Experimental and Theoretical Investigation of Novel Phase Change Materials for Thermal Applications

By

Sayem Zafar

A Thesis Submitted in Partial Fulfillment of the
Requirements for the Degree of Doctor of
Philosophy in Mechanical Engineering

Faculty of Engineering and Applied Science,
University of Ontario Institute of Technology

Oshawa, Ontario, Canada

Abstract

An experimental investigation is conducted to test the thermal properties, behaviour and characteristics of R134a clathrates with additives, as phase change materials (PCMs). PCMs' charging characteristics are analysed and evaluated for cooling applications. The formation of refrigerant clathrates is investigated due to their potential use in active as well as in passive cooling applications. PCMs are formed using R134a clathrate and distilled water with different refrigerant fractions and five different additives. The main objective of using additives is to study their potential for enhancing the clathrate formation and their thermal properties under direct contact heat transfer. PCMs are formed in glass tubes to determine their freezing onset time, transformation time and thermal properties. The thermal properties determined are the liquid phase thermal conductivity, mushy phase thermal conductivity, and specific latent heat of the PCMs. Refrigerant R134a fractions of 0.15, 0.2, 0.25, 0.3, 0.35 and 0.4 are used to form clathrate. For the additives, ethanol, sodium chloride, magnesium nitrate hexahydrate, copper and aluminum are used. Additive mass fraction is varied from 0.01 to 0.05 with 0.01 interval. Time for on set and end set is recorded after regular intervals. PCM's temperatures, after regular intervals, at two different locations inside the tube are also recorded. Discharge tests are also conducted for which the PCMs are used to cool the hot air as well as to cool down a battery. Energy and exergy analyses are performed to assess PCMs' performance. R134a fraction of 0.35 is found to be the best mass ratio for clathrate formation while Ethanol as best additive.

Acknowledgments

I would like to express my deep and sincere gratitude to my supervisor, Dr. Ibrahim Dincer, for his valuable guidance and continuous support. His enthusiasm and passion has been a constant source of inspiration and encouragement.

A great deal of this research is inspired and made possible through the teamwork of Dr. Dincer's research group. I would like to appreciate them for helping me throughout.

Last but not least, I want to thank my family for their endless support throughout my studies. The honor of this degree truly belongs to them. Their blessings and prayers have always been with me.

To all of whom I have missed during this brief acknowledgement, please rest assure that your support has been vital and it cannot be forgotten.

Table of Contents

List of Tables

List of Figures

Nomenclature

C_P	Specific heat capacity, J/kg K
D	Dipole moment, Debye
dp	Diameter of the particle, m
Ex	Exergy, J
ex	Specific exergy, J/kg
$\dot{e}x$	Specific exergy rate, W/kg
f_{TE}	Thermoeconomic cost factor
H	Volumetric enthalpy, J/m^3
h	Specific enthalpy, J/kg
k	Thermal conductivity coefficient, W/m K
l	Length, height, m
M	Molar mass, g/mol
m	Mass, kg
$\dot{m}$	Mass flow rate, kg/s
Pr	Prandtl number; $(\frac{\mu C_P}{k})$
Q	Heat, J
$\dot{Q}$	Heat flow rate, W
R^2	Coefficient of determination
R_b	Thermal boundary resistance, m^2 K/W
Re	Reynolds Number; $(\frac{\rho v d_p}{\mu})$
$\dot{S}$	Entropy rate, W/K
s	Specific entropy, J/kg K
T	Temperature, K
t	Time, s
u	Specific internal energy, J/kg
U	Heat transfer coefficient, W/m^2 K
V	Volume fraction
$\dot{W}$	Work rate, Power, W

w	Mass fraction
x	Distance, m
Z	Coordination number
Z_k	Cost of items, $

Greek Letters

α	Biot number; (hL/k)
β	Thermal diffusivity; ($k/\rho C_P$), m^2/s
Δ	Difference
ρ	Density, kg/m^3
η	Energy efficiency
Ψ	Exergy efficiency
λ	Specific latent heat of fusion, J/kg
ξ	Energy cost, $/J

Subscripts

amb	Ambient
b	Base fluid
c	Charging
cm	Critical
d	Discontinuous
dst	Destruction
e	Exit
ele	Electrical
f	Final
gen	Generation
i	Initial
m	Mixture

Superscript

Q	Heat

Acronyms

CFC	Chlorofluorocarbons
HCFC	Hydro- chlorofluorocarbons
HFC	Hydrofluorocarbons
LiPo	Lithium polymer
$Mg(NO_3)_2$	Magnesium nitrate
NaCl	Sodium chloride
PCM	Phase change material
TES	Thermal energy storage

Chapter 1 Introduction

The use of energy has excessively increased in recent years. Energy appears to be the engine of progress towards modernity. It is widely believed that the global energy demand is bound to increase at an exponential rate. To meet the growing demand, natural resources are being consumed at an alarmingly high rate. One way to slow down the rate of natural resource consumption is the use of alternative energy. Apart from using the alternative ways to produce energy, an effective way is to manage it properly. A major use of energy is for heating and cooling applications. Energy storage systems have been recently introduced to help harvest the energy, manage it and use it accordingly. The study related to energy storage systems is divided into the analyses of the heat exchanger while the other aspect looks at the materials to be used to store the energy.

Applicable materials for the energy storage come in all shapes, varieties and sizes. Materials that change their phase, liquid-solid-gas, appear more feasible for energy storage applications. Primary reason for their effectiveness is their latent heat capability which tends to result in higher amount of energy storage without changing their own temperature [1,2]. One of the ways to form a useable phase change material (PCM) is by introducing gas into the water molecules. These materials, with trapped gas molecules inside the water molecules, are called clathrates. When the gas is a refrigerant, they are referred as clathrates of refrigerants. Refrigerant clathrates are important to study since they can be used with the existing refrigeration and air conditioning cycle. Refrigerant clathrates can be altered to change their phase under desired temperatures by adding additives and changing the component mixture fractions. Such feature enables refrigerant

clathrates to be effective for active and as well as passive cooling applications [3]. This feature also makes them very effective not only for comfort cooling but also for heat absorption for food, electronics and medical industries.

The possible application of cold thermal energy storage PCMs is wide ranging from comfort cooling to electronic cooling. For example, most commercial buildings in tropical parts of the world use a huge amount of energy for heating, ventilation, and air conditioning (HVAC) systems [4]. As a result, the electricity demand increases during the day time while it drops at night. Implementing direct cold thermal energy storage system with conventional air conditioning system helps shift the electricity load from day time (peak time) to night time. This shifting is done by storing cold energy during the night and then utilized it when needed primarily during the day time.

With the increasing demand for electronics, the heat generated by electronic devices has been a problem that needs to be dealt with [5]. The heat generation in electronics not only limits their performance, but it also presents a safety hazard as the electronic item can easily burn. Cold PCMs can be used to cool down electronics for long enough periods to maintain their temperature and allow safe usage. Cooling electronics, using PCMs, appears to be a viable option because of their ability to be made into any size and shape. They offer a more economical solution than the conventional cooling methods currently available.

1.1 Thesis Outline

This section gives an overview of the thesis. The thesis starts with introduction stating the background and possible applications of the product. The second chapter gives the details of motivation behind the research and a complete list of objectives of the research. The third chapter includes a literature review of thermal energy storage system, description and types of phase change materials, refrigerant clathrate and thermal properties. The fourth chapter explains the background of refrigerant clathrates for cooling applications. The fifth chapter lists out the design techniques, experimental set-ups, system descriptions and challenges faced during the course of experimental work.

The sixth chapter explains the analyses based on energy and exergy evaluations including the equations for mass, energy, entropy and exergy. This chapter also includes the equations for energy and exergy efficiencies.

The seventh chapter includes the results and discussion of the research. There are several main sections which are follows:

- First a brief description of the tested material is presented with contents of each test run.
- Second section of this chapter provides the detail description of the test results conducted for base PCM. Base PCM is basically the refrigerant clathrate without any additive. Clathrate formation time is determined for different mass fractions of the refrigerant. It also shows the test results for clathrate formation at two different bath temperatures.

- Third section shows the test results for charging time of the PCMs with additives. Additives are studied for refrigerant mass fraction of 0.35 with a range of additive mass fraction. This section also shows the test results for constant energy bath test where temperature readings are recorded at two different locations inside the PCM after regular interval.
- Fourth section shows the results of varying the additive fraction on charging time. Different additives are used to study their influence on charging time.
- Fifth section shows the effects of changing the aspect ratio on charging time. Two different aspect ratios are studied to see their impact on charging time.
- Sixth section shows the test results for discharge tests. Discharge tests are conducted using hot air and with hot battery. Discharging times are recorded for each PCM with hot air discharge. With battery discharge, battery temperatures and battery cooling times are presented.
- Seventh section includes the thermal properties determined through the set of experiments. The thermal conductivity, specific heat and latent heat values are evaluated for each PCM. The evaluated thermal properties are compared with the analytical calculations. Optimization study is also presented in this chapter along with the validation of results.
- Eighth section presents the energy and exergy values for charging and discharging of each PCM. The energy and exergy evaluation is presented for base PCM as well as for PCMs including the additives.
- Ninth section includes the thermoeconomic study of PCMs.

- Tenth section presents the uncertainty analysis for all the tested PCMs. Uncertainty analyses are presented for charging temperature values, discharging temperature values and thermal property values.
- Eleventh section shows the analytical study conducted to determine the thermal properties. Analytical study presents the thermal properties of PCMs based on some more refrigerants and additives than the ones used for experiments.
- Twelfth section presents the results of optimizations. Optimizations are conducted on simple charging and discharging as well as on battery cooling. Optimization functions are developed which is presented in the analyses chapter.
- Thirteenth section presents the validation of the results. Results are compared with some other published values to validate the findings of the experiments.
- Finally, future work and further improvement that can be made with the experimental study are presented.

In the last chapter, the conclusions and recommendations of the thesis are presented. It lists the findings of the experimental work and gives suggestions for utilizing the findings of the work.

Chapter 2 Motivation and Objectives

2.1 Motivation

The demand for cooling applications is currently high and is expected to increase in the coming years. The cooling applications can either be for comfort, food or for electronics. A cooling mechanism is required to provide cooling for the required capacity yet have the ability to be used for portable and small applications. The entire refrigeration system is usually expensive and undesirable to be used for small portable applications due to its bulky size.

Refrigerant clathrates can either be used for large scale cooling or they can be encapsulated to provide cooling for small portable applications. Clathrates of several refrigerants already exist and are used as PCMs. The existing refrigerant based PCMs take a very long time to charge. They also have limited capacity and have undesired operating temperatures. The motivation behind the current research is to change the effective thermal properties of the PCMs in order to improve the charging and discharging times. It is believed that the latent heat can also be improved to enhance the capacity. The improvement in the desired parameters can be achieved by adding metal particles, salt particles and liquid additive.

2.2 Specific Objectives

The specific objectives of this study are to conduct theoretical and experimental studies along with thermodynamic assessments on clathrates with different additives and mass fractions. Refrigerant R134a and R141b are used to form clathrates with additives. To

come up with novel PCMs, different salts, ethanol and metal micro particles, to come up with a novel PCM. The experiments are conducted to determine the thermal properties, charging and discharging times of the tested PCMs.

The specific objectives of the thesis study are given as follows:

1. To select appropriate refrigerant and additives for experimental studies. An extensive literature review is undertaken to select appropriate refrigerants for the experimental and analytical studies. For experimental study, refrigerants that are currently being used are selected. For analytical study, refrigerants with low global warming potential and possible retro-fit replacements are selected. Literature survey is conducted to select appropriate additives for the experimental and analytical study. At least one additive candidate from solid metal, solid nonmetal and liquid is selected.

2. To form refrigerant clathrates based on R134a and R141b. Experiments are conducted in which refrigerants R134a and R141b are mixed with water to form refrigerant clathrates. The refrigerant clathrates are formed to establish baseline parameters against which the novel PCMs' parameters are compared. The established parameters are charging times, thermal properties and discharging times. The clathrate formation is studied over a range of refrigerant mass fractions. The refrigerant mass fractions of 0.15, 0.2, 0.25, 0.3, 0.35 and 0.4 are studied.

3. To develop novel PCMs by adding sodium chloride, magnesium nitrate hexahydrate, aluminum particles, copper particles and ethanol additives in the R134a clathrate. Experiments are conducted to make novel PCMs by adding the

above mentioned additives in the refrigerant R134a clathrates. The PCM, comprising of refrigerant, water and additive, are formed with mass fraction of the additives varying from 0.01 to 0.05 with 0.01 intervals. Additives change thermal properties of the PCMs which in turn change the charging and discharging times.

4. To evaluate the specific heat capacity using analytical methods. Using the equations available in the literature, the specific heat of the new PCMs is predicted. Later, the PCMs are made and test results are collected. The collected test results included the values of temperatures and the mass. With specific heat capacity of the PCMs calculated, the heat flow from the PCM is determined.
5. To model the thermal conductivities using analytical methods and experimentally. Using the empirical equations available in the literature, the thermal conductivities the new PCMs are predicted. Later, the PCMs are made and test results collected. The collected test results included the values of temperatures and geometric dimensions of the PCMs. With these values, thermal conductivities are determined for the tested PCMs.
6. To calculate the latent heat of fusion experimentally. The heat of fusion of the PCMs is measured using the acquired data.
7. To measure the onset and end set charging times experimentally. During the experiments, the PCMs are continuously observed to pin point the time they start changing their phase and the time the freezing process is completed. The phase change onset and end times is recorded. This established the operating range of the novel PCMs.

8. To measure the discharging times experimentally. For active cooling test, the PCMs are discharged using hot air. The times PCMs takes to completely discharge are recorded. Along with the times, the PCM temperatures are also recorded to maintain the baseline for analyses. For passive cooling applications, PCMs are discharged with the battery heat. PCM is formed in a jacket designed for the battery test while the battery is heating. Discharging times and battery temperatures are continuously recorded for the test.
9. To perform energy analysis for charging and discharging. The energy analysis is conducted, using the equations described in the Analysis chapter, to evaluate the energy efficiency during the charging and discharging process.
10. To perform exergy analysis for charging and discharging. The exergy analysis is conducted, using the equations described in the Analysis chapter, to evaluate the energy efficiency during the charging and discharging process.
11. To encapsulate the newly developed PCMs in cylindrical container with glass walls and square container with metal walls. Difference in charging and discharging times are recorded along with two different aspect ratios. The shapes and sizes are studied such that the PCMs can be utilized for electronic cooling applications.
12. To conduct the thermoeconomic analysis on each PCM. Thermoeconomic analysis will be conducted for the novel PCMs to understand the economic viability of the PCMs.

Chapter 3 Literature Review

The ability to utilize energy is a great scientific achievement of the human recent-past and it continues to reform at a gradual pace. It is the same ability that fueled the industrial revolution and governs our way of living even today. The recent global trend has changed from rudimentary energy production or rejection to precisely manage and absorb energy. The energy management is a challenge that needs to be dealt with in order to achieve the goal of sustainable growth. Energy storage works as an equalizer between the energy availability and its demand while help making the system more energy conserving hence improving the performance [6]. Energy storage systems can be divided with respect to the types of energy being stored. Generally energy storage systems are divided into mechanical, electrical and thermal energy storage systems [7].

Mechanical energy storage systems include gravitational energy storage, pumped hydro systems, compressed air storage or spinning flywheels. Gravitational energy storage relates to a system that converts the available energy to put either liquids or solids at a higher altitude. This gain in altitude increases the available potential energy which can be later utilized by converting it into kinetic energy or pressure head, in the case with liquids. Compressed gasses or pumped liquids can be stored using the available energy to be utilized for later use. Such fluids can be utilized by converting their pressure into a useful form of energy required. Electrical energy storage is the most common type of energy storage in public use. It requires the use of a battery that stores the electrical energy in it. When needed, the stored electrical energy can be utilized as an electrical

output. Thermal energy storage system is of interest hence discussed further in the section below.

3.1 Thermal Energy Storage Systems

Thermal energy storage (TES) refers to the storage of heat by increasing or decreasing the temperature of a substance or by changing the phase of a substance [8]. TES is the temporary storage of high- or low temperature energy for later use. With the growing demand for energy management, it is also essential to look for ways to manage thermal energy. Thermal energy management can be associated to either heat storage for later use or heat absorption for cooling purposes. The materials for thermal energy storage systems can be divided into sensible heat storage, thermochemical heat storage and latent heat storage [9]. Sensible heat storage is when the temperature of the substance changes. Thermochemical heat storage systems refer to the system in which heat is absorbed or released due to formation or breaking of a molecular bond. Latent heat storage is referred to the system in which a substance changes its crystalline structure as a solid or its phase either from solid to solid, solid to liquid, liquid to gas, solid to gas or vice versa.

3.1.1 Latent Heat Storage

This thesis focuses on latent heat storage as it usually offers higher change in thermal energy than the sensible heat change for a given medium [8].Materials used in the latent heat storage system are referred as phase change materials (PCMs). When the PCM is introduced to the environment, it changes its phase instead of changing its temperature. The process of material phase change, however, changes the temperature of the

environment since the change of phase occurred due to heat loss or heat gain by the material.

Latent heat storage also appears more attractive for thermal management since it provides a high-energy storage density and has the capacity to store energy at a relatively constant temperature [10]. The latent heat storage system has to have a storage material, which goes through a phase change for the desired operating temperature, and a heat exchange surface for heat transfer to or from the latent heat storage material [8, 11]. Latent heat storage materials are referred as phase change materials (PCMs) because they tend to change their phase. The advantage of using PCMs, over sensible heat change material, is superior heat transfer at almost constant PCM temperature. Constant PCM temperature means the PCM does not need special handling with respect to temperature. Latent heat storage PCMs store 5 to 14 times more heat per unit volume than everyday available sensible storage materials [9].

PCMs are of importance for thermal energy systems since latent heat storage is one of the techniques of managing thermal energy. Several researchers have worked on PCMs for a wide range of applications with studies on types of material, their characteristics and their advantages and disadvantages. It is suggested that the use of PCM's latent heat allows the thermal energy storage systems to be smaller in size hence becomes more feasible for a wider range of applications [8]. Several substances have been nominated as effective PCMs while some of them have also been commercialized [9]. The PCMs can be chosen based on their temperature range, application space availability, interaction with the environment or the desired amount of heat rejection/absorption from the system.

3.1.2 Phase Change Materials (PCMs)

PCMs can be classified as solid–solid, solid–liquid, solid–gas or liquid–gas. These classifications are based on their transformation phase before and after heat absorption or rejection. Solid-solid PCMs are materials that change their crystalline structure at a specific temperature. They have small volume changes and do not generally require encapsulation, unlike liquids and gases. Such features make them easy to handle and can be used in many situations for desired dimensions, without the added constraints of containment [12, 13]. The drawback of solid-solid PCMs is their low latent heat values compared to solid-liquid or liquid-gas phase changes. Solid/liquid–gas PCMs usually have higher latent heat of phase transition compared to solid-solid and solid-gas phase change [9]. However their large volume changes on phase transition increases the containment problems hence makes them complex and impractical [11].

For several thermal energy storage applications, it is required for the PCMs to flow in a system which is not possible for solid-solid PCMs. Solid to liquid PCMs absorb heat to become liquid while releasing heat to become solid. These types of PCMs usually have lower latent heat compared to solid/liquid-gas type PCM but higher than the solid-solid PCMs. Unlike solid-solid PCMs, they require containment and a heat exchange mechanism. Compared to solid/liquid-gas PCMs, these have lower volume change not to mention it does not have gas which makes their containment easier and more economical. Due to the better heat absorption/rejection properties and manageable containment issues, solid-liquid PCMs are preferable for most of the applications. These types of PCMs are the focus of research for this thesis.

Phase change materials are the latent heat storage materials since the heat absorption or discharge causes the material to change its phase. When the PCM goes from solid to liquid, it absorbs heat. This heat absorption means that the heat is taken away from another body. In this process, the other body loses its heat and either becomes cooler or changes its phase. When the PCM goes from liquid to solid, it gives away heat. The surrounding or nearby body tends to absorb heat. This heat absorption, by the surrounding body, makes it either warmer or it changes its phase.

Almost every material changes its phase when the required amount of heat is supplied or taken away from it. However, in order to be considered for use as a latent heat storage material, the PCM has to have certain desired properties. These desired properties make the PCM feasible for use for cooling applications. The desired properties are discussed as follows:

- The PCM should have the appropriate phase-change temperature. The phase-change temperature should match with the working temperature range. If the PCM changes phase outside the range of working temperature, it would be of no use for the application.
- The PCM should have high latent heat capacity to affect the other body/environment heat as much as possible. High latent heat per unit volume is considered for most applications as this optimizes the container volume.
- The PCM should have high thermal conductivity coefficient. Thermal conductivity coefficient helps in the charging or discharging process. Lower thermal conductivity coefficient results in slow heat transfer while high coefficient results in faster heat transfer.

- The PCM should also show feasible chemical properties. It should not be toxic as to cause health hazard. It should be non-reactive to the containment or contacting material as well as to the environment. For commercial safely aspects, it should not be a fire hazard either since it may be used near or around high temperatures, ignition or spark.
- The PCM and its constituents should be readily available and be cost effective. This feature is required to allow for large quantity production and use at an economical rate. Moreover, the entire system cost is already high so an inexpensive PCM would attract more usage.

PCMs can be further divided into organic or inorganic materials. Organic and inorganic materials behave differently and have different thermal properties. Organic materials are advantageous because they melt and freeze repeatedly without phase segregation and loss in their latent heat of fusion [6]. They are also noncorrosive due to their inability to make salt hence it makes them easy to contain. Comparisons of properties and attributes of organic and inorganic materials are listed in Table 3.1.

As can be seen from Table 3.1, both the organic and inorganic materials have their pros and cons. Paraffin wax is a common type of PCM. It is widely used and commercially available due to its favorable behavior over a wide range of temperatures. At room temperature paraffin's phase depends on its molecular structure and its melting point increases as the chain length increases [21]. Paraffin are gaseous with less than 5 carbon atoms per molecule, with 5 to 15 carbon atoms are usually liquids while the straight-chain paraffin having more than 15 carbon atoms per molecule are solids. Although paraffin is relatively easy to handle and usually inexpensive, it has low thermal

conductivity and it is considered flammable. Due to these undesirable characteristics, researchers are looking for better materials to be used as PCMs.

Table 3.1 Attributes and properties of common organic and inorganic materials as PCMs [9, 14 - 20].

Organic	Inorganic
• Unable to make salts due to the covalence of carbon	• Make salts
• Lower melting and boiling points	• Higher melting and boiling points
• Insoluble in water, soluble in organic solvents	• Readily soluble in water, insoluble in organic solvents
• Highly inflammable and volatile	• Not inflammable and non – volatile
• Poorer conductors of heat and electricity in aqueous solutions	• Better conductors of heat and electricity in aqueous solutions
• Melt and freeze repeatedly without phase segregation and loss in their latent heat of fusion	• Double volumetric latent heat storage capacity than the organic compounds
• Noncorrosive	• Heat of fusion does not change with cyclic phase change over long durations
• Paraffin have favorable behavior over a large range of temperatures	• Salt hydrates freezes or melts at a variety of temperatures
• Low thermal conductivity	• High thermal conductivity
• Flammable	• Mildly corrosive and toxic
• High heat of fusion	• Inexpensive and abundant
• Low specific heat	• Poor nucleating properties
• High toxicity	• Incongruent melting

The other types of organic materials, suitable as PCMs, are generally described as non-Paraffin organic materials. Esters, fatty acids, alcohols and glycols are found to be effective PCMs with certain advantages and disadvantages [15, 16]. These materials have the advantage of having high heat of fusion which means they can store large quantity of heat. But these materials have certain drawbacks which makes them commercially undesirable as an appropriate PCM. They have low thermal conductivity which means they would take longer to get heated, charged, or to discharge. These materials are also

toxic, corrosive to usual containment materials, flammable with relatively low flash point and are highly instable at high temperatures. Another hindrance towards their widespread use is their high cost compared to paraffin.

Several inorganic materials show properties that makes them a desirable PCM. In general inorganic compounds have almost double volumetric latent heat storage capacity than the organic compounds [9]. They also have long term advantages as their heat of fusion does not change with cyclic phase change over long durations. Salt hydrates are common type of inorganic PCM in use and have been extensively studied for the use as latent heat storage material. These are a mixture of inorganic salt and water which freezes or melts at a variety of temperatures, depending on the percent composition of the two materials or the salt. Salt hydrates demonstrate properties that make them a very effective PCM [9, 10].

- They have high latent heat of fusion per unit volume which results in high quantity of heat to be stored or absorbed without large changes in their volume. This enables them to be stored is limited space making their containment very easy.
- They have high thermal conductivity which means they can be charged or discharged quickly. This ability of quick charge or discharge means they can be used for smaller cycles and short durations.
- They are mildly corrosive and toxic while being compatible with plastics and other usual containment materials. This means that they pose little problems with containment and handling.

- Many salt hydrates are inexpensive and abundant. This feature makes their widespread use possible, even for the non-commercial use.

Salt hydrates have their own share of problems. They have poor nucleating properties which results in super-cooling of the liquid before crystallization beings [9]. The most effective salt hydrates are known to have the problem of incongruent melting. Incongruent melting is considered when the salt is not completely dissolved in the water at the phase change point [22]. This results in undissolved salt not being part of the solidification process which results in greater amount of undissolved salt as the cycle continues. The problem of incongruent melting can be addressed by mechanical steering, encapsulation, adding agents to prevent salt settlement or by having access water to avoid supersaturating solution [17-20]. Eutectics are a mixture of materials that changes phase completely at a fixed temperature. They form a mixture of the component crystals during crystallization while melting or freezing congruently [23].

3.1.3 Clathrates of Refrigerant

Clathrate is a solidified form of water that contains gas molecules in its molecular cavities [23, 24]. Clathrates form when water and gas combine under low temperatures and high pressures [25]. Using refrigerant clathrates has appeared to be a promising way to store thermal energy for cooling applications. Since the phase change temperature of clathrate is above the freezing point of water, yet low enough to be used for comfort cooling, its use in air conditioning has been studied and found to be useful [26 - 30]. Refrigerant clathrates are considered more effective compared to the other type of PCMs as they can be used through refrigerant loops as they can be easily circulated [31, 32]

Clathrates have certain properties that make them very good PCM for cold storage. Clathrates have high heat of fusion which means that they can store higher amount of energy. They also have high density therefore the storage can be smaller per unit energy rate. Clathrates do not have added corrosive or toxicity hence normal refrigeration unit can be used to form clathrates of refrigerants. And since they require the mixture of water and refrigerant, it is economical and available in abundance.

Many chlorofluorocarbons (CFCs), hydro- chlorofluorocarbons (HCFCs), and hydrofluorocarbons (HFCs) can form clathrates of refrigerant [33]. In order to be used for cold thermal energy storage, an effective refrigerant clathrate should form at atmospheric pressure and temperature range between 278 K to 285 K [34-36]. Several refrigerants form the clathrates but only handful is commercialized. Table 3.2 shows the latent heat of fusion, formed pressure and phase change temperature of some selected refrigerant clathrates [37].

Table 3.2 Phase change temperature, formation pressure and heat of fusion for several refrigerant clathrates [37].

Types	Refrigerants	Phase change temperature (^{o}C)	Pressure (kPa)	Heat of fusion (kJ/ kg)
Chlorofluorocarbon				
CFC 12	R12	11.8	439	316
CFC-11	R11	8.5	55	334
Hydro-chlorofluorocarbon				
HCFC-21	R21	8.7	101	337
HCFC-31	R31	17.8	282	427
HCFC-142b	R141b	8.4	42	344
HCFC-22	R22	16.3	815	380
HCFC-141b	2141b	8.4	42	344
HFC-134a	R134a	10	410	358
HFC-152a	R152a	15	434	383
HFC-125	R125	11.2	944	362

Due to the environmental concerns, CFC clathrates are forbidden. This restriction leaves only the hydro-chlorofluorocarbon and hydrofluorocarbons to be used for PCM. Refrigerant clathrates with R-134a have been proposed as a PCM which demonstrated to be the most promising candidates for this goal [34-36]. Another refrigerant considered feasible for refrigerant clathrates is R141b due to its available engineering applications, low saturated vapor pressure, low cost, and its low pressure character [38]. Refrigerant R32 should also be of interest as it has low global warming potential, is accessible and it makes an effective PCM due to its high thermal conductivity, compared to its counterparts [39-40]. Due to the availability, wide spread use and relatively low working pressure, R134a is used for the experiments. R134a is extensively used for domestic air conditioning application therefore; research efforts have been made to develop R134a clathrate for cool storage applications [41]. The other refrigerant used in this study is R141b because of its availability and very low working pressure. Low working pressure makes the refrigerant easy to contain and handle. R32 and R1234yf are also potential candidates for this study but their unavailability in the market and their price made it out of reach.

Conventional PCMs, especially the ones based on refrigerant clathrates, have poor heat transfer properties. To further enhance the performance of refrigerant clathrates, to be effective PCMs, additives of different materials have been studied. For instance, adding calcium hypochlorite or benzenesulfonic acid sodium salt improved the cold energy storage capacity and the cold energy transfer rate of R141b based clathrate [42]. For organic material, adding alcohol in R134a based clathrate accelerates the cool storage rate and eliminates the floating clathrate during the hydration process [41].

In order to increase thermal conductivity, metallic nanoparticles have also been added to the existing heat transfer fluid. It has been reported that even a small fraction of nanoparticles of low thermal conductivity metallic oxides can favorably increase the thermal conductivity of pure substances, such as water [43, 44]. Even for organic compounds such as monoethylene glycol and paraffin fluids, copper oxide nanoparticles can improve the thermal conductivity [45]. Addition of pure copper nanoparticles in ethylene glycol increases the thermal conductivity by 40% [46]. For the refrigerant hydrate, nanoparticles of copper are also studied which shows that the heat transfer and charging times increases with the addition of nanoparticles of copper [47]. This improvement in thermal transport properties depends on the particle size, dispersion and the operating temperature [48-53]. It is believed that this phase change temperature can be lowered by using additives such as salt, alcohol and ethylene glycol to make clathrates more suitable for cooling applications [54-55].

Liquid additives have also been studied as they do not pose significant hindrance when used for active cooling/heating applications. Liquid additives are of interest as they can easily run through pumps and compressors, without causing any significant damage or loss of efficiency. However, liquid additives namely propylene glycol and ethylene glycol have been used for passive cooling applications as well [56]. Ethylene glycol is commonly used as automotive engine coolant hence presents itself as a strong candidate for liquid additive [57]. Apart from thermal properties improvement, additives help enhance the performance and usability of PCMs. The melting temperature of some refrigerant clathrates is a little higher than what is generally required for comfort, food or electronics cooling. It is believed that this phase change temperature can be lowered by

using additives such as salt, alcohol and ethylene glycol to make clathrates more suitable for cooling applications [54].

For the research in this thesis, at least one candidate from pure metal, salt and liquid additive is selected. Sodium chloride, magnesium nitrate hexahydrate, copper, aluminum and ethanol are the additives studied in this thesis. Metals are selected because they tend to have high thermal conductivities hence they may help improve the thermal conductivity of the refrigerant clathrate. Copper is selected due to its high thermal conductivity and aluminum is selected due to its low density while it has a relatively good thermal conductivity. Salts are selected due to their low densities and their ability to mix well with liquids. Sodium chloride is the most common salt so it is selected of its abundance in commercial market. Magnesium nitrate hexahydrate is selected for experiments due to its low cost, easy handling characteristics and solubility in water [58]. For liquid additive, ethanol is selected for tests since previous researchers have studied alcohol, as an additive, to see the effect on active cooling [41].

Apart from thermal properties improvement, additives have other advantages to enhance the PCMs performance and usability. As shown in Table 3.2, the melting temperature of some refrigerant clathrates is a little higher than what is generally required for comfort, food or electronics cooling. This thesis describes the model study to model the effects of adding additives in the selected refrigerant clathrates to enhance their thermal properties. At a preliminary level, the most appropriate refrigerant clathrates are proposed and the suitable additives are also suggested.

Chapter 4 Background

Global reliance on energy has increased many folds over the last few decades and it continues to do so, at an alarming rate. According to the international energy outlook, global energy consumption growth is 53 percent from 2008 to 2035 [59]. In order to meet the growing energy demand, natural resources are being depleted faster than they can be replenished [60]. Destruction of natural resources can be associated not only to global increase in energy demand but also to our heavy reliance on non-renewable sources of energy.

4.1 Energy Use for Cooling

Energy use for refrigeration and air conditioning accounts for about 15% of the total electricity consumption in the world [61]. Since the energy used for electricity production is 13%, the refrigeration and air conditioning amounts to about 2% of the entire energy consumption [62]. It is believed that this high consumption of energy for cooling applications can be significantly reduced by opting for a thermal energy system. A thermal energy system is an energy management system which stores the excess energy while releases it when required. The excess energy, which gets stored, is otherwise dumped to the atmosphere causing harmful and unwanted environmental effects. This system of energy harvesting has a potential to reduce the use of electricity and other energy sources that are harmful to the environment.

Another area that will see increase in demand is the ability to absorb heat from electronics. As modern electronics are getting smaller and faster, the demand for a mechanism to reject or absorb heat from the electronics is ever increasing. The increase

in demand can also be associated with the increased electric machines and devises. One such use of electric devices is for transportation. In order to achieve more sustainable global environment, modes of transportation are being designed, and made, to run on electric power. The demand for electric power requires the use of electric storage, usually using batteries. The problem with batteries is that as the battery power output increases, the battery temperature tends to increase [63]. Similarly, as more processing power is squeezed into electronics, thermal management has become more critical for successful design of electric devices. Moreover, electric devices and electric storage systems operate best within a limited temperature range so their packages must be designed to remove the excessive heat [64].

Since the application for heat absorption ranges from thermal energy storage to electric cooling, a mechanism is required that can be used for both the applications. Research on a solution that can be used for both the applications will be valuable. A material that can absorb heat is considered to be a viable solution for both the applications mentioned before. Furthermore, it is even better if the material changes its phase during the heat absorption process. The phase change process not only absorbs more energy but also the phase change process does not change the material temperature significantly. Materials that can be incorporated for such processes are phase change materials (PCMs) that tends to change their phase from solid-liquid-gas or vice versa while absorbing heat within the operating temperature range. Such materials can be stored in large containers to provide cooling or can be encapsulated in desired geometries or sizes for electronic cooling applications. Latent heat of PCMs is greater than their specific heat that is why they tend to absorb more heat during the phase change process

or even when compared to non-phase change materials. The other advantage of PCMs is their ability to roughly maintain their own temperature during the heat absorption process. This feature allows for surroundings to be kept at the design temperature and not get affected by cooling of a part of the system.

4.1.1 Refrigerant Clathrates with Additives

Thermal energy storage through PCM is an efficient method to store thermal energy. PCM in latent storage are used to increase the thermal energy capacity of the system. Using PCM in latent heat storage provides a higher thermal energy storage/discharge capacity. Refrigerant based phase change materials are one of the many mechanisms available for electric thermal management and thermal energy storage. Clathrates of refrigerants are considered effective as they tend to have high heat of fusion compared to eutectics, paraffin and fatty acids.

When the phase change is required from solid to liquid (above 273 K or 0 ^{o}C) the refrigerants are mixed with water to form clathrates. Clathrate of refrigerant is a compound formed by the inclusion of molecules of one kind of guest substance in the cavities of the crystal lattice of another host substance [65-66]. In other words, they are formed by mixing water and refrigerants at a certain pressure and temperature. Clathrates of several refrigerants already exist and are used as PCMs. The addition of additives improves the performance of the refrigerant clathrates. Performance improvement is due to improvement in charging and discharging times, change in phase change temperatures to fit the desired range, or improvement in the thermal properties of the refrigerant clathrates.

Chapter 5 Experimental Setup

This chapter describes the experimental setup to determine the latent heat, phase change temperature, thermal conductivity and heat capacity of the PCM. It also provides the system description for the equipment and apparatus to be used for the experiments.

5.1 System Description

For the experiments, a cold constant temperature bath from *The Clifton Range* is used as a constant temperature source [67]. The refrigerant clathrate with additive, named PCM, are formed in glass tubes from *ACE Glass Incorporated* [68]. The tubes are submerged in the constant temperature water bath for which the temperature is set at 276 K and 278 K. The constant temperature bath works by providing cold energy and heat simultaneously to the distilled water in the bath to maintain its temperature at a set value. The graphic illustration of the experimental system is shown in Figure 5.1.

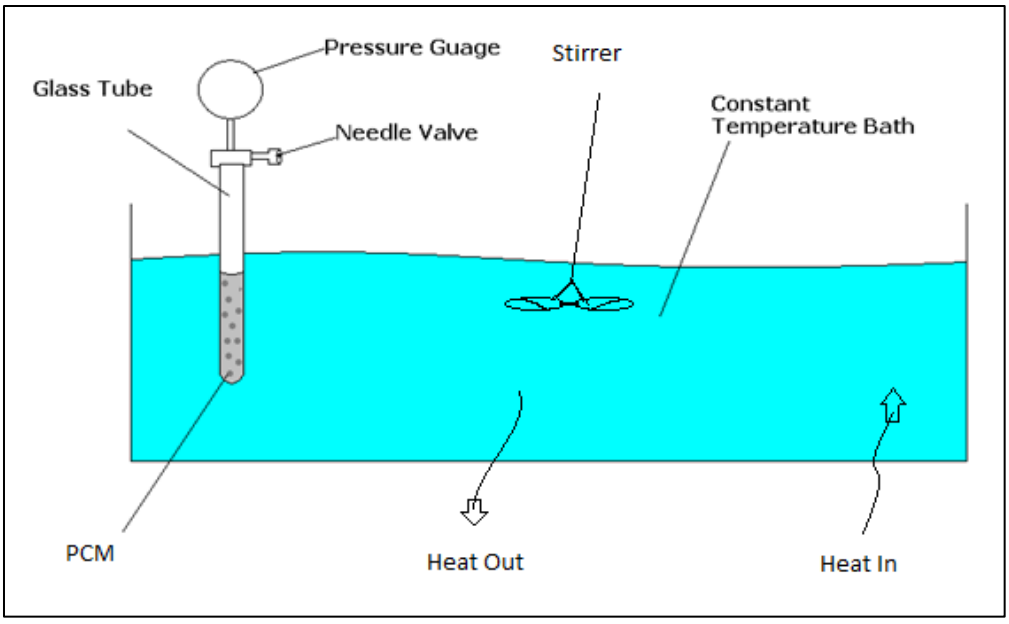

Figure 5.1 A schematic diagram of the proposed PCM testing system

A refrigeration system with cooling coils around the water bath pumps out the heat. A controller constantly monitors the water temperature in the bath while continues to provide the desired heat to maintain the desired temperature. The bath is converted into constant energy bath for thermal properties experiments. A constant cold and hot energy is provided to the water in the bath to maintain the amount of energy. A stirrer is also used which circulated the water in the bath. Without the stirrer, the water near the hot or cold source would change its temperature while the water away from the source would see its effect later.

The PCM is formed in the glass tubes. First the glass tube is filled with distilled water and the desired additive. The exact mass of the tube with its constituents is measured using a high accuracy digital weighing scale. The tube is sealed and then vacuumed to get rid of excess air. The last step is to fill the desired refrigerant using a needle valve that allows one way flow. The glass tube is then submerged into the cold temperature water bath for charging. The tubes are visually observed after regular interval to observe the onset and end set of freezing. The freezing times, PCM temperatures and pressures are recorded for each test. Onset of freezing is usually east to detect as the top layer starts freezing. The end set is challenging to pin point so it is important to continue observing the PCM until after the last observed changes in the PCM structure. PCM usually rises as it freezes so height is observed for the end set.

The K-type thermocouples are attached to a reader to read the temperatures. For initial charging test, only one temperature reading is taken. For thermal property tests, temperatures are taken at two different locations. The tube is comprehensively tested for leaks and provisions are made to make sure there are no leaks. It is important to use a

glass tube since the onset of phase change needs to be observed visually. The illustrative figure of the glass tube, its connections and used systems are shown in Figure 5.2.

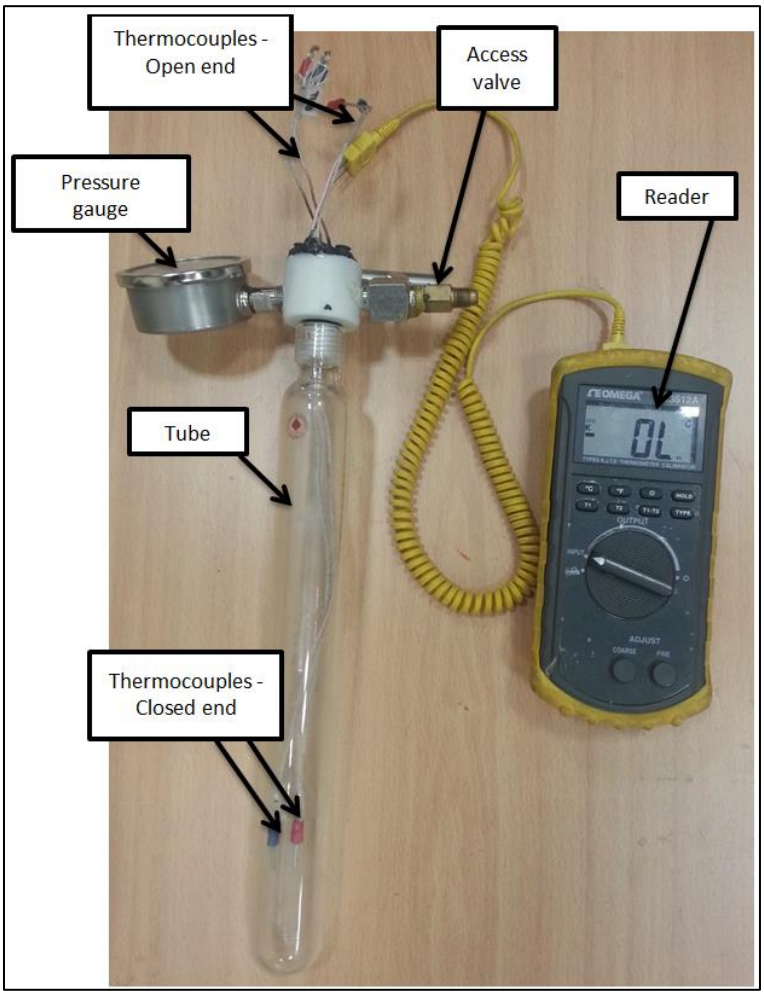

Figure 5.2 Instruments for experimental measurements

The PCM discharge using hot air is also part of the experimental investigation as it helped cross check the values of thermal properties. Hot air at 315 K is used to melt the PCM in the glass tube. The process of melting the PCM from solid to liquid is the discharge of energy hence called PCM discharge. The temperature of the PCM is recorded at regular interval and the phase of the PCM is observed. The time it takes for each PCM to discharge is noted. Figure 5.3 shows the illustrative picture of the discharge

setup. Figure 5.3(a) shows the side view of the setup while Figure 5.3(b) shows the top view of the same setup.

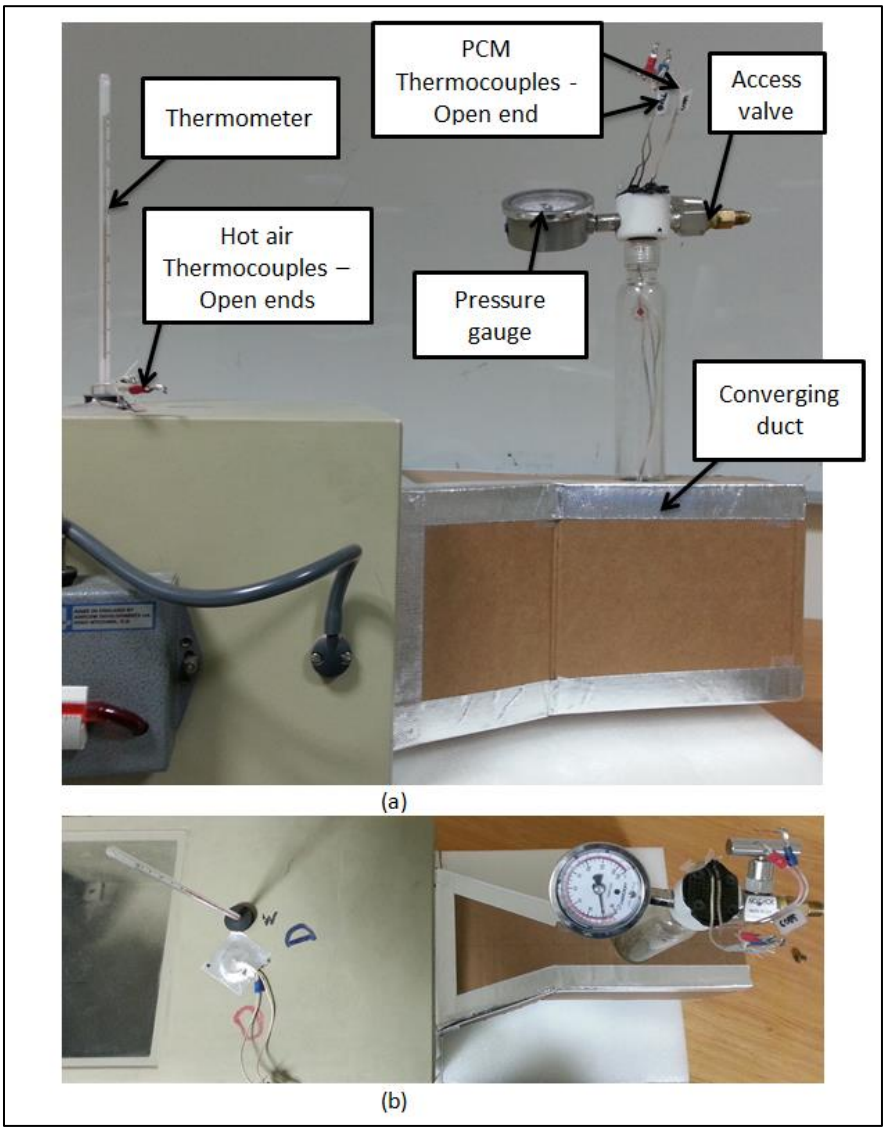

Figure 5.3 Illustration of the system for discharge (a) side view, (b) top view

The procedure to determine the thermal properties of the PCM are described as follows:

- Used 16.24 kg of distilled water with the density of 998 kg/m^3 and specific heat of 4200 J/kg K in the constant temperature bath.

- Operated the bath with constant supply of chiller and heater initially at room temperature i.e. ambient temperature.
- Started noting down the time from the initiation when the bath temperature is ambient (T_{amb}) until the time bath temperature does not change (T_{ss}).
- The amount of energy is calculated by the equation $Q=m_{bath}C_{Pwater}(T_{amb}-T_{ss})$.
- The value of Q is divided by time, in seconds, to determine the heat rate $\dot{Q}$ in J/s or Watts.
- The PCM tubes are submerged in the bath.
- Temperature (T_i), time (t_i) and phases (solid, mushy or liquid) of the PCM is recorded after regular interval.
- Two probes are inserted for temperature readings 14 mm away from each other. One is at the center location r_1 and the other one 14 mm away at r_2.
- The center location reads temperature T_{core} of the tube cross-section while the other is 14 mm away, T_{away}, from it.
- The PCM is discharged using hot air.
- The temperatures T_{core} and T_{away} are recorded during discharge after regular interval.
- Specific heat, C_P, is determined using the governing equation $Q=m_{PCM}C_P(\Delta T_i)$.
- Latent heat is determined by adding the total amount of heat Q from the time of onset until the end set.

- Thermal conductivity, k, is determined using $k = \frac{\dot{Q} \ln(\frac{r_2}{r_1})}{2\pi l \, \Delta T \, \Delta t}$

A 6s LiPo 5000 mAh 60C battery is used to conduct the battery cooling tests. An aluminum jacket is made to house the battery and filled by the desired PCM. Since no observations are needed for these tests, the jacket can be of non-transparent material. Aluminum is used since it is light and can easily be welded. Welding is preferred over binding with glue since sealing the jacket with glue binder is very difficult. The jacket has the pressure gauge and it is sealed using a gasket from the threaded regions. Figure 5.4 shows the dry fit close up of the jacket and battery.

Figure 5.4 Dry fit setup of the battery and the PCM jacket

The battery, while inside the PCM jacket, is connected to a motor with load which is operated at maximum power. A voltmeter is attached to the battery to read its voltage while a thermocouple is placed between the battery cells to read the battery temperature. Battery is charged to its maximum voltage of 4.18 Volts and discharged until it reaches cutoff voltage of 3.6 Volts. It is not safe to operate the battery below the cutoff. Figure 5.5 shows the set-up of the battery cooling experiment with labels of components used.

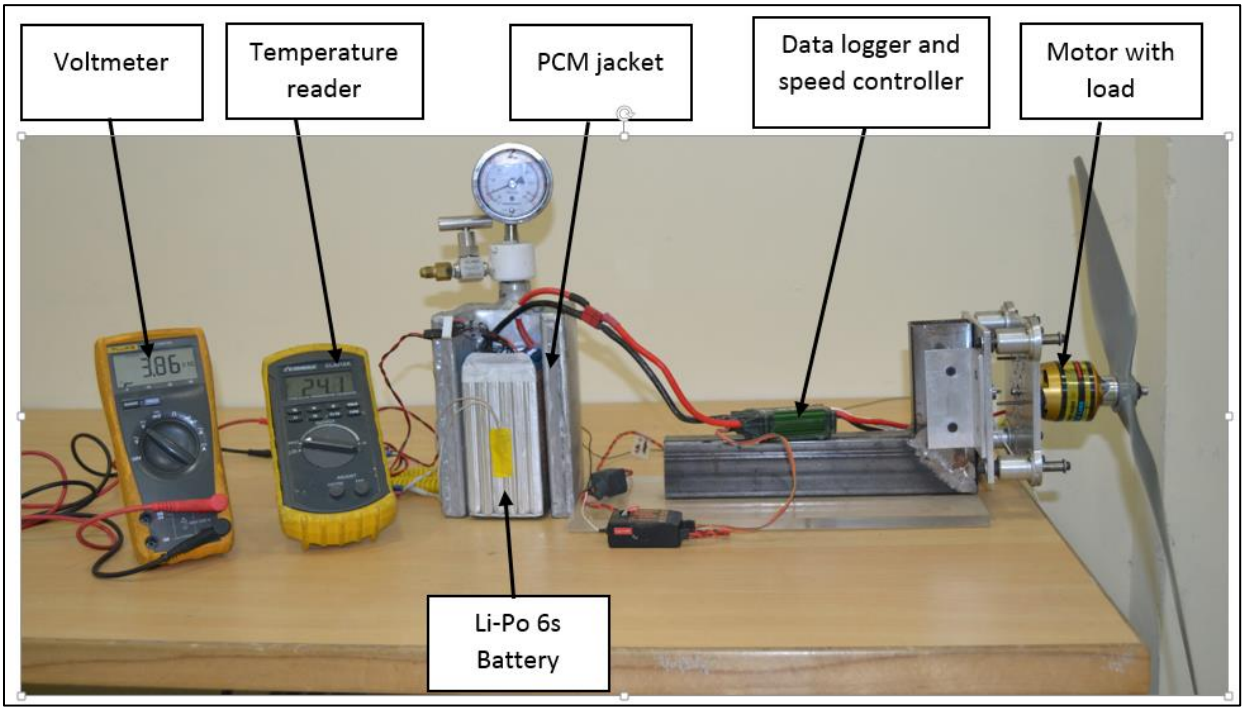

Figure 5.5 Illustration of the battery cooling test setup

5.2 Experimental Equipment

Several equipment are used in this study to achieve the desired objectives. Their individual description is described in this section. The following information is extracted from their corresponding manuals [67-71].

5.2.1 Glass Tubes

The tubes are made up of borosilicate glass material. The tubes are designed and tested for use at 1400 kPa by the manufacturer. The tubes have strain-free closure with two o-rings and seated on a specially formed tubing surface. The tubing surface has no screw threads, clamps or any other strain producing hardware. The strain producing hardware may cause glass failure under pressure and temperature. The tubes have a tube retainer, size *118 FKM* seal o-rings, gasket and an anodized aluminum end cap. End cap is tapped to accept a 3.17 mm (0.125 inches) National Pipe Thread (N.P.T.) threaded accessory.

5.2.2 Constant Temperature Bath

A cold constant temperature bath is used to maintain a constant desired temperature around a specimen or tube in this case. The equipment comprises of a bath to contain the working liquid. Distilled water is used for the experiments. The working liquid should not freeze or evaporate under the desired operating temperatures. A refrigeration system is used to cool the water to the desired temperature. Instrumentation and control unit provides the set point temperature and the required power. The control unit, a proportional-integral-derivative (PID) controller, maintains the set point temperature by supplying heat at short bursts. When constant energy is required, refrigeration system is operated and constant heat is supplied using the heater. The refrigeration system installed provides enough cool energy to freeze the bath water. Since the refrigeration system cannot be regulated, to stop the bath water from freezing, heater is used with an alternating current (AC) regulator. Heat input to the bath water is varied until the desired temperature is reached.

5.2.3 Temperature Sensors

To read the temperature inside the PCMs, the *OMEGA® CL3512A* calibrator/thermometer is used. The *CL3512A* simulates type J/K/T/E thermocouple signals. Each signal is adjustable by using the coarse and fine dials. The *CL3512A* can also be used as a dual type J/K/T/E thermocouple input thermometer. Features include a large 3½ digit display with backlighting and display selections of HOLD, °C/°F, and0.1/1°. The source mode of the *CL3512A* simulates the thermocouple output to check the operation of a thermocouple meter and make rough calibration adjustments. For thermocouple wires, K-type thermocouples are used with functional range from 200°C to 1372°C and a minimum reading capability of 0.1°C. Type K thermocouples are a mixture of chromel and alumel material. Chromel is an alloy made of approximately 90% nickel and 10% chromium. Alumel is an alloy consisting of approximately 95% nickel, 2% manganese, 2% aluminum and 1% silicon.

5.2.4 Battery Test Equipment

A test bench is set-up to conduct the battery cooling tests. A small direct current (DC) outrunner motor is used as a load for the battery. A stand is connected to a bench to hold the motor firmly while it operates. The DC outrunner motor used in the experiment is *AXi 5325/24* with a propeller. The battery used for the experiments is 6s Lithium Polymer (LiPo) 5000 mAh *60C* because of its availability. To operate the motor, the electronic speed controller used for the experiment is *Phoenix ICE HV 85* from Castle Creation. The current and voltage are read through on board power supply unit's ammeter and voltmeter. The *EagleTree eLogger V3* with *MPRV3-LEADS-100* is used for electric current and voltage readings. The *EagleTree eLogger V3* is capable to log current up to

100 Amps and voltage from about 5 V to 70 V. Current is measured with Halls effect sensor hence the current sensor does not interfere with the electric power. The *EagleTree eLogger V3* plugs to a computer and runs with its provided software. The *EagleTree* Magnetic RPM sensor is used to take rotational speed readings for the motor-prop system. The RPM sensor plugs to *EagleTree eLogger V3* hence the readings appear on the computer screen. The sensor contains an infra-red light source and an infra-red detector. The *EagleTree* Magnetic RPM sensor works by interfering with the magnetic field of the stationary magnet hence generating a signal.

5.2.5 Hot Air Duct

The hot air duct comprises a variable speed radial acting axial flow fan discharging into a 250mm square duct. The square duct has electrical heaters and orifice plate for airflow measurement. The heaters are rated for 1kW each with two such heaters. A tube holding nozzle-shaped duct is made at the end of the existing duct. A nozzle is placed to narrow down the exit flow to have the maximum possible contact with the tube. A thermometer is placed at the end of the duct to read the duct air temperature. Tube temperature and nozzle exit temperatures are read using the thermocouple.

5.3 Experimental Layouts

This sections presents the layout of the experiments conducted for this thesis. Three different sets of experiments are conducted for this thesis. First set of experiments are constant temperature bath charging where PCMs are charged using the cold bath. Tubes are submerged in the cold bath and the PCM temperatures are recorded after regular interval until it is completely charged. The second set of tests are conducted to determine

the thermal properties of the PCMs. Tubes are submerged in the cold constant energy bath with two temperature probes. Once again the temperature readings are recorded after regular interval for both the probes. Third set of experimnets are discharge tests. The PCMs are discharged using hot air and electrical battery. For hot air discharge, temperatures inside the tube are recorded after regular internal until the PCM is completely discharged. For battery cooling tests, a special jacket is made to house the selected battery. Battery is placed in the jacket and operated on a load. The cutoff temperature, cutoff time and cooling time until the battery reached ambient temperature is recorded. All the readings are later evaluated and presented in chapter 7.

First set of experiments are conducted to achieve three primary goals. First goal is to find out which refrigerant, among R134a and R141b, is better at forming clathrates. The time it takes to form the clathrate and the formation pressure established determined which refrigerant is better. The second goal is to determine the better bath temperature for charging the clathrate. Bath temperature of 276 K and 278 K are used. Although it is clear that it takes more energy to cool the bath down to 3 ^{o}C (276 K), as compared to 278 K. But it is to be established if the charging time for the clathrate is the same or different. Once the charging times are determined, the energy and exergy evaluations established which bath temperature requires the least amount of energy. The third goal is to find out the most appropriate refrigerant mass fraction for clathrate formation. Charging times and clathrate structure are some of the parameters used to establish the most appropriate mass fraction. Refrigerant mass fractions of 0.15, 0.2, 0.25, 0.3, 0.35 and 0.4 are used to form the clathrate. For the sake of simplicity, clathrate with percent refrigerant is used to describe the clathrate. Energy and exergy values are also evaluated to determine the

amounts required to form clathrate with each refrigerant mass fraction. Figure 5.6 shows the experimental layout of the first set of experiments.

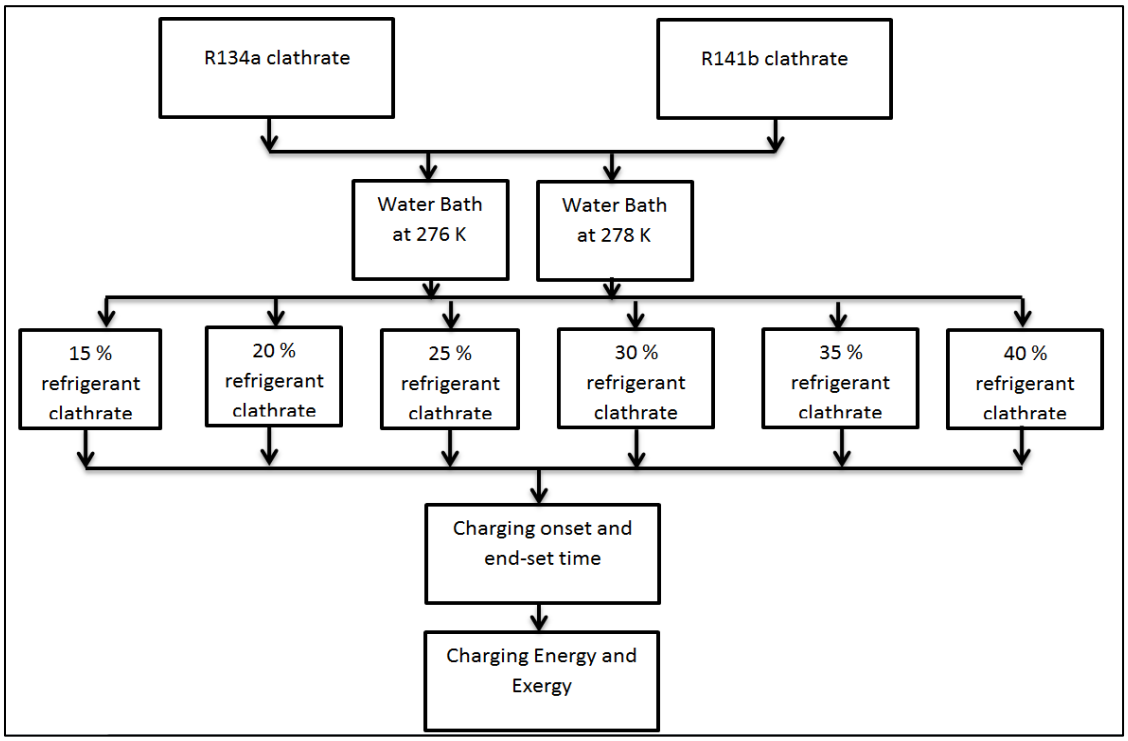

Figure 5.6 Experimental layout of the first set of experiments

For the second set of experiments, PCMs are formed by adding five different additives in 0.35 mass fraction R134a clathrate. The five additives used are copper, aluminum, ethanol, magnesium nitrate hexahydrate and sodium chloride. The refrigerant clathrate without any additive is considered to be the base PCM. These experiments are conducted to achieve four primary goals. The first goal is to find out the charging times of each PCM. The charging times included the onset and end set of PCM freezing. Using the charging onset and end set times, energy and exergy values of charging are evaluated. The second goal is to find out the charging times of each PCM with additive mass fractions varied from 0.01 to 0.05 with an interval of 0.01. It is desired to find out the

effects of additive fractions on the charging times, charging energy values and charging exergy values. The charging times included the onset and end set of PCM freezing. The third goal is to find out the discharging times of each PCM using hot air. The discharging times only included the end set of PCM freezing since onset almost starts immediately. Using the discharging times, energy and exergy values of discharging are evaluated. The fourth goal is to find out the discharging times of each PCM using battery heat. A special jacket is made to house the selected battery and PCMs are formed inside the jacket. Parameters recorded for this set of tests for each PCM are battery run times, battery temperature at cutoff voltage and time for the battery to cool to a minimum possible temperature to recharge the battery safely. Using the cooling times, energy and exergy values of discharging are also evaluated. Figure 5.7 shows the experimental layout of the second set of experiments.

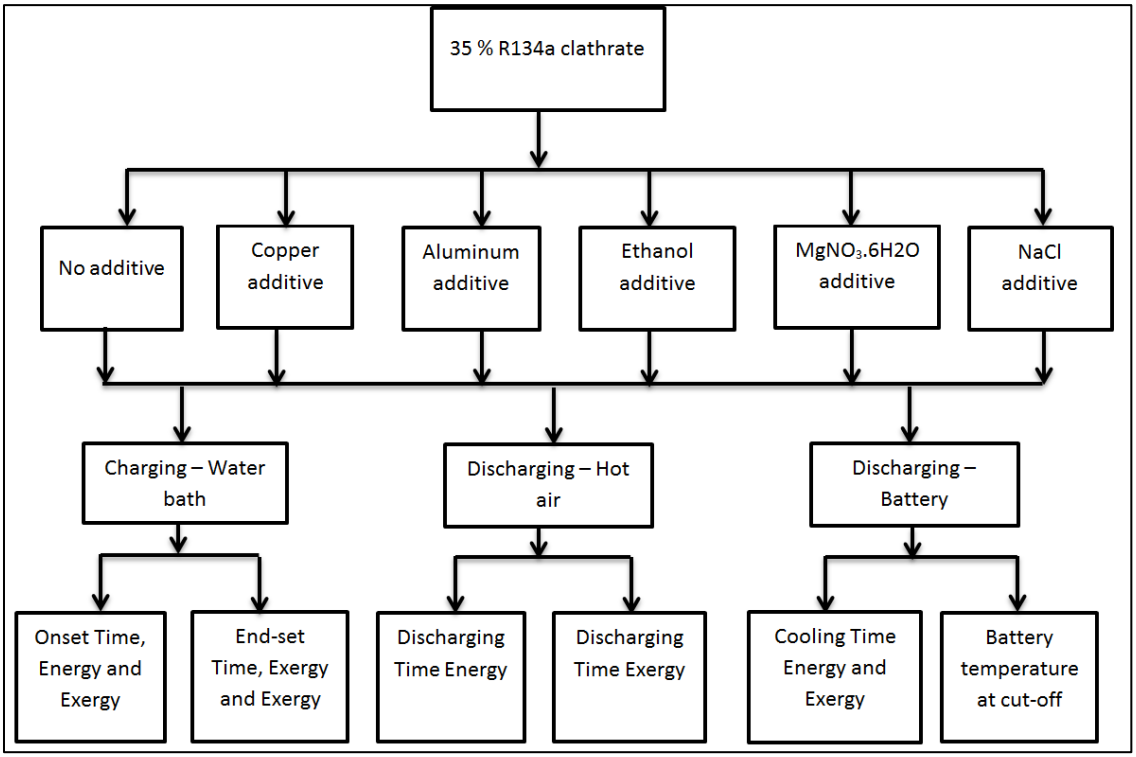

Figure 5.7 Experimental layout of the second set of experiments

The third set of experiments is conducted to determine the thermal properties of each PCM and establish which additive is better. Five different additives are used namely copper, aluminum, ethanol, magnesium nitrate hexahydrate and sodium chloride. Tubes with two temperature probes are used for these experiments. Charging times for each PCM is recorded along with its temperatures for each temperature probe. Using the temperature data, thermal properties of each PCM is determined. Thermal properties determined included specific heat, latent heat, liquid phase thermal conductivity and solid phase thermal conductivity. Comparing the charging times and structure of each PCM, performance of each PCM is predicted. Soft fluffy structure takes short time to charge but it cannot provide cool energy for long. Alternatively, a hard solid structure may take longer to charge but it can provide cool energy longer. Charging times are used to evaluate the energy and exergy values of each PCM. Figure 5.8 shows the experimental layout of the third set of experiments.

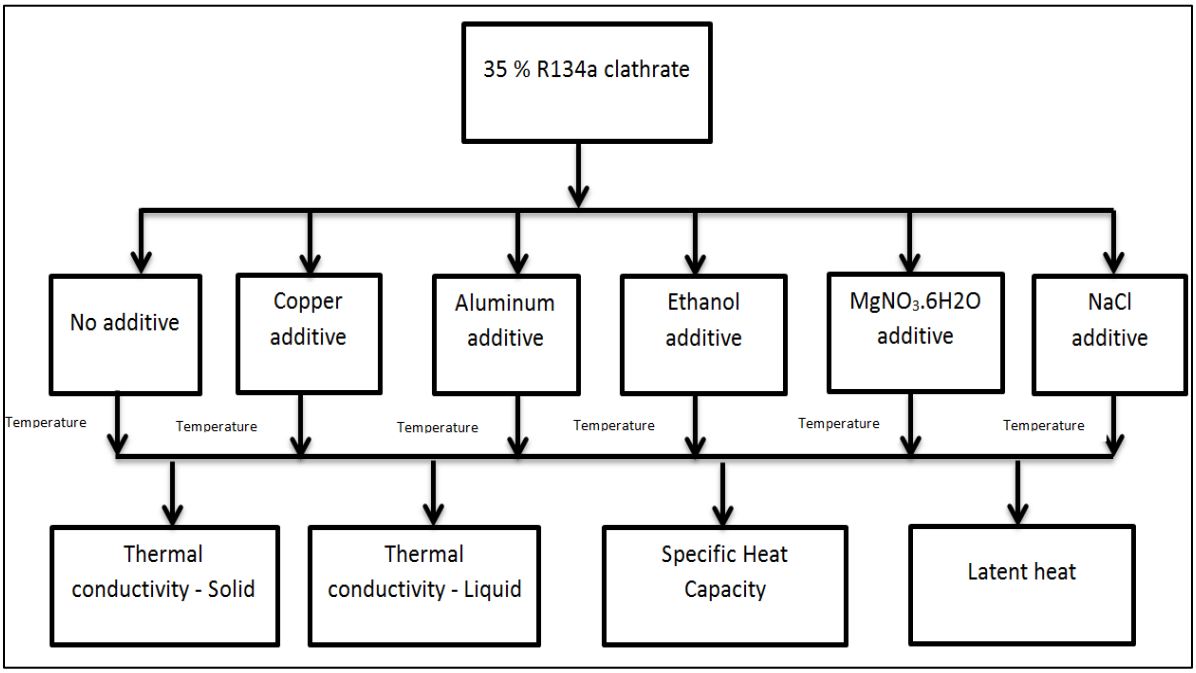

Figure 5.8 Experimental layout of the third set of experiments

5.4 Challenges

Refrigerant is stored under high pressure since at atmospheric pressure, it vaporizes. In order to use the refrigerant as a liquid, it has to be maintained at high pressure. For R134a, the pressure at 298 K is 455 kPa which is the pressure inside the container. Storing the refrigerant in the tank is not a concern but keeping the glass tube pressurized is a big challenge. It is to be noted that a transparent testing container is required to visually see the onset and end set of freezing. If the visual part is not required, welded metal tubes would have been a better option. There are limited numbers of tubes and the test procedure requires the tube to be vacuumed out before every test run. This requirement meant there has to be a needle valve to fill the refrigerant and a main threaded stopper. The two openings had to be tightly sealed or else the refrigerant leaked. Clathrate formation does not take place whenever there is even a minor refrigerant leak. The challenge magnified for the thermal properties' experiments. Since two more openings are required for two sets of thermos-couples, the chances of refrigerant leaks magnified. It is particularly tricky to seal the thermocouple wire since it has to be a single wire that needs to perfectly seal with the cork material. The sealing usually did not last more than two runs and for discharging, when the pressure reached 590 kPa, it leaked for every second run.

5.5 Applications

The system and experimental work studied in this thesis has several experimental and practical applications. The system and experimental layout described in this chapter lays out the foundation for studying several properties of refrigerant clathrates. The designed system allows direct measurement of onset and end set times of each PCM formation. Since it uses glass tubes, visual observations can be made to see the onset and end set of freezing. An opaque PCM container does not allow visual inspection hence makes it very difficult to determine the PCM formation stages. The tube has a pressure limit of 840 kPa for safe operations so refrigerants with higher pressure than that of R134a can also be used. The other aspect is the ability to safely determine the thermal properties within acceptable ranges. The systems available prior to this one have complex mechanism which makes them impractical for applications where pressurized gas is used. They also have a special requirement for current to flow through the wire going in the container. A wire with flowing current, however small, not only makes the system unsafe but also makes it very difficult to completely seal it. This tube system is small enough to be carried yet big enough to allow sizable PCM formation. It has attached temperature and pressure sensors so it is easy to take readings. It can conveniently be used with most usual fluid for charging or discharging tests. The designed for battery cooling tests has many experimental applications as well. It is small enough to fit in usual cooling baths or most hose-hold refrigerators. It is made up of metal with sides welded to prevent any possibility of leaks. Its size allows it to be used for most common types of batteries in use for radio control electronics, LiPo 6s. It has a pressure gauge to allow for instant pressure readings.

Apart from experimental applications, the system and the studied PCMs have several particle applications. The tested PCM results determine the PCM's properties which can be used for any desired applications. For cooling applications, the additive that yields the cooling longest can be chosen while for applications related to underwater gas pipeline clogging, additive that delays the clathrate formation is suitable. The PCMs can be used for either active cooling for passive cooling. PCM can be formed in cold thermal energy storage systems at night to be used in the morning peak hours. This allows the energy load demand to be leveled for day and night, instead of peaking during day and dropping down at night. The other practical application is for electrical and electronic devises. With growing demand of electronics and their processing power, heat dissipation is a challenge. PCMs can be used to cool electronics since they can be formed in any shape and size while providing enough cool energy to maintain the electronics temperature under safe operating range. With global trend switching to electric vehicles, battery cooling is a problem to be dealt with. The jacket developed in this thesis can be directly used to cool LiPo 6s batteries. Similar jackets can be developed, according to the size and shape of the batteries, to prevent them from overheating. The advantage of PCM is the latent heat, which is greater than the specific heat. Since PCMs maintain the same temperature while absorbing heat, they are preferred over other commonly used materials for heat absorption.

Chapter 6 Analyses

This chapter presents the overall and part analyses of the PCMs under investigation. It also presents the energy and exergy analyses of the entire system.

A single-component pure substance changes its phase at a precise temperature. The material temperature does not change until the material has completely changed its phase. Such materials are considered as one-region materials as the temperature change occurs only when the material is in a particular phase region. In a multi-component PCM, as the one under investigation, phase change occurs over a range of temperature, instead of being at a particular temperature. This phase between the solid and liquid region is described as a mushy region where the temperature as well as the phase, both, changes. Since such PCMs would have a solid, liquid and mushy region, the problem associated with such materials is described as multi-region or moving boundary problems. Predicting the behavior of phase-change systems is difficult due to its inherent non-linear nature at moving interfaces, for which displacement rate is controlled by the latent heat lost or absorbed at the boundary [72].

The governing equation for heat can be written as follows:

$$Q = (mC_p \Delta T)_{solid} + m\lambda + (mC_p \Delta T)_{liquid} \quad (6.1)$$

where m is the mass of the PCM, C_P is the specific heat, T is the temperature and λ is the specific latent heat of PCM.

The amount of heat rejected from the PCM tube to the bath is given as follows:

$$Q = m_{bath} C_{P,water} (T_{amb} - T_{ss}) = m_{bath} (h_{amb} - h_{ss}) \quad (6.2)$$

where T_{amb} is the ambient bath temperature and T_{ss} is the steady state temperature of the water bath. Similarly h_{amb} is the ambient bath specific enthalpy and h_{ss} is the steady state specific enthalpy. Specific heat, C_P, is determined using the energy balance equation as follows:

$$Q = m_{PCM} C_P \Delta T_i \tag{6.3}$$

where ΔTi is the temperature difference of the same location in the PCM.

Thermal conductivity, k, is determined using

$$k = \frac{\dot{Q} \ln(\frac{r_2}{r_1})}{2\pi l \, \Delta T} \tag{6.4}$$

where, r_1 and r_2 is the inner and outer radius of the PCM inside the tube, '*l*' is the height of the PCM inside the tube, ΔT is the difference in temperature between location r_1 and r_2.

In order to theoretically estimate the thermal properties, empirical equations are used to validate the trend. Specific heat can be calculated by adding the product of the mass fraction and specific heat of the pure species present in the PCM.

$$C_{P,PCM} = w_1 C_{P,1} + w_2 C_{P,2} + w_3 C_{P,3} \tag{6.5}$$

where $C_{P,i}$ is the heat capacity of species i and *w* its mass fraction.

The other important parameter is the heat of fusion which can be described for two-dimensional problem, as follows [73, 74]:

$$\frac{\partial h}{\partial t} = \frac{\partial}{\partial x}(\beta \frac{\partial h_{latent}}{\partial x}) - \rho_L \lambda \frac{\partial f}{\partial t} \tag{6.6}$$

where 'h' is the enthalpy, β is the thermal diffusivity, λ is the spacific latent heat of fusion, 't' is time, ρ is density, and 'f' is liquid fraction describes as follows:

$$f = \begin{cases} 0 & T < T_m \quad \text{solid,} \\ [0,1] & T = T_m \quad \text{mushy,} \\ 1 & T > T_m \quad \text{liquid.} \end{cases} \tag{6.6a}$$

with the thermal diffusivity β defined as:

$$\beta = \frac{k}{C_P \rho} \tag{6.7}$$

where 'k' is the thermal conductivity coefficient and ρ is the density.

Substituting equation (6.7) into equation (6.5) yields the enthalpy of fusion with respect to thermal conductivity and density as follows:

$$\frac{\partial h}{\partial t} = \frac{\partial}{\partial x}\left[\left(\frac{k}{C_P \rho}\right)\frac{\partial h}{\partial x}\right] - \rho_L \lambda \frac{\partial f}{\partial t} \tag{6.8}$$

Note that PCM in solid phase has higher density as compared to liquid phase PCM while it is in the middle during the 'mushy' region. In order to further simplify the equation (6.8) to obtain a preliminary result, it could be assumed that the heat of fusion does not change with respect to the time hence treating it as steady state condition. With this assumption, the equation becomes as follows:

$$\rho_L \lambda \frac{\partial f}{\partial t} = \left(\frac{k}{C_P \rho}\right)\frac{\partial^2 h}{\partial x^2} \tag{6.9}$$

Assuming the change is linear with respect to time for 'f' and distance for 'h', equation (6.9) can be simplified to:

$$\rho_L \lambda \frac{\Delta f}{\Delta t} = \left(\frac{k}{C_P \rho}\right)\frac{\partial^2 h}{\partial x^2} \tag{6.10}$$

Since it is difficult to predict the exact density during phase change, it is important to have the density eliminated with something that tends to stay constant during phase change. Unlike density, mass of the material tends to stay the same so an expression can be arrived upon without density of the PCM.

Since ‘h’ is the enthalpy, substituting mass per unit volume in place of density would yield the enthalpy value. The equation becomes:

$$\rho_L \lambda \frac{\Delta f}{\Delta t} = \left(\frac{k}{C_P m}\right) \frac{\partial^2 H}{\partial x^2} \tag{6.11}$$

where ‘m’ is the mass and ‘H’ is the volumetric enthalpy of fusion.

The thermal conductivity ‘k’ for any material, in Cartesian coordinates, is defined as:

$$\dot{Q} = \frac{\mathrm{kA\Delta T}}{\Delta l} \tag{6.12}$$

where $\dot{Q}$ is the heat rate, A is the cross-sectional area and *l* is the distance between two temperature readings.

The thermal conductivity ‘k’ for the refrigerant clathrate can be described as follows [68]:

$$k = 0.4 \times \exp\left(\frac{T}{T_{cm}} - 1\right)\left(\frac{D_1}{D_2}\right)^2 \times M^{0.5} w_1 w_2 \left(\frac{k_2}{M_2^{0.5}} - \frac{k_1}{M_1^{0.5}}\right) \tag{6.13}$$

where D is the dipole moment, *w* is the mass fraction and M is the molar mass of the species.

Refrigerants are mixed with water to form the clathrate in liquid phase. Adding solid additives, to improve thermal conductivity, improves the thermal transport properties of the PCM. It requires a different set of equations to predict the thermodynamic properties of the PCM with solid additives, be it salts or nanoparticles.

Several models are presented to predict the thermal conductivity of the fluids containing small solid particles [75]. The thermal conductivity of the PCM having solid particles is not easy to calculate as it yields complex parameters upon which the values are based [76]. One of the models is the extension of Effective Medium Theory (EMT) described as [77-80]:

$$\sum_{i=1}^{n} V_i \frac{k_m - k_{ith}}{k_i + \left(\frac{Z}{2} - 1\right)k_m} = 0 \quad (6.14)$$

where V is the volume fraction, Z is the coordination number, k_{ith} is the thermal conductivity of the i^{th} element and k_m is the thermal conductivity of the mixture.

Another model is a two component three dimensional model for isotropic material thermal conductivity as follows [81 - 85]:

$$k = k_b \left[\frac{1-J}{1-J(1-V_d)}\right] \quad (6.15)$$

where

$$J = V_d^2 \left(1 - \frac{k_d}{k_b}\right) \quad (6.16)$$

where k is the overall thermal conductivity of the system, k_b and k_d are the thermal conductivities of the continuous and discontinuous component(s), respectively, and V_d is the volume fraction of the discontinuous phase.

The third model that can be used to predict the thermal conductivity of the PCM is based on potential theory as follows [86, 87]:

$$k = k_b \left[\frac{1-(1-a(k_d/k_b))b}{1+(a-1)b}\right] \quad (6.17)$$

where

$$a = \frac{3k_b}{2k_b + k_d} \quad (6.18)$$

and

$$b = \frac{V_d^3}{V_d^3 + V_c^3} \quad (6.19)$$

In equations 6.17-6.19, k_c and k_d are the thermal conductivities of the continuous and discontinuous component(s), respectively. V_d is the volume fraction of the discontinuous phase while V_c is the volume fraction of the continuous phase.

Some models propose prediction of thermal conductivity based on the effect of interfacial layer formed around the nanoparticle, which makes calculations more difficult [88]. An effective model to present the improvement in thermal conductivity of fluid with nanoscale particles is through Single Phase Brownian Model (SPBM) as follows [89]:

$$k = k_b(1+A\ Re^m\ Pr^{0.333}\ V_d)\ \frac{[k_d(1+2\alpha)+2k_b]+2\ V_d[k_d(1-\alpha)-k_b]}{[k_d(1+2\alpha)+2k_b]-\ V_d[k_d(1-\alpha)-k_b]} \quad (6.20)$$

where V is the volume fraction while A and m are constants. A is independent of fluid type while m depends on the fluid and particle type. Biot number α is:

$$\alpha = 2R_b k_c/d_p \quad (6.21)$$

The equation yields the thermal conductivity of the fluid with nanoparticles that incorporates the conduction contribution of the particles, particle-fluid thermal boundary resistance and the convection contribution. Overall, this equation (6.20) takes care of the localized convection due to Brownian motion as well; something that previous models failed to address. When the additives are used that are not nanoscale particles, the equation simplifies to only the static thermal conductivity as follows:

$$k = k_b\frac{[k_d(1+2\alpha)+2k_b]+2\ V_d[k_d(1-\alpha)-k_b]}{[k_d(1+2\alpha)+2k_b]-\ V_d[k_d(1-\alpha)-k_b]} \quad (6.22)$$

For an uncertainty analysis, the standard deviation is described as follows:

$$\sigma = \sqrt{\frac{\Sigma(x_j - \bar{x})^2}{n-1}} \quad (6.23)$$

where $\bar{x}$ is the mean value and n is the number of trials.

The errors in calculated values, ΔR, is determined using the following equation:

$$\Delta R = \frac{\partial R}{\partial x_1} + \frac{\partial R}{\partial x_2} + \ldots + \frac{\partial R}{\partial x_n} \quad (6.24)$$

where x is the individual parameter making up the calculated result R.

The thermoeconomic analysis on the PCMs is also conducted with the following equation [90]:

$$f_{TE} = \frac{Z_k}{Z_k + \xi\, Ex_{dst}} \quad (6.25)$$

where Z_k is the total cost of the items used in the PCM in dollars, ξ is the energy cost in $/J and and f_{TE} is the thermoeconomic factor.

6.1 System Analyses

Three primary systems are used to conduct the tests and attain the test results. Cold water bath is used for charging the PCMs, hot air for discharge the PCM and battery cooling system to see the effects of PCM cooling. Their analyses are presented in this section.

6.1.1 Analysis of Constant Temperature Bath

Cold bath water absorbs the heat from the PCM during the charging process. The bath has a built in refrigeration system that works on basic vapor compression refrigeration cycle. Since it is a close loop system, the mass balance equation for every single component of the constant temperature bath is as follows:

$$\dot{m}_i = \dot{m}_e \quad (6.26)$$

Compressor pressurises the refrigerant while increasing the refrigerant's temperature, enthalpy and entropy. Compressor takes the electrical energy in to produce the work. The work done by the compressor is increasing the pressure and temperature of the refrigerant. The energy balance equation simplifies as follows:

$$\dot{m}_i h_i + \dot{W}_{ele} = \dot{m}_e h_e + \dot{Q} \quad (6.27)$$

For all the practical systems, exergy is destroyed due to irreversibilities present in it. The exergy balance equation can be written as follows:

$$\dot{m}_i ex_i + \dot{W}_{ele} = \dot{m}_e ex_e + \dot{E}x_{dst} + \dot{E}x^Q \quad (6.28)$$

The refrigerant system enters the condenser. The condensore rejects the heat to the surrounding, ideally only changing the refrigerant phase. However, practicaly, the temperature of the refrigerant also drops while the pressure remains the same. The energy balance equation for the condenser refrigerant is given as follows:

$$\dot{m}_i h_i = \dot{m}_e h_e + \dot{Q} \text{ (Phase change involved)} \quad (6.29)$$

Similarly, the exergy balance equation is as follows:

$$\dot{m}_i ex_i = \dot{m}_e ex_e + \dot{E}x_{dst} + \dot{E}x^Q \quad (6.30)$$

After condensor, the refrigerant enters the expansion valve. Expansion valve decompresses the refrigerant droping its pressure, subsequently its pressure as well. The enthaly across the expansion vale is designed to remain the same. The energy balance equation is described as follows:

$$\dot{m}_i h_i + \dot{Q} = \dot{m}_e h_e \quad (6.31)$$

The exergy balance equation is described as follows:

$$\dot{m}_i ex_i + \dot{E}x^Q = \dot{m}_e ex_e + \dot{E}x_{dst} \quad (6.32)$$

After the expansion valve, the refrigerant system enters the evalorator. Avaporator coils are wraped around the water bath to cool the bath. As the refrigerant goes through the evaporator, it absorbs the heat from the water bath. This addition of heat ideally only changing the refrigerant phase. However, practicaly, the temperature of the refrigerant also rises while the pressure remains the same. The energy balance equation for the condenser refrigerant is given as follows:

$$\dot{m}_i h_i + \dot{Q} = \dot{m}_e h_e \text{ (Phase change involved)} \quad (6.33)$$

Similarly, the exergy balance equation is as follows:

$$\dot{m}_i ex_i + \dot{E}x^Q = \dot{m}_e ex_e + \dot{E}x_{dst} \quad (6.34)$$

6.1.2 Analysis of Hot Air Duct

Hot air gives away the heat to the PCM during the discharging process. The hot air duct has a built in electric heater that heats up the air flowing across it. Since it a simple duct with one inlet and one exit (ignoring leaks), the mass balance equation can be written as follows:

$$\dot{m}_i = \dot{m}_e \quad (6.35)$$

The air goes across the eletric heater where its temperature is raised while its pressure remains the same. Heater takes the electrical energy to produce heat. The heat is provided to the flowing air. The energy balance equation simplifies as follows:

$$\dot{m}_i h_i + \dot{Q} = \dot{m}_e h_e \quad (6.36)$$

For all the practical systems, exergy is destroyed due to irreversibilities present in it. The exergy balance equation can be written as follows:

$$\dot{m}_i ex_i + \dot{E}x^Q = \dot{m}_e ex_e + \dot{E}x_{dst} \quad (6.37)$$

6.1.3 Analysis of Battery Cooling

When electrical energy in lithium polymer battery is discharged as it runs an electrical motor, it tends to heat up. PCM is used to absorb the heat from the battery and cool the battery down. The battery has a resistance, so when the current is drawn from that battery, the current goes through a certain resistance heating up the battery. For the battery cooling test, no mass transfer is associated with it as only the heat transfer is experienced. The heat from the battery goes through the PCM jacket to the PCM. The PCM heats up and changes its phase by absorbing the energy. The heat released by the battery is associated with the battery's internal energy change which can be described as follows:

$$m\Delta u_{ch} = \dot{Q}\ \Delta t \quad (6.38)$$

The exergy balance equation can be written with respect to the chemical exergy as follows:

$$m\Delta\ ex_{ch} = + \dot{E}x^Q\ \Delta t + \dot{E}x_{dst} \quad (6.39)$$

6.2 Energy and Exergy Analyses

The general energy and exergy balance equations for the PCM charging and discharging are presented in this section. Charging is described as the process of solidification while

discharge is described as the process of melting. PCM gives away the heat during the process of charging while it takes in the heat during the process of discharging.

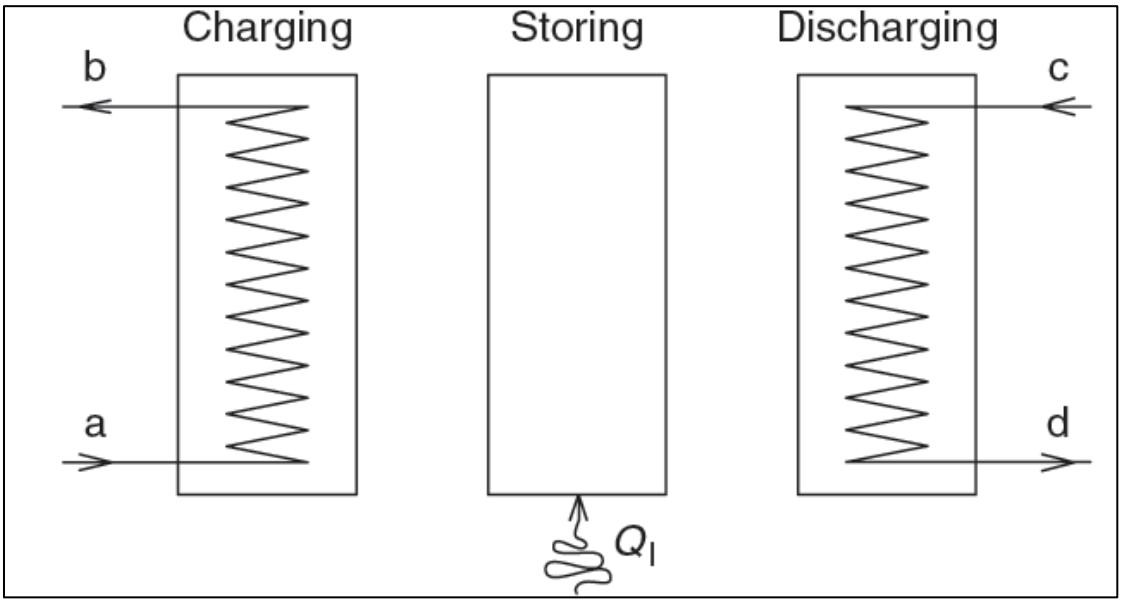

Figure 6.1 Schematic diagram of the charging, storage and discharging process for the PCM [91]

For charging the PCM, mass balance equation for the charging fluid can be described as follows:

$$(\dot{m}_{in})\,\Delta t = (\dot{m}_{out})\,\Delta t = (\dot{m}_{c})\,\Delta t \quad (6.40)$$

where $\dot{m}$ is the mass flow rate, subscript 'c' is refers to the charging fluid while 'in' and 'out' refers to the incoming and exiting fluid, respectively.

The energy balance equation between the charging fluid and PCM for the flow can be described as follows:

$$[(\dot{m}_{c}h_{c})\Delta t]_{out} - [(\dot{m}_{c}h_{c})\Delta t]_{in} = [(\dot{m}_{PCM}h_{PCM})\Delta t]_{in} - [(\dot{m}_{PCM}h_{PCM})\Delta t]_{out} + \dot{Q}_{gain}\,\Delta t \quad (6.41)$$

where ‘h’ is the specific enthalpy of the substance while subscript ‘gain’ referrers to the heat gained from the surrounding over the period of Δt.

When the charging is done using stationary fluids to a stationary PCM over a time period, the equation becomes as follows:

$$(m_c h_c)_f - (m_c h_c)_i = (m_{PCM} h_{PCM})_i - (m_{PCM} h_{PCM})_f + \dot{Q}_{gain}\,\Delta t \quad (6.42)$$

The entropy balance equation between the charging fluid and PCM for the flow can be described as follows:

$$(\Delta \dot{m}_c \Delta s_c \Delta t) = [(\dot{m}_{PCM} s_{PCM})\Delta t]_{in} - [(\dot{m}_{PCM} s_{PCM})\Delta t]_{out} + \frac{\dot{Q}_{gain}}{T_0}\Delta t + \dot{S}_{gen}\,\Delta t \quad (6.43)$$

where ‘s’ is the specific entropy of the substance, T_0 is the ambient temperature and $\dot{S}_{gen}$ is the entropy generation rate.

When the charging is done using stationary fluids to a stationary PCM over a time period, the equation becomes as follows:

$$(m_c s_c)_f - (m_c s_c)_i = (m_{PCM} s_{PCM})_i - (m_{PCM} s_{PCM})_f + \frac{\dot{Q}_{gain}}{T_0}\,\Delta t + \dot{S}_{gen}\,\Delta t \quad (6.43)$$

The exergy balance equation between the charging fluid and PCM for the flow can be described as follows:

$$(\Delta \dot{m}_c \Delta ex_c \Delta t) = [(\dot{m}_{PCM} ex_{PCM})\Delta t]_{in} - [(\dot{m}_{PCM} ex_{PCM})\Delta t]_{out} + \dot{E}x_{dst}\,\Delta t + \dot{E}x^{Q}\,\Delta t \quad (6.44)$$

where ‘ex’ is the specific exergy, $\dot{E}x_{Dst}$ is the exergy destruction and $\dot{E}x^{Q}$ is the thermal exergy loss of the substance.

The thermal exergy loss can be described as:

$$\dot{E}x^{Q} = (1 - \frac{T_0}{T})\dot{Q} \quad (6.45)$$

When the charging is done using stationary fluids to a stationary PCM over a time period, the equation becomes as follows:

$$(m_c ex_c)_f - (m_c ex_c)_i = (m_{PCM} ex_{PCM})_i - (m_{PCM} ex_{PCM})_f + \dot{E}x_{dst}\,\Delta t + \dot{E}x^{Q}\,\Delta t \quad (6.46)$$

For discharging the PCM, mass balance equation for the charging fluid can be described as follows:

$$(\dot{m}_{in})\,\Delta t = (\dot{m}_{out})\,\Delta t = (\dot{m}_c)\,\Delta t \quad (6.47)$$

The energy balance equation between the discharging fluid and PCM for the flow can be described as follows:

$$[(\dot{m}_{PCM} h_{PCM})\Delta t]_{out} - [(\dot{m}_{PCM} h_{PCM})\Delta t]_{in} = [(\dot{m}_c h_c)\Delta t]_{in} - [(\dot{m}_c h_c)\Delta t]_{out} + \dot{Q}_{gain}\,\Delta t \quad (6.48)$$

When the discharging is done using stationary fluids to a stationary PCM over a time period, the equation becomes as follows:

$$(m_{PCM} h_{PCM})_f - (m_{PCM} h_{PCM})_i = (m_c h_c)_i - (m_c h_c)_f + \dot{Q}_{gain}\,\Delta t \quad (6.49)$$

When the heat is being absorbed from a stationary solid, the energy balance equation becomes as follows:

$$(m_{PCM} h_{PCM})_f - (m_{PCM} h_{PCM})_i = \dot{Q}\,\Delta t \quad (6.50)$$

The entropy balance equation between the discharging fluid and PCM for the flow can be described as follows:

$$(\Delta \dot{m}_{PCM} \Delta s_{PCM} \Delta t) = [(\dot{m}_c s_c)\Delta t]_{in} - [(\dot{m}_c s_c)\Delta t]_{out} + \frac{\dot{Q}_{gain}}{T_0}\Delta t + \dot{S}_{gen}\Delta t \quad (6.51)$$

When the discharging is done using stationary fluids to a stationary PCM over a time period, the equation becomes as follows:

$$(m_{PCM}s_{PCM})_f - (m_{PCM}s_{PCM})_i = (m_c s_c)_i - (m_c s_c)_f + \frac{\dot{Q}_{gain}}{T_0}\Delta t + \dot{S}_{gen}\Delta t \quad (6.52)$$

When the heat is being absorbed from a stationary solid, the entropy balance equation becomes as follows:

$$(m_{PCM}s_{PCM})_f - (m_{PCM}s_{PCM})_i = -\frac{\dot{Q}_{supply}}{T_0}\Delta t + \dot{S}_{gen}\Delta t \quad (6.53)$$

The exergy balance equation between the discharging fluid and PCM for the flow can be described as follows:

$$(\Delta \dot{m}_{PCM}\Delta ex_{PCM}\Delta t) = [(\dot{m}_c ex_c)\Delta t]_{in} - [(\dot{m}_c ex_c)\Delta t]_{out} + \dot{E}x_{dst}\Delta t + \dot{E}x^{Q}\Delta t \quad (6.54)$$

When the discharging is done using stationary fluids to a stationary PCM over a time period, the equation becomes as follows:

$$(m_{PCM}ex_{PCM})_f - (m_{PCM}ex_{PCM})_i = (m_c ex_c)_i - (m_c ex_c)_f + \dot{E}x_{dst}\Delta t + \dot{E}x^{Q}\Delta t \quad (6.55)$$

When the heat is being absorbed from a stationary solid, the equation becomes as follows:

$$(m_{PCM}ex_{PCM})_f - (m_{PCM}ex_{PCM})_i = \dot{E}x_{dst}\Delta t - \dot{E}x^{Q}_{supply}\Delta t \quad (6.56)$$

where $\dot{E}x^{Q}_{supply}$ is the thermal exergy.

6.1.1 Analyses of Energy and Exergy Efficiencies

In order to determine the efficiencies, it is first important to describe the useful input and required output of the system.

For the charging process, the heat absorbed by the charging fluid $Q_{in,c}$ is described as:

$$[(\dot{m}_c h_c)\Delta t]_{out} - [(\dot{m}_c h_c)\Delta t]_{in} = Q_{in,c} \quad (6.57)$$

While heat given out by the PCM $Q_{out,PCM}$ is

$$(m_{PCM} h_{PCM})_i - (m_{PCM} h_{PCM})_f = Q_{out,PCM} \quad (6.58)$$

The thermal exergy absorbed by the charging fluid $Ex^{Q}_{in,c}$ is described as:

$$[(\dot{m}_c ex_c)\Delta t]_{out} - [(\dot{m}_c ex_c)\Delta t]_{in} = Ex^{Q}_{in,c} \quad (6.59)$$

While thermal exergy given out by the PCM $Ex^{Q}_{out,PCM}$ is defined as:

$$(m_{PCM} ex_{PCM})_i - (m_{PCM} ex_{PCM})_f = Ex^{Q}_{out,PCM} \quad (6.60)$$

For the discharging process, the heat absorbed by the PCM $Q_{in,PCM}$ is described as:

$$(m_{PCM} h_{PCM})_f - (m_{PCM} h_{PCM})_i = Q_{in,PCM} \quad (6.61)$$

The heat released by the discharging fluid $Q_{out,c}$ or the heat emitted by the stationary solid is described as:

$$(m_c h_c)_i - (m_c h_c)_f = Q_{out,c} = \dot{Q}\,\Delta t \quad (6.62)$$

The thermal exergy absorbed by the PCM $Ex^{Q}_{in,PCM}$ is described as:

$$(m_{PCM} ex_{PCM})_f - (m_{PCM} ex_{PCM})_i = Ex^{Q}_{in,PCM} \quad (6.63)$$

The thermal exergy released by the discharging fluid $Ex^{Q}_{out,c}$ or the thermal exergy released by the stationary solid is described as:

$$(m_c ex_c)_i - (m_c ex_c)_f = Ex^{Q}_{out,c} = \dot{E}x^{Q}_{supply}\,\Delta t \quad (6.64)$$

The overall system efficiencies can now be described since useful output and required inputs have been established. The required input is the energy/exergy released by the charging material to change the phase or charge the PCM. The useful output is the energy/exergy absorbed by the discharging material which in turn is absorbed by the PCM. The overall system's energy efficiency can be described as:

$$\eta_{oa} = \frac{Q_{in}}{Q_{out}} \tag{6.65}$$

The overall system's exergy efficiency can be described as:

$$\Psi_{oa} = \frac{Ex_{in}}{Ex_{out}} \tag{6.66}$$

6.3 Optimization Study

Optimization study and its dependent variables are presented in this section. Objective function is developed to evaluate the most optimal PCM. Functions constraints are also presented in this section.

Six different phase change materials are tested for this thesis for charging, discharging and battery cooling. Charging energy alone is not a suitable variable to determine if the PCM is efficient since it may have very little discharge capacity. Additionally, energy efficacy is not the only factor to be considered since the PCM cost plays a vital role in making it viable. Similarly for the battery test case, cooling times are not the only factor determining the success of a PCM since its cost and cutoff time are also important factors.

6.3.1 Optimization Study of Glass Tube Tests

For charging and discharging tests, a simple equation is developed to yield a factor, Y_{sc} that relates the charging energy, discharging energy and the PCM cost.

The objective function equation is given as follows:

$$Y_{sc} = \frac{(Z_{k,PCM})(E_c)}{(\xi_d)(E_d)} \tag{6.67}$$

The constraints are as follows:

$0.22 < \xi_d < 0.32$ (Per unit energy rate in the province of Ontario) (6.67a)

$E_c > E_d$ (To satisfy 2nd law of thermodynamics) (6.67b)

For cost optimization, the variables are $Z_{k,PCM}$ and ξ_d. The ratio of the term E_d and E_c can be defined as efficiency which remains constant for each PCM. The numerator is the PCM cost $Z_{k,PCM}$ and the charging energy, E_c. The denominator is the discharge energy rate, ξ_d, and discharge energy, E_d. The ratio between energy utilized to charge the PCM and energy given out by the PCM are the variables used in equation (6.67). PCM cost and discharge energy are the other two variables. The PCM that yields the smallest Y_{sc} value is the most optimal PCM. Low ratio of charging and discharging energy is desired because it would mean high energy efficiency. The value of Y_{sc} cannot be less than or equal to zero since, according to the first and second law of thermodynamics, discharge energy cannot be greater or equal to the energy required to charge the PCM.

6.3.2 Optimization Study of Battery Cooling Tests

For battery cooling tests, a relationship is separately developed. Factor Y_{bc} relates the battery cooling time, cutoff time and PCM cost. The objective function equation is given as follows:

$$Y_{bc} = \frac{(Z_{k,PCM})(t_{cooling})}{(\xi_d)(E_d)(t_{cut-off})} \quad (6.68)$$

The constraints are as follows:

$0.22 < \xi_d < 0.32$ (Per unit energy rate in the province of Ontario) (6.67a)

$E_c > E_d$ (To satisfy 2nd law of thermodynamics) (6.67b)

$t_{cut-off} < 6990$ (Battery cutoff time, in seconds, under ambient conditions) (6.67c)

For cost optimization, the variables are $Z_{k,PCM}$ and ξ_d.The numerator is the PCM cost $Z_{k,PCM}$ and the battery cooling time, $t_{cooling}$. The denominator is the discharge energy rate, ξ_d, discharge energy, E_d, and battery cutoff time, $t_{cut-off}$. The variables in ratio are the battery cooling time until it reaches safe recharging temperature and battery cutoff time when the voltage drops low enough to shut down the motor. PCM cost and discharge energy are, once again, the other two variables The PCM that yields the smallest Y_{bc} value is the most optimal PCM. Low time ratio is desirable since it means battery is unusable for short period of time. The scalar multiple beside each variable signifies the importance of each variable in the factor. The value of Y_{bc} cannot be less than zero since total cooling time cannot be less than cutoff time.

Chapter 7 Results and Discussion

This chapter provides the results and discussion of the study conducted on novel PCMs. Experimental results of charging, discharging, battery cooling test results, thermoeconomic, uncertainty analysis, analytical study, optimization and validation are presented here. Energy and exergy evaluation of the charging and discharging process is also given in this section.

After the literature review, the two refrigerant candidates isolated are R141b and R134a. Initially, the tests are conducted to find out if the selected refrigerant formed clathrate at temperature above 0 ^{o}C (273 K). Furthermore, the most appropriate refrigerant percent composition is determined. Later, several different additives are added with the refrigerant clathrates to test the improvement in the thermal properties. Sodium chloride (NaCl), magnesium nitrate hexahydrate ($Mg(NO_3)_2.6H_2O$), aluminum particles, copper particles and ethanol are selected as additives. The additives are added to study the improvement in the thermal properties of the clathrate based on the before mentioned refrigerants. The thermal properties are determined for a variable fraction of additives since their solubility changes with the change in temperature [92, 93].

The safety, handling and storing characteristics of the used materials are discussed as follows:

- R134a is a class common refrigerant used in a variety of domestic and commercial applications. It is classified as A1 in the American Society of Heating, Refrigeration, and Air Conditioning Engineers safety group [94]. It means that R134a has low toxicity and does not propagate flame. R134a operates

at about 340 kPa at 298 K so containment is required to prevent leaks and needs to be stored under 323 K. R134a however has high global warming potential and more environmentally friendly alternatives will soon be available in the market.

- R141b is nonflammable and has a very low operating pressure [95]. It does not require any specialized pressurized system to contain it but it must be stored below 323 K.
- Ethanol is considered flammable so it must be kept away from ignition, spark or extreme high temperatures. Ethanol is toxic if ingested and it causes irritation to skin and eyes [96].
- Magnesium nitrate hexahydrate may be flammable at high temperatures. It can cause irritation to skin and eyes in case of contact. It is considered hazardous to ingest or to inhale it [97].
- Aluminum is slightly hazardous in case of skin contact as it causes irritation. It does not cause any irritation to the eyes and is considered non-hazardous in case of ingestion. Aluminum is considered nonflammable [98].
- Copper is considered very hazardous, if ingested. It is hazardous in case of inhalation, skin contact and eye contact as it causes irritation. It can be flammable at high temperatures [99].
- Sodium chloride is slightly hazardous in case of skin contact as it causes irritation. It can also cause irritation to the eyes and is considered non-hazardous in case of ingestion. Sodium chloride is considered nonflammable [100].

7.1 Test Results of Base PCM

Experiments are conducted to determine the onset and end set times of R134a and R141b clathrates without additives. Refrigerant mass fraction is varied from 0.15 to 0.4 with 0.05 intervals. Figure 7.1 shows the graphical illustration of water and refrigerant mass for each fraction.

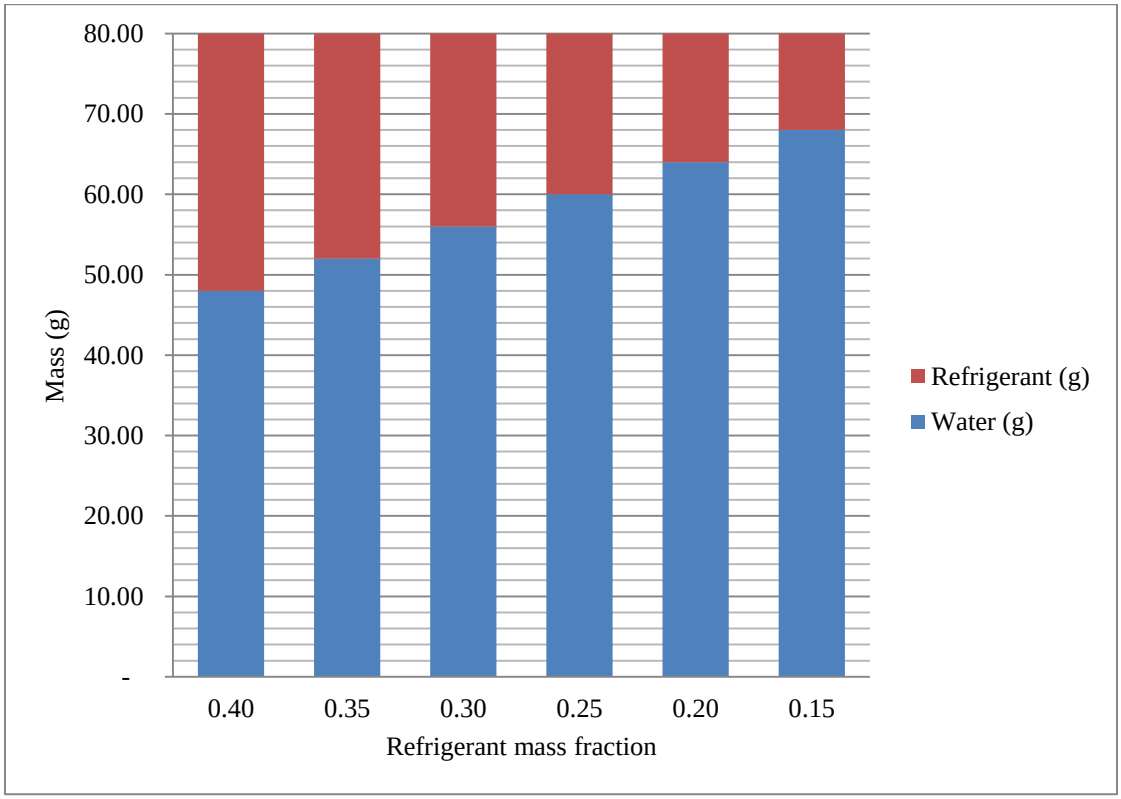

Figure 7.1 Graphical illustration of water and refrigerant masses for each fraction

Different fractions of refrigerant and water ratios are tested to find out the most appropriate combination. Table 7.1 shows the values of water and refrigerant mass used for each fraction. The total mass of the tested clathrate is maintained at the value of 80 gram.

Table 7.1 Values of water and refrigerant mass for each fraction

Mass (g)	Refrigerant mass fraction	Water (g)	Refrigerant (g)
80	0.40	48	32
80	0.35	52	28
80	0.30	56	24
80	0.25	60	20
80	0.20	64	16
80	0.15	68	12

Refrigerant clathrate is tested at two different bath temperatures for charging. Refrigerant clathrates are tested at 3 ^{o}C (276 K) and 5 ^{o}C (278 K). Water at 5 ^{o}C (278 K) temperature requires lower energy while 3 ^{o}C (276 K) water temperature requires greater energy to bring the bath to their desired temperatures. Charging times are important to determine as they yield the total energy used to form the PCMs. Less charging time means low energy while more time means large amount of energy required to form the PCMs. R141b did not form clathrate at 3 ^{o}C (276 K) for all the tested refrigerant fractions. No more tests are conducted on R141b since it failed to form the clathrate at lower temperature. Test result readings for R134a clathrate at 3 ^{o}C (276 K) are presented in Table 7.2. The table shows the observed transformation the clathrate structure i.e. 1st 2nd or 3rd and the clathrate pressure at formation. Table 7.3 shows the results of refrigerant R134a mixed with distilled water at 0.15, 0.2, 0.25, 0.3, 0.35 and 0.4 mass fractions. With bath temperature of 3 ^{o}C (276 K), onset and end set times are recorded along with the remarks on the structure and appearance of the clathrate in the tube.

Table 7.2 Test result readings for R134a clathrate at 3 ^{o}C (276 K)

R134a clathrate at 3 ^{o}C (276 K)					
Ratio	Onset (minutes)	1st Observation (minutes)	2nd Observation (minutes)	3rd Observation (minutes)	Pressure (kPa)
0.15	20	5	15	-	3207
	40	5	5	60	241
	20	5	15	-	241
	100	5	25	30	220
0.2	20	10	10	-	241
	120	5	10	20	241
	80	10	10	-	241
	20	5	15	-	241
0.25	40	5	5	-	220
	120	5	25	-	207
	120	5	10	30	255
	20	5	20	-	241
0.3	20	5	25	40	248
	100	5	5	-	241
	80	5	15	-	241
	80	5	5	20	220
0.35	60	5	-	-	241
	60	5	15	10	234
	40	5	5	20	262
	20	5	5	50	241
0.4	60	20	-	-	241
	40	10	50	-	269
	60	5	5	20	227
	60	5	5	20	241
	110	5	5	-	241

Table 7.3 Observations, onset and end set time values for selected mass fractions of R134a refrigerant clathrate at 276 K

#	Contents	Refrigerant Fraction	Onset times (minutes)	End set times (minutes)	Remarks
1	R134a + water	0.15	45	89	Small amount of clathrate
2	R134a + water	0.2	60	84	Small amount of clathrate
3	R134a + water	0.25	93	122	Complete fluffy clathrate
4	R134a + water	0.3	64	102	Complete fluffy denser clathrate
5	R134a + water	0.35	35	70	Complete solid clathrate
6	R134a + water	0.4	49	73	Complete solid clathrate

Figure 7.2 shows the formed R134a clathrate in the glass tubes at 300 kPa and 276 K. Fugure (a) represents the clathrate with 0.15 refrigerant mass fraction, (b) is 0.2, (c) is 0.25, (d) is 0.3, (e) is 0.35 and (f) is 0.4. In Figure (a) and Figure (b), water can be seen that has not contributed towards clathrate formation. This is due to lack of refrigerant in the tube which leaves some water to remain liquid and not form clathrate. From Figure (c) to Figure (f), an almost complete utilisation of water can be observed. The illustrations in Figure 7.2 shows that refrigerant mass fractions of 0.15 and 0.2 do not form complete clathrate hence should not be considered for any further analysis.

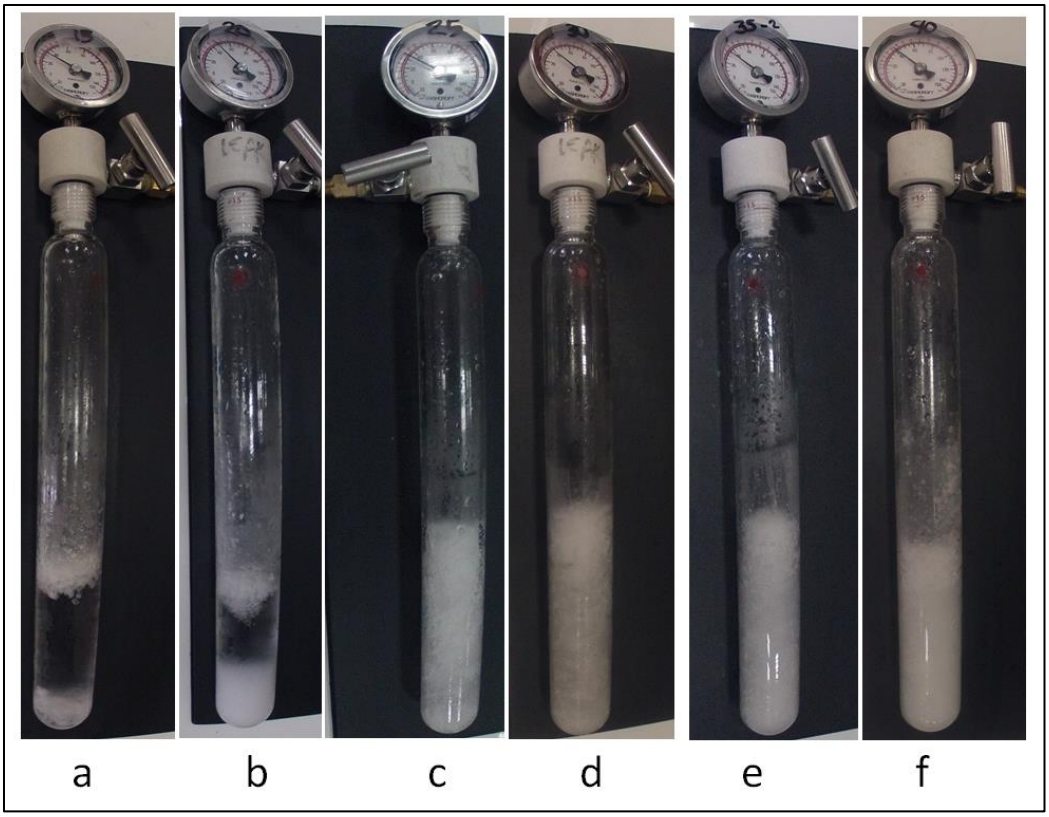

Figure 7.2 R134a clathrates in tubes (a) 0.15, (b) 0.2, (c) 0.25, (d) 0.3, (e) 0.35 and (f) 0.4 refrigerant mass fraction at 276 K

Figure 7.3 shows the R134a clathrate onset and end set average times for clathrate formation at different refrigerant mass fractions. Onset time is the time clathrate takes to start freezing while end set is when the process of freezing is complete. It is to be noted that complete freezing does not necessarily mean everything in the tube is frozen. For some fractions, either the water or the refrigerant remains liquid and does not freeze at the water bath temperature of 276 K. Refrigerant mass fractions of 0.15 to 0.40 are shown in the figure. Below 0.25, a large fraction of the water remains unmixed, as shown in Figure 7.2. Above 0.4, the refrigerant does not have enough water to mix with hence does not get utilized. The graph shows that the charging time reduces until 0.35 refrigerant

mass fraction and then it starts to increase. From the tests, it is concluded that 0.35 is the most optimal mass fraction for refrigerant since it takes the least amount of time.

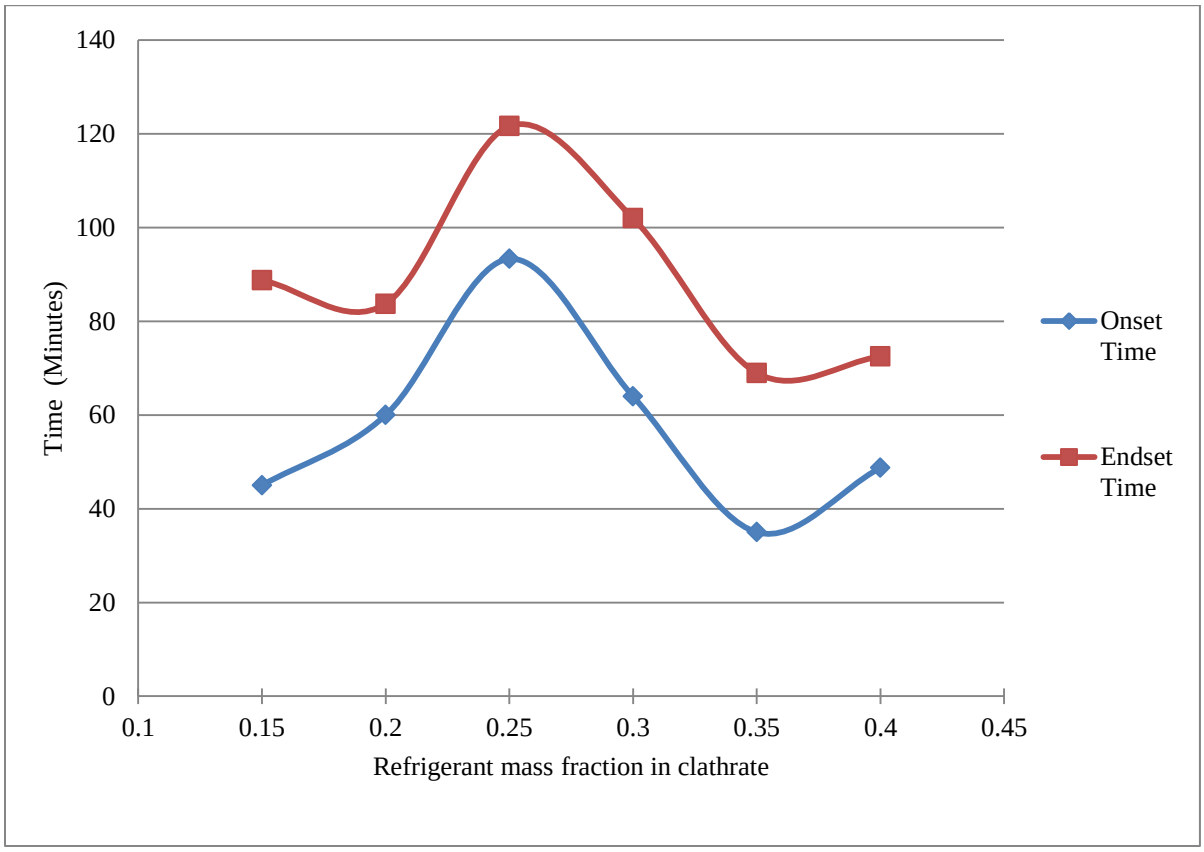

Figure 7.3 R134a clathrate times for onset and end set at different refrigerant mass fractions at 278 K

R134a clathrate is also tested with bath temperature of 278 K for onset and end set times. Test result readings for R134a clathrate at 278 K are presented in Table 7.4. The table shows the observed transformation the clathrate structure i.e. 1st 2nd or 3rd and the clathrate pressure at formation. Table 7.5 shows the results of refrigerant R134a mixed with distilled water at 0.15, 0.2, 0.25, 0.3, 0.35 and 0.4 mass fractions. The times are recorded along with the remarks on the structure and appearance of the clathrate in the tube.

Table 7.4 Test result readings for R134a clathrate at 5 ^{o}C (278 K)

R134a clathrate at 5 ^{o}C (278 K)					
Mass fractions	Onset time (minutes)	1st Observation (minutes)	2nd Observation (minutes)	3rd Observation (minutes)	Pressure (kPa)
0.15	80	5	25	-	255
	40	5	55	-	311
	100	5	15	-	290
	60	10	50	-	311
0.2	80	5	15	-	290
	20	5	35	-	255
	80	5	15	20	234
0.25	110	5	-	-	297
	80	5	25	-	311
	40	5	5	50	227
	50	5	15	20	220
0.3	20	5	25	40	248
	100	5	5	-	241
	80	5	15	-	241
	80	5	5	20	220
0.35	60	5	-	-	241
	60	5	15	10	234
	40	5	5	20	262
	20	5	5	50	241
0.4	60	20	-	-	241
	40	10	50	-	269
	60	5	5	20	227
	60	5	5	20	241
	110	5	5	-	241

Table 7.5 Observations, onset and end set time values for selected mass fractions of R134a refrigerant clathrate at 278 K

#	Contents	Refrigerant Fraction	Onset times (minutes)	End set times (minutes)	Remarks
1	R134a + water	0.15	70	112.5	Small amount of clathrate
2	R134a + water	0.2	62.5	93.3	Small amount of clathrate
3	R134a + water	0.25	70	104	Small amount of clathrate
4	R134a + water	0.3	70	102.5	Small amount of clathrate
5	R134a + water	0.35	62.5	94	Small amount of clathrate
6	R134a + water	0.4	67.5	96	Small amount of clathrate

Figure 7.4 shows the formed R134a clathrate in the glass tubes at 278 K. Fugure (a) represents the clathrate with 0.15 refrigerant mass fraction, (b) is 0.2, (c) is 0.25, (d) is 0.3, (e) is 0.35 and (f) is 0.4. In some of the tube figure, water can be seen that has not contributed towards clathrate formation. This is due to lack of refrigerant in the tube and higher temperatures which leaves some water to remain liquid and not form clathrate. Figure (e) and Figure (f) show better utilisation of water to form clathrate and more solidified clathrate can be observed. The observations, shown in Figure 7.4 (a) to (f), shows that refrigerant mass fraction of 0.15 and 0.2 form the least amount of clathrate. When compared with the results for 276 K clathrate, the clathrate formed at 278 K is low in quantity and takes longer to form.

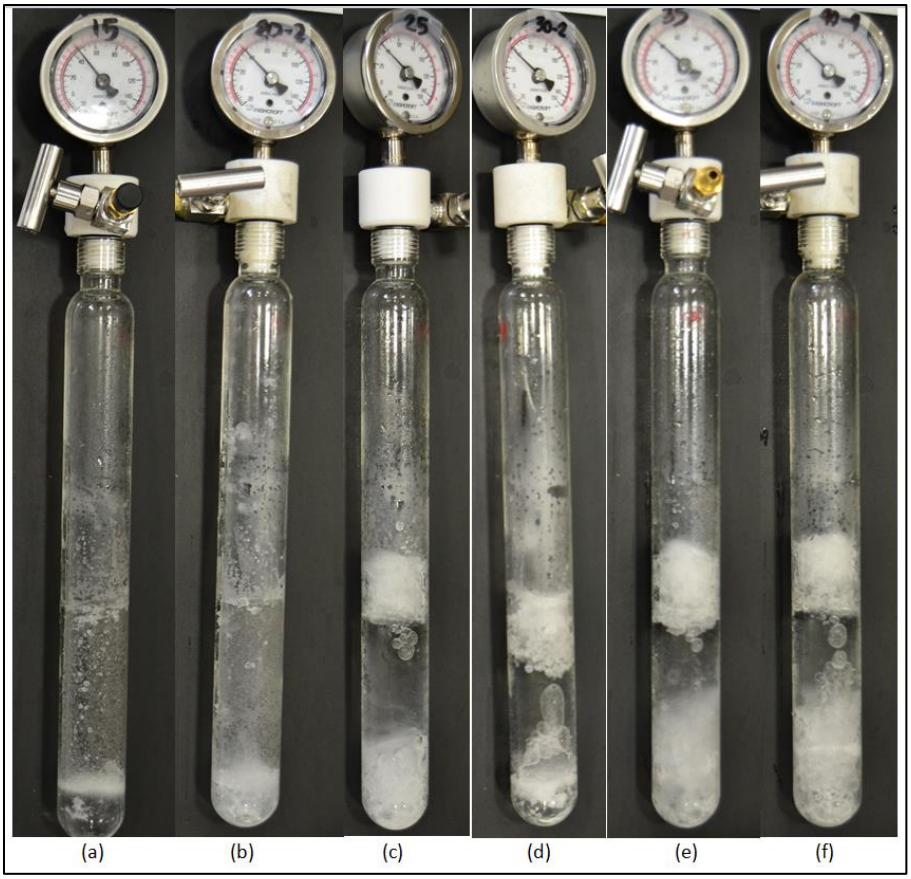

Figure 7.4 R134a clathrates in tubes (a) 0.15, (b) 0.2, (c) 0.25, (d) 0.3, (e) 0.35 and (f) 0.4 refrigerant mass fraction at 278 K

Figure 7.5 shows the R134a clathrate onset and end set average time for clathrate formation at different refrigerant mass fractions. The graph shows the onset and end set time for bath temperature of 278 K. It is to be noted that complete freezing does not necessarily mean everything in the tube is frozen. For some fractions, either the water or the refrigerant remains liquid and does not freeze at the water bath temperature of 278 K. Refrigerant mass fractions of 0.15 to 0.4 are shown in the figure. Below 0.3, a large fraction of the water remains unmixed, as shown in Figure 7.4. Above 0.4, the refrigerant does not have enough water to mix with hence does not get utilized. The graph shows that the charging times reduce until 0.35 refrigerant mass fraction and then it starts to

increase. From the tests, it is concluded that 0.35 is the most optimal mass fraction for refrigerant since it takes the least amount of time.

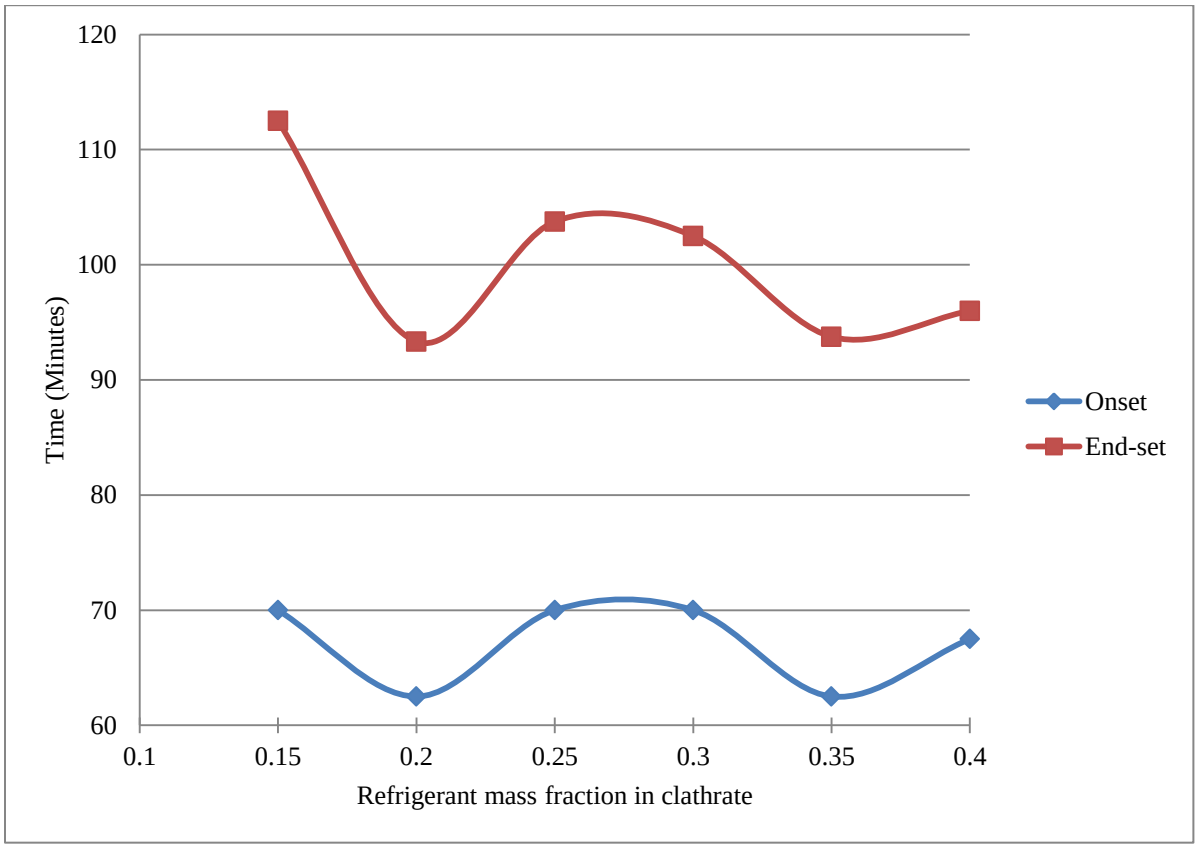

Figure 7.5 R134a clathrate times for different refrigerant mass fractions at 268 K bath temperature

Figure 7.6 shows the charging times for R134a clathrate at 276 K and 278 K bath temperature. The charging times includes onset and end set of freezing. The results show that 276 K bath temperature starts the onset of charging faster. It also shows that 276 K finishes the freezing faster as well for the tested refrigerant mass fractions. It is concluded that bath temperature of 276 K is more appropriate to charge than 278 K.

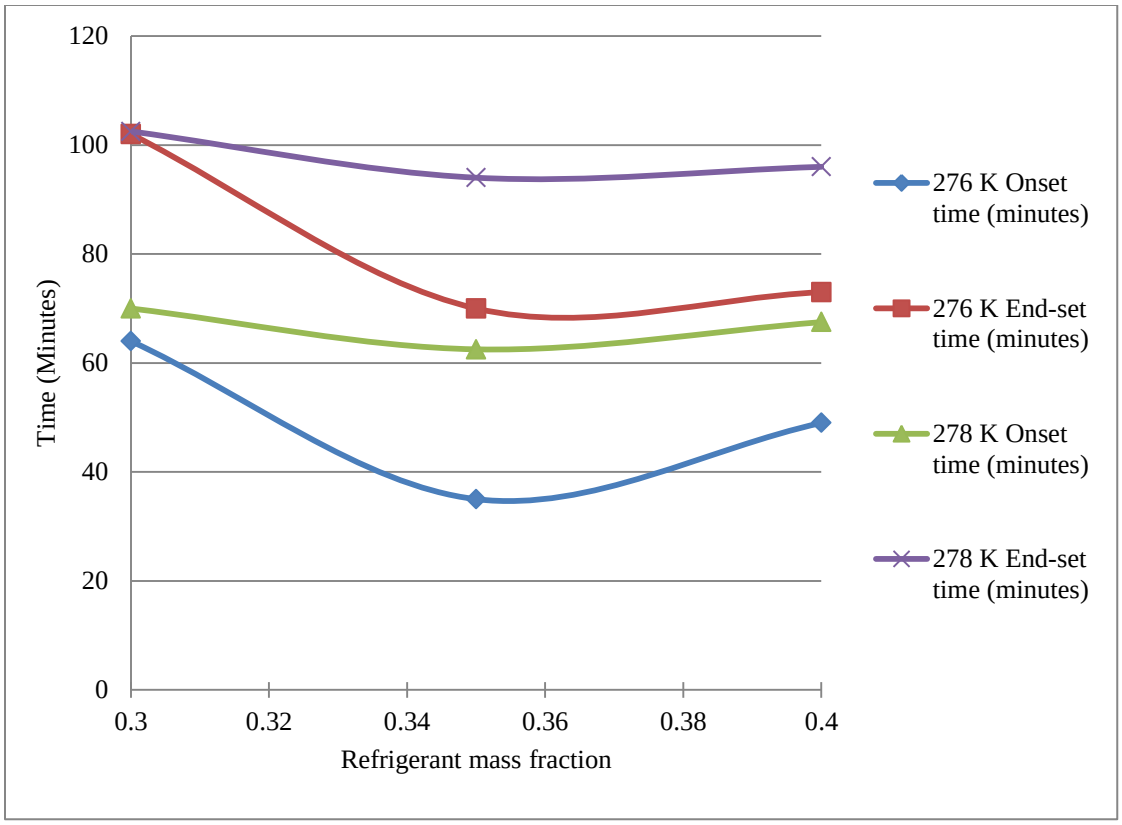

Figure 7.6 Charging process times for R134a clathrate at 276 K and 278 K bath temperatures

7.2 Test Results of PCMs with Additives

After figuring out the most appropriate percent composition for refrigerant clathrate, additives are included to see the improvement in the charging times. For the additives, ethanol, sodium chloride, magnesium nitrate hexahydrate, copper and aluminum are used. Additives are added from 0.01 by mass fraction to 0.05 by mass fraction to see their effects on charging times.

Figure 7.7 shows the graphical illustration of water, refrigerant and additive mass for each fraction. Additive tests are conducted for 0.35 refrigerant mass fraction as it resulted in the least charging times. The total mass of the tested clathrate is maintained at

the value of 80 gram. Additive mass fraction is varied from 0.01 to 0.05 with 0.01 intervals.

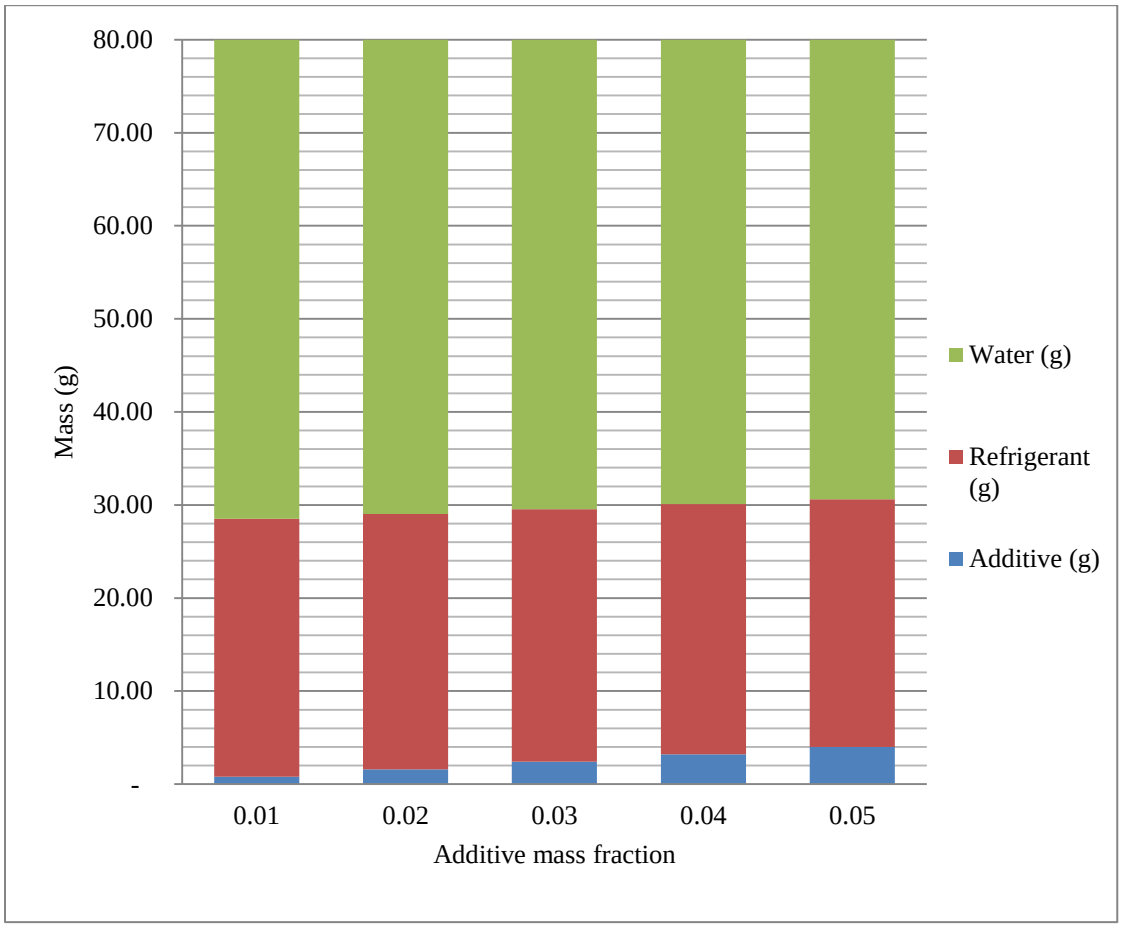

Figure 7.7 Graphical illustration of water, refrigerant and additive masses for each fraction

Tests are conducted with bath temperature of 276 K with selected additives. R134a clathrate with selected additives are tested at bath temperature of 276 K for onset and end set times. Table 7.6 shows the values of water, refrigerant and additive mass for each fraction. Test result readings for R134a clathrate with additives at 276 K are

presented in Table 7.7. The table shows the times of change in structure observation, additive types and the clathrate pressures at formation.

Table 7.6 Values of water, refrigerant and additive masses for each fraction

Mass (g)	Refrigerant mass fraction	Water (g)	Refrigerant (g)	Additive fraction	Additive (g)
80	0.35	51	28	0.01	0.8
80		51	27	0.02	1.6
80		50	27	0.03	2.4
80		50	27	0.04	3.2
80		49	27	0.05	4.0
80	0.3	55	24	0.01	0.8
80		55	24	0.02	1.6
80		54	23	0.03	2.4
80		54	23	0.04	3.2
80		53	23	0.05	4.0
80	0.25	59	20	0.01	0.8
80		59	20	0.02	1.6
80		58	19	0.03	2.4
80		58	19	0.04	3.2
80		57	19	0.05	4.0
80	0.2	63	16	0.01	0.8
80		63	16	0.02	1.6
80		62	16	0.03	2.4
80		61	15	0.04	3.2
80		61	15	0.05	4.0
80	0.15	67	12	0.01	0.8
80		67	12	0.02	1.6
80		66	12	0.03	2.4
80		65	12	0.04	3.2
80		65	11	0.05	4.0

Table 7.7 Observation times, additive types and clathrate pressures at formation

35% R134a refrigerant clathrate at 276 K						
Additive	Additive fraction	Onset (Minute)	1st Observation (Minutes)	2nd Observation (Minutes)	3rd Observation (Minutes)	Pressure (kPa)
none	none	15	5	5	45	227
	none	15	5	5	45	227
Copper	0.01	10	10	10	-	241
	0.01	10	5	5	40	220
	0.01	10	5	5	50	227
	0.02	10	5	5	70	227
	0.02	10	5	15	60	227
	0.02	10	5	5	30	227
	0.03	10	5	15	60	220
	0.03	10	5	35	50	227
	0.04	10	5	5	60	213
	0.04	10	5	25	10	220
	0.05	10	5	15	50	213
	0.05	10	5	35	30	227
$MgNO_3.6H_2O$	0.01	10	10	10	-	227
	0.01	20	5	15	-	220
	0.02	20	10	20	-	220
	0.02	20	5	5	30	227
	0.03	20	5	15	-	220
	0.03	20	5	15	-	227
	0.04	10	5	5	30	213
	0.04	20	5	5	20	227
	0.05	10	5	15	20	207
	0.05	30	5	15	20	227
	0.05	10	5	15	-	227

Table 7.7 Change in structure observation times, additive type and clathrate pressure at formation *(cont.)*

Additive	Additive fraction	Onset (Minutes)	1st Observation (Minutes)	2nd Observation (Minutes)	3rd Observation (Minutes)	Pressure (kPa)
Ethanol	0.01	20	10	10	30	227
	0.01	30	10	20	-	234
	0.02	50	5	15	-	213,
	0.02	10	5	5	30	207
	0.02	20	10	10	-	227
	0.03	10	5	5	10	213
	0.03	60	5	5	-	207
	0.04	50	5	5	-	220
	0.04	70	5	5	-	234
	0.05	70	10	10	-	255
	0.05	40	10	10	-	220
Aluminum	0.01	10	5	15	40	241
	0.01	10	5	15	40	213
	0.02	20	5	15	30	234
	0.02	10	5	25	-	207
	0.02	30	5	15	-	234
	0.02	20	5	15	-	207
	0.03	10	5	15	40	220
	0.03	10	5	25	40	220
	0.04	10	20	40	20	213
	0.04	10	20	40	20	220
	0.05	20	5	15	-	193
	0.05	10	5	15	60	220
	0.05	10	5	45	-	234
Sodium chloride	0.01	50	5	35	-	227
	0.01	30	5	-	-	220
	0.01	20	5	25	-	234
	0.02	100	10	-	-	207
	0.02	100	5	25	-	241
	0.03	50	5	45	-	207
	0.03	70	5	45	-	227

Charging times for onset and end set are recorded regarding the structure of the clathrate as shown in Table 7.8. Observations regarding the structure of the clathrate help predict the energy storage capability. If the structure is hard solid, it can release the cool energy longer than the structure that is soft and fluffy.

Table 7.8 R134a clathrate onset time, end set time and observational remarks

#	Contents	Type of additives	Additive mass fraction	Onset times (minutes)	End set times (minutes)	Remarks
1	0.35 R134a + water + copper	Metal, solid micro particles	0.01	10	53	> Mildly soft fluffy clathrate structure > Does not mix well with the clathrate > Large crystals >Additive appears to settle at the bottom
			0.02	10	77	
			0.03	10	95	
			0.04	10	65	
			0.05	10	80	
2	0.35 R134a + water + magnesium nitrate hexahydrate	Nonmetal, solid particles	0.01	17	32	> Soft fluffy clathrate structure > Mixes well with the clathrate, > Additive does not appears to settle at the bottom > Small crystals
			0.02	20	43	
			0.03	20	40	
			0.04	15	50	
			0.05	17	50	
3	0.35 R134a + water + aluminum	Metal, solid micro particles	0.01	10	70	> Mildly soft fluffy clathrate structure > Large crystals > Does not mix well with the clathrate >Additive appears to settle at the bottom
			0.02	15	55	
			0.03	10	75	
			0.04	10	90	
			0.05	13	63	
4	0.35 R134a + water + sodium chloride	Nonmetal, solid particles	0.01	33	58	> Mixes well with the clathrate, > Additive does not appears to settle at the bottom > Small crystals
			0.02	63	78	
			0.03	60	110	
			0.04	-	-	> No clathrate formation
			0.05	-	-	
5	0.35 R134a + water + ethanol	Nonmetal, liquid	0.01	25	65	> Hard solid clathrate structure, >Additive does not settle at the bottom
			0.02	26	53	
			0.03	35	50	
			0.04	60	70	
			0.05	55	75	

7.2.1 Test Results of Constant Energy Charging

Tests are conducted with two temperature probes inserted in the PCM tube. These tests are done to find out temperature at two different locations in the PCM. These tests are done with constant energy bath setting where the amount of energy is maintained. Two different location reading are required to determine the thermal properties of the PCM namely thermal conductivity and specific heat. Table 7.9 shows the test readings recorded and observations made during the tests.

Figure 7.8 shows the temperature readings recorded during the charging process of the PCM without additive. The variation of two different temperatures is shows in above figure. One of them is core temperature reading which is at the cross-sectional center of the tube and the "out" which is 14 mm away from the core. Core takes longer to cool down as it is further away from the cold bath water. The temperature in the tube decrease until 20 minute mark as the water bath continues to cool the tube. After a short period of time, the temperature increases suddenly, after 50 minutes, as R134a clathrate nucleates, giving off heat. Once nucleation is complete, the heat being given off by R134a clathrate reduces and the temperature inside the tube starts to drop again.

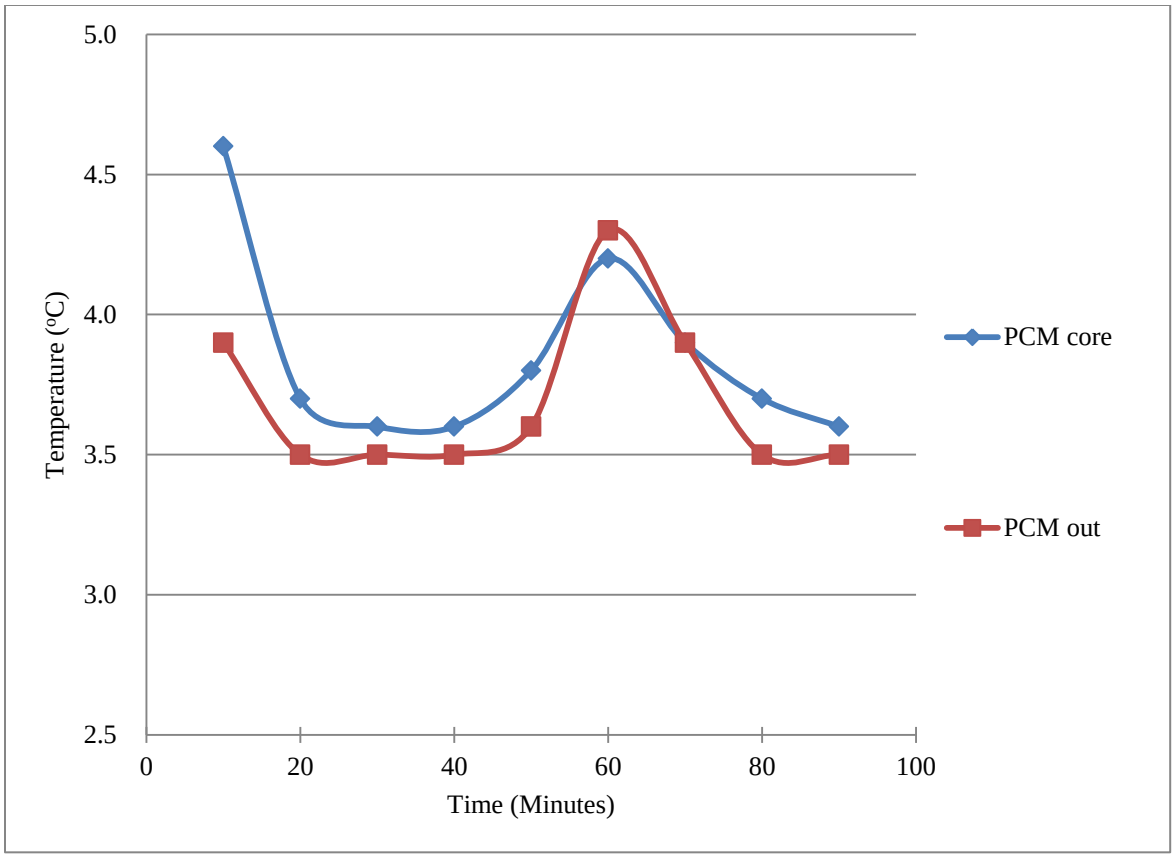

Figure 7.8 Recorded temperature readings during the charging process of the PCM without additive

Figure 7.9 shows the temperature readings recorded during the charging process of the PCM with copper additive. Core temperature reading is the temperature at the cross-sectional center of the tube and the "out" which is 14 mm away from the core. Core takes longer to cool down as it is further away from the cold bath water. For copper additive, the temperature in the tube decrease almost continuously until complete freezing is achieved. After 20 minutes, the temperature increases suddenly as R134a clathrate nucleates, giving off heat. Once nucleation is complete, the heat being given off by R134a clathrate reduces and the temperature inside the tube starts to drop again. The height and length of the temperature peaks is small with copper additives.

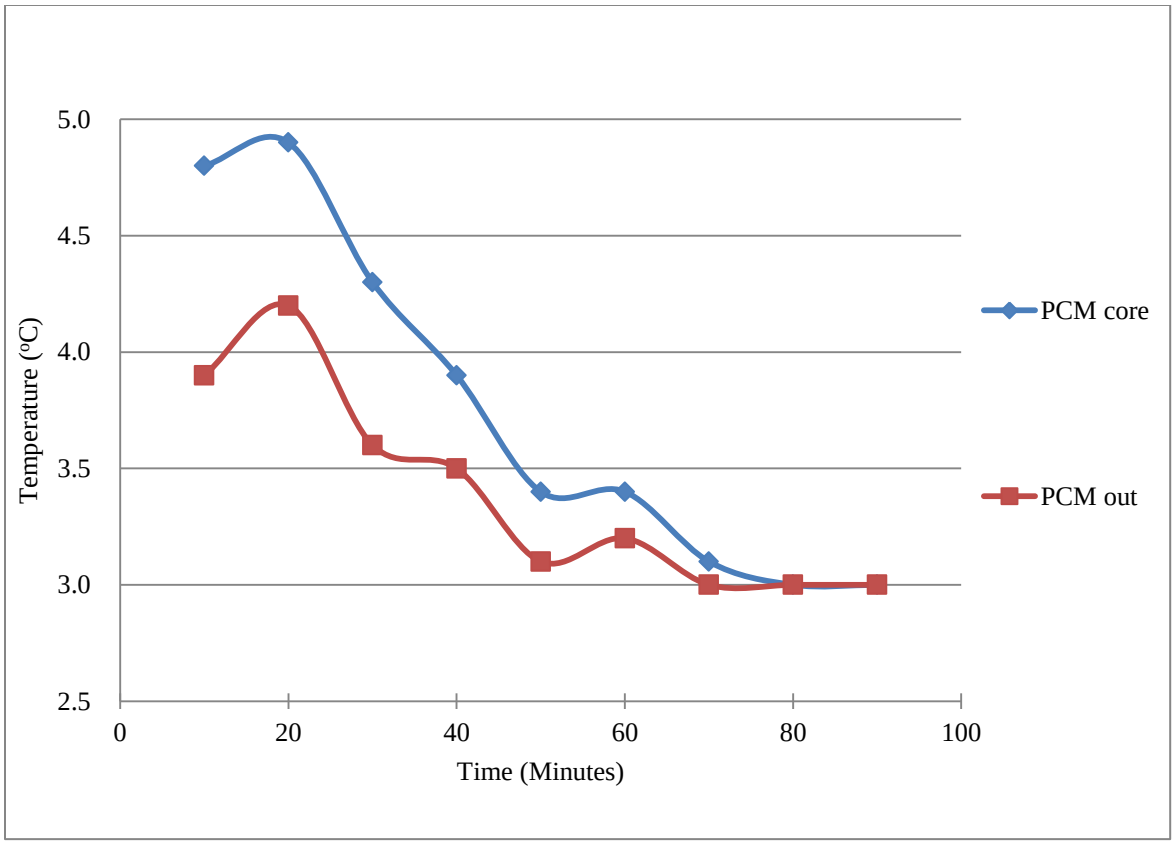

Figure 7.9 Recorded temperature readings during the charging process of the PCM with copper additive

Figure 7.10 shows the temperature readings recorded during the charging process of the PCM with ethanol additive. Core temperature reading is the temperature at the cross-sectional center of the tube and the "out" which is 14 mm away from the core. Core takes longer to cool down as it is further away from the cold bath water. For ethanol additive, the temperature in the tube decrease until 20 minute mark. After 20 minutes, the temperature increases suddenly a little as R134a clathrate nucleates, giving off heat. The temperature drops after 30 minutes until 50 minute mark. After 50 minutes, temperature increase significantly due to nucleation. Once nucleation is complete after 70 minutes, the heat being given off by R134a clathrate reduces and the temperature inside the tube starts

to drop again. The height and length of the temperature peaks depend on the amount of formation heat and the heat transfer rates of the clathrate nucleation. The height and length of the temperature peaks is big with ethanol additive.

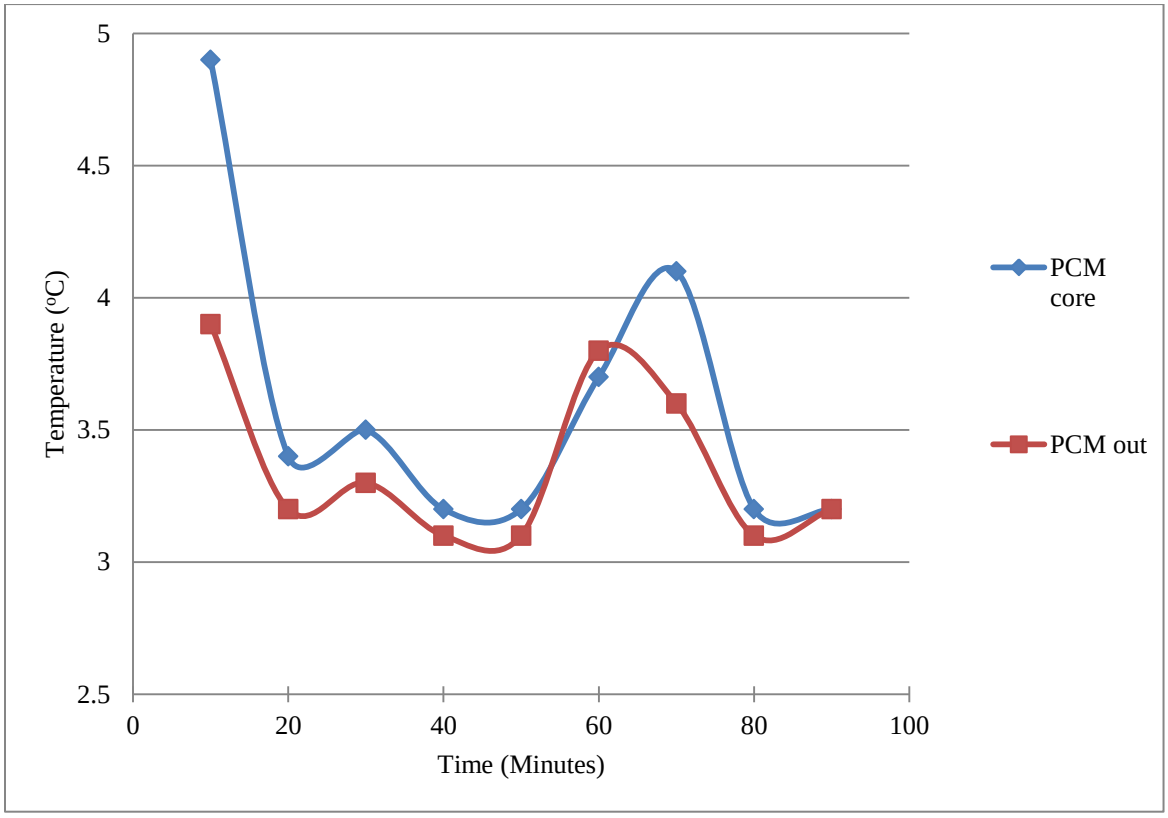

Figure 7.10 Recorded temperature readings during the charging process of the PCM with ethanol additive

Figure 7.11 shows the temperature readings recorded during the charging process of the PCM with magnesium nitrate hexahydrate additive. Core temperature reading is the temperature at the cross-sectional center of the tube and the "out" which is 14 mm away from the core. Core takes longer to cool down as it is further away from the cold bath water. For magnesium nitrate hexahydrate additive, the temperature in the tube decrease until 30 minute mark. After 30 minutes, the temperature increases a little as

R134a clathrate nucleates, giving off heat. The temperature drops after 40 minutes mark, once nucleation is complete. The height and length of the temperature peaks depends on the amount of formation heat and the heat transfer rates of the clathrate nucleation. Since magnesium nitrate hexahydrate have better thermal properties than ethanol, the peak is comparatively smaller.

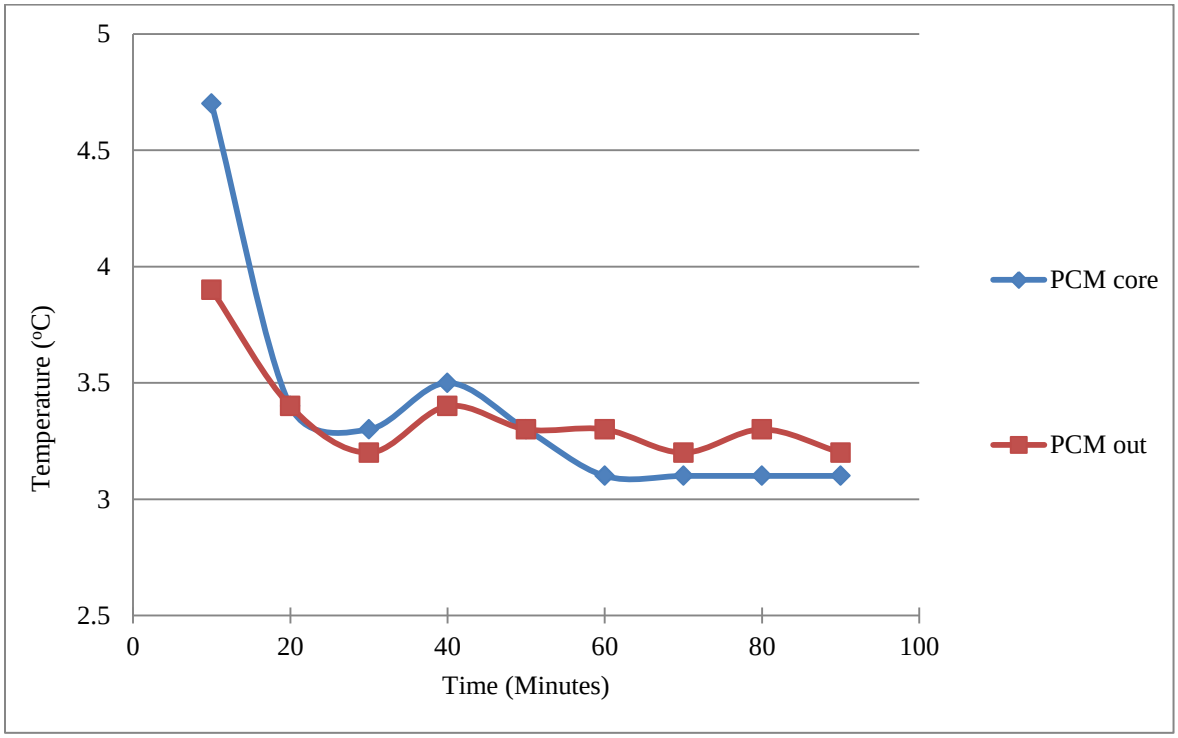

Figure 7.11 Recorded temperature readings during the charging process of the PCM with magnesium nitrate hexahydrate additive

Figure 7.12 shows the temperature readings recorded during the charging process of the PCM with sodium chloride additive. Core temperature reading is the temperature at the cross-sectional center of the tube and the "out" which is 14 mm away from the core. Core takes longer to cool down as it is further away from the cold bath water. For sodium chloride additive, the temperature in the tube decrease until 20 minute mark. After 20

minutes, the temperature increases gradually as R134a clathrate nucleates, giving off heat until 50 minute mark. The height and the length of the temperature peaks depends on the amount of formation heat and the heat transfer rates of the clathrate nucleation. Since sodium chloride has bad thermal properties, the peak is high and very wide. Wide peak shows that nucleation lasted long and it takes a very long time for PCM with sodium chloride to cool down again.

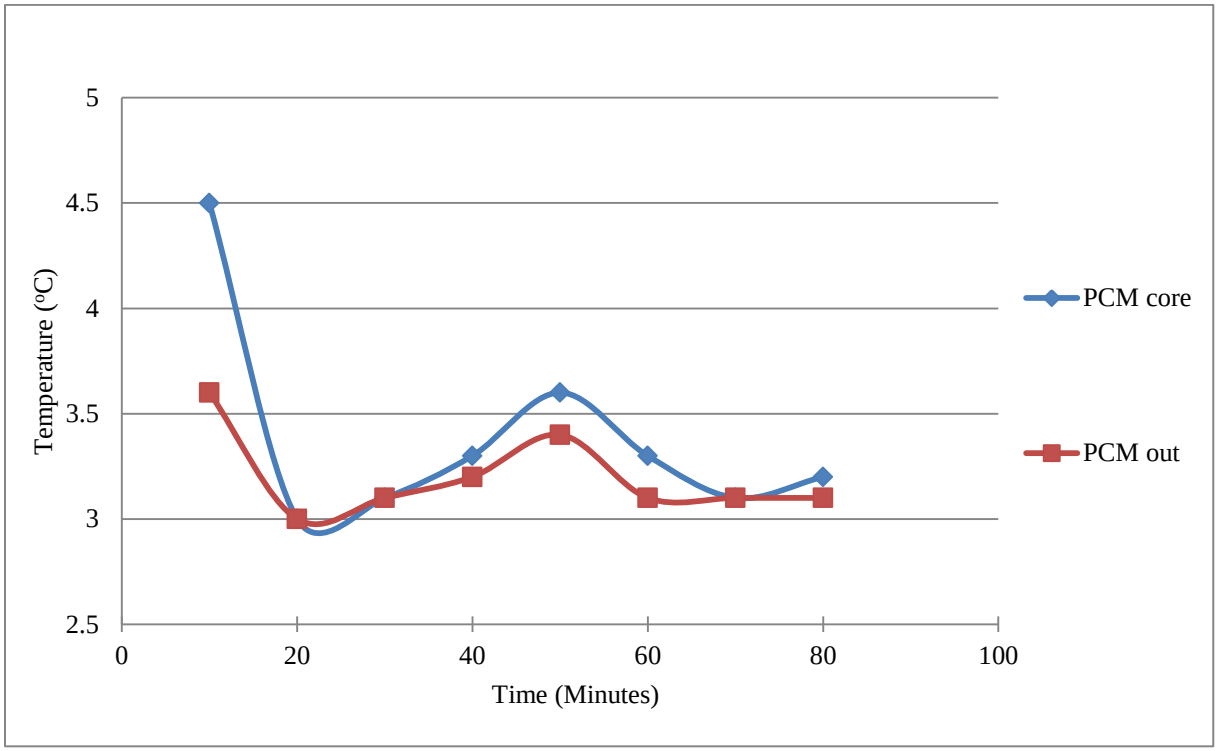

Figure 7.12 Recorded temperature readings during the charging process of the PCM with sodium chloride additive

Figure 7.13 shows the temperature readings recorded during the charging process of the PCM with aluminum additive. Core temperature reading is the temperature at the cross-sectional center of the tube and the "out" which is 14 mm away from the core. Core takes longer to cool down as it is further away from the cold bath water. For

aluminum additive, the temperature in the tube decrease until before 10 minute mark (from room temperature to the initial reading is not shown in the graph). After 10 minutes, the temperature increases a bit as R134a clathrate nucleates, giving off heat until 20 minute mark. Since aluminum has good thermal properties, the peak is low and not as wide as sodium chloride additive. Narrow peak shows that nucleation did not last long and since aluminum additive improved the thermal conductivity, it does not take very long for PCM to cool down again.

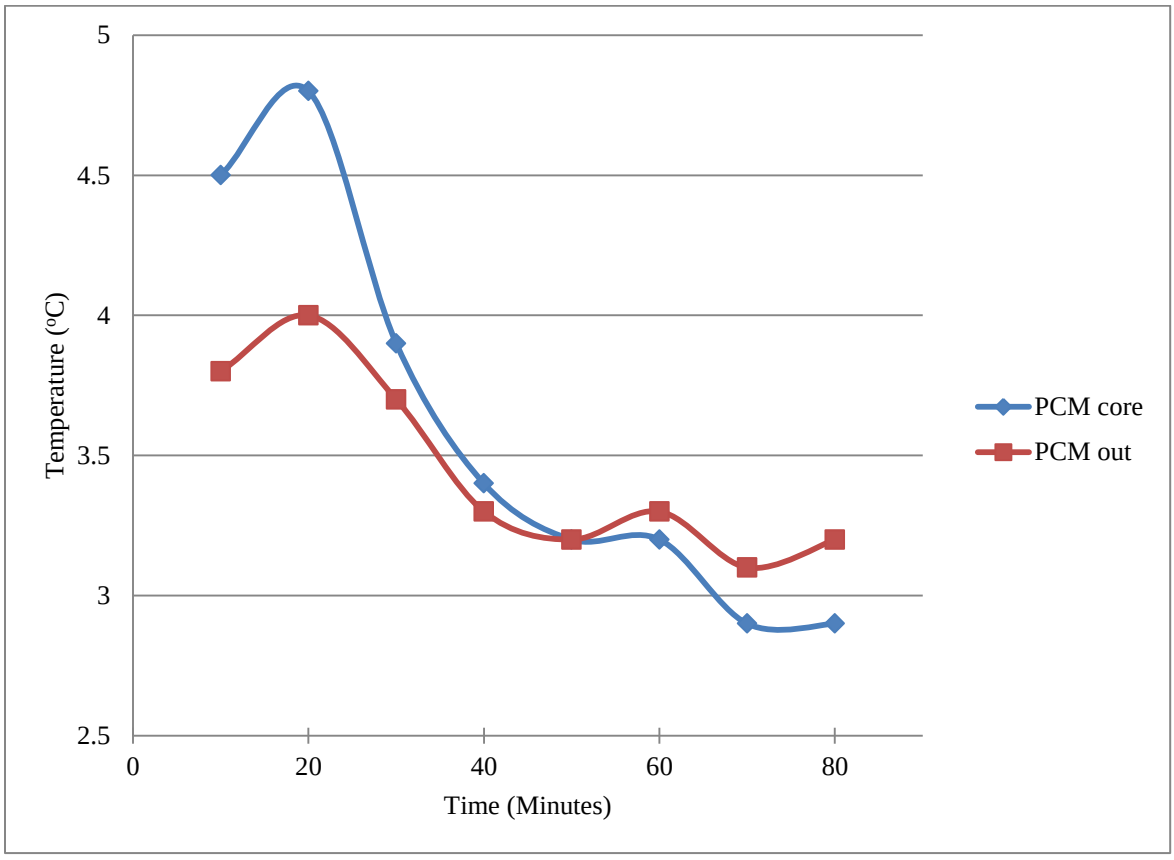

Figure 7.13 Recorded temperature readings during the charging process of the PCM with aluminum additive

Table 7.9 Readings and observations during tests

273 K charging for 0.35 R134a refrigerant				
Time (Minutes)	r_1 temperature ^oC	r_2 temperature ^oC	Bath temperature ^oC	Remarks
PCM without additive				
0	20.7	21.1	3.2	
40	4	3.8	3.4	onset
50	3.9	3.7	3.2	1st change
80	3.8	3.5	3.3	2nd change
0	21.7	21.4	3.2	
50	3.8	3.6	3.2	onset
60	4.2	4.3	3.2	1st change
90	3.6	3.5	3.2	2nd change
		0.01 Copper		
0	21.8	23.2	2.9	
10	3.7	4.2	3.2	onset
20	3.8	3.6	3.4	1st change
50	3.5	3.3	3.2	2nd change
0	22.1	22.3	3.2	
10	4.8	3.9	3.4	onset
20	5	4.2	3.1	1st change
60	3.4	3.2	2.9	2nd change
		0.01 Ethanol		
0	22.4	23.1	2.8	
60	3.7	3.8	3	onset
70	4.1	3.6	3	1st change
10	3.2	3.1	3.1	
90	3.2	3.2	3.3	2nd change
0	22.1	22.1	3.3	
30	3.9	3.9	3.2	onset
40	4.4	4.1	3.4	1st change
70	3.8	3.9	3.7	2nd change

Table 7.9 Readings and observations during tests *(cont.)*

		0.01 $MgNO_3.6H_2O$		
0	21.4	21.5	3.4	
30	4.2	4.2	4	onset
40	4.7	4.4	4.1	1st change
70	4.2	4.2	4.1	2nd change
0	22.6	22.1	3	
30	3.3	3.2	3.2	onset
40	3.5	3.4	3.1	1st change
70	3.1	3.2	3.3	2nd change
		0.01 NaCl		
0	13.5	13.6	4	
40	6.3	3.6	6.2	onset
50	4.5	4.5	4.1	1st change
80	3.9	4.1	4.1	2nd change
0	18.3	18.4	2.9	
40	3.3	3.2	2.8	onset
50	3.6	3.4	2.8	1st change
70	3.1	3.1	3	2nd change
		0.01 Aluminum		
0	22	21.9	3.4	
10	4.5	3.8	3.5	onset
20	4.8	4	3.3	1st change
40	3.4	3.3	3.2	2nd change
70	2.9	3.1	3.1	3rd change
0	22.5	22.6	3	
10	4	3.6	2.8	onset
20	3.5	3.6	2.9	1st change
40	2.9	3.2	2.9	2nd change
70	2.8	3.1	2.7	3rd change

7.3 Test Results at Different Additive Fractions

Figure 7.14 shows the results of the tests conducted on R134a clathrate with copper particles as additives. Copper mass fraction is varied from 0.01 to 0.05 while their onset and end set times are recorded. The onset time with copper particles is found to be the same for all five cases at 10 minutes. The end set time varied from 60 minutes for 0.01 additive mass fraction to 90 minutes for 0.05 additive mass fraction. The onset time remains the same since the same amount to additive interacts to initiate the solidification process. The end set time increases with the increase in additives fraction. Copper particles settle at the bottom of the tube and the ones that are present in the clathrate are not evenly distributed. This causes clathrate to remain liquid in some sections while frozen in the other. The heat transfer process is slow in the frozen region hence the freezing time increases.

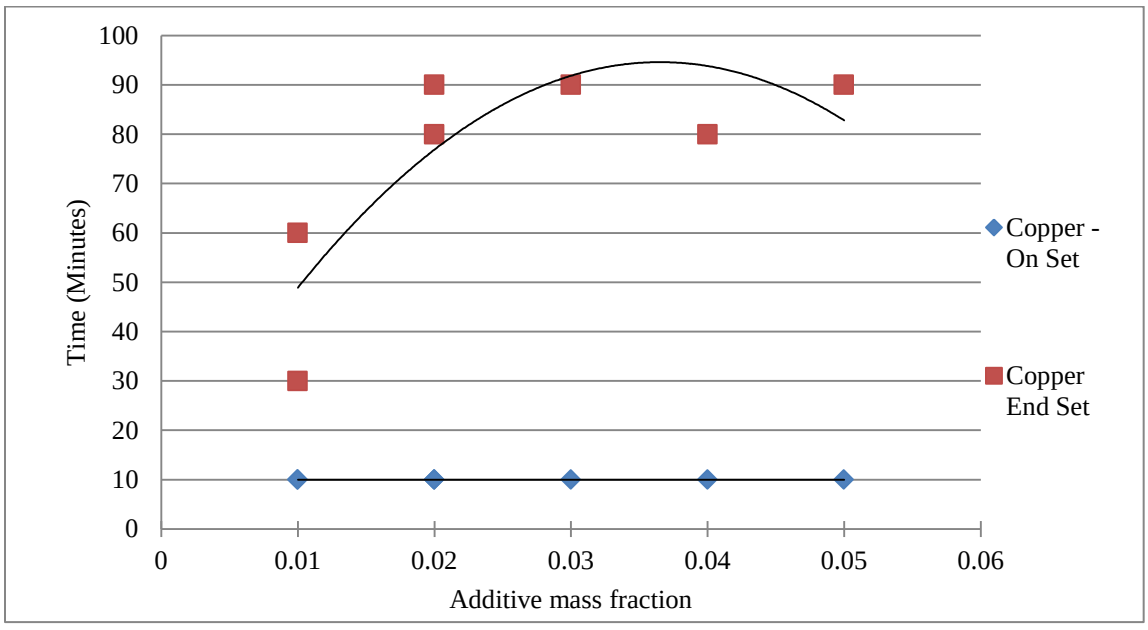

Figure 7.14 Charging process times for clathrate formation with copper additive at different additive fractions

Figure 7.15 shows the test results for R134a clathrate with magnesium nitrate hexahydrate as additive. The average onset time with magnesium nitrate hexahydrate is found to 20 minutes. The end set time varied from 30 minutes for 0.01 additive mass fraction to 50 minutes for 0.05 additive mass fraction. The onset and end set time increase slightly with the increase in additives. The clathrate appeared to have small crystals with visible air gaps in between and the crystals are small. At low additive ratios and for onset, magnesium nitrate hexahydrate improves the clathrate formation time because of its slightly better thermal conductivity compared to water. However, end set time for high additive fractions tends to increase due to the nature of salts to resist clathrate formation.

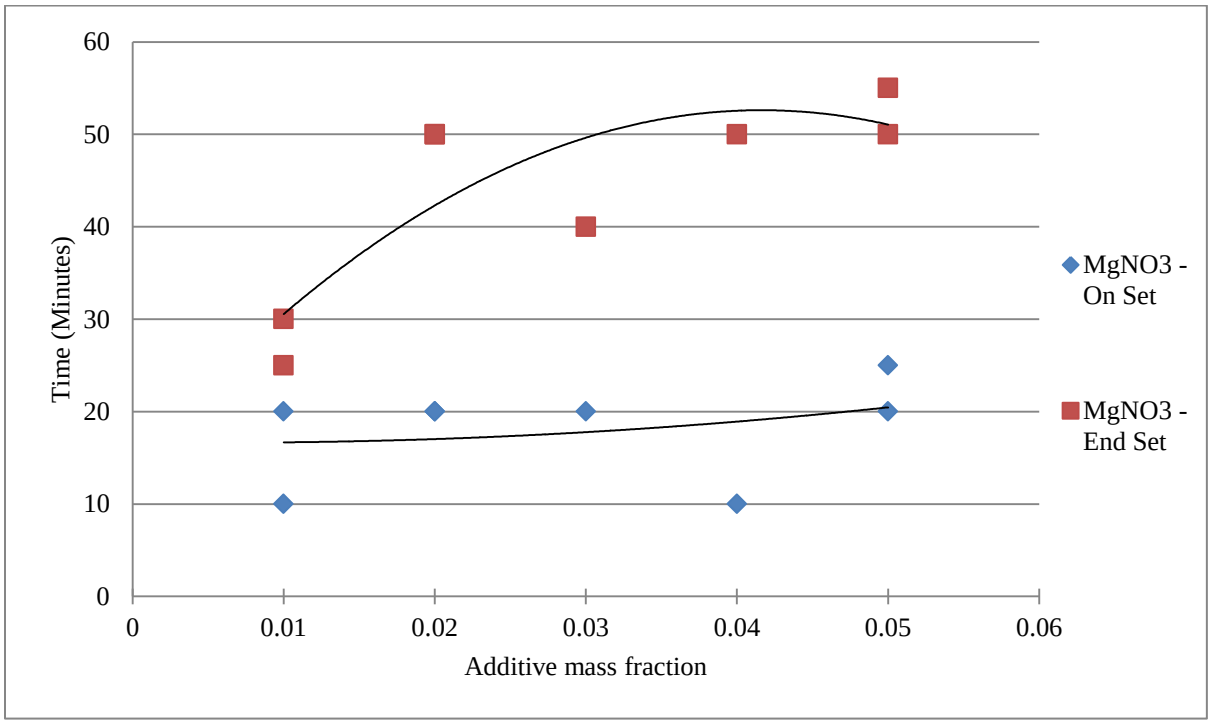

Figure 7.15 Charging process times for clathrate formation with magnesium nitrate hexahydrate additive at different additive fractions

Figure 7.16 shows results for R134a clathrate with ethanol. The onset time with ethanol increased from 25 minutes to 60 minutes. The end set time varied from 65 minutes for 0.01 additive mass fraction to 85 minutes for 0.05 additive mass fraction. The onset and end set time increases with the increase in additives. Although the onset time for ethanol is high, the end set is achieved rather fast once the solidification begins. Since ethanol is liquid, it mixes well with the clathrate hence the heat transfer is fairly uniform.

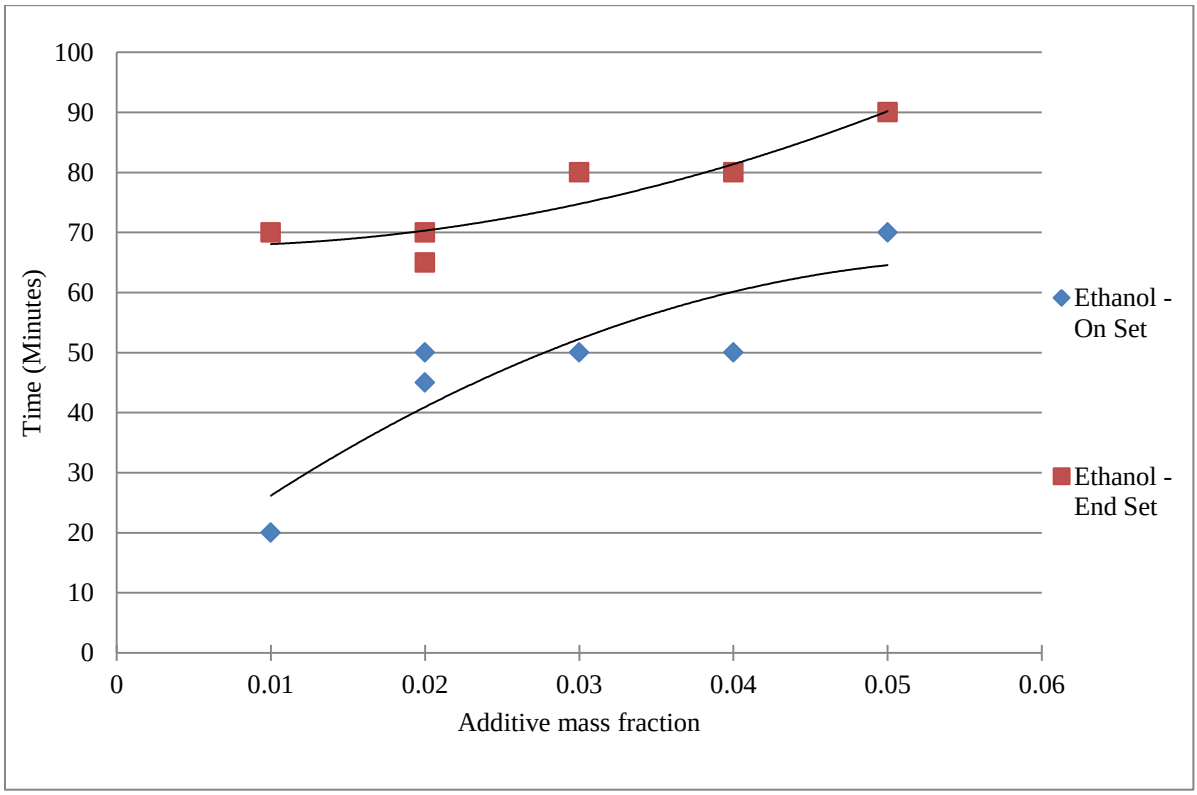

Figure 7.16 Charging process times for clathrate formation with ethanol additive at different additive fractions

Figure 7.17 shows the results of the tests conducted on R134a clathrate with aluminum particles as additives. The onset time with aluminum particles is found to be 11 minutes for all five cases. The end set time varied from 65 minutes for 0.01 additive

mass fraction to 90 minutes for 0.05 additive mass fraction. Aluminum, like copper particles, settles at the bottom of the tube and the ones that are present in the clathrate are not evenly distributed. Clathrate remains liquid in some sections while frozen in the other. In the frozen section, the heat transfer process is slow which increases the solidification time.

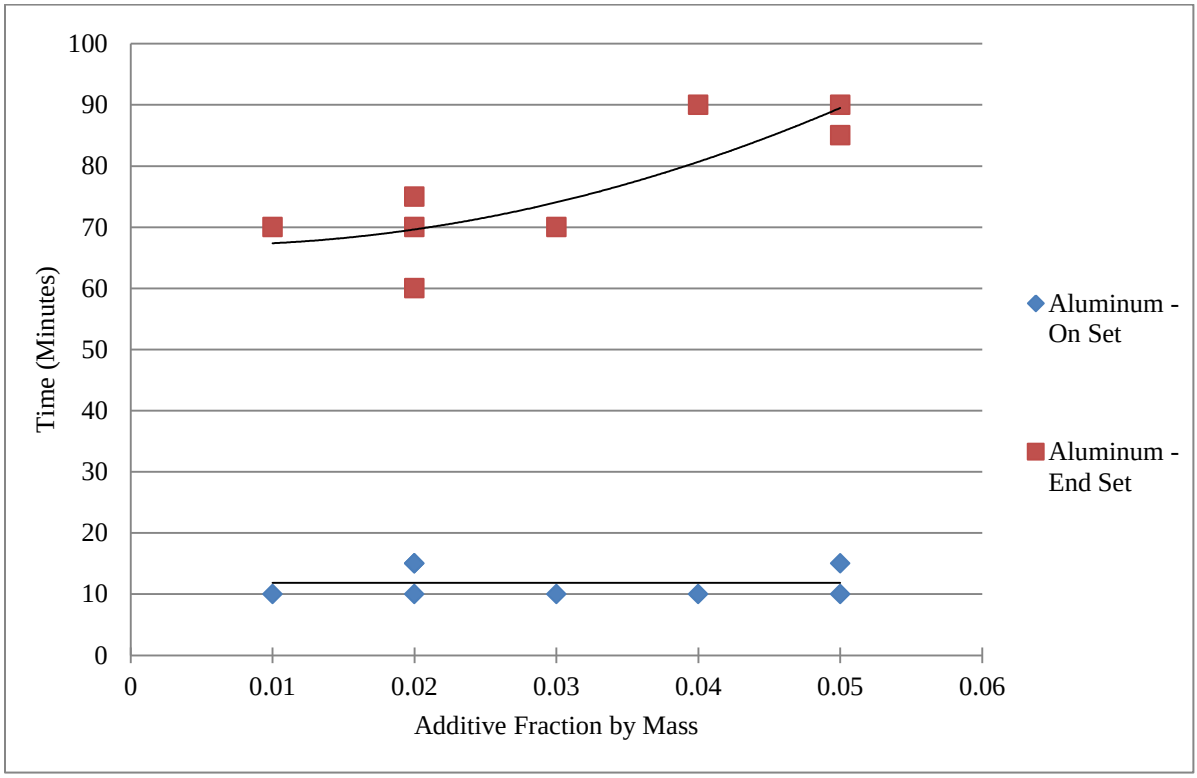

Figure 7.17 Charging process times for clathrate formation with aluminum additive at different additive fractions

Figure 7.18 shows the test results for sodium chloride as additive in R134a clathrate. The average onset time varied at 40 minute for 0.01 additive mass fraction to 65 minutes for 0.03 additive mass fraction. The end set time varied from 80 minutes for 0.01 additive mass fraction to 110 minutes for 0.03 additive mass fraction. For sodium

chloride, the R134a clathrate did not form for higher additive fractions. The onset and end set time increase with the increase in additives fraction. Sodium chloride increased the onset and end set time for all the tested fractions. Sodium chloride has lower thermal conductivity than the water. It also slows the clathrate formation since salt particles interact with the water molecules hence stop refrigerant molecules to form the clathrate.

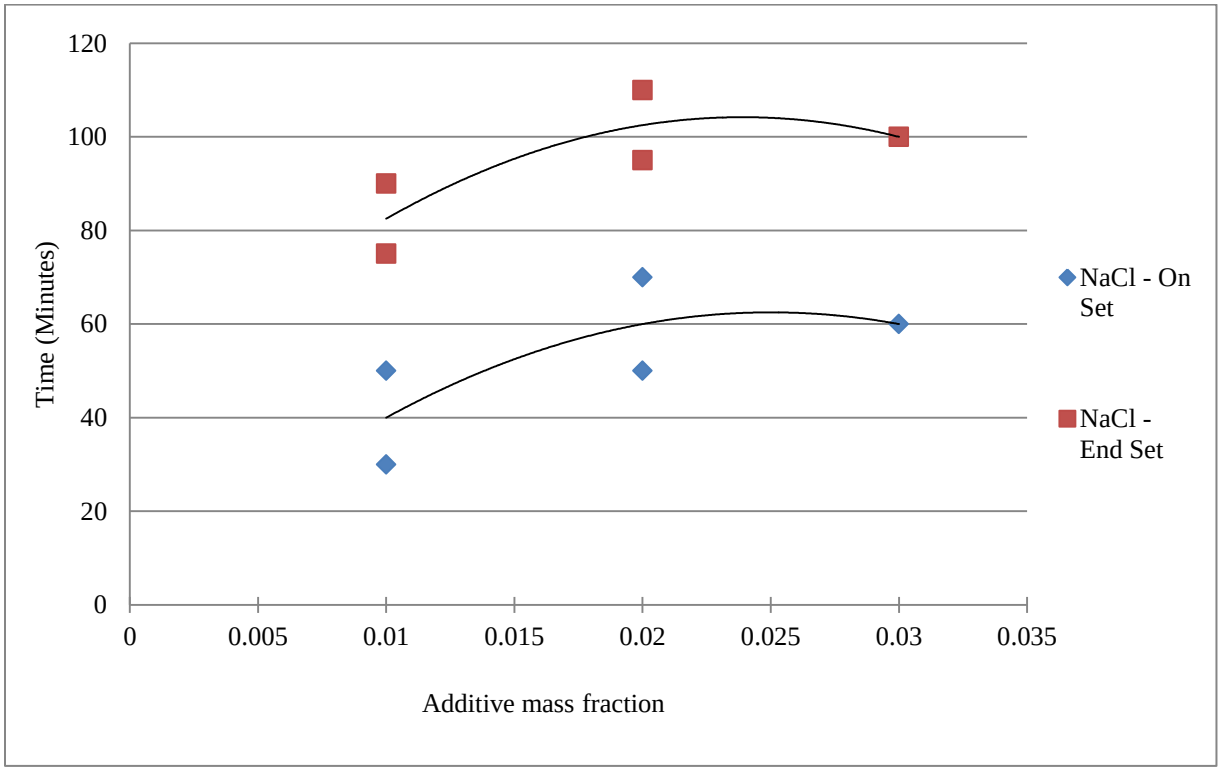

Figure 7.18 Charging process times for clathrate formation with sodium chloride additive at different additive fractions

Figure 7.19 shows the average onset time for the five tested additives. The graph shows that copper and aluminum have the lowest onset time followed by magnesium nitrate hexahydrate, ethanol and then sodium chloride. For 0.01 additive mass fraction, the onset time decreased by 25 minutes for copper and aluminum when compared to

refrigerant clathrate without additive. This is an improvement of 71%. Magnesium nitrate hexahydrate decreased the time by 20 minutes while ethanol reduced it by 10 minutes showing improvement of 57% and 28% respectively. Sodium chloride maintained the onset time. At high additive concentrations, onset time decreased by 25 minutes for copper and aluminum. For magnesium nitrate hexahydrate, the improvement is of 15 minutes. For ethanol, the clathrate formation time increased to above 25 minutes while for sodium chloride, the increase is of 30 minutes.

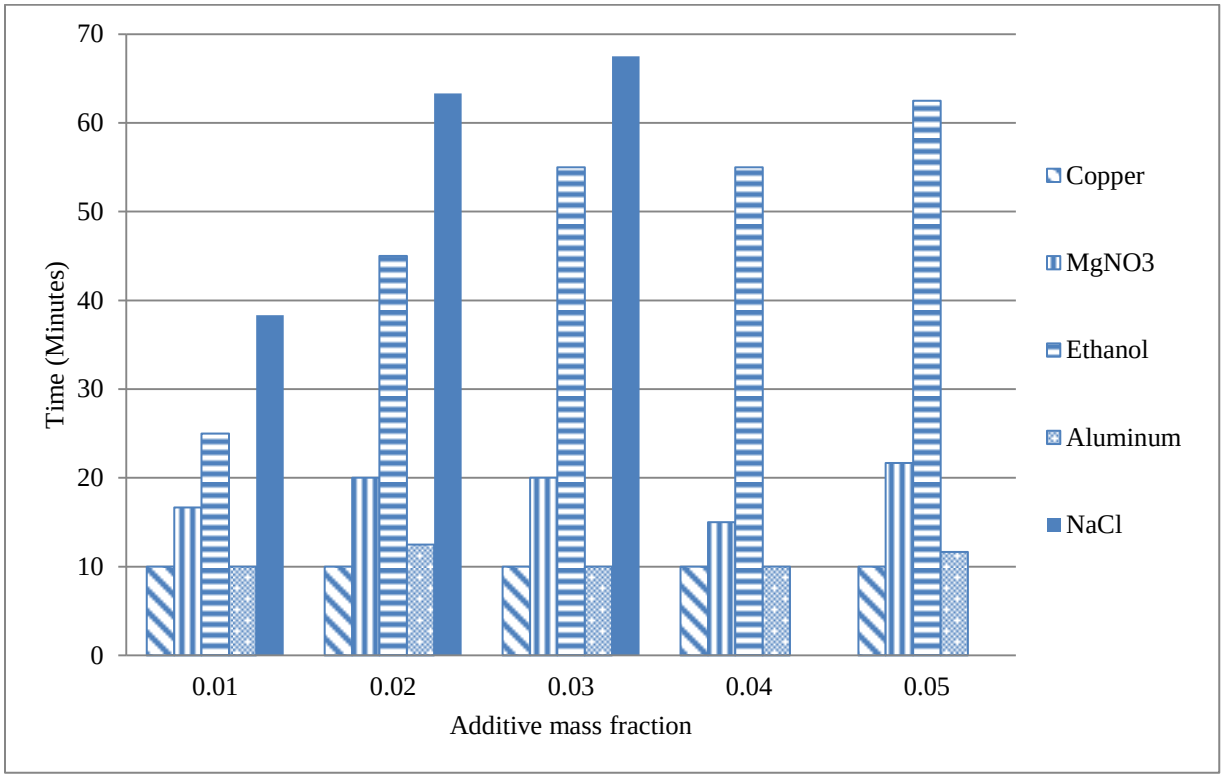

Figure 7.19 Onset time comparison between different additives

Figure 7.20 shows the end set time for R134a clathrate with five tested additives. The graph shows that magnesium nitrate hexahydrate has the lowest end set time

followed by copper ethanol, aluminum and then sodium chloride. For 0.01 additive mass fraction, the end set time decreased by 35 minutes for magnesium nitrate hexahydrate and 15 minutes for copper. It comes out to be an improvement of 55% for magnesium nitrate hexahydrate and 24% for copper. Ethanol and aluminum maintained the end set time relatively the same as the base R134a clathrate. Sodium chloride increased the end set time by 10 minutes. At high additive concentrations, the end set time decreased by 20 minutes for magnesium nitrate hexahydrate showing an improvement of 28% for charging time. All the other additives either maintained the end set time or increased it.

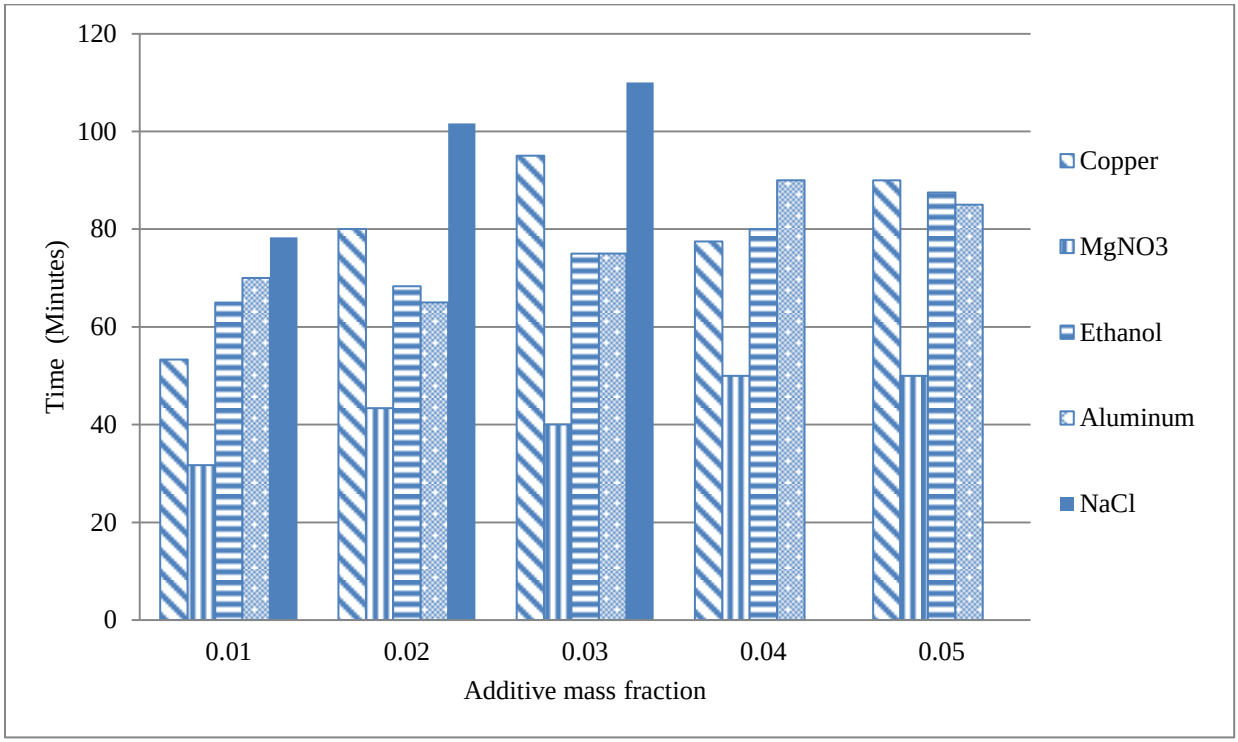

Figure 7.20 End set time comparison between different additives

Figure 7.21 compares the end set time differences between base PCM and PCMs with additives. All the PCMs with additives are compared with the base PCM for their

end set charging times. Negative time shows that the charging time is reduced while positive time shows that the charging time increased. Magnesium nitrate hexahydrate reduced the time the most by 38 minutes while sodium chloride increased the charging time with 8 minutes. It must be noted that reduced charging times do not necessarily mean it is the best additive. The PCM structure plays an important role in determining an additive's effectivity.

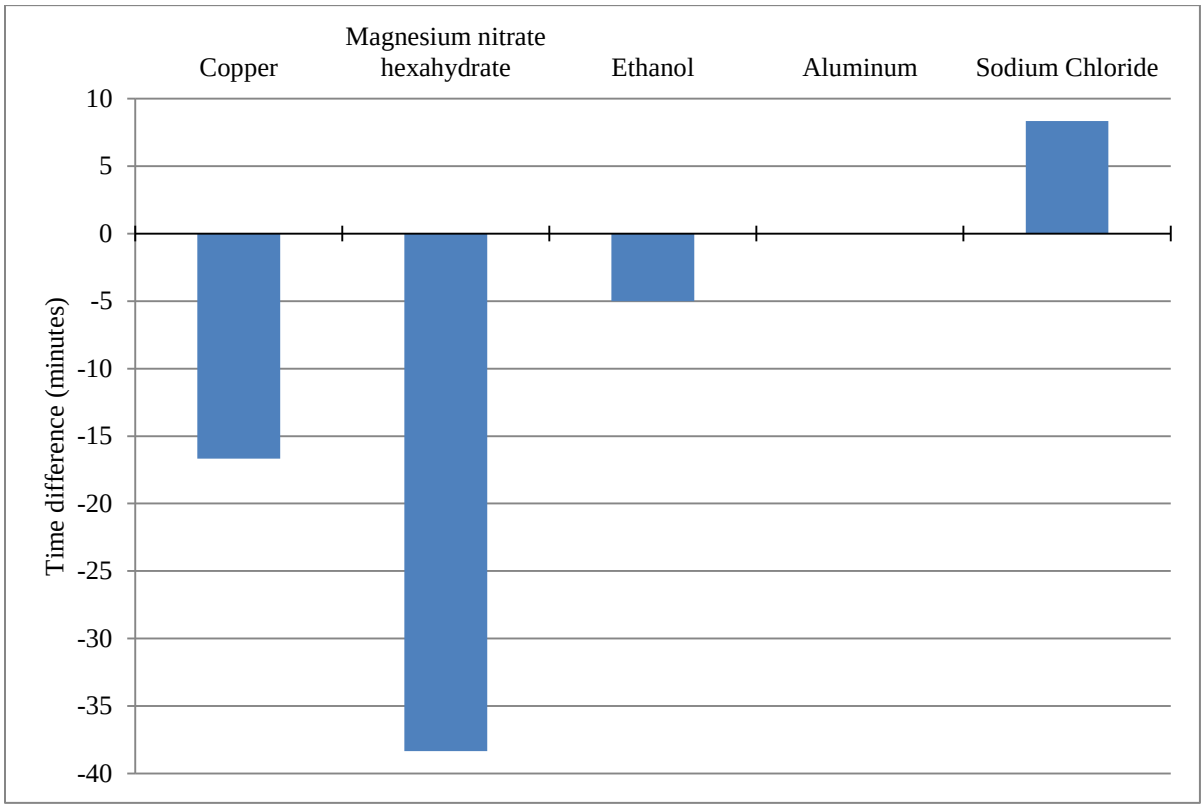

Figure 7.21 End set time difference between base PCM and PCMs with additives

7.3.1 Development of Charging Time Correlations

The trend of charging time with respect to additive type and additive mass fraction is important to study. In this regard, correlations are developed to predict the charging times

of each PCM. These correlations are derived for onset and end set times as studied and illustrated in Figures 7.14 to 7.18. These correlations depict the trend observed during the charging process of R134a clathrate having the additives mass fractions of 0.01, 0.02, 0.03, 0.04 and 0.05. The sodium chloride is the only exception as it did not form the clathrate for 0.04 and 0.05 so the correlation is limited to 0.03 mass fraction for sodium chloride additive. For each additive, the charging time "t", in minutes, can be related to additive mass ratio '*w*' as follows:

For Copper:

Onset: $t = 10$ (Constant) (7.1)

$R^2 = 0.557$ (7.1a)

End set: $t = -46301\ w^2 + 3493.6\ w + 25.382$ (Second order polynomial) (7.2)

$R^2 = 0$ (7.2a)

For Magnesium Nitrate Hexahydrate:

Onset: $t = 65.16\ w + 16.941$ (Linear relation) (7.3)

$R^2 = 0.5099$ (7.3a)

End set: $t = -9184.3\ w^2 + 979.17\ w + 23.961$ (Second order polynomial) (7.4)

$R^2 = 0.0591$ (7.4a)

For Ethanol:

Onset: $t = -25753\ w^2 + 2384.6\ w + 5.5$ (Second order polynomial) (7.5)

$R^2 = 0.8308$ (7.5a)

End set: t = 571.74 w + 57.913 (Linear relation) (7.6)

R^2 = 0.8074 (7.6a)

For Aluminum:

Onset: t = 11.154 (Constant) (7.7)

R^2 = 0.622 (7.7a)

End set: t = 519.23 w + 61.346 (Linear relation) (7.8)

$R^2 = 2x10^{-30}$ (7.8a)

For Sodium Chloride:

Onset: t = -104167 w^2 + 5625 w - 7.5 (Second order polynomial) (7.9)

R^2 = 0.7265 (7.9a)

End set: t = -75000 w^2 + 4583.3 w + 40 (Second order polynomial) (7.10)

R^2 = 0.6944 (7.10a)

7.3.2 Development of Heat Transfer Correlations

The trend of charging times with respect to additive mass fractions also helps determine the overall heat transfer correlations. Heat transfer correlations are prepared to predict unknown values for each PCM. These correlations are derived from section 7.4.1 for end set times.

Starting with the basic heat transfer governing equation

$\dot{Q} = U\ A\ \Delta T$ (7.11)

where U is the heat transfer coefficient with units $(\frac{W}{m^2\ K})$.

For each additive, the charging energy can be related to additive mass ratio '*w*' as follows:

For Copper:

$$U = \frac{\dot{Q}\,\Delta t}{A\,\Delta T\left[-46301\left(\frac{m_a}{m_{PCM}}\right)^2 + 3493.6\left(\frac{m_a}{m_{PCM}}\right) + 25.382\right]} \tag{7.12}$$

For Magnesium Nitrate Hexahydrate:

$$U = \frac{\dot{Q}\,\Delta t}{A\,\Delta T\left[-9184.3\left(\frac{m_a}{m_{PCM}}\right)^2 + 979.17\left(\frac{m_a}{m_{PCM}}\right) + 23.961\right]} \tag{7.13}$$

For Ethanol:

$$U = \frac{\dot{Q}\,\Delta t}{A\,\Delta T\left[571.74\left(\frac{m_a}{m_{PCM}}\right) + 57.913\right]} \tag{7.14}$$

For Aluminum:

$$U = \frac{\dot{Q}\,\Delta t}{A\,\Delta T\left[519.23\left(\frac{m_a}{m_{PCM}}\right) + 61.346\right]} \tag{7.15}$$

For Sodium Chloride:

$$U = \frac{\dot{Q}\,\Delta t}{A\,\Delta T\left[-75000\left(\frac{m_a}{m_{PCM}}\right)^2 + 4583.3\left(\frac{m_a}{m_{PCM}}\right) + 40\right]} \tag{7.16}$$

7.4 Results of Charging Times at Different Aspect Ratio

Figure 7.22 shows the onset times for square container for two different PCMs at two different aspect ratios. The two different PCMs are R134a clathrate without additive and R134a clathrate with 0.01 mass fraction ethanol additive. Ethanol additive is used for this study since it tends to mix well with the clathrate and forms hard solid structure. The graphs show the onset freezing time of the PCMs. Graphs show that increasing the aspect ratio lowers the freezing onset time irrespective of the constituents of the PCMs.

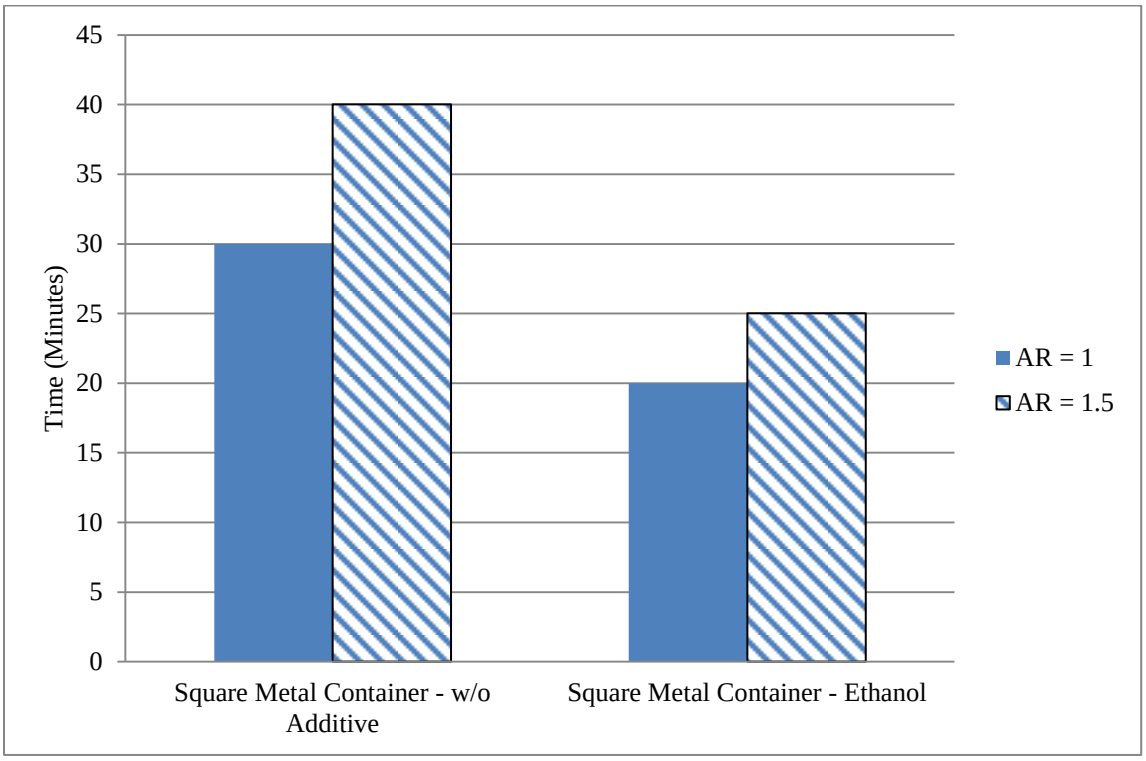

Figure 7.22 Onset times for square container for two different PCMs at two different aspect ratios

7.5 Discharge Test Results

The experiments are conducted to determine discharge capability of the PCMs. The PCMs are discharged using hot air to find out their discharge capacity. Furthermore, a battery jacket is made to cool down the battery using the PCMs. Cooling down the battery using the PCMs shows the potential application.

7.5.1 Results of Discharging using Hot Air

Hot air is used to find the cooling capacity of each PCM. Table 7.10 shows the parameters and values used for the discharge experimentations.

Table 7.10 Values of parameters used in experimental study

Parameters	Symbol	Value
Discharge air mass flow rate	$\dot{m_{air}}$	0.05 kg/s
PCM mass	m_{PCM}	0.08 kg
Specific heat of air	C_{Pair}	1005 J/kg K
Incoming air temperature	T_{in}	315 K
Exiting air temperature	T_{out}	311 K
Battery cool down temperature	-	299 K
Ambient temperature	T_{amb}	298 K

Discharge tests are conducted on the PCM having R134a clathrate with and without additives. Two temperature sensors are inserted in the glass tube to record the temperature of two different locations inside the tube. These temperature readings are later used to find the thermal properties of the PCMs. Two set of tests are conducted for each PCM where the readings are taken after one minute interval. Table 7.11 shows the temperature readings taken for each PCM.

Table 7.11 Temperature readings for each PCM

276 K Discharge for 35% R134a refrigerant				
Times (minutes)	Air Temperature ^{o}C	r_1 Temperature ^{o}C	r_2 Temperature ^{o}C	Remarks
	PCM without additive			
0	39	3.1	3.3	
3	42.2	14.3	14.8	discharged
0	40.1	3.1	4.1	
4	42.3	9.3	15.7	discharged
	0.01 Copper			
0	38.4	3	3.5	
3	41.4	10	15.2	discharged
0	40.1	3.4	4.3	
4	41.7	15.8	16.9	discharged
	0.01 Ethanol			
0	39.4	4.1	3.8	
8	42.1	15.4	16	discharged
0	39.1	4.2	4.3	
8	42.2	20.9	22.5	discharged
	0.01 Magnesium nitrate			
0	39.5	4.2	4.2	
2	41.9	10.7	12.9	discharged
0	39.8	3.6	4.5	
4	42.7	17.9	20	discharged
	0.01 Sodium chloride			
0	39.5	3.8	4.4	
3	42.5	13.6	15	discharged
0	39.3	3.4	3.8	
3	42.2	13.7	14.6	discharged
	0.01 Aluminum			
0	39.4	2.8	3.3	
4	42	13.3	15.7	discharged
0	40.1	3.6	4.2	
5	42.6	15.6	17.4	discharged

Figure 7.23 shows the temperature readings recorded during the discharging process of the PCM without additive. The discharge is done using hot air while two probes recorded the inside temperature. One of them is core temperature reading which is at the cross-sectional center of the tube and the "out" which is 14 mm away from the core. Core takes longer to heat up as it is further away from the hot air. Compared to charging, discharging takes shorter since the temperature difference for discharging is greater than that of charging. The temperature in the tube almost gradually increases until the entire PCM is melted. There is a small drop between 1 minute and 2 minute mark where the temperature increase slowed down. This slow increase in temperature shows that the PCM is going through the phase change and most of the heat provided by the hot air is being converted into changing the phase; i.e. latent heat. After 2 minute mark, the temperatures at both the stations start increasing. The PCM discharged in 3 minutes reaching 15 degree temperature.

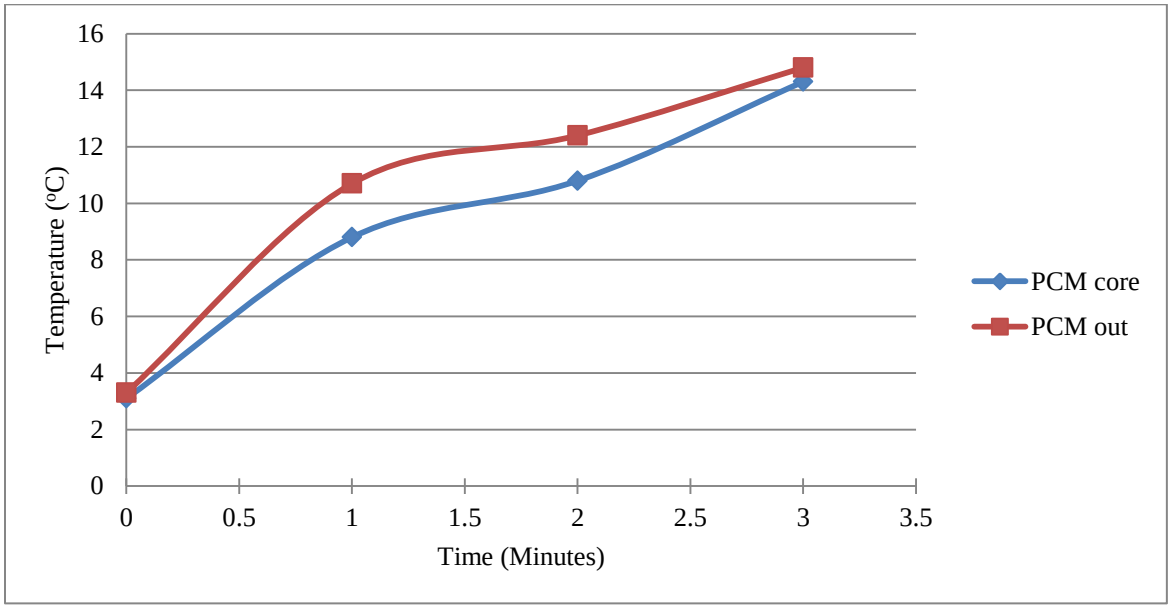

Figure 7.23 Temperature readings during the discharging process of the PCM without additive

Figure 7.24 shows the temperature readings recorded during the discharging process of the PCM with copper additive. Core takes longer to heat up as it is further away from the hot air. Compared to charging, discharging takes shorter since the temperature difference for discharging is greater than that of charging. The temperature in the tube almost gradually increases until the entire PCM is melted. There is a small drop between 1 minute and 2 minute mark where the temperature increase slowed down. This slow increase in temperature shows that the PCM is going through the phase change and most of the heat provided by the hot air is being converted into changing the phase; i.e. latent heat. After 2 minute mark, the temperatures at both the stations start increasing. The PCM discharged in 3 minutes reaching 15 degree temperature. Copper additive showed same discharge time and cooling temperature as the base PCM. So when comparing their usefulness, their charging time determines which one is better.

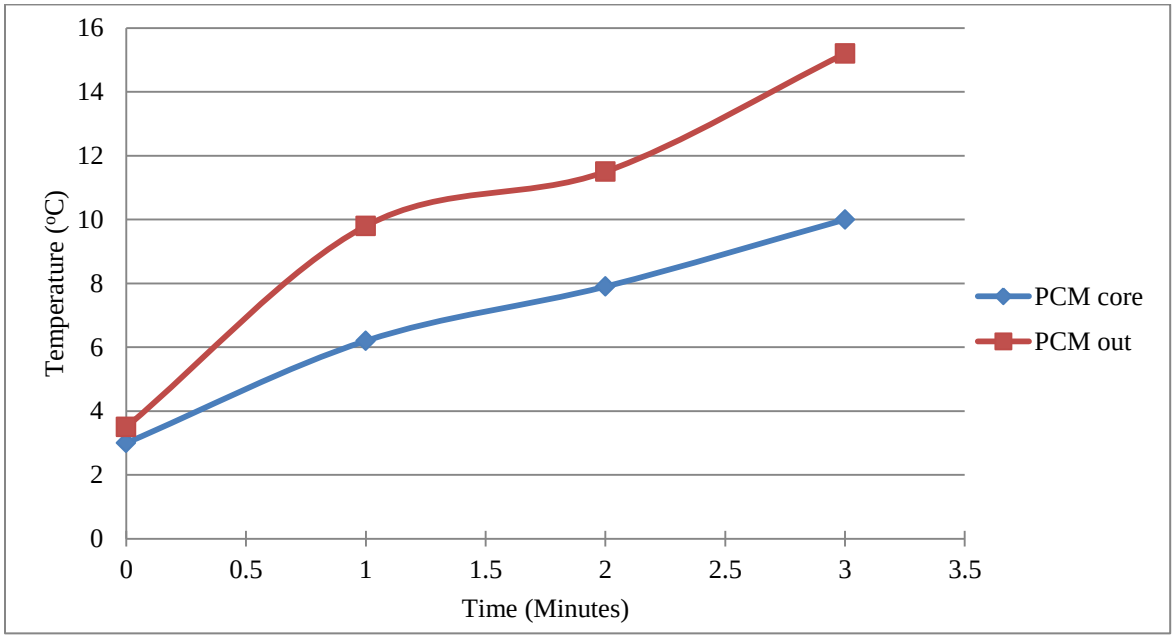

Figure 7.24 Temperature readings during the discharging process of the PCM with copper additive

Figure 7.25 shows the temperature readings recorded during the discharging process of the PCM with ethanol additive. The temperature in the tube almost gradually increases until 1 minute mark. After that, the ethanol PCM temperature does not change and remain at around 10 degrees until the 6 minute mark. This no change in temperature shows that the PCM is going through the phase change and most of the heat provided by the hot air is being converted into changing the phase; i.e. latent heat. It takes longer for ethanol PCM since its structure is hard solid, taking longer to completely melt. Ethanol PCM has the highest discharge time of 8 minutes. It also has the most latent heat absorbed hence it took longest to change the temperature.

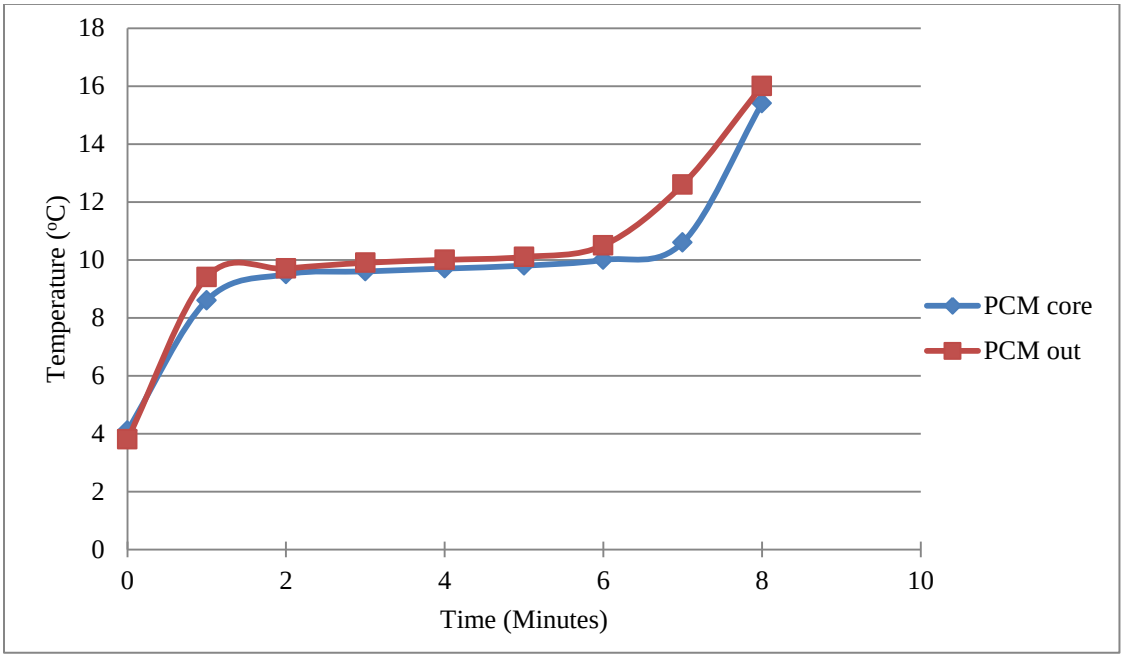

Figure 7.25 Temperature readings during the discharging process of the PCM with ethanol additive

Figure 7.26 shows the temperature readings recorded during the discharging process of the PCM with magnesium nitrate hexahydrate additive. The temperature in the

tube almost gradually increases until the entire PCM is melted. There is a slight drop between 1 minute and 1.5 minute mark where the temperature increase slowed down. This slow increase in temperature shows that the PCM is going through the phase change and most of the heat provided by the hot air is being converted into changing the phase; i.e. latent heat. After 2 minute mark, the temperatures at both the stations start increasing. Magnesium nitrate hexahydrate PCM has a small time span for no temperature change period since the clathrate structure is very soft hence it does not store a lot of cold energy and melts easily. The PCM discharged in 3 minutes reaching 15 degree temperature. Magnesium nitrate hexahydrate PCM showed same discharge time as the base PCM. So when comparing their usefulness, their charging time determines their respected effectiveness.

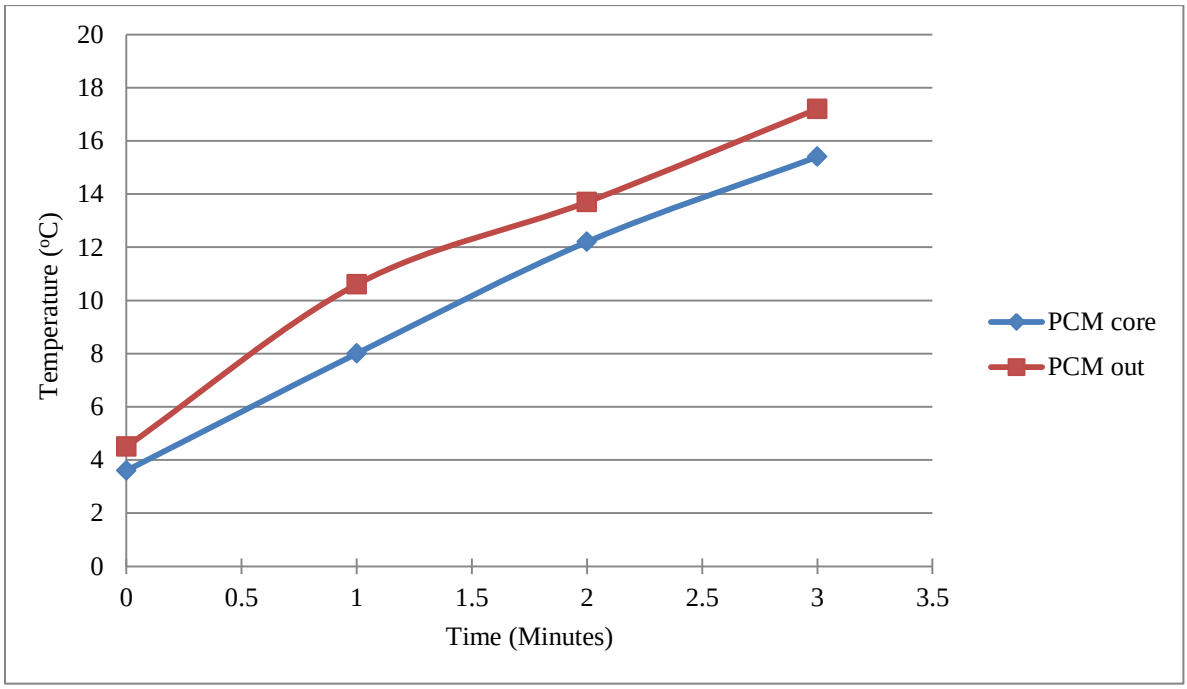

Figure 7.26 Temperature readings during the discharging process of the PCM with magnesium nitrate hexahydrate additive

Figure 7.27 shows the temperature readings recorded during the discharging process of the PCM with sodium chloride additive. The temperature in the tube almost gradually increases until the entire PCM is melted. Once again, there is a slight drop between 1 minute and 2 minute mark where the temperature increase is slowed down. This slow increase in temperature shows that the PCM is going through the phase change and most of the heat provided by the hot air is being converted into changing the phase; i.e. latent heat. After 2 minute mark, the temperatures at both the stations start increasing. Sodium chloride PCM has a small time span for no-temperature-change period since the clathrate structure is very soft hence it does not store a lot of cold energy and melts easily. The PCM discharged in 3 minutes reaching 15 degree temperature. Sodium chloride PCM showed same discharge time as the base PCM hence its charging time determines if sodium chloride, as an additive, is effective or not.

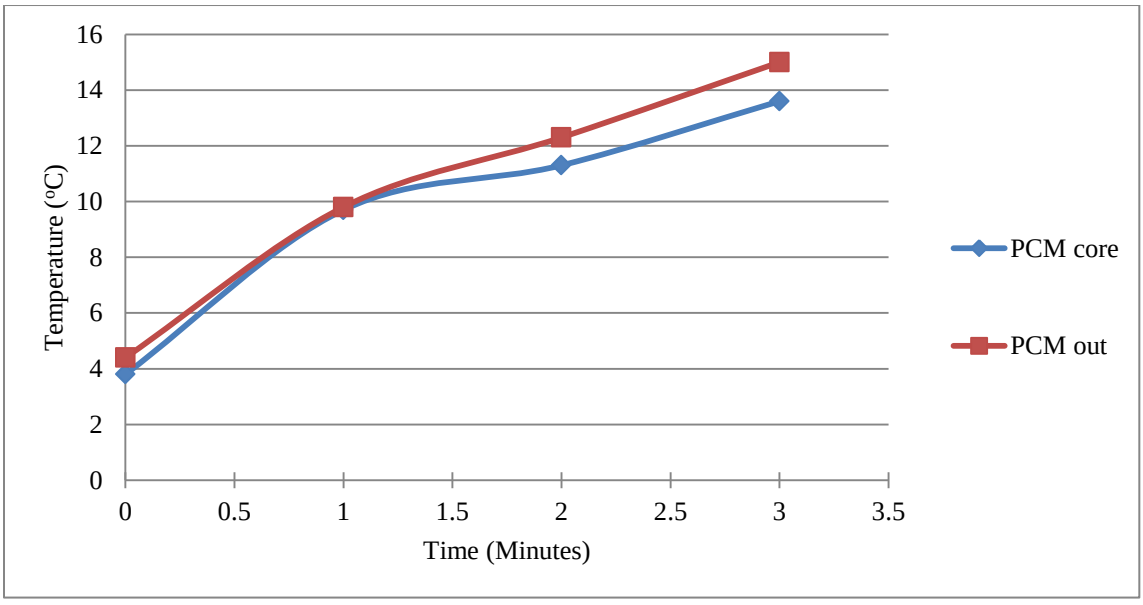

Figure 7.27 Temperature readings during the discharging process of the PCM with sodium chloride additive

Figure 7.28 shows the temperature readings recorded during the discharging process of the PCM with aluminum additive. The temperature in the tube increases for the initial first minute. A slight drop in temperature increase is observed between 1 minute and 2.5 minute mark. This slow increase in temperature shows that the PCM is going through the phase change and most of the heat provided by the hot air is being converted into changing the phase. After 2.5 minute mark, the temperatures at both the stations start increasing. Aluminum PCM has 1.5 minute time span for no temperature change period where latent heat is absorbed. This latent heat absorption period for aluminum PCM is superior to salt additive PCMs but inferior to ethanol PCM. The PCM discharged in 4 minutes reaching 15 degree temperature. Aluminum PCM showed better discharge time as the base PCM hence it showed to have better potential for cooling applications compared to base PCM.

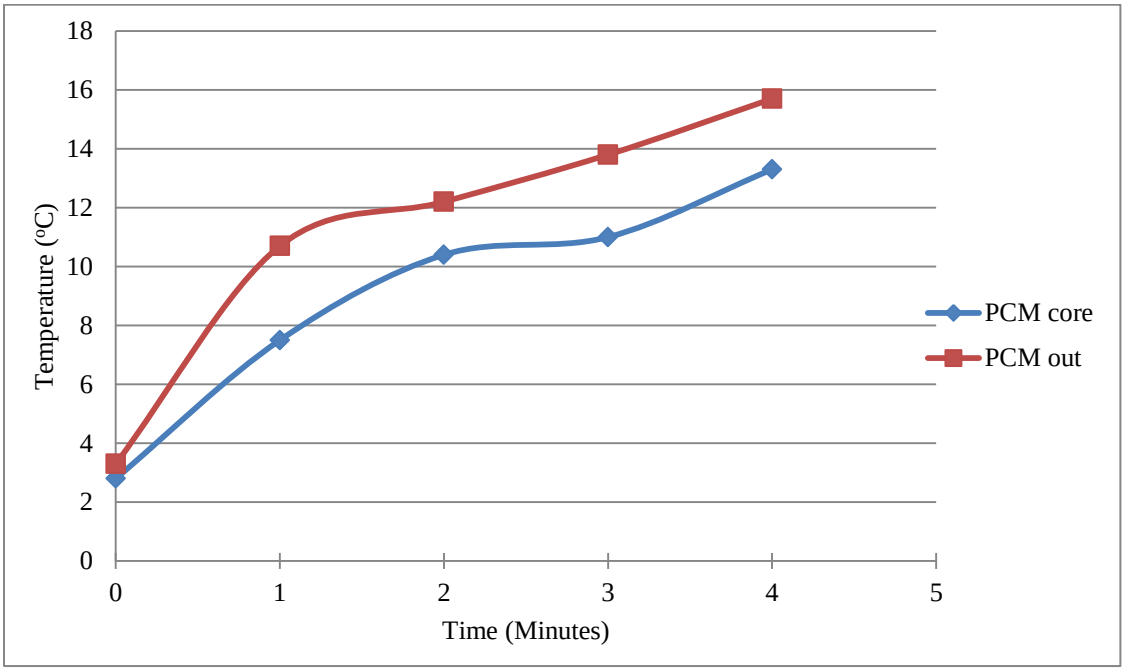

Figure 7.28 Temperature readings during the discharging process of the PCM with aluminum additive

Figure 7.29 shows the time each PCM takes to completely melt and reach 15 ^{o}C. Hot air at 42 ^{o}C and 50 g/s is blown at the tube containing the PCMs. Ethanol additive lasts the longest for 435 seconds followed by aluminum, copper, base clathrate and sodium chloride. Magnesium nitrate based PCM lasts the shortest; for only 180 seconds. Ethanol additive makes a strong solid structure with the refrigerant clathrate hence it is able to release the cool energy longer. Aluminum and copper based PCMs also form relatively hard solid structure with large crystals. Since the additives settle at the bottom of the tube and do not mix well with the clathrate, their impact on discharge is not significant. Sodium chloride based PCMs are also mildly solid structures and it mixes well with the clathrate. Sodium chloride delays the clathrate formation and leave gaps in the clathrate structures. On the other hand, magnesium nitrate hexahydrate makes a soft fluffy clathrate structure which discharges early.

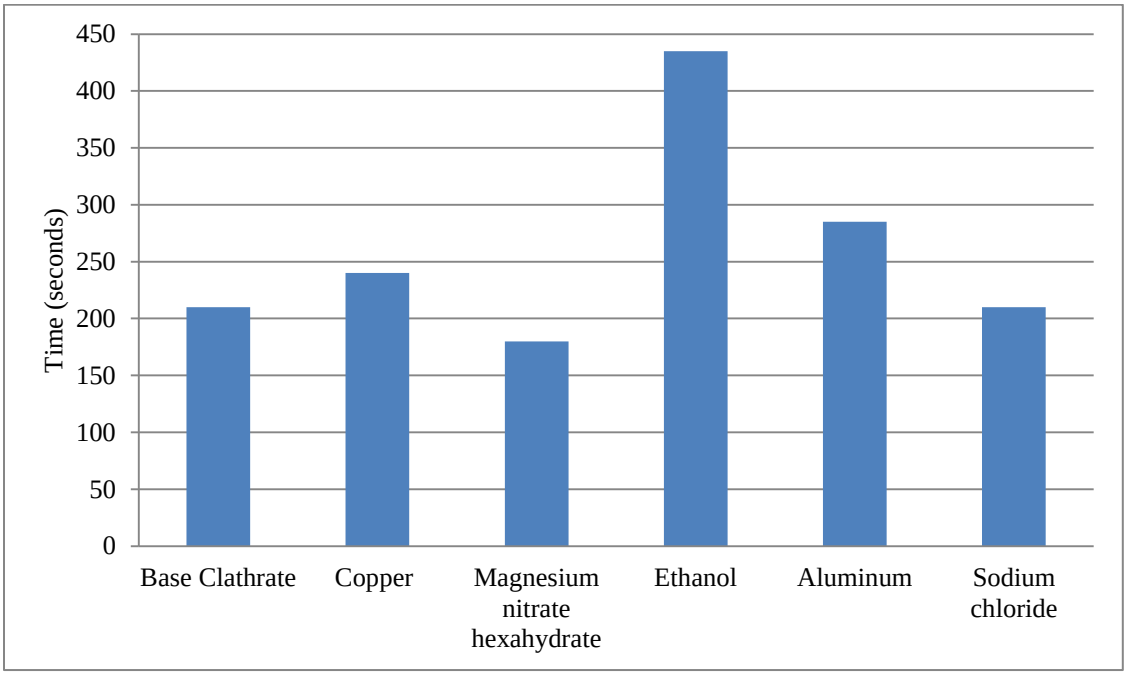

Figure 7.29 Illustration of time to liquefy for each PCM

7.5.2 Results of Battery Cooling Tests

Figure 7.30 shows the total time battery takes to cool down using each PCM type. The pattern bars in the above graph shows the averaged value of the time readings for each case. The battery is considered to have cooled down and ready to be charged again when the battery temperature reaches 26 ^{o}C. When the battery jacket is empty, it tends to prevent battery cooling compared to the case when the battery is exposed to ambient air. The results show that PCM with ethanol additive cools down the battery fastest with copper, aluminum and no additive PCM have similar cooling time. Salt additives have higher cooling time compared to other additives because of their mildly soft structure and low cool energy storage capacity. It is interesting to note that no additive base clathrate PCM performs very well, compared to other PCMs, while cooling the battery.

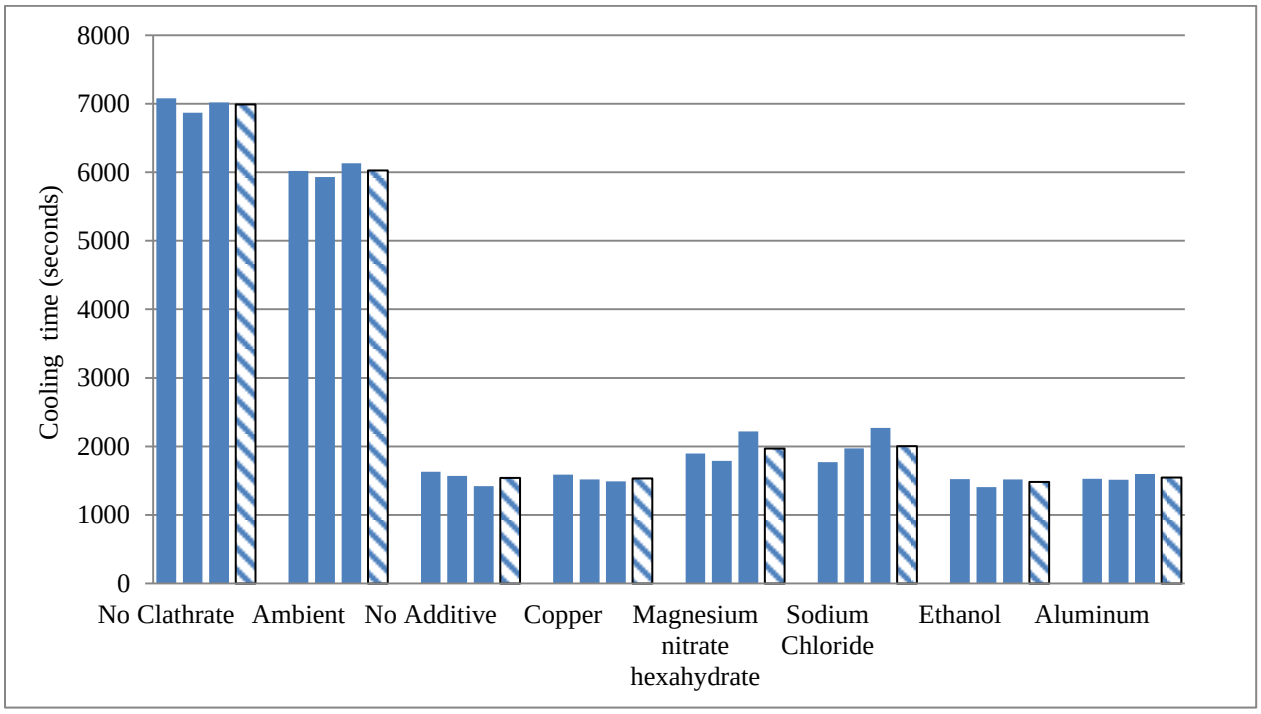

Figure 7.30 Total battery cooling down time using each PCM

Figure 7.31 shows the battery temperature at the time when the battery reaches the cutoff voltage. The battery temperature at cutoff is recorded for each case. The pattern bars in the above graph shows the averaged value of the temperature readings for each case. It is important to find this temperature since it effects the total cooling time of the battery. It is also of significance since a cooler battery can be operated longer or more power burst can be extracted from it. The results show that empty jacket with no clathrate in it tends to heat up the battery when compared to the case when the battery is exposed to ambient air. This heating of battery can be associated due to the heat being trapped in the jacket with little dissipation to the surroundings. PCM with ethanol and aluminum additive helps battery maintain the lowest temperature. PCMs with salt additives keep the battery temperature higher than the other PCMs. Overall; the PCMs reduce the battery temperature by approximately 6 ^{o}C.

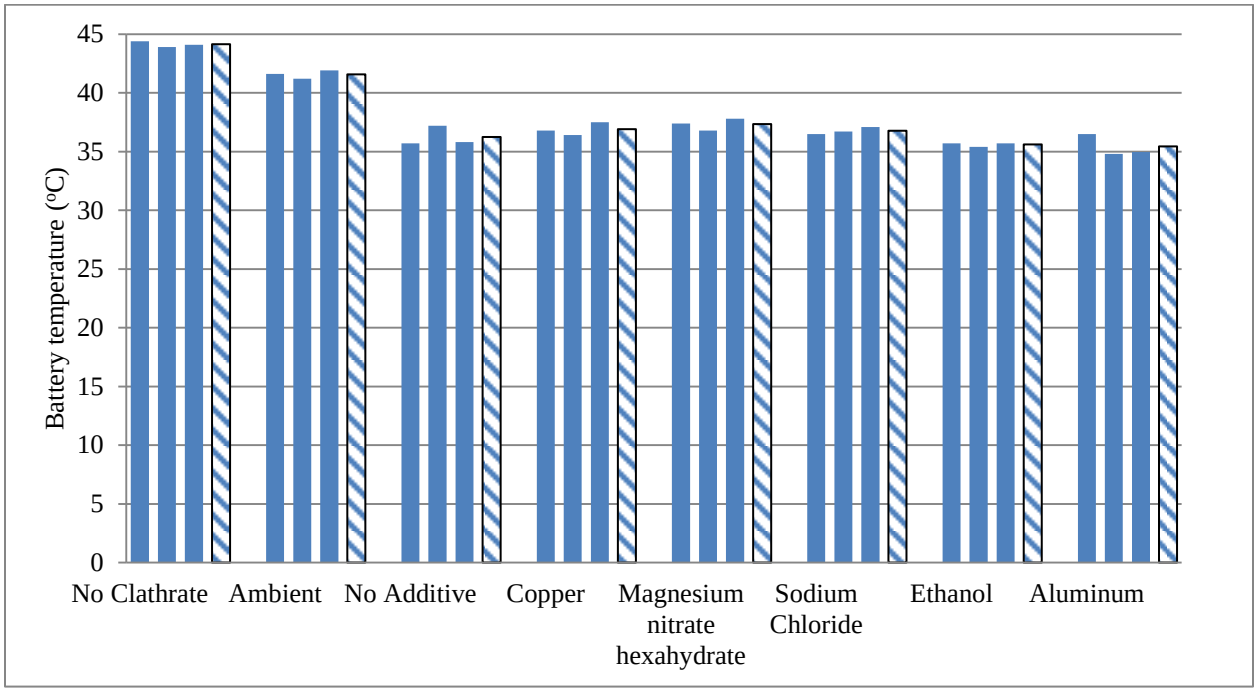

Figure 7.31 Battery temperature at cutoff voltage

Figure 7.32 shows the battery run times until the battery reaches the cutoff voltage. For the “Ambient” case, no jacket is used as it is desired for the battery to be cooled through surrounding air. The pattern bars in the above graph shows the averaged value of the time readings for each case. Ethanol and aluminum based PCMs reduced the run time to around 380 seconds. Jacket without clathrate case increased the run time to 510 seconds. The results show that cooling down the battery reduces its run time while heating it up, the “No clathrate” case, improves its run time. Under low temperatures, the internal resistance increases hence the battery yields low run time. Whereas, under higher temperature, it gives out higher run time because of reduced internal resistance. However, heating up the battery shortens the life span of the battery.

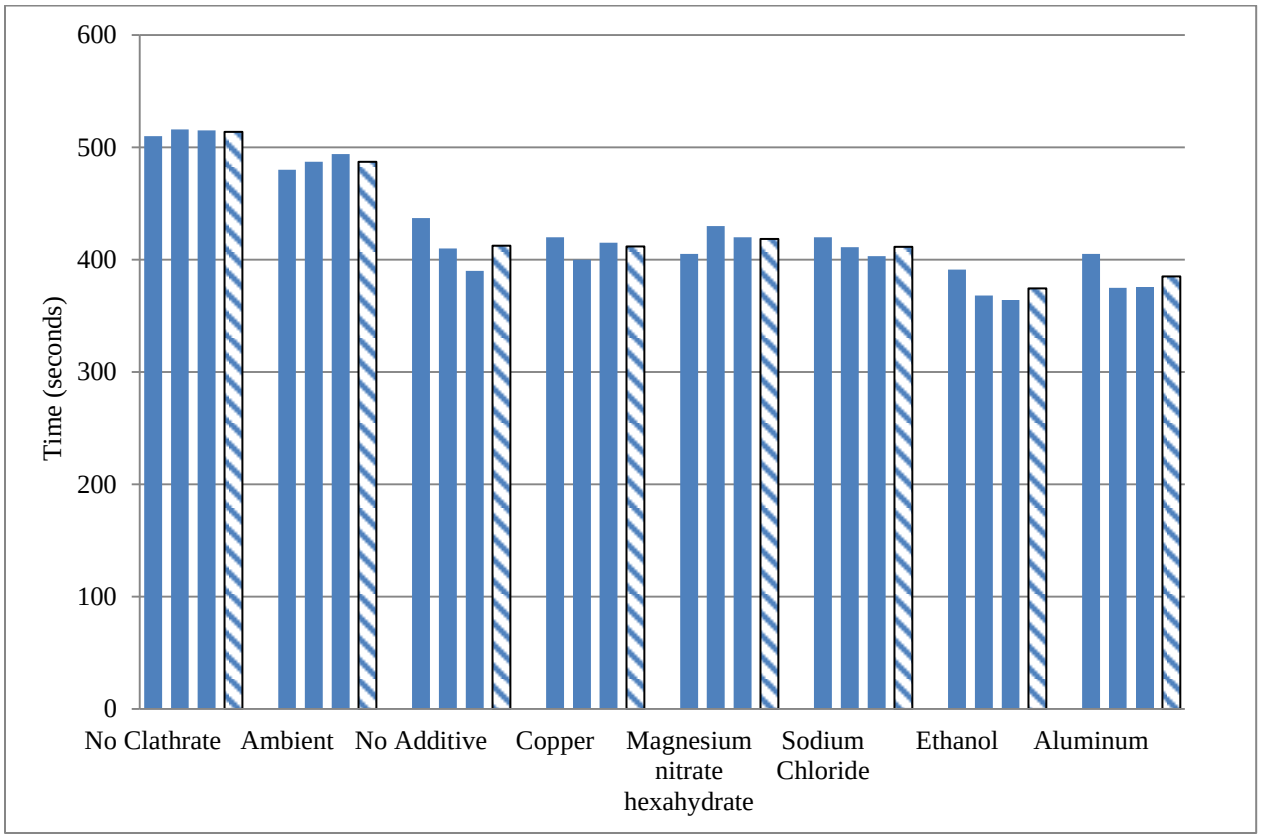

Figure 7.32 Battery run times until the cutoff voltage

7.6 Results of Calculations of Thermal Properties

Further experiments are conducted to determine the thermal properties of PCM. Refrigerant, water and the desired additive are mixed in a pressurized glass tube to form PCMs. Refrigerant R134a is used as the refrigerant to form clathrate with distilled water. The refrigerant mass fraction of 0.35 is used as it tends to be the most optimized fraction for clathrate formation. Five different materials are used as additives. The additives are copper particles, aluminum particles, ethanol, sodium chloride and magnesium nitrate hexa-hydrate. The mass fraction of the additives is 0.01. Figure 7.33 shows the temperature readings against time for the water bath. Bath stability test is conducted to find out the steady state temperature for bath at the given voltage. The graph shows the time bath takes to reach study state is 25 minutes.

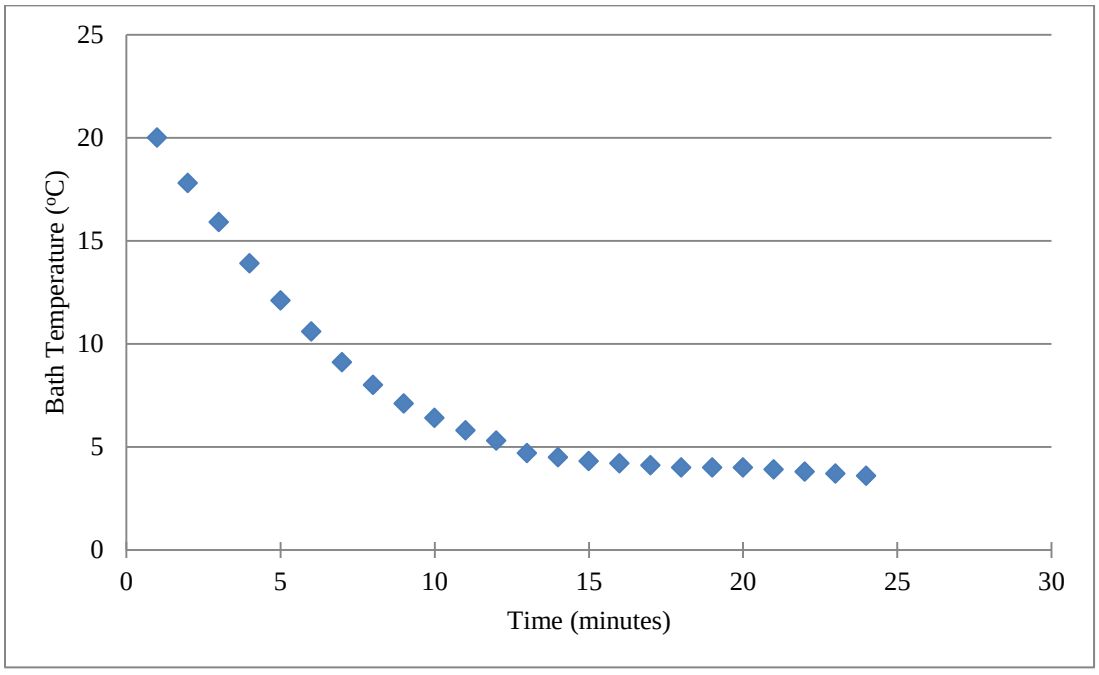

Figure 7.33 Temperature readings against time for water bath

The PCMs consists of R134a clathrate with and without additives. Thermal properties are important to determine as they determine the appropriate application of the PCM and its feasibility of use. High thermal property value means either fast charge and discharge rate or simply greater capacity to retain heat. The measured parameters used are shown in Table 7.12 below.

Table 7.12 Baseline parameters for experimental study

Parameters	Symbol	Value
Water bath mass	m_{bath}	16.24 kg
PCM mass	m_{PCM}	0.08 kg
Specific heat of distilled water [101]	C_{Pwater}	4200 J/kg K
Distance between two thermocouples	Δx	0.014 m
Density of distilled water	ρ	998 kg/m^3
Temperature of water in bath	T_{bath}	276 K
Height of the PCM inside the tube	l	0.175 m
Inner thermocouple location (core)	r_1	0.1 mm
Outer thermocouple location (out)	r_2	14 mm

7.6.1 Values of Experimental Thermal Properties

Experimental readings are taken for the temperature at two different locations, r_1 (core) and r_2 (out), inside the glass tube. The temperature readings are recorded after regular intervals during charging as well as for discharging process. Using the equations described in the Analysis section, thermal properties of the R134a clathrate with and without additives are calculated for each test.

Figure 7.34 shows the specific heat values attained through the experiments for all the tested PCMs. The values are obtained after experimental results using equation (6.2) and equation (6.3). It can be observed from the graph that additives, overall, slightly decreased the specific heat. Since water has better specific heat value than any other

tested material, PCM without additive has better specific heat value. Copper and ethanol PCMs have similar specific heat values even though their pure are not exactly the same; copper has higher. Since ethanol is liquid, it mixes well hence improves the specific heat of the PCM. Similarly, salts also mix well in the PCM hence in spite have lower specific heat values compared to metal particles, the salts perform better in improving the specific heat of the PCM. Sodium chloride has a very low specific heat capacity value which is why sodium chloride PCM has the lowest specific heat capacity.

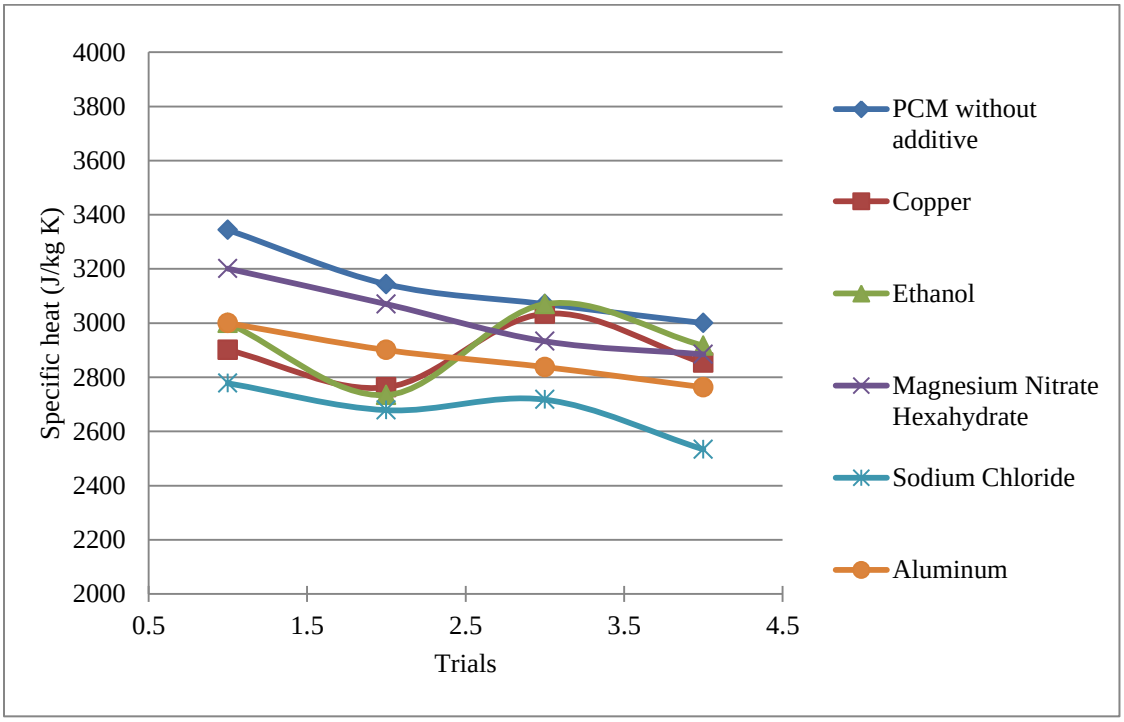

Figure 7.34 Experimental specific heat values for all the tested PCMs

Figure 7.35 shows the specific latent heat values attained through the experiments for all the tested PCMs. The values are obtained after experimental results using eq. (6.1) and eq. (6.2). It can be observed from the graph that some additives improve the specific latent heat while others drop it. Latent heat is directly related to the PCM structure type

and its grain structure. As evident from the above graph, ethanol PCM has far superior specific latent heat than any other PCM, around 67 kJ/kg. Magnesium nitrate hexahydrate PCM has the lowest specific latent heat of around 3 kJ/kg. Ethanol PCM has a strong solid structure which helps it store greater amount of cool energy than any other PCM. Ethanol also mixes well with R134a clathrate which allows it to form a homogeneous PCM without any significant gaps in the structure. On the other hand, Magnesium nitrate hexahydrate PCM has soft fluffy structure which means it does not store a lot of cool energy and discharges fast.

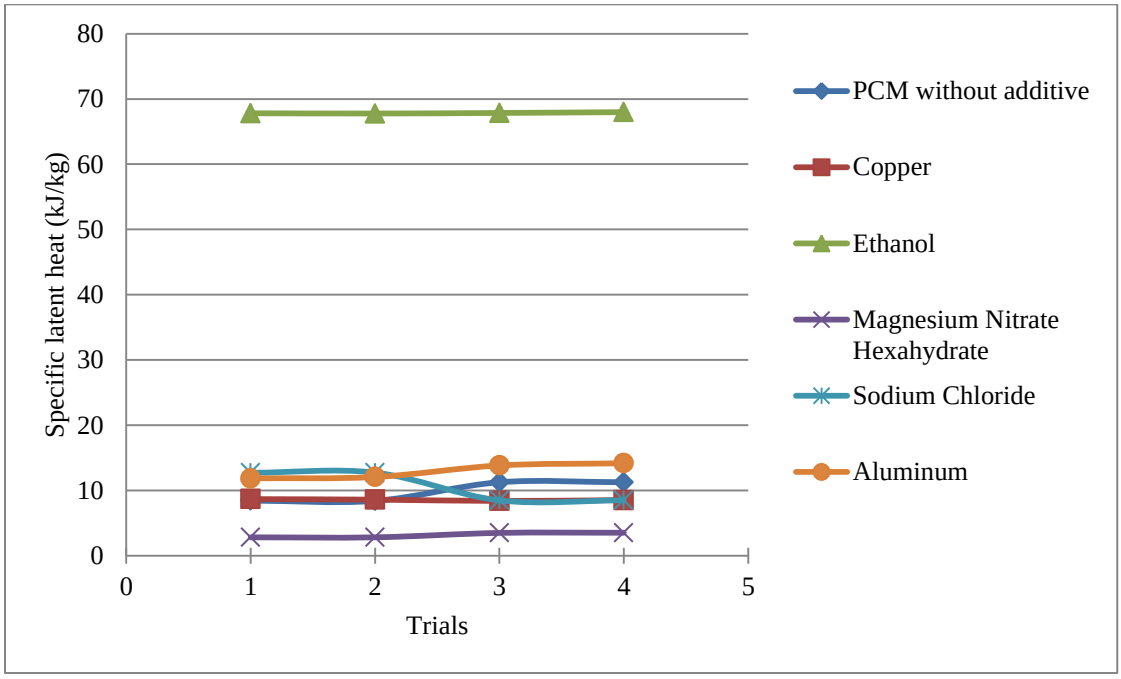

Figure 7.35 Experimental specific latent heat values for all the tested PCMs

Figure 7.36 shows the liquid phase thermal conductivity values attained through the experiments for all the tested PCMs. The values are obtained after experimental results using equation (6.2) and equation (6.4). It can be observed from the graph that

additives generally improve the liquid phase thermal conductivity. The trend is observed that followed the additive's thermal conductivity. Copper having the highest thermal conductivity as a pure species improved the thermal conductivity the most, followed by aluminum, salts and then ethanol. Thermal conductivity of metal additives is several times greater than other additives. But since they do not mix well in the PCM, the bulk thermal conductivity of the PCM does not improve as much.

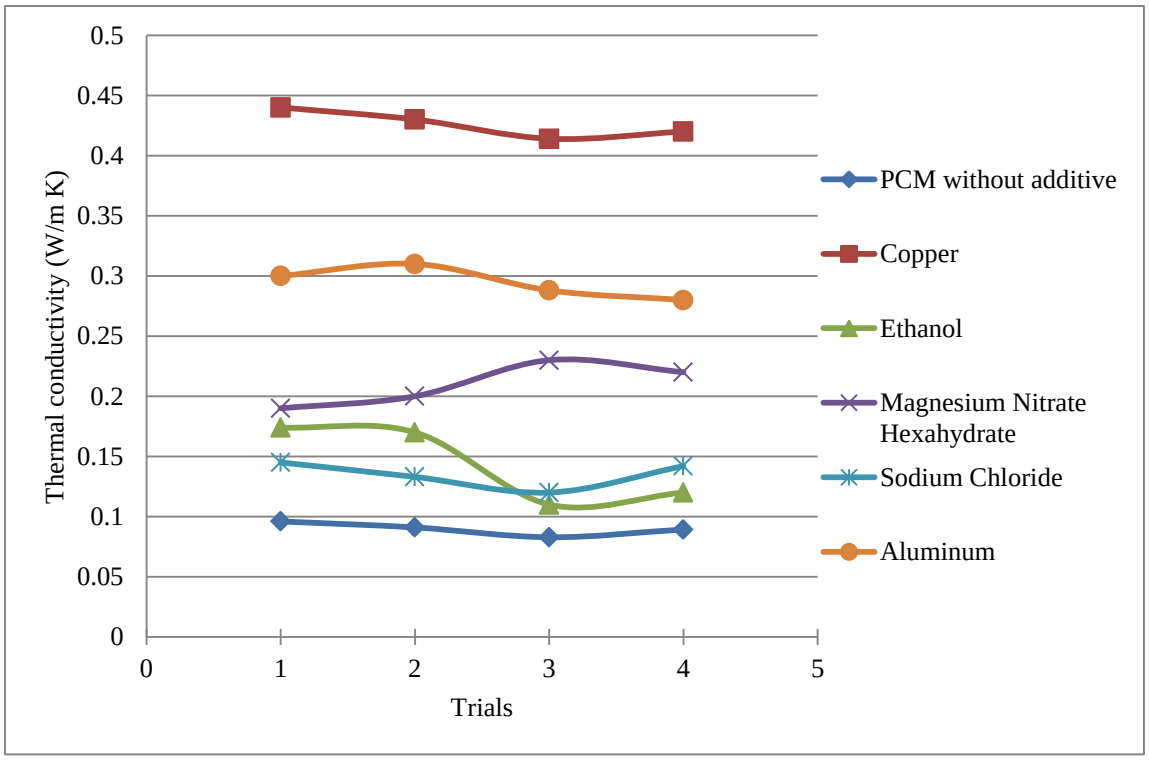

Figure 7.36 Experimental liquid phase thermal conductivity values for all the tested PCMs

Figure 7.37 shows the mushy phase thermal conductivity values obtained through the experiments for all the tested PCMs. The values are obtained after experimental results using equation (6.2) and equation (6.4). It can be observed from the graph that all

the additives improve the thermal conductivity of the base PCM except for sodium chloride. Once again, the trend is observed that followed the pure specie additive's thermal conductivity. Copper having the highest thermal conductivity as pure species improved the thermal conductivity the most, followed by aluminum, salts and then ethanol. Thermal conductivities of metal additives are several times greater than other additives. But since they do not mix as well, the bulk thermal conductivity of the PCM does not improve as significantly as it could. On the other hand, salts and ethanol mixes well in the clathrate so they yield their highest possible impact.

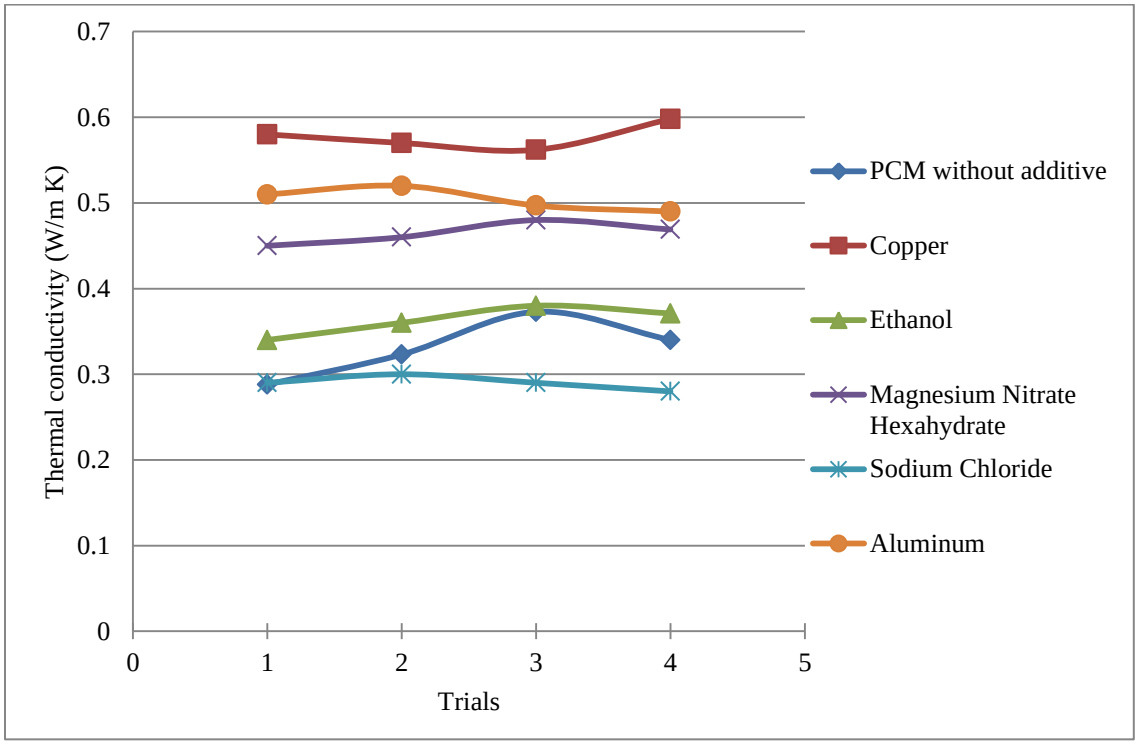

Figure 7.37 Experimental mushy phase thermal conductivity values for all the tested PCMs

Figure 7.38 shows the averaged specific heat capacity values calculated through the experiments. PCM without any additive has the highest specific heat capacity,

followed by magnesium nitrate hexahydrate, ethanol, copper and aluminum. Sodium chloride PCM has the lowest specific heat capacity value amongst the tested additives. Sodium chloride has the lowest specific heat capacity as pure species which makes the combined specific heat capacity value to be low. The PCM without any additive has a high specific heat capacity value since the total amount of water is greater there compared to any other combination. Since water has the highest specific heat capacity, this presence of extra water improves the specific heat capacity of the PCM. Metal additives do not mix well so they do not show true potential when their impact on thermal properties is observed.

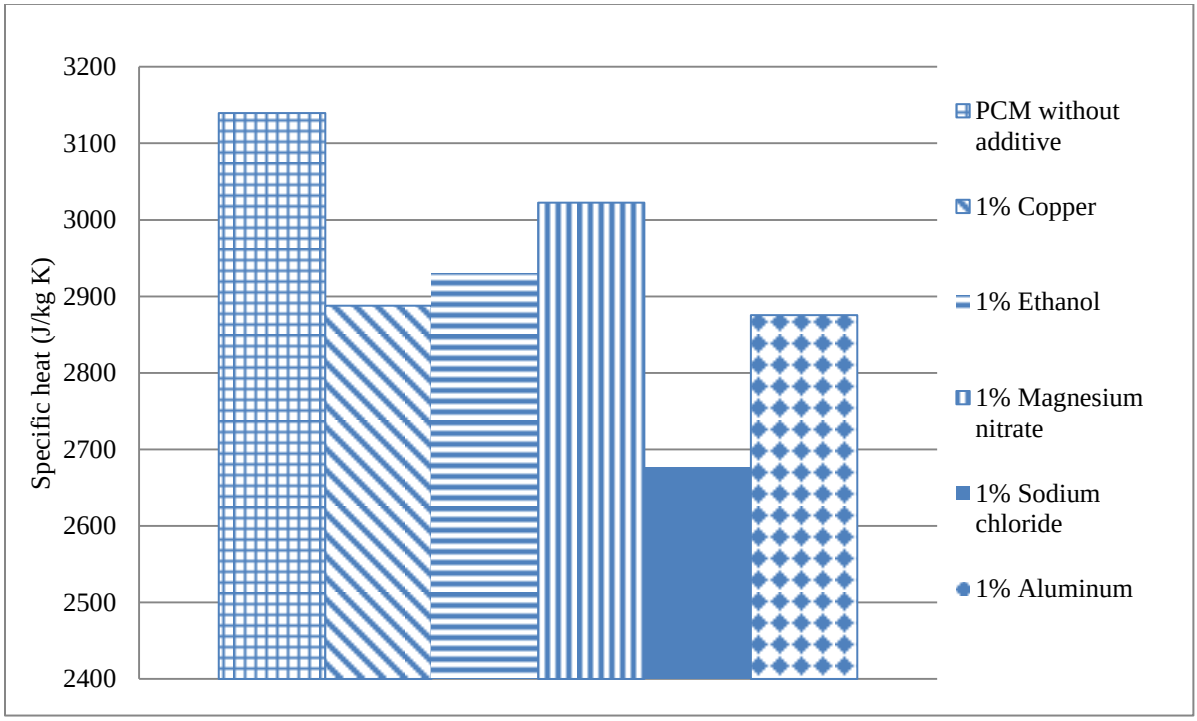

Figure 7.38 An illustration of liquid phase specific heat capacity values for PCMs with different additives

Figure 7.39 shows the thermal conductivity values of the tested PCMs calculated through the experiments. These thermal conductivity values are during the liquid phase. PCM with copper additive has the highest thermal conductivity, followed by aluminum PCM, magnesium nitrate hexahydrate PCM, ethanol PCM and sodium chloride PCM. PCM without any additive has the lowest thermal conductivity amongst all the tested PCMs. PCM with copper additive has the highest thermal conductivity because, amongst the used additives, copper has the highest thermal conductivity. This high thermal conductivity addition in the PCM makes the combined thermal conductivity high. The PCM without any additive has the lowest thermal conductivity.

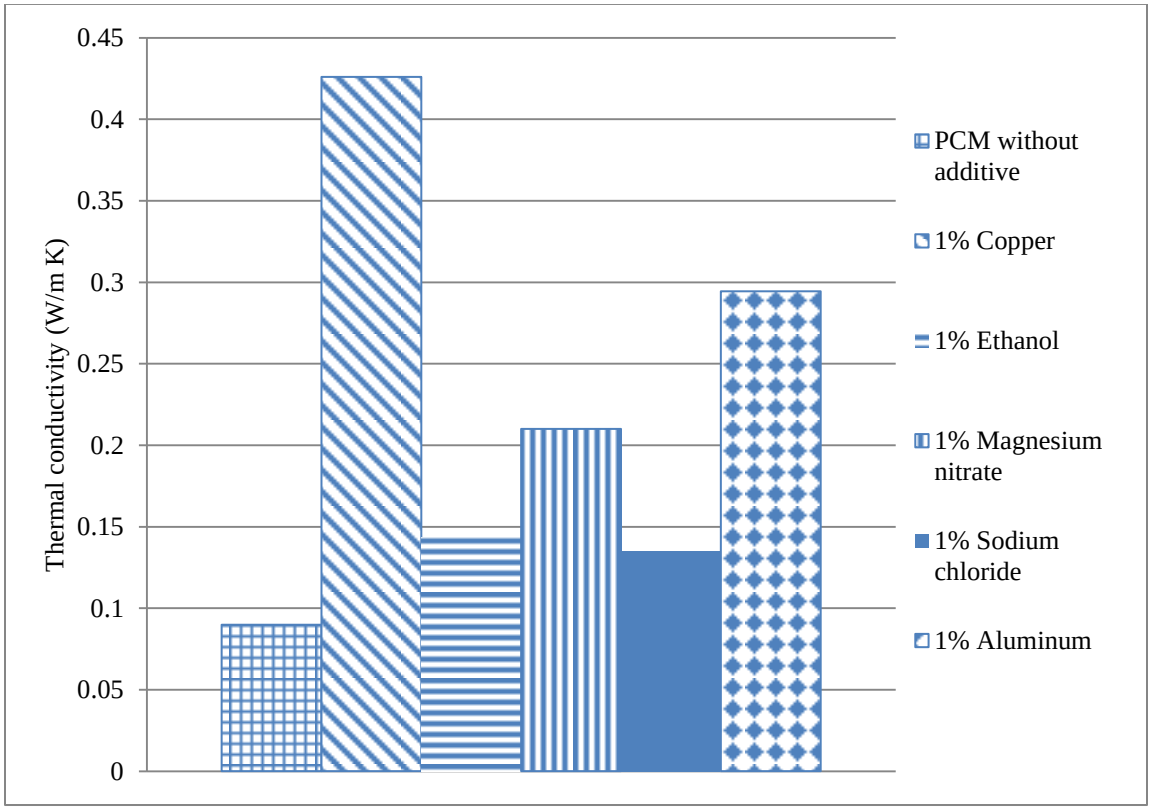

Figure 7.39 An illustration of liquid phase thermal conductivity values for PCMs with different additives

Figure 7.40 shows the thermal conductivity values of the tested PCMs during the mushy phase. The mushy phase is when the PCM is partly liquid and partly fluffy solid. PCM with copper additive has the highest thermal conductivity because of copper's high thermal conductivity and the large crystal formations during freezing. After copper PCM, aluminum PCM has the highest thermal conductivity, followed by ethanol PCM and PCM without additive. PCM with sodium chloride has the lowest thermal conductivity because of its comparative low thermal conductivity, compared to other solid additives used. The other factor for its low thermal conductivity is small crystals with gaps in between. These gaps in between gets filled with air or refrigerant gas which lowers the thermal conductivity of the PCM with sodium chloride.

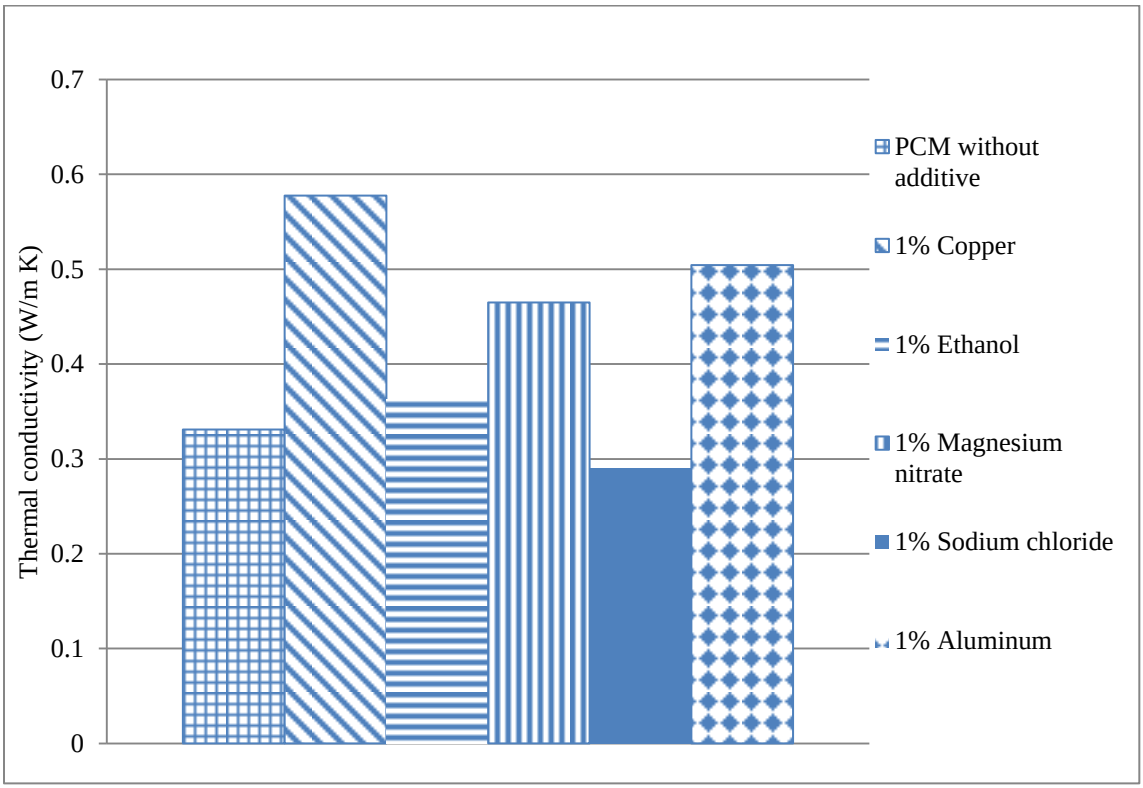

Figure 7.40 An illustration of mushy phase thermal conductivity values for PCMs with different additives

Figure 7.41 shows the specific latent heat values calculated through the experiments. The specific latent heat is the heat required to change the phase of the unit mass of PCM. PCM with ethanol additive has the highest specific latent heat while PCM with magnesium nitrate has the lowest specific heat. PCM with ethanol makes dense solid structure which requires great amount of heat release. This ability also enables it to absorb more heat during discharge. PCM with magnesium nitrate additive has soft structure which charges and discharges relatively fast. This fast charge and discharge means it does not require a lot of energy to change its phase.

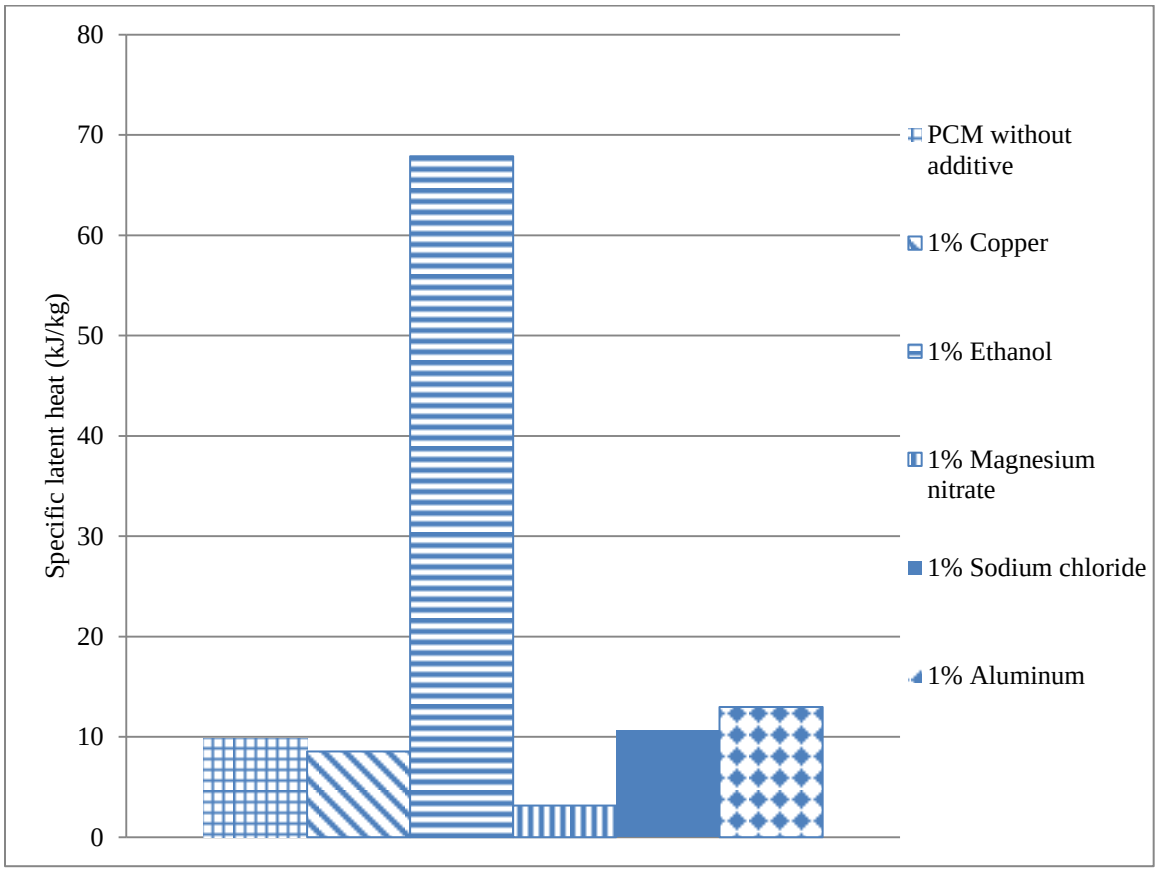

Figure 7.41 An illustration of specific latent heat values for PCMs with different additives

7.6.2 Comparison of Experimental and Analytical Results

An attempt is made to theoretically calculate the liquid phase specific heats and thermal conductivities of the PCMs with the additives. Thermal conductivity values of liquid phase PCMs are calculated using equations (6.20) and (6.22). Table 7.13 shows the values of the parameters used to analytically determine the thermal conductivity values. Specific heat values of the clathrate are calculated using equation (6.5). The properties used to calculate the specific heats are listed in Table 7.14.

Table 7.13 Parameters and their corresponding values for thermal conductivities [88, 108-111]

Parameters	Values
Thermal interface resistance - R_b	1.2×10^{-8} K m^2/W
Metal particle diameter - d_p	10^{-6} m
Nonmetal particle diameter - d_p	10^{-9} m
Constant 'A'	40000
Constant 'm' for Copper	1.5
Constant 'm' for Aluminum	1.6
Constant 'm' for nonmetals	2
Thermal conductivity - Aluminum	210 W/m K
Thermal conductivity - Copper	410 W/m K
Thermal conductivity - Ethanol	0.18 W/m K
Thermal conductivity – Sodium chloride	6.5 W/m K
Thermal conductivity – Magnesium nitrate hexahydrate	0.7 W/m K

Table 7.14 Materials and their corresponding specific heat capacities [102-108]

Materials	Specific heats (J/kg K)
R134a	850
Water	4200
Sodium chloride	880
Magnesium nitrate hexahydrate	4700
Aluminum	910
Copper	390
Ethanol	2460

Figure 7.42 shows the specific heat capacity values of the liquid phase PCMs. The figure shows that, overall, the empirical equations over predicts the values irrespective of the material contents. The comparative low values during the experiments can be associated with the non-homogeneous mixing of the additives, particle amalgamation where the additives cluster together, error in additive mass calculation and presence of interfacial layer. The highest difference between the analytical and experimental values of liquid specific heat capacity is for salt additive at 14%. All the others are found to be below 14%. This comparison of experimental values with the analytical values show the experimental values are satisfactory.

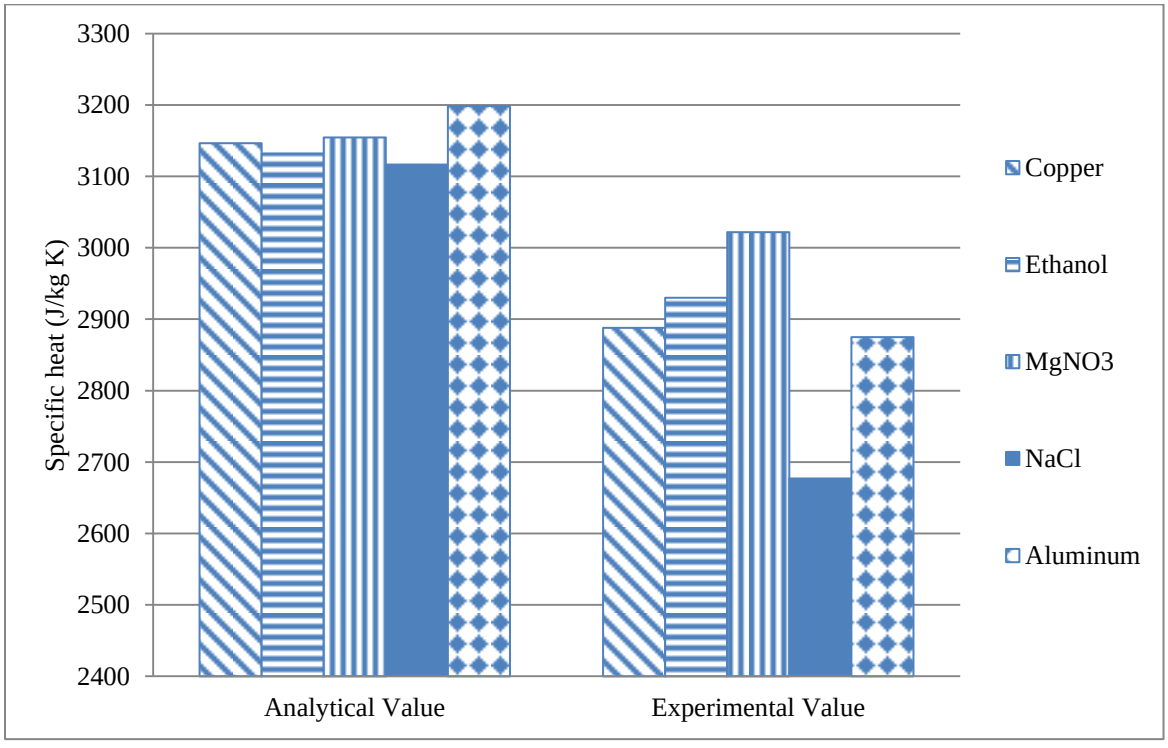

Figure 7.42 Illustrative comparison between analytical and experimental liquid phase specific heat capacities

Figure 7.43 shows the thermal conductivity values of the liquid phase PCMs. The analytical calculations predicted the thermal conductivity values higher than compared to the experimental calculations. The comparative low values calculated for the experimental evaluation is due to non-homogeneous mixing of the additives, particle amalgamation where the additives cluster together, error in additive mass calculation and presence of interfacial layer. Sodium chloride yielded the highest percent difference, at 26%, when the analytical and experimental values of liquid phase thermal conductivities are compared. All the others are found to be below 26%. Although further improvements can be made to improve the results, the overall results are within the reasonable range.

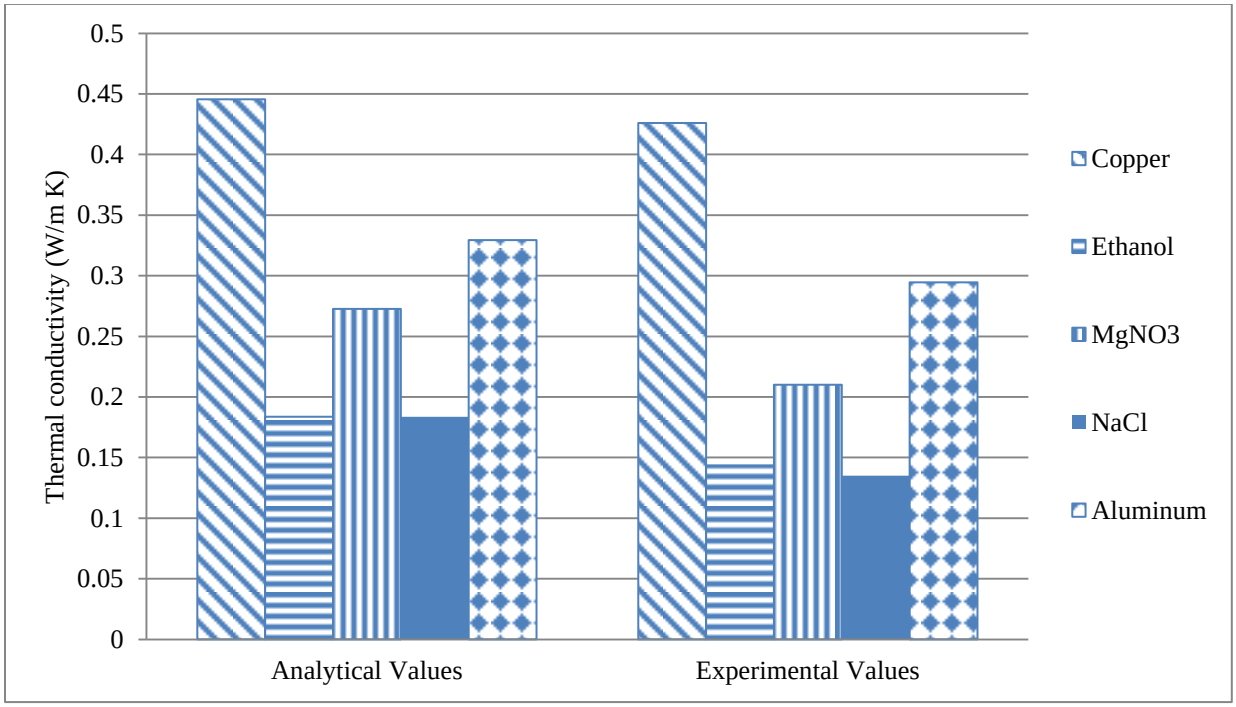

Figure 7.43 Illustrative comparison between analytical and experimental liquid phase thermal conductivities

7.7.3 Effects of Additives on Thermal Properties

The effects on thermal properties by adding the additives are also studied. Adding the additive is desired to improve the thermal properties as it would help in cooling application. Each additive is evaluated to see its effects on the specific heats and thermal conductivities.

Figure 7.44 shows the difference in liquid phase specific heat each additive made to base PCM. Specific heat is one of the variables desired to be improved for an effective PCM. However, it is not as important as some other parameters since this study is to find the most optimal phase change material where latent heat storage is desired. Material with high specific heat changes its own temperature after higher amount of energy is provided compared to a material with low specific heat capacity. It can be seen from the graph that the additives reduced the specific heat capacity of the base PCM. Sodium chloride reduced the most at almost 15%, aluminum reduced it by 8.5%, copper by 8%, ethanol by 6.5% while magnesium nitrate reduced it by 4%. Figure 7.45 shows the difference in liquid phase thermal conductivity each additive made to base PCM. Liquid phase thermal conductivity is one of the variables desired to be improved for an effective PCM. It is an important parameter as higher thermal conductivity allows for faster charging and possibly lower temperature discharge. Material with high thermal conductivity changes its phase after lower amount of energy is provided as compared to a material with low liquid phase thermal conductivity. It can be seen from the graph that the additives increased the liquid phase thermal conductivity of the base PCM. Copper additive improved the thermal conductivity by 350%, followed by aluminum at 230%, magnesium nitrate hexahydrate at 134%, ethanol at 60% and sodium chloride at 50%. In

spite the fact that they delay the clathrate formation, the results shows that sodium chloride and ethanol improve the thermal conductivity of the PCM.

Figure 7.46 shows the difference in solid phase thermal conductivities measured when additives are added to base PCM. Mushy phase thermal conductivity is also one of the parameter desired to be improved for an effective PCM. It is an important parameter as higher thermal conductivity allows for lower temperature discharge. Material with high mushy phase thermal conductivity changes discharges cool energy faster as compared to a material with low thermal conductivity. It can be seen from the graph that all additives increased the solid phase thermal conductivity of the base PCM, except sodium chloride. Copper additive improved the thermal conductivity by 74%, followed by aluminum at 52%, magnesium nitrate hexahydrate at 40% and ethanol at 9%. Sodium chloride reduced the solid phase thermal conductivity by 12%. Figure 7.47 shows the difference made by the additives in specific latent heat of the base PCM. Most of the additives made negligible difference with the exception of ethanol and, to some extent, magnesium nitrate hexahydrate. Magnesium nitrate hexahydrate additive lowers the specific latent heat of the PCM since it forms soft fluffy structures. This structure type does not allow for a lot of energy storage hence the phase change is relatively quick. PCM with ethanol forms hard solid structure which requires more energy and takes longer to discharge it. The specific latent heat of the PCM with ethanol is found to be almost 600% more than the base PCM.

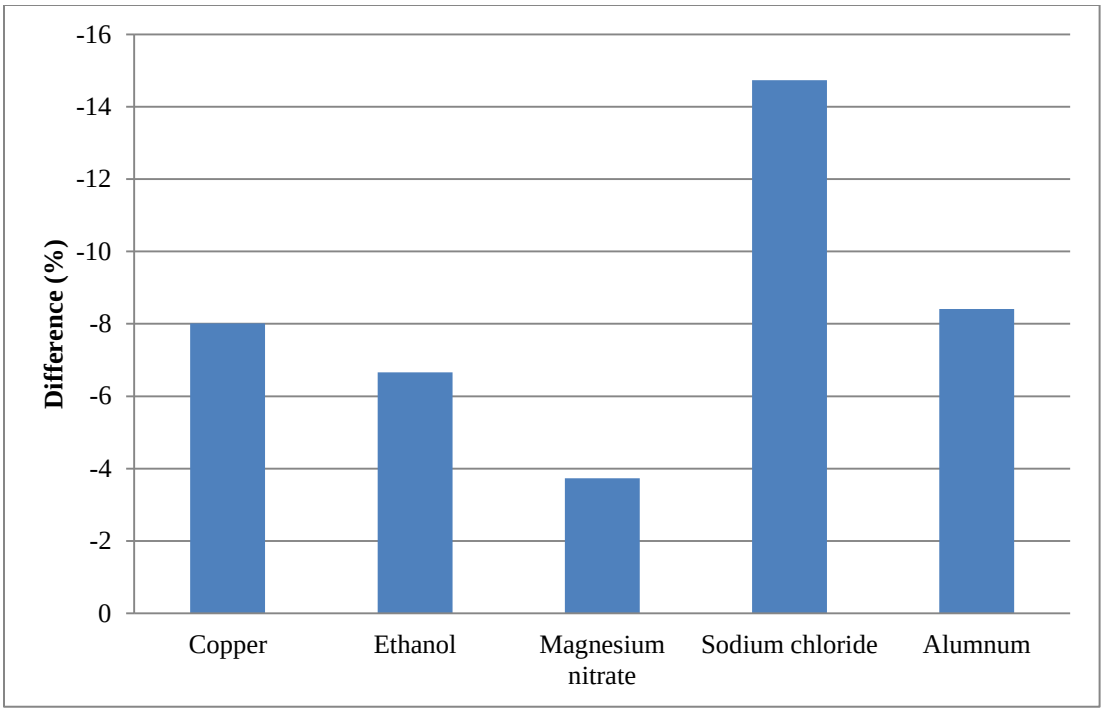

Figure 7.44 Differences in liquid phase specific heat capacities compared to base PCM without additive

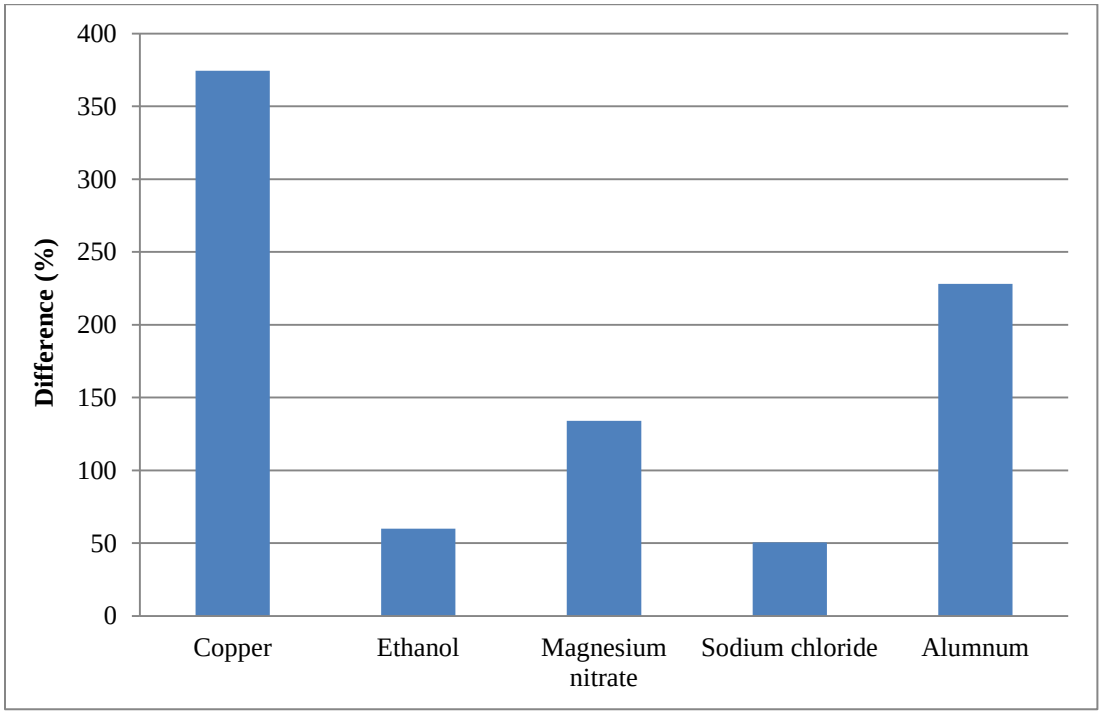

Figure 7.45 Differences in liquid phase thermal conductivities compared to base PCM without additive

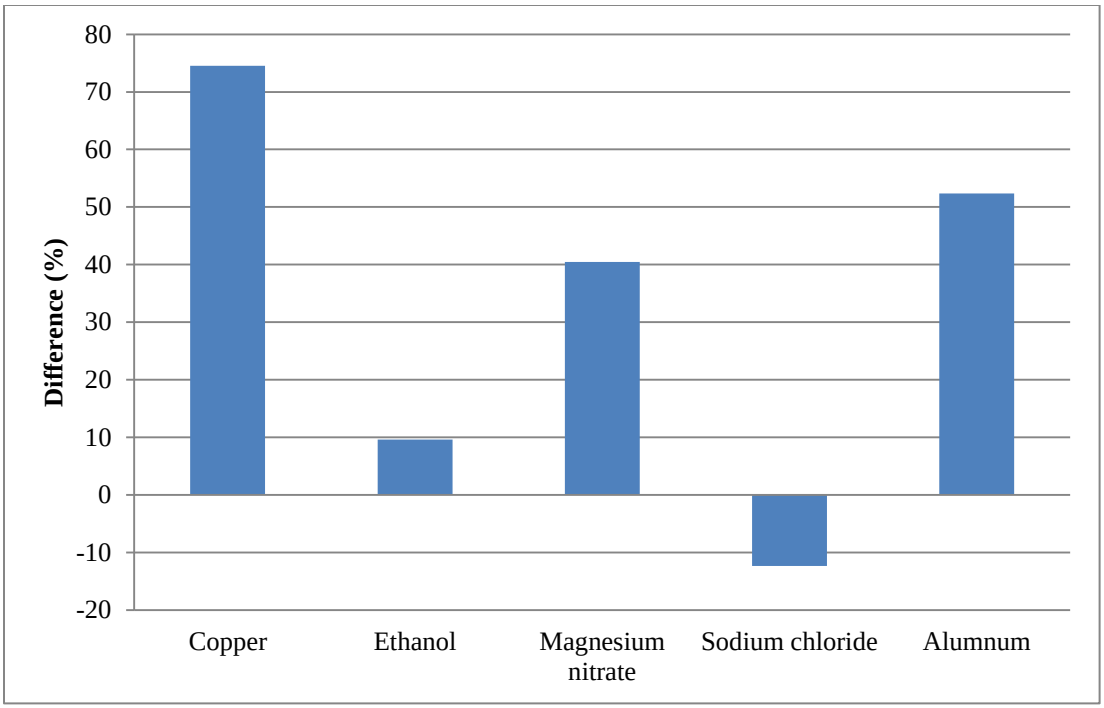

Figure 7.46 Differences in mushy phase thermal conductivities compared to base PCM without additive

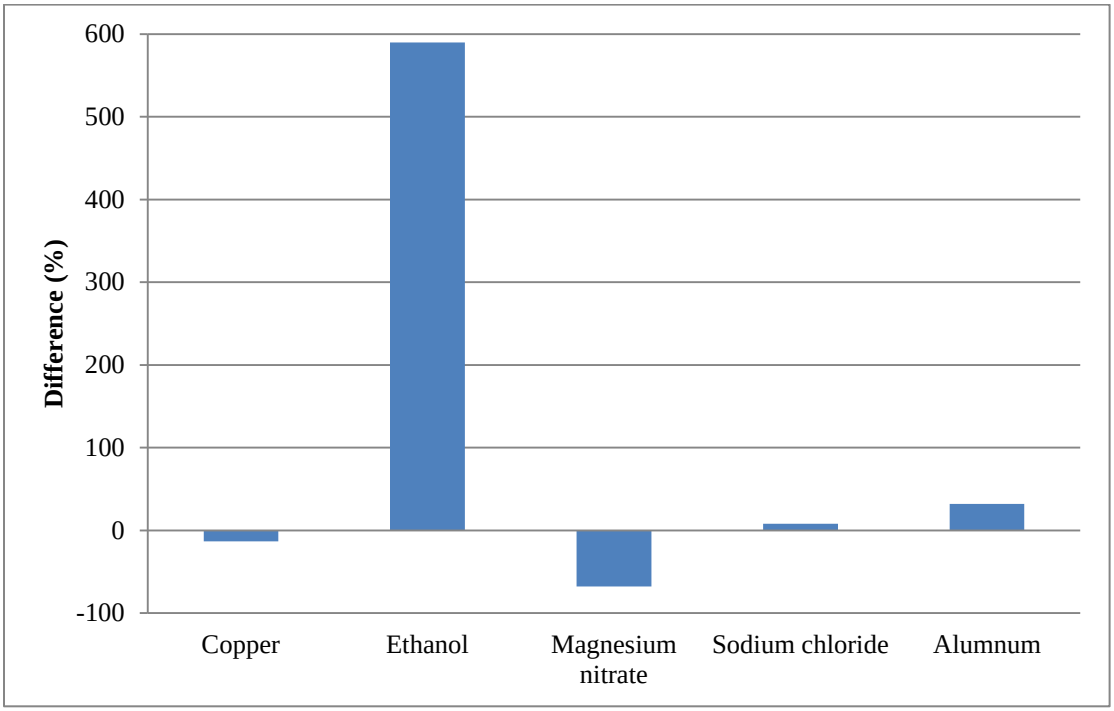

Figure 7.47 Differences in specific latent heat compared to base PCM without additive

7.7 Results of Energy and Exergy Analyses

Analyses are conducted to evaluate the energy and exergy values for charging of the tested R134a clathrate with and without additives. Energy and exergy values are determined for R134a clathrates at different fractions and then with different additives over a range of mass fractions. Energy analysis is done to quantify the amount of energy required to charge the desired PCMs. The exergy analysis, on the other hand, determines how much of that energy is available to be utilized later.

7.7.1 Results of Energy and Exergy Analyses on Base Clathrate

Energy and exergy analyses are conducted on the base PCM (R134a clathrate without any additive). These analyses determined the amount of energy and exergy required to charge the PCMs. The analyses are also conducted to compare the two different bath temperatures of 276 K and 278 K for charging. Table 7.15 shows the energy and exergy values calculated for the onset and end set of charging the base clathrate. The energy and exergy values calculated are for water bath temperature of 278 K.

Table 7.15 Energy and exergy values for onset and end set times of charging process of base clathrate at 278 K bath temperature

End Set at 278 K				**Onset at 278 K**			
$\dot{Q}$ (W)	**Q (kJ)**	**$\dot{E}x$ (W)**	**Ex (kJ)**	**$\dot{Q}$ (W)**	**Q (kJ)**	**$\dot{E}x$ (W)**	**Ex (kJ)**
95	639	68	457	95	398	68	284
95	531	68	379	95	355	68	254
95	590	68	421	95	398	68	284
95	583	68	416	95	398	68	284
95	533	68	380	95	355	68	254
95	546	68	390	95	384	68	274

Figure 7.48 shows the energy and exergy values of R134a clathrate at different refrigerant mass fractions for 278 K bath temperature. The energy and exergy values are for the charging of the R134a clathrate without any additive. The energy and exergy analyses are done based on the end set time of R134a clathrate. Refrigerant fractions of 0.15 to 0.4 are shown in the figure. For 0.15, 0.2 and 0.25 mass fractions, the excess water or the refrigerant remains liquid and does not freeze at the water bath temperature of 278 K. Because these three fractions do not form clathrate comprehensively, they are not considered for any further analysis. The charging time reduces until 0.35 refrigerant mass fraction and then it starts to increase, as is the case with the charging time. The analysis shows that 0.35 refrigerant mass fraction is the most optimal mass fraction for clathrate charging since it takes the least amount of energy. The energy required at 0.35 refrigerant fraction is 532 kJ and the exergy is at 380 kJ. Table 7.16 shows the energy and exergy values calculated for the end set of charging process of the base clathrate. The energy and exergy values calculated are for water bath temperature of 276 K.

Table 7.16 Energy and exergy values for onset and end set times of charging process of base clathrate at 276 K bath temperature

End Set at 276 K				**Onset at 276 K**			
$\dot{Q}$ (W)	**Q (kJ)**	**$\dot{E}x$ (W)**	**Ex (kJ)**	**$\dot{Q}$ (W)**	**Q (kJ)**	**$\dot{E}x$ (W)**	**Ex (kJ)**
107	572	68	360	107	290	68	183
107	540	68	340	107	387	68	243
107	784	68	494	107	601	68	379
107	657	68	414	107	412	68	260
107	444	68	280	107	225	68	142
107	467	68	294	107	314	68	198

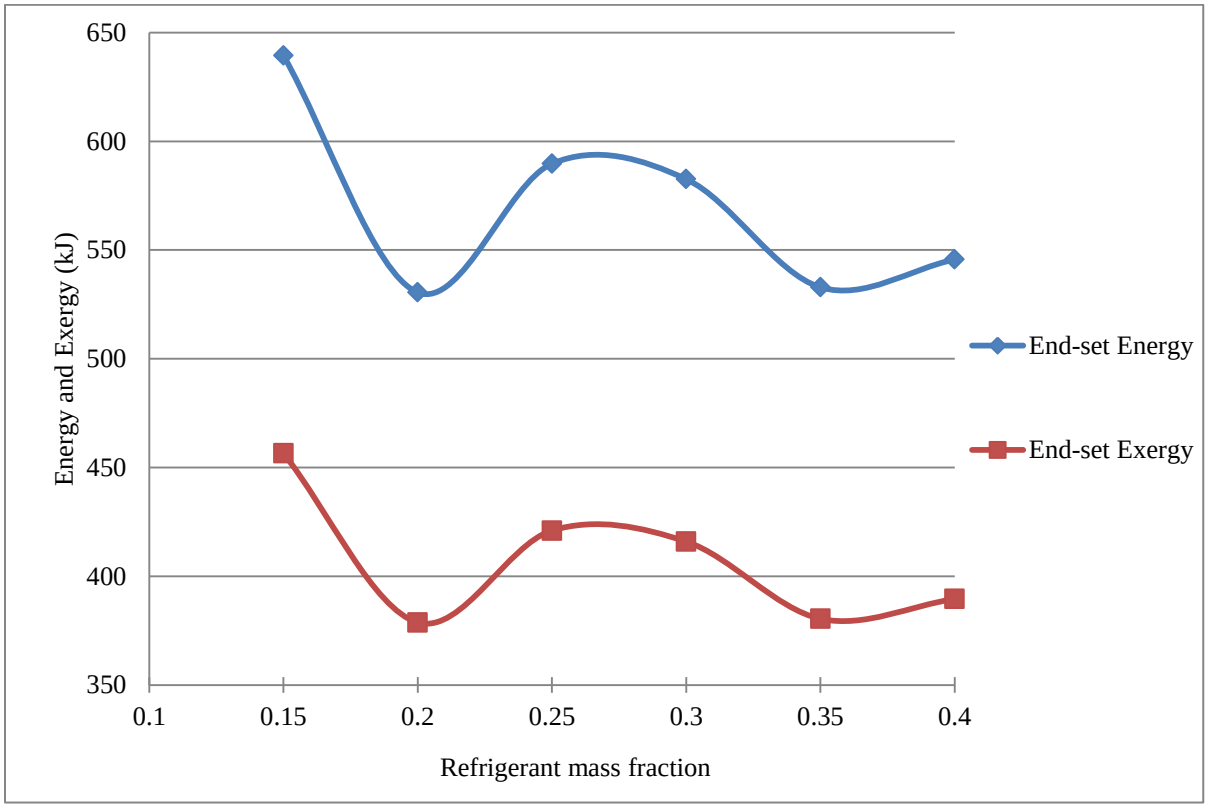

Figure 7.48 End set energy and exergy values at different refrigerant mass fractions for 278 K bath temperature

Figure 7.49 shows the R134a clathrates' energy and exergy values at different refrigerant mass fractions for 276 K bath temperature. The energy and exergy values are for the charging of the R134a clathrate without any additive. The energy and exergy analyses are done based on the end set time of R134a clathrate. Refrigerant mass fractions of 0.15 to 0.4 are shown in the figure. For 0.15 and 0.2 mass fractions, the excess water or the refrigerant remains liquid and does not freeze at the water bath temperature of 276 K. Because these two fractions do not form clathrate comprehensively, they are not considered for any further analysis. The graph shows that the charging time reduces until 0.35 refrigerant mass fraction and then it starts to

increase, as is the case with the charging time. The analysis shows that 0.35 refrigerant mass fraction is the most optimal mass fraction for clathrate charging since it takes the least amount of energy. The energy required at 0.35 refrigerant mass fraction is 445 kJ and the exergy is at 280 kJ.

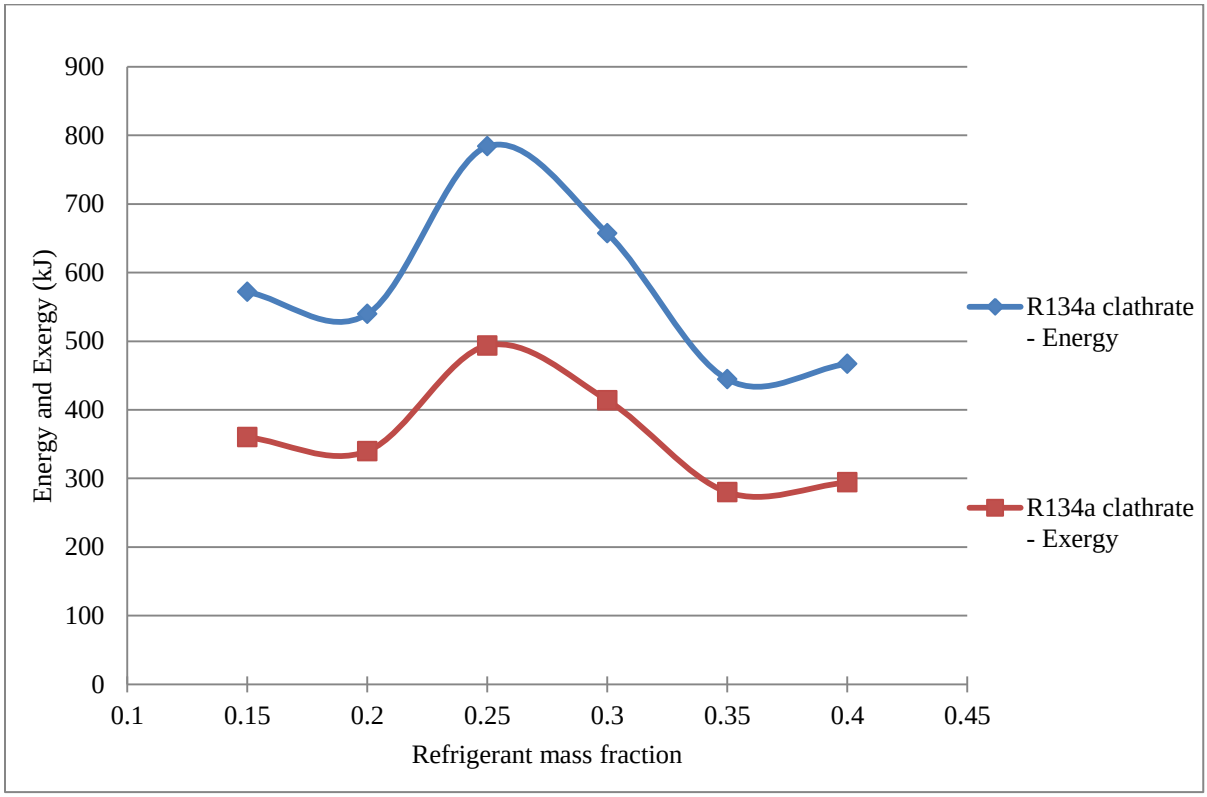

Figure 7.49 End set energy and exergy values at different refrigerant mass fractions for 276 K bath temperature

Figure 7.50 shows end set energy and exergy amounts required to charge the base PCM with water bath temperatures of 276 K and 278 K. The graph shows the energy and exergy for refrigerant mass fraction of 0.3, 0.35 and 0.4. Both energy and exergy amounts required to charge the base PCM is lower when the bath temperature is 276 K compared to when the bath temperature is 278 K. Although it takes greater energy to cool the bath to 276 K, the PCM takes shorter time to get charged at lower temperature. Since it takes

shorter to charge the PCM at 276 K, the total energy and exergy amounts required to charge the PCM is lower at this bath temperature.

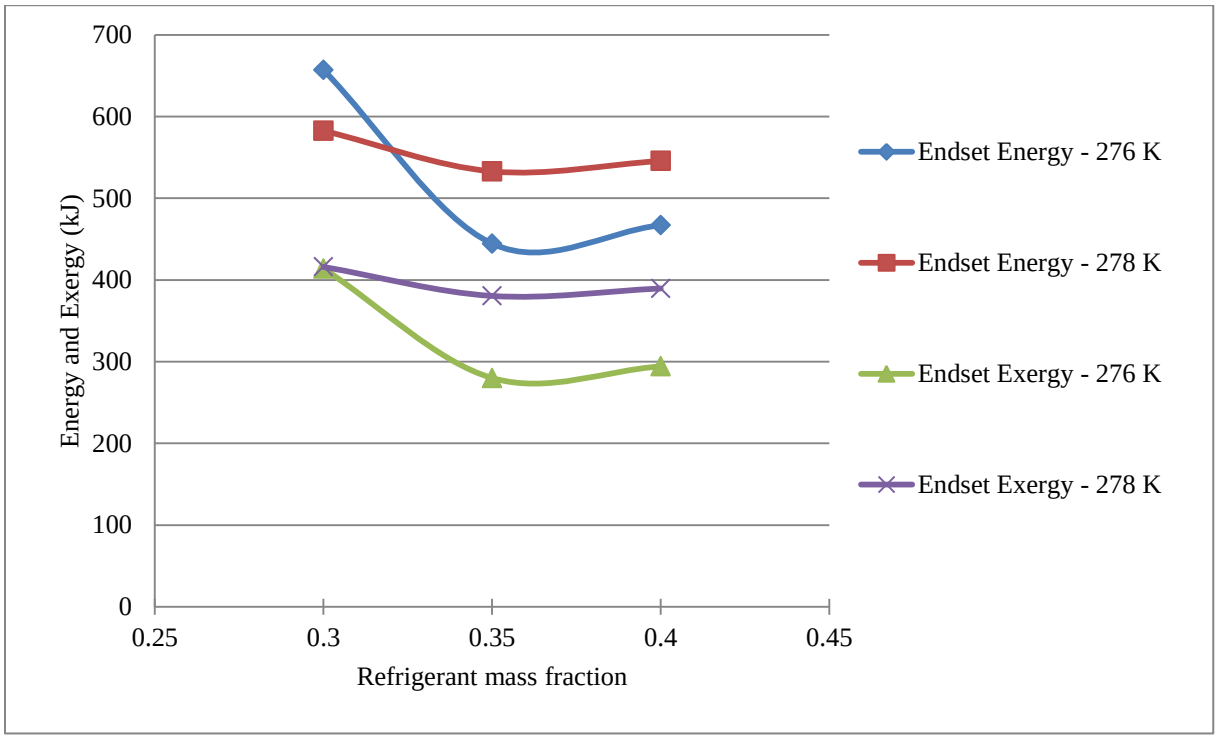

Figure 7.50 Base PCM end set energy and exergy values for charging process at 276 K and 278 K

7.7.2 Results of Energy and Exergy Analyses on PCMs with Additives

Figure 7.51 shows the energy and exergy amounts required for charging R134a clathrate having copper additives. Copper mass fraction is varied from 0.01 to 0.05 while their energy and exergy values are analyzed. The energy and exergy analyses are done on the end set time since it determines the total charging. The required energy varied from 344 kJ for 0.01 additive mass fraction to 580 kJ for 0.05 additive. Similarly, the exergy value varied from 216 kJ for 0.01 additive mass fraction to 365 kJ for 0.05 additive. The energy and exergy values increase with the increase in additives fraction since the end set time

increases. Low additive fraction requires lower energy to charge while more copper in the clathrate increases the required energy. Copper, as an additive does not mix well with the clathrate and settles at the bottom of the tube. This settled copper does not contribute to clathrate formation but it continues to change its own temperature, in turn, utilizing energy.

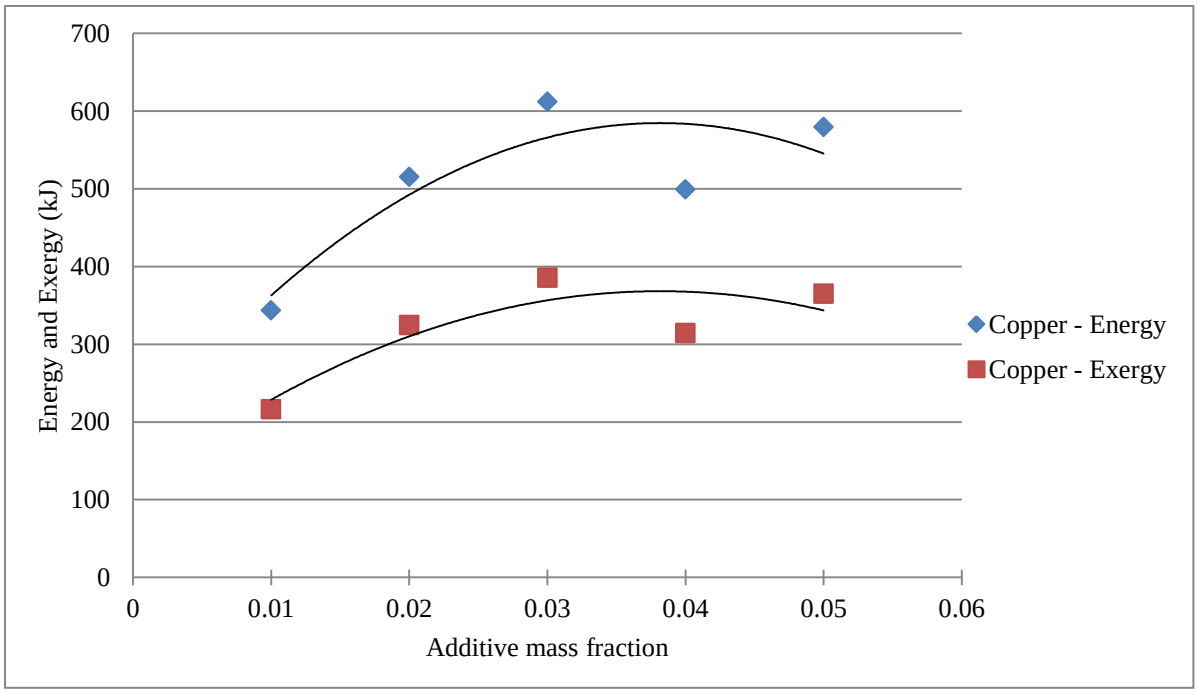

Figure 7.51 Charging process energy and exergy values for copper additive at different additive fractions

Figure 7.52 shows the energy and exergy values for charging R134a clathrate with magnesium nitrate hexahydrate additive. The energy varied from 204 kJ for 0.01 additive mass fraction to 322 kJ for 0.05 additive mass fraction. Similarly, exergy varied from 128 kJ for 0.01 additive mass fraction to 203 kJ for 0.05 additive mass fraction. The energy and exergy increases almost linearly with the increase in additives. The energy

and exergy values increase with the increase in additives fraction since the end set time has the same trend. Low additive fraction requires lower energy to charge while more magnesium nitrate in the clathrate increases the required energy. Magnesium nitrate hexahydrate, being a salt, tends to resist clathrate formation since its molecules like to occupy the cage like space present in the water molecules. So as the additive fraction is increased, clathrate formation is delayed as more magnesium nitrate hexahydrate particles are present to occupy the water molecules.

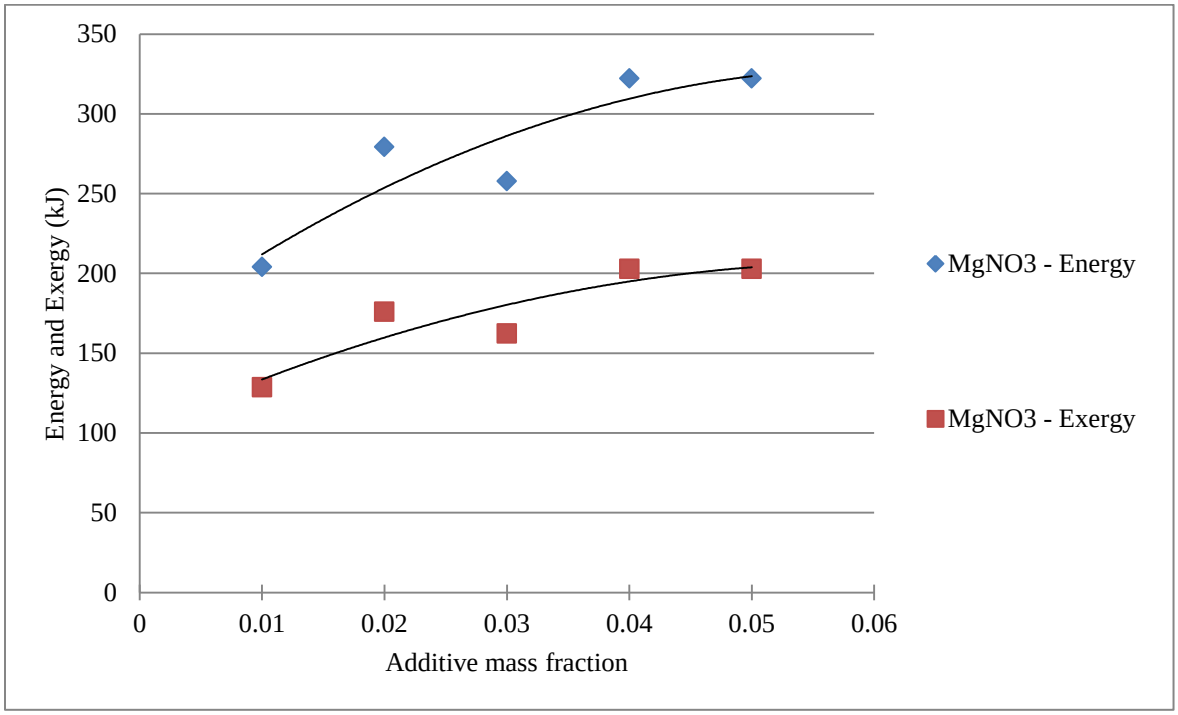

Figure 7.52 Charging process energy and exergy values for magnesium nitrate additive at different additive fractions

Figure 7.53 shows energy and exergy values for R134a clathrate having ethanol additive. The energy utilization varied from 419 kJ for 0.01 additive mass fraction to 564 kJ for 0.05 additive mass fraction. The exergy utilization varied from 264 kJ for 0.01

additive mass fraction to 355 kJ for 0.05 additive mass fraction. The figure shows that energy and exergy values increase with the increase in ethanol mass fraction. Once again, the end set time dictated the energy and exergy values which follow the same trend as observed for charging time. Low additive fraction requires lower energy to charge while more ethanol in the clathrate increases the required energy. Although ethanol mixes well with the clathrate, having poor specific heat, it absorbs higher amount of heat to change its temperature than the base clathrate. This low specific heat contributes in slower temperature change hence slower charging time and energy. So as the additive fraction is increased, clathrate formation is delayed as more ethanol is present in the tube.

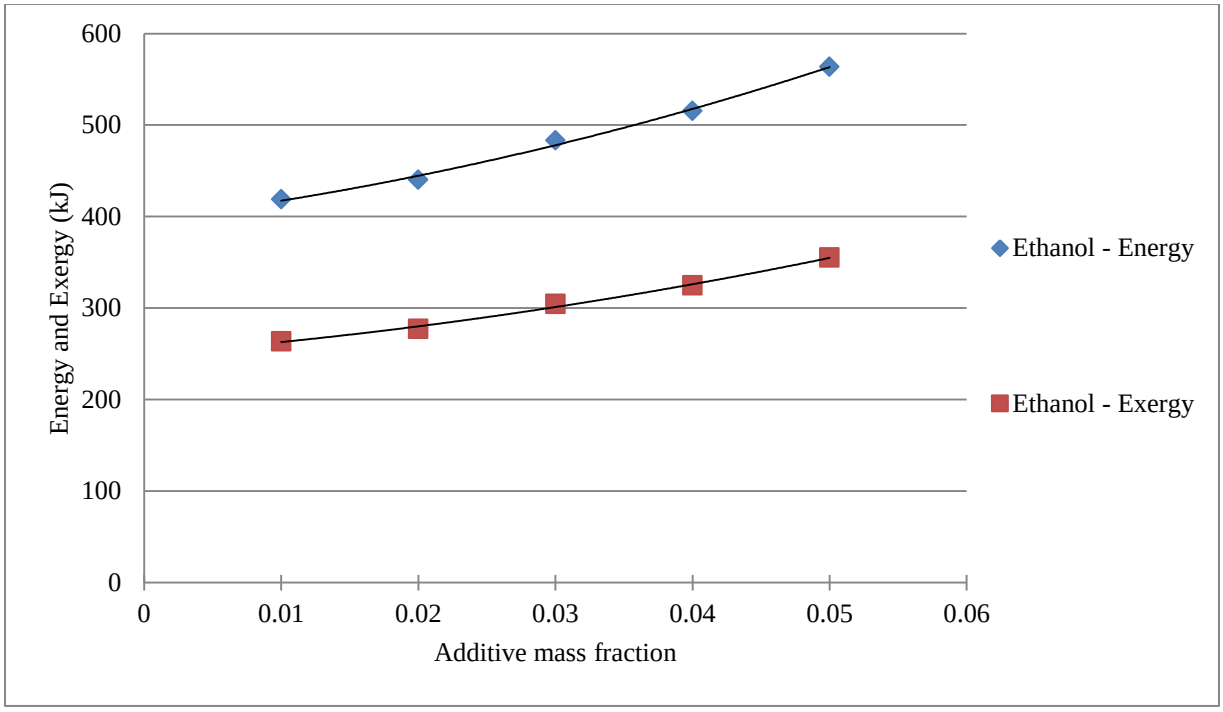

Figure 7.53 Charging process energy and exergy values for ethanol additive at different additive fractions

Figure 7.54 shows the energy and exergy values of R134a clathrate having aluminum particles as additives. The energy utilization varied from 451 kJ for 0.01 additive mass fraction to 547 kJ for 0.05 additive mass fraction. The exergy utilization varied from 284 kJ for 0.01 additive mass fraction to 345 for 0.05 additive mass fraction. The figure shows that energy and exergy values increase linearly with the increase in aluminum mass fraction. As is the case with previous additives, the end set time dictated the energy and exergy values which follow the trend of charging time. Low additive fraction requires lower energy to charge while more copper in the clathrate increases the required energy. Like copper, aluminum as an additive, does not mix well with the clathrate and settles at the bottom of the tube. This settled aluminum does not contribute to clathrate formation but it continues to change its own temperature, in turn, utilizing energy.

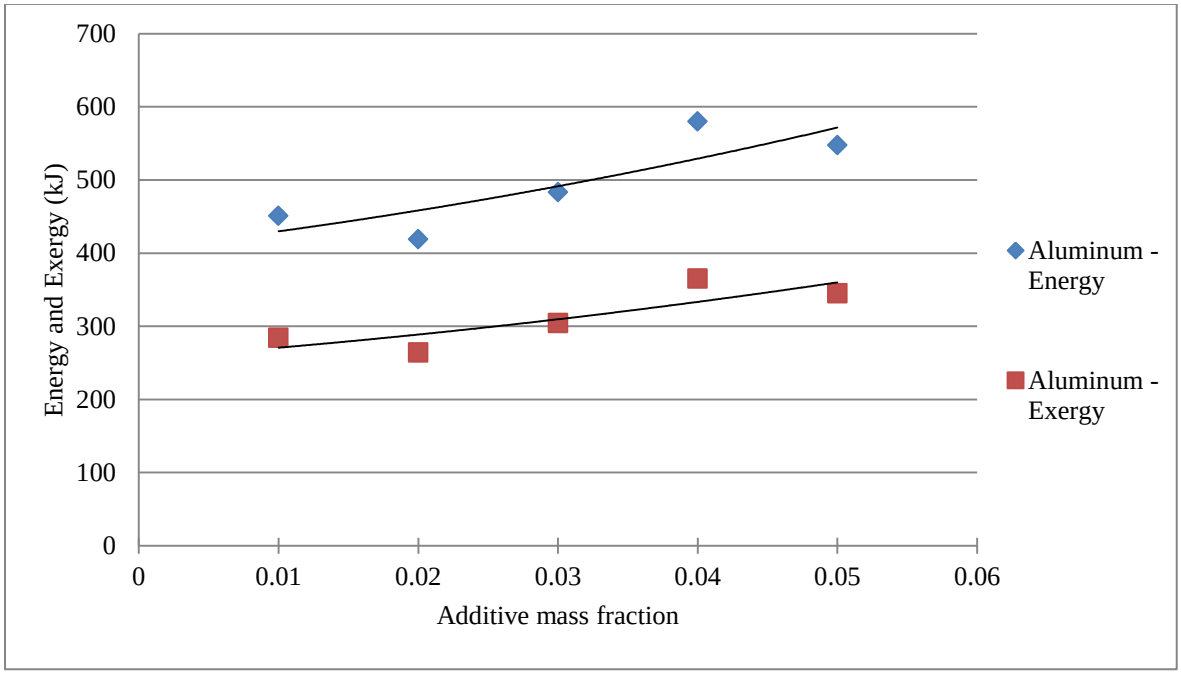

Figure 7.54 Charging process energy and exergy values for aluminum additive at different additive fractions

Figure 7.55 shows the energy and exergy values of R134a clathrate having NaCl particles as additives. The energy utilization varied from 505 kJ for 0.01 additive mass fraction to 709 kJ for 0.03 additive mass fraction. The exergy utilization varied from 318 kJ for 0.01 additive mass fraction to 447 kJ for 0.03 additive mass fraction. For sodium chloride, the R134a clathrate did not form for higher additive fractions. Energy and exergy values tend to increase with the increase in sodium chloride mass fraction. Like other additive trends, the end set time dictated the energy and exergy values. Low additive fraction requires lower energy to charge while more sodium chloride in the clathrate increases the required energy. Sodium chloride, being a salt, tends to resist clathrate formation since its molecules like to occupy the cage like space present in the water molecules. So as the additive fraction is increased, clathrate formation is delayed as more sodium chloride particles are present to occupy the water molecules.

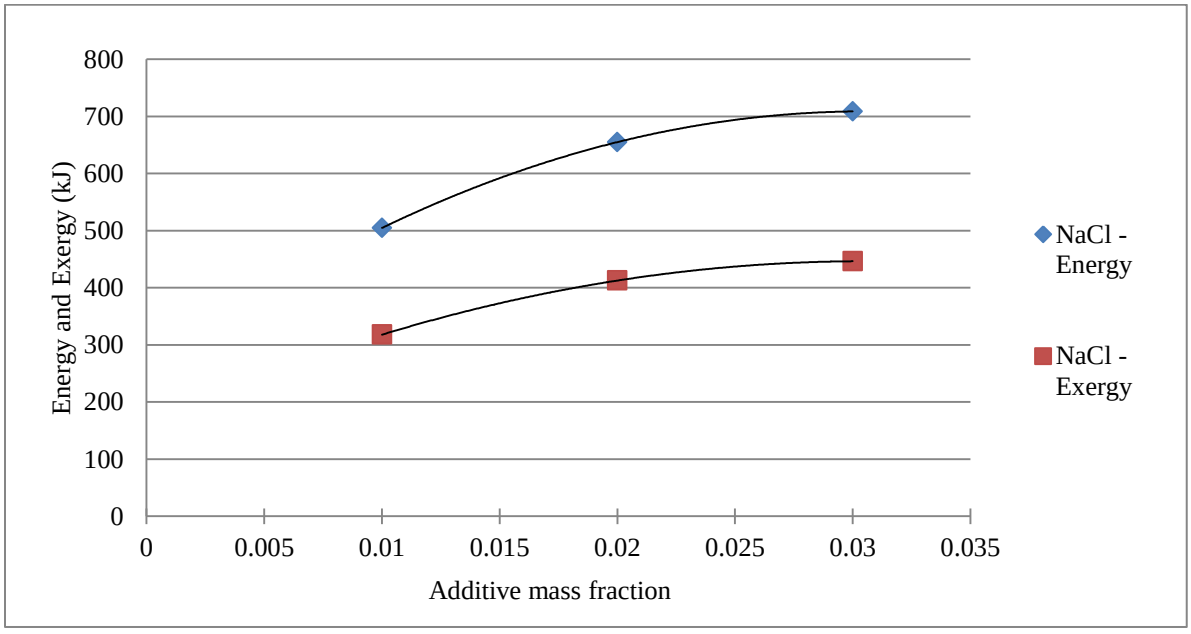

Figure 7.55 Charging process energy and exergy values for sodium chloride additive at different additive fractions

Figure 7.56 shows the average energy utilizations for charging R134a clathrate using five tested additives. The graph shows that magnesium nitrate hexahydrate has the lowest overall energy utilization followed by copper, ethanol, aluminum and then sodium chloride. For 0.01 additive mass fraction, the energy decreased by 55% for magnesium nitrate hexahydrate and 22% for copper. Ethanol and aluminum maintained the energy utilization relatively the same as required by the base R134a clathrate. Sodium chloride increased the energy utilization by 13%. At high additive concentrations, the energy utilization decreased by 27% for magnesium nitrate hexahydrate. Copper, ethanol, aluminum and sodium chloride increased the energy utilization by 27%, 26%, 23% and 60% respectively.

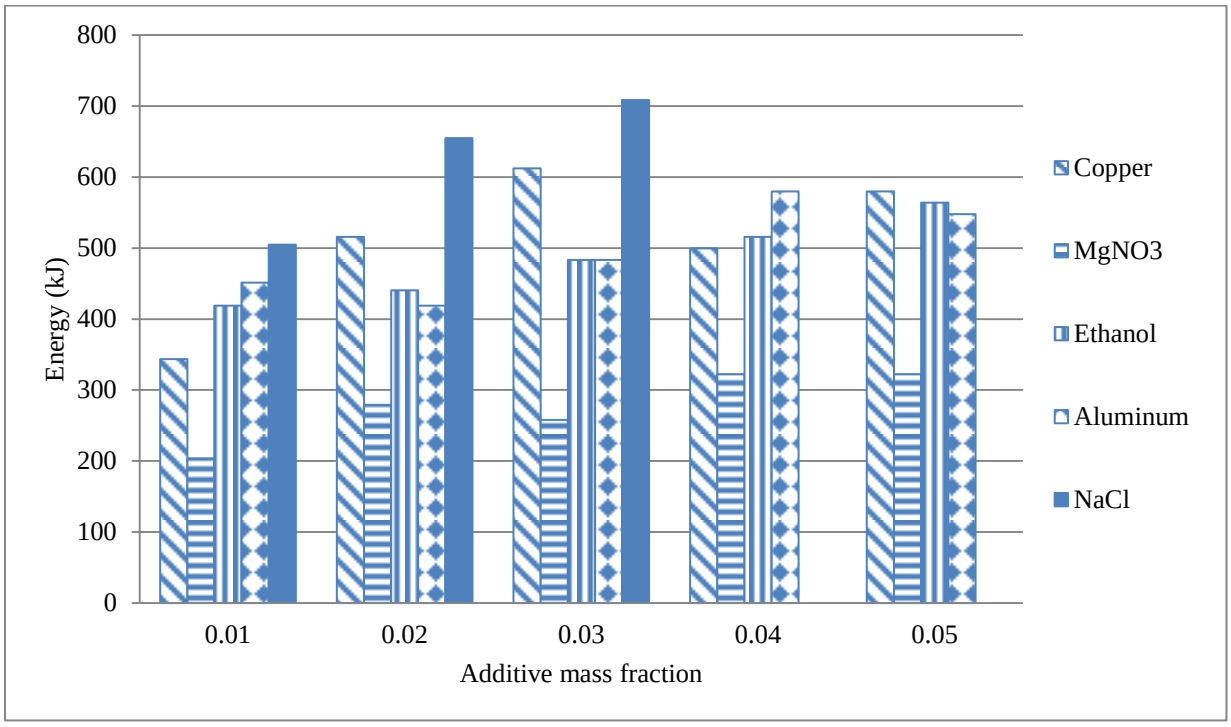

Figure 7.56 Charging energy comparison between additives

Figure 7.57 shows the average exergy utilizations during charging process of R134a clathrate for the five tested additives. Similar to the energy utilization trend, magnesium nitrate hexahydrate has the lowest overall energy utilization followed by copper, ethanol, aluminum and then sodium chloride. For 0.01 additive mass fraction, the exergy decreased by 55% for magnesium nitrate hexahydrate and 33% for copper. Ethanol and aluminum maintained the energy utilization relatively the same as required by the base R134a clathrate. Sodium chloride increased the energy utilization by 13%. At high additive concentrations, the energy utilization decreased by 27% for magnesium nitrate hexahydrate. Copper, ethanol, aluminum and sodium chloride increased the energy utilization by 27%, 26%, 23% and 60% respectively.

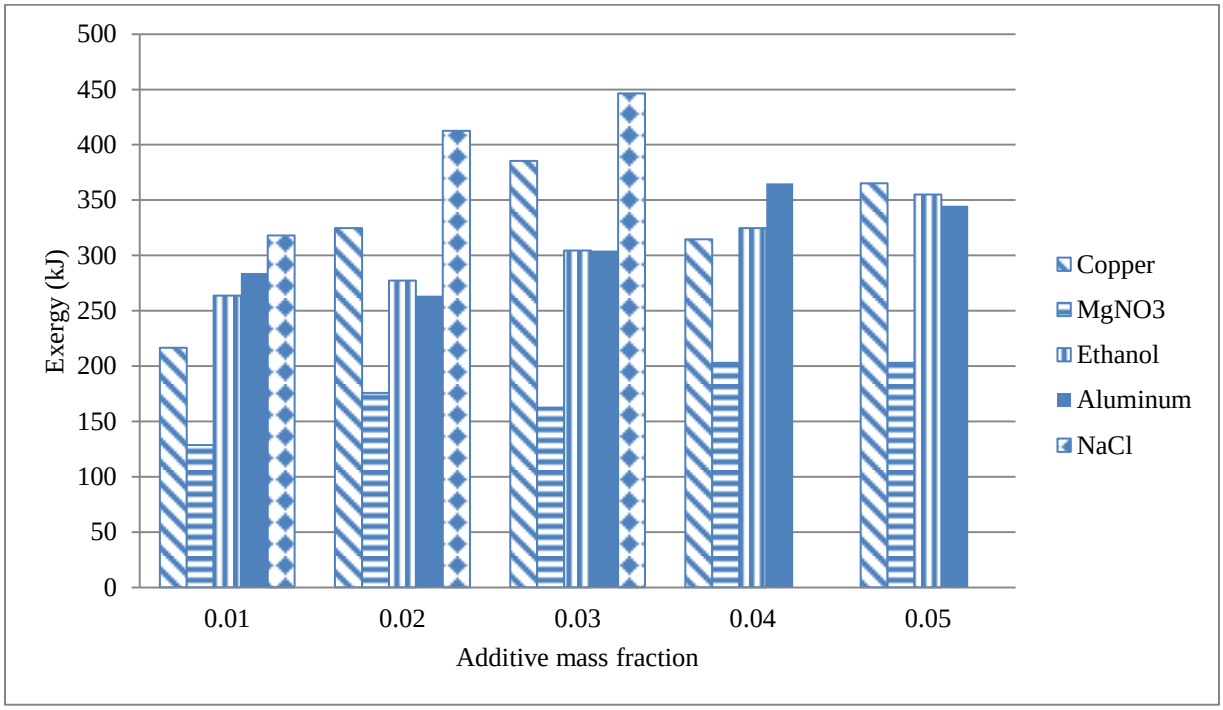

Figure 7.57 Charging exergy comparison between additives

Figure 7.58 shows the average cool energy released by each PCM during the discharge phase. The graph shows that ethanol additive has the highest overall energy release followed by aluminum, copper, base clathrate and magnesium nitrate hexahydrate. The reason for magnesium nitrate hexahydrate additive's low energy release is its soft clathrate structure. Additives that make soft small clathrate structures tend to absorb low energy. Another factor that hampers the energy absorption is non-homogenous mixing of additives. The metal additives would absorb more energy if they mix well in the clathrate. Ethanol on the other hand, makes hard solid clathrate which allows it to provide cool energy longer than the others.

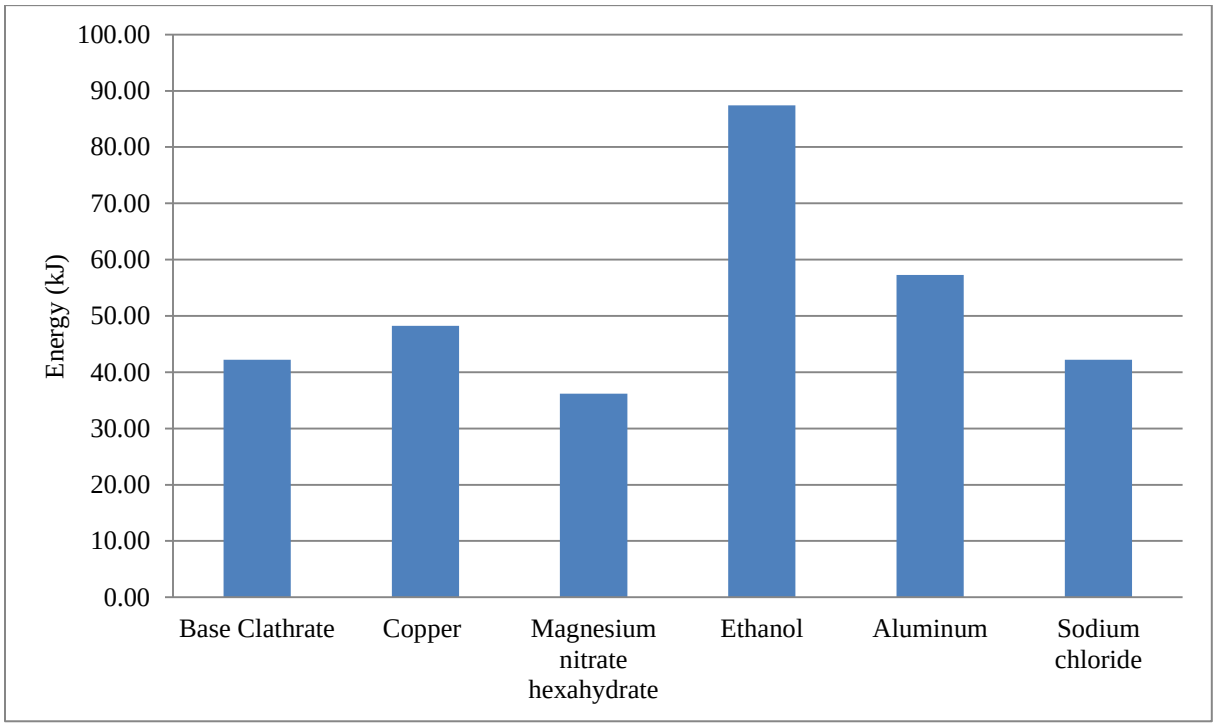

Figure 7.58 Cool energy discharge values of each PCM

Figure 7.59 shows the average cool exergy released by each PCM during the discharge phase. Exergy follows the same trend as energy. Magnesium nitrate

hexahydrate, again, has the lowest exergy while ethanol additive has the highest. The reason for magnesium nitrate hexahydrate additive's low energy release is its soft clathrate structure. Ethanol, on the other hand, makes hard solid clathrate which allows it to provide cool energy longer than the others.

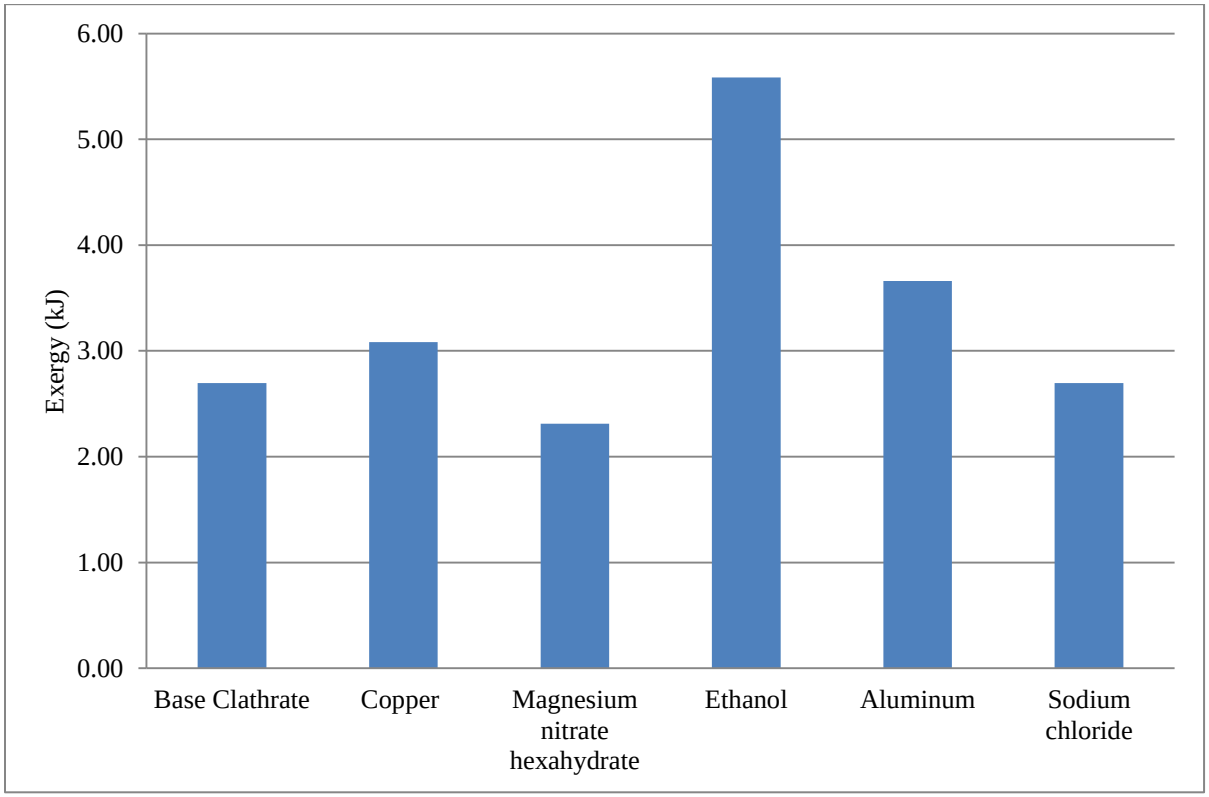

Figure 7.59 Cool exergy discharge values of each PCM

Figure 7.60 shows the overall energy and exergy efficiencies of each PCM. The solid bar represents the exergy values while bars with pattern fill represent the energy. The input and output values are utilized to evaluate these efficiencies. The efficacy graph shows the true picture of which additive results in most gain. Ethanol additive shows the highest efficiency while sodium chloride shows the least. Ethanol, in spite taking long to freeze, yields the most during discharge hence proved to be the most useful. Sodium

chloride additive talks long to charge while does not last very long during discharge which makes it the least efficient additive.

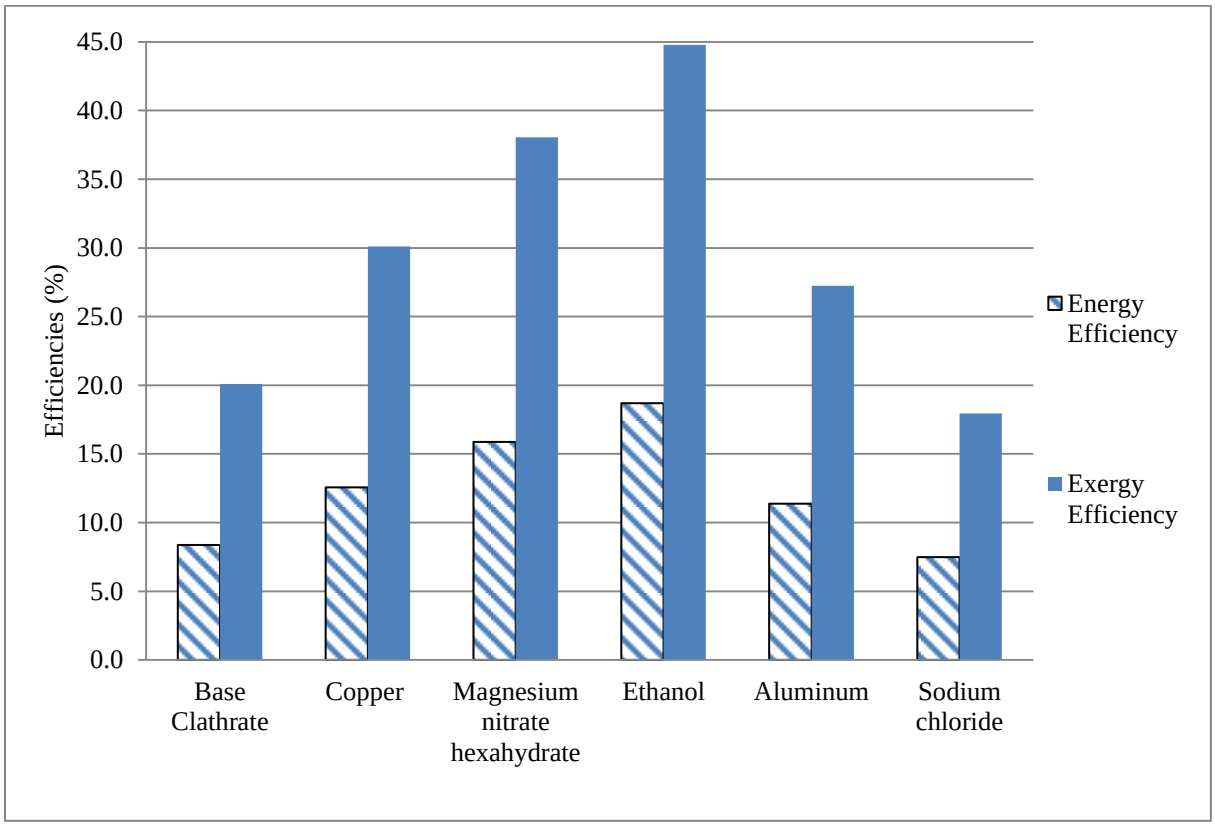

Figure 7.60 Overall energy and exergy efficiencies of each PCM

Figure 7.61 shows the exergy destruction for each PCM used in the experiments. Sodium chloride based PCM has the highest exergy destruction of 12 kJ. Magnesium nitrate hexahydrate based PCM has the lowest exergy destruction of 4 kJ. Sodium chloride based PCM has high charging time and a comparative low discharge time which results in high exergy destruction. Magnesium nitrate hexahydrate based PCM has low charging time which results in relatively low exergy destruction. It is to be noted that

even though magnesium nitrate hexahydrate based PCM has the lowest exergy destruction, it may not necessarily be the most useful PCM, overall.

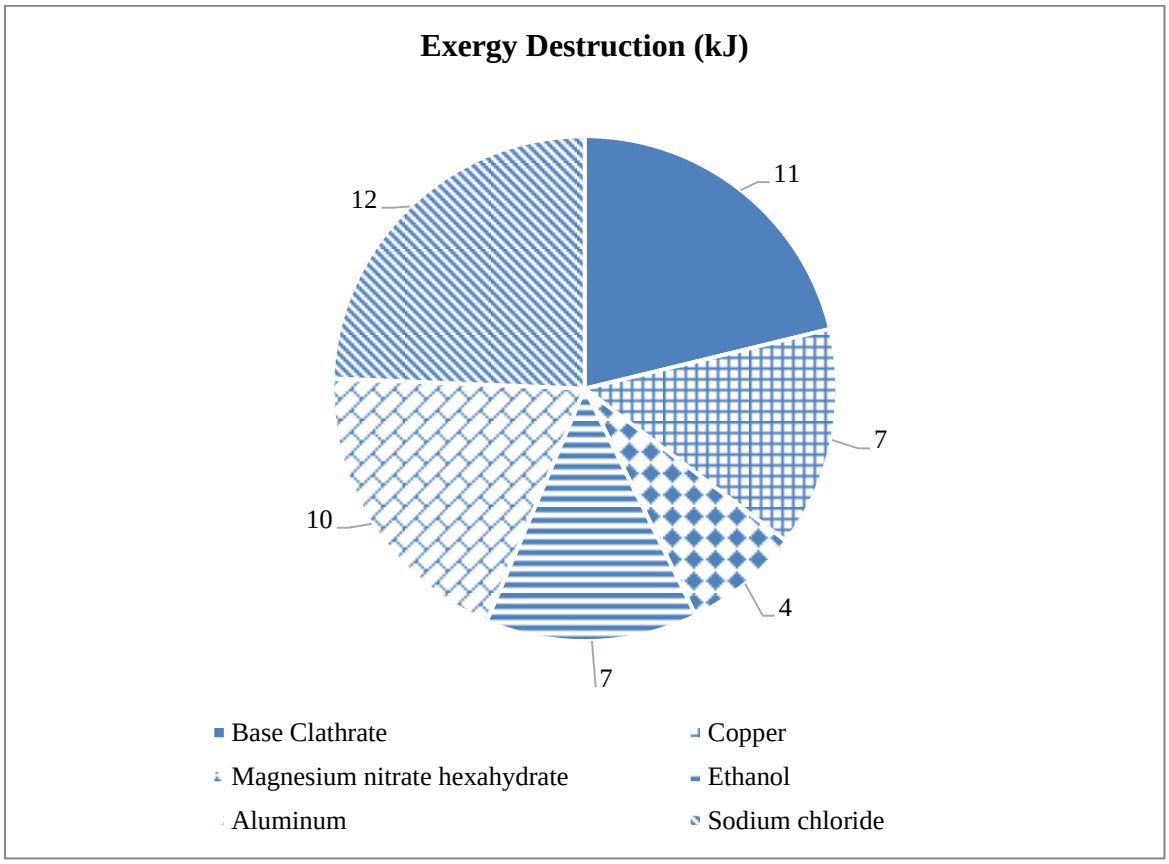

Figure 7.61 Exergy destruction values of each PCM

7.8 Results of Thermoeconomic Analysis

Using the equations described in the Analyses section, thermoeconomic analyses are conducted on the PCMs used in the experiments. Thermoeconomic analyses include the evaluation of thermoeconomic factor and cost-benefit analyses for the PCMs. Figure 7.62 shows the variation of thermoeconomic variable, f_{TE} as it changes with respect to each PCM. Thermoeconomic variable, f_{TE}, is studied for each PCM including its energy,

containment and PCM components costs. For thermoeconomic factor, higher the value, more feasible it is. The results show that magnesium nitrate hexahydrate based PCM has the highest thermoeconomic factor while sodium chloride based PCM has the lowest thermoeconomic factor. The low thermoeconomic factor for magnesium nitrate hexahydrate based PCM is due to its low exergy destruction. Similarly, high thermoeconomic factor for sodium chloride based PCM is due to its high exergy destruction.

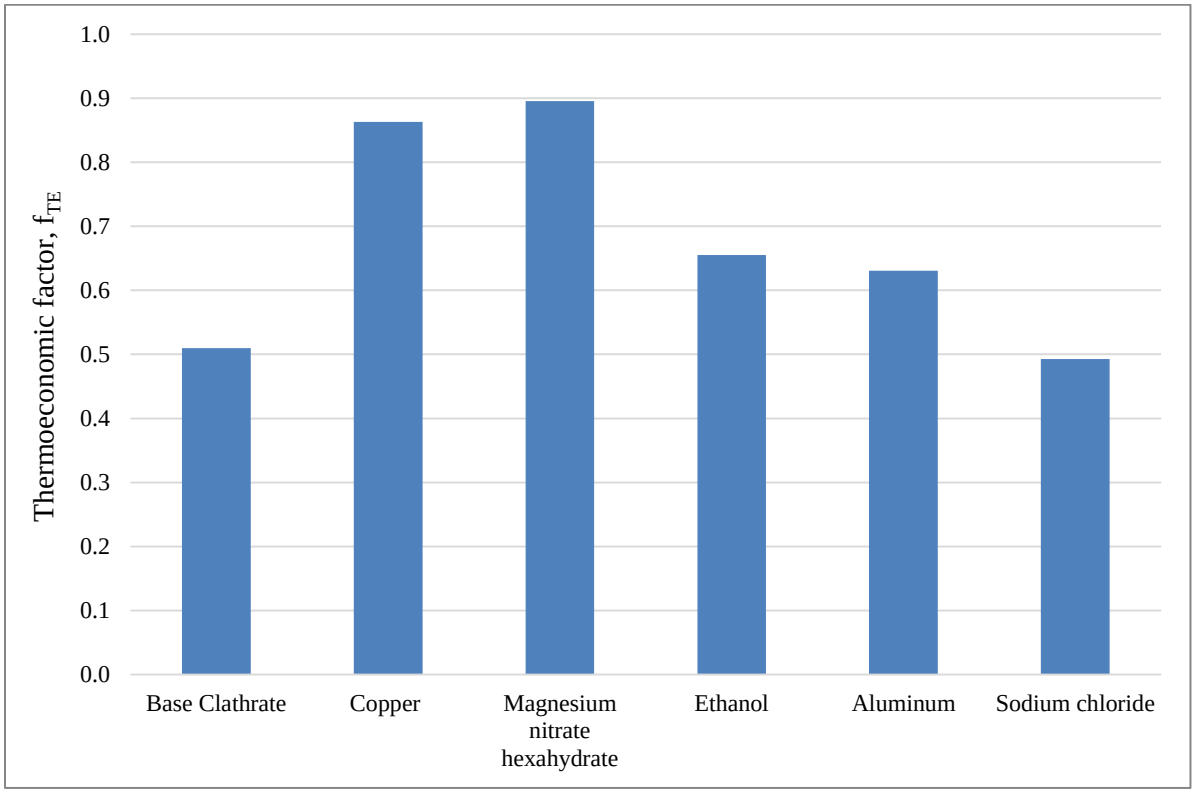

Figure 7.62 Thermoeconomic variable values of each PCM

Figure 7.63 shows the energy cost of producing the PCM and amount saved using the PCM. The energy cost is calculated using the electricity unit rate of $0.32. Ethanol,

having the highest efficiency, gives the highest return in terms of discharge energy. Sodium chloride has the greatest difference between charging and discharging price due to its low efficiency. As it can be seen from the graph that the energy cost of charging 100 units is not very high and it remains below $5. Magnesium nitrate hexahydrate shows to have the lowest energy cost but it also has the lowest return.

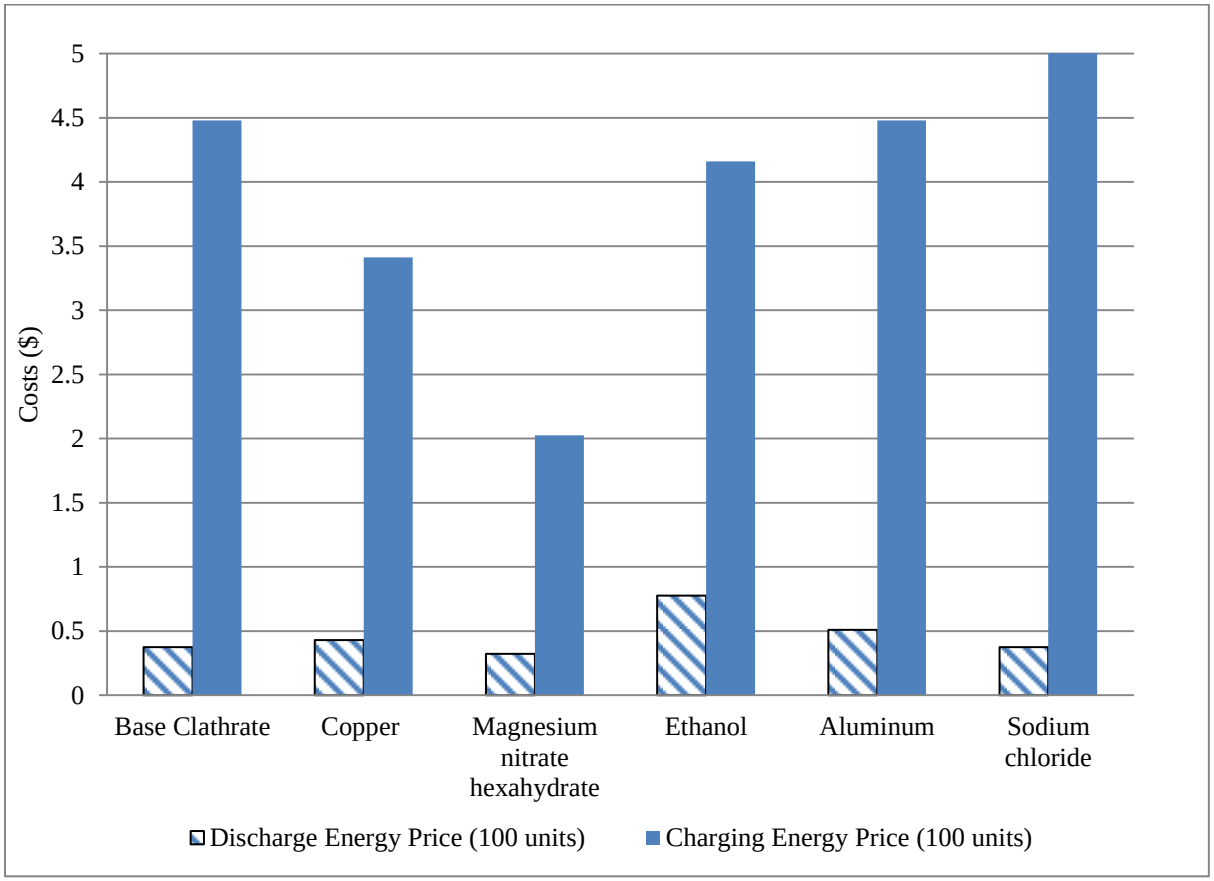

Figure 7.63 Energy costs of producing and using PCM

Figure 7.64 shows the costs of producing 100 units of each PCM with additives compared to the base PCM without any additive. This figure includes the price for 80 gram additive and the costs of energy to charge it. The energy cost is calculated using the

electricity unit rate of $0.32. Copper additive proves to be the most expensive primarily due to the price of copper particles. Magnesium nitrate hexahydrate has low cost since it does not take long to get charged. It should be noted that magnesium nitrate hexahydrate does not produce a lot either so its low price is somewhat deceiving. Ethanol has the second lowest cost due to its low price. Ethanol additive makes the most economical PCM since it costs relatively low to produce it yet it gives the highest efficiency.

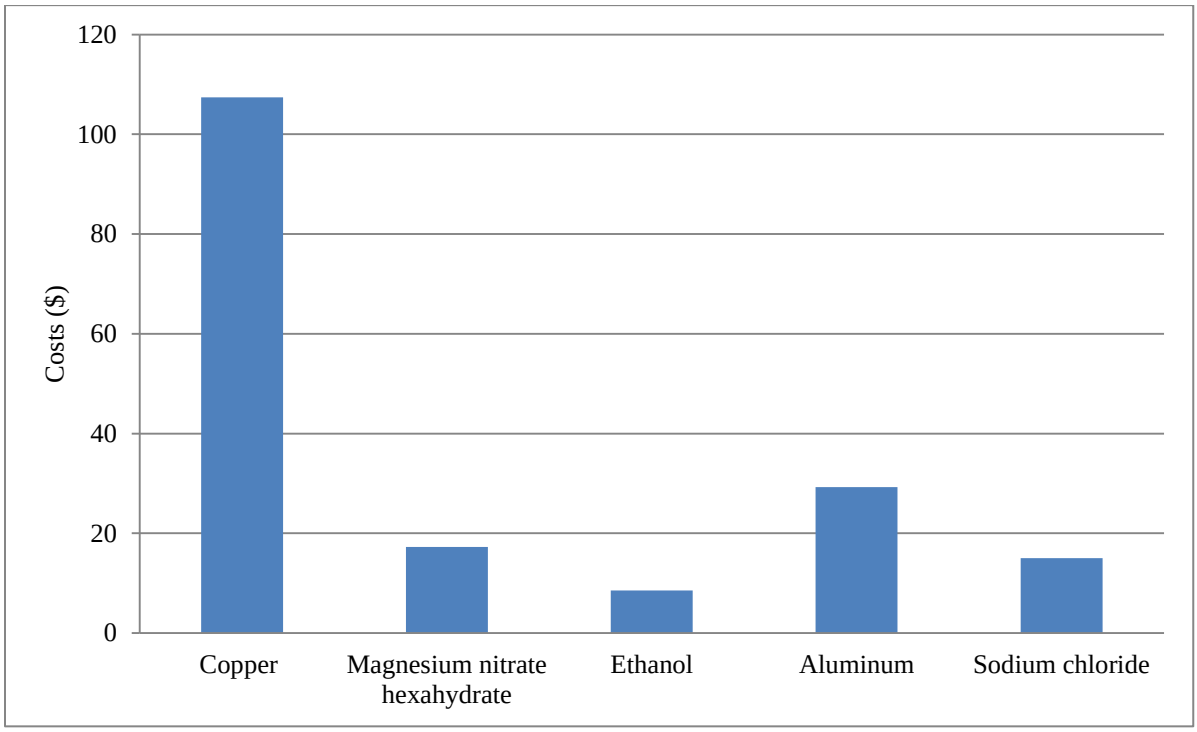

Figure 7.64 Costs of producing 100 units of each PCMs

7.9 Uncertainty Analysis Results

Uncertainty analyses are conducted on the measured and calculated values. The uncertainly analyses include the error analysis resulting from the measured values from

the instruments. Standard deviation is also analyzed for the charging time to show how the recorded times varied.

7.9.1 Error Analysis Results

Error analyses are conducted on the calculated values of thermal properties. The uncertainly analyses also includes the error resulting from the measured values from the instruments. Table 7.17 shows the errors associated with the various measured and calculated properties used in this paper. The error readings are due to the used instruments, experimental reading error, measurement approximation or calculated result values. The charging time is due to the average interval between the observation and the time alarm. Energy and exergy error values are due the errors of individual variable used in their equations.

Table 7.17 Errors associated with the measured and calculated properties

Properties	Errors	Remarks
Mass of PCM	$\pm 2.5 \times 10^{-3}$ g	Depended on the digital weighing scale
Charging Time	± 30 s	Average interval between the alarm and the observation
Temperature	± 0.005 K	Instrumental error associated with the thermocouple
Mass of Bath water	± 0.2 kg	Calculated using the measured volume of the container
Energy	± 5.35 J	Calculated error using error analysis equation
Exergy	± 10.85 J	Calculated error using error analysis equation
Averaged C_P of PCMs	± 510 J/kg K	Calculated error using error analysis equation
Averaged k of PCMs	± 0.0153 W/m^2 K	Calculated error using error analysis equation

7.9.2 Standard Deviations of the Experimental Readings

Several readings are recorded during the experiments for thermal properties, charging and discharging process of the PCM. The readings, taken during charging process, are for onset time and end set time of the PCM. The discharge phase included the hot air discharge of the PCM and the cool energy discharge used for battery cooling. For thermal properties' experiments, thermal conductivities, specific heat and specific latent heat are determined. Figure 7.65 shows the standard deviation associated with the PCM charging time recorded for the onset of freezing. Copper additive shows the least standard deviation only at 0.05 additive mass fraction. Aluminum also shows to start the onset at similar time readings and has the second lowest standard deviation. Magnesium nitrate hexahydrate has the third lowest standard deviation, followed by ethanol and then sodium chloride.

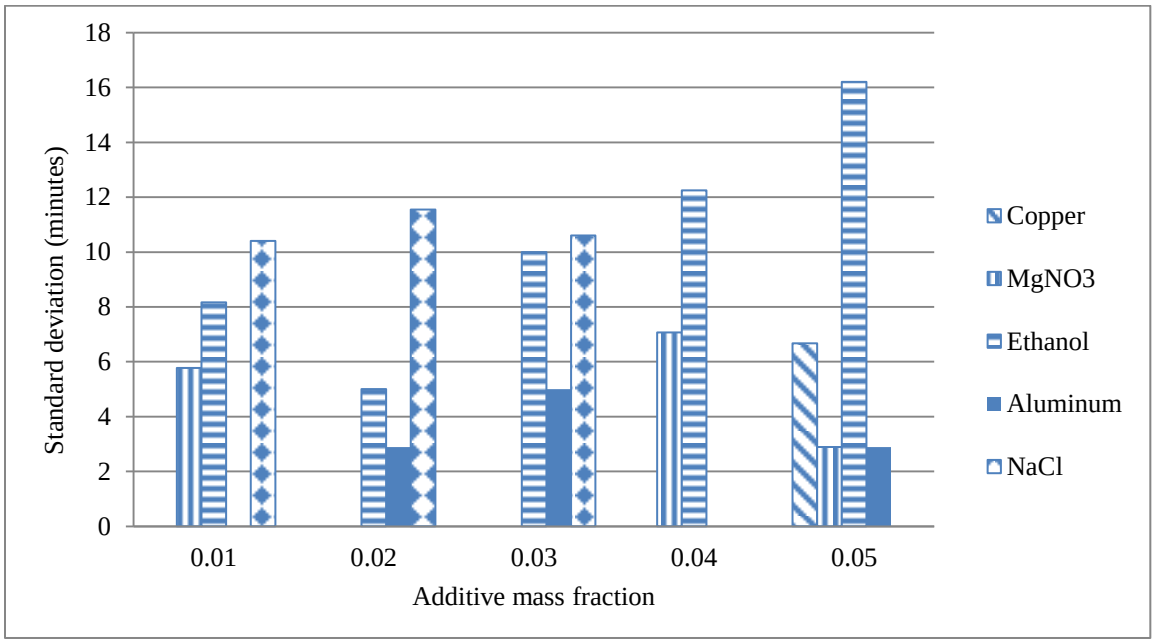

Figure 7.65 Standard deviations of onset times of PCMs

Figure 7.66 shows the standard deviation associated with the PCM charging time recorded for the end set of freezing. Copper additive shows the highest standard deviation with low additive fraction while it reduced when the additive fraction increased. Aluminum, ethanol and magnesium nitrate hexahydrate shows relatively stable standard deviation readings for the end set time. Sodium chloride has higher standard deviation for its results then the other additives. Standard deviation shows a decreasing trend as the additive fraction increases.

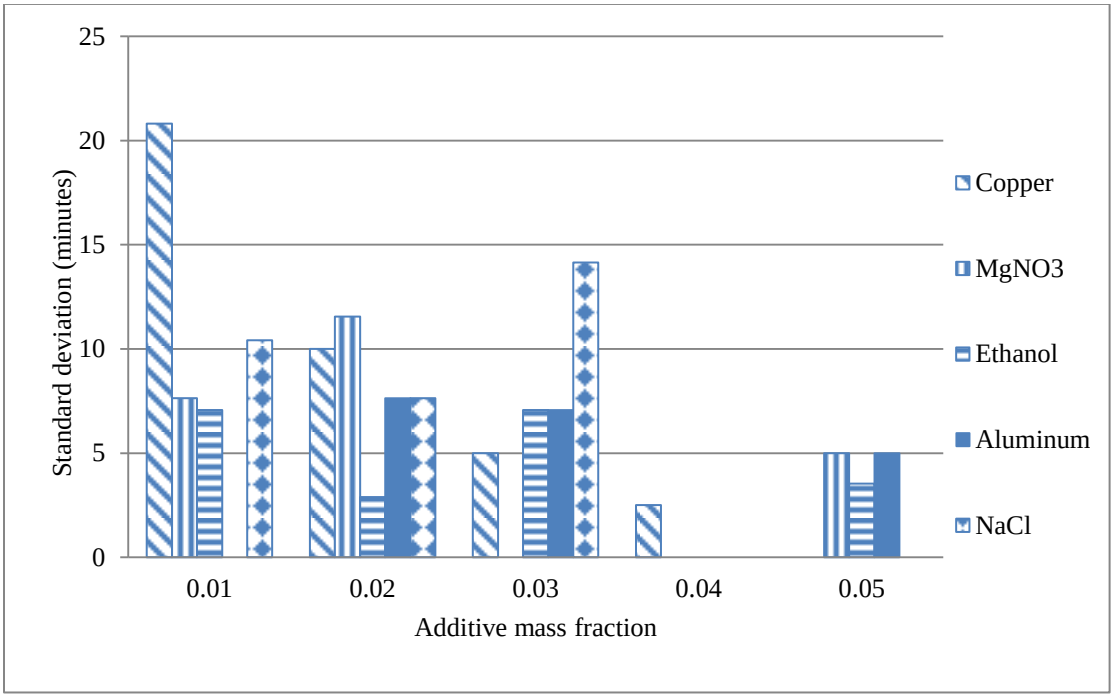

Figure 7.66 Standard deviations of end set times of PCMs

Figure 7.67 shows the standard deviation in time until battery cutoff voltage for each case. Base PCM with no additive has the highest standard deviation at 23 seconds, followed by aluminum at 17 seconds, then ethanol at 14 seconds, magnesium nitrate

hexahydrate at 12 seconds, copper at 10 seconds and sodium chloride at 8 seconds. The empty jacket with no clathrate has the lowest standard deviation reading of 3 seconds.

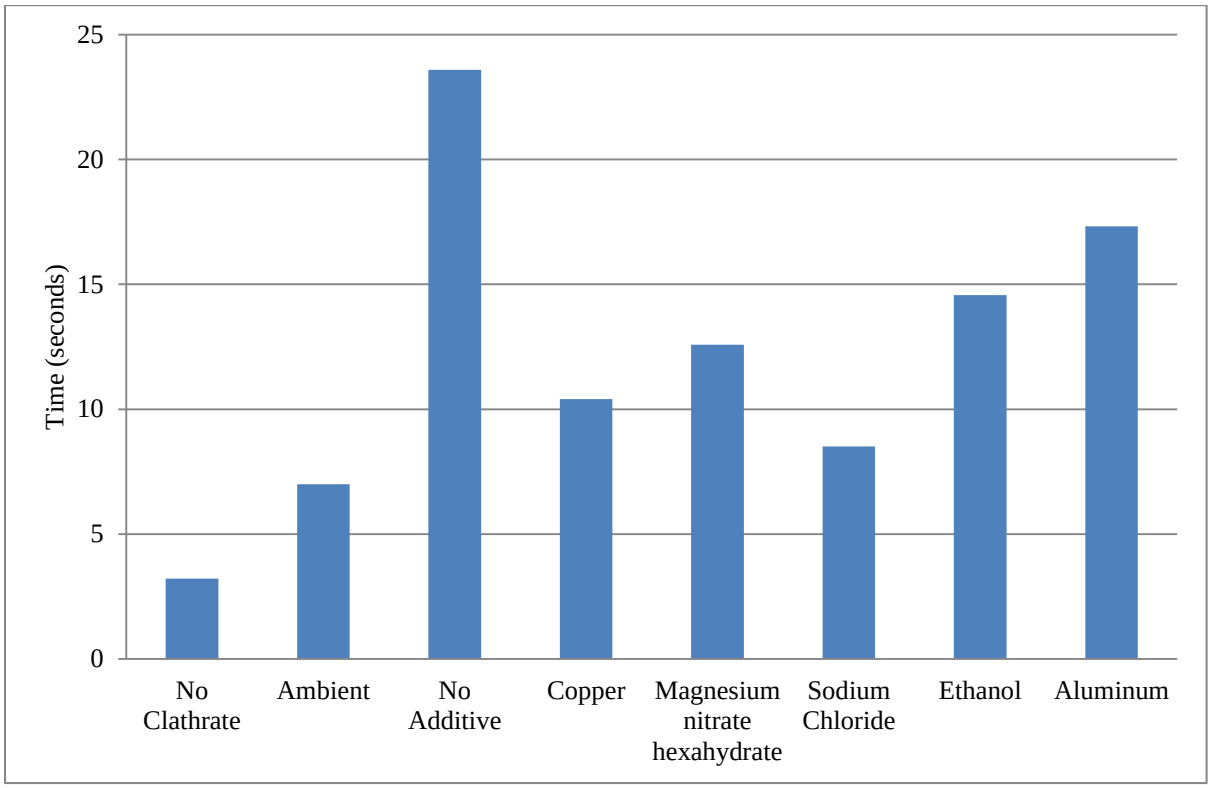

Figure 7.67 Standard deviations of battery cutoff times of PCMs

Figure 7.68 shows the standard deviation time until the battery cooled down. Battery is considered rechargeable when it reaches 26 ^{o}C. Salt additives have high standard deviation compared to others. Sodium chloride has the highest at 252 seconds while copper has the lowest at 51 seconds. Figure 7.69 shows the standard deviation in temperature at cutoff voltage for each case. The standard deviation is lowest when the battery is exposed to the ambient temperature. Base PCM with no additive has the highest standard deviation at 1.4 ^{o}C while ethanol additive has the lowest at 0.17 ^{o}C.

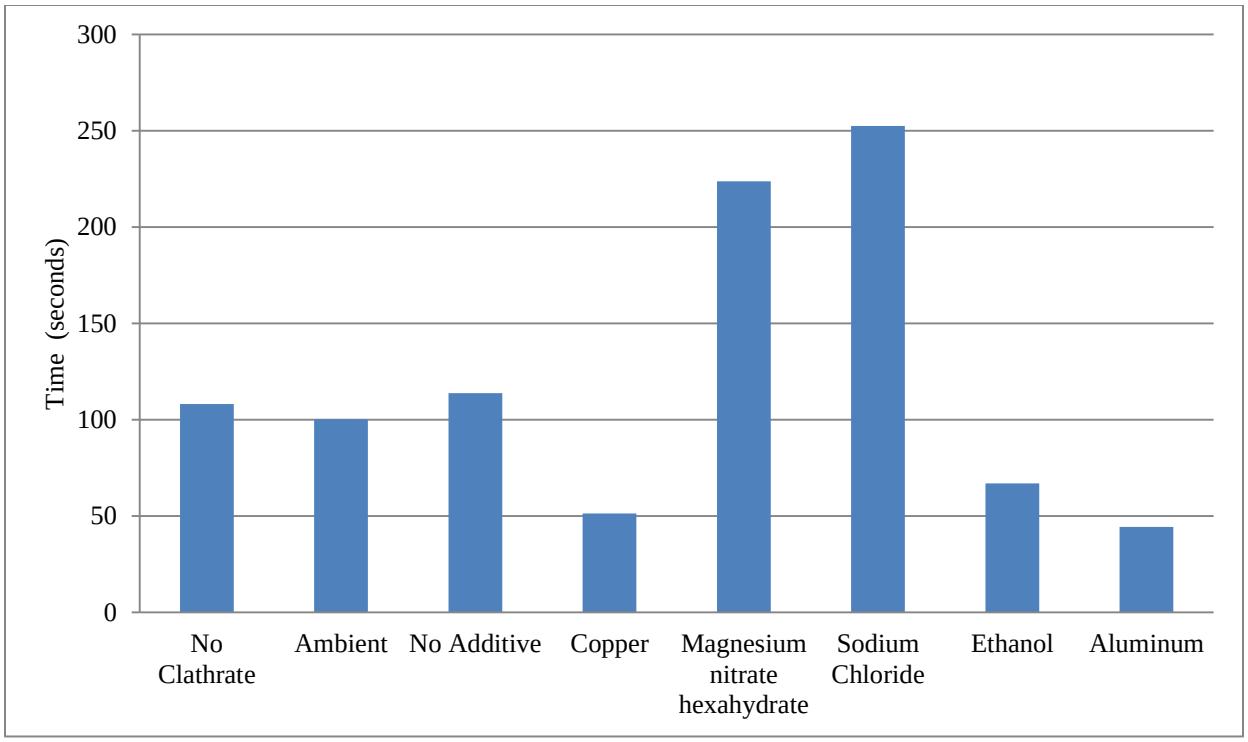

Figure 7.68 Standard deviations of battery cooling times of PCMs

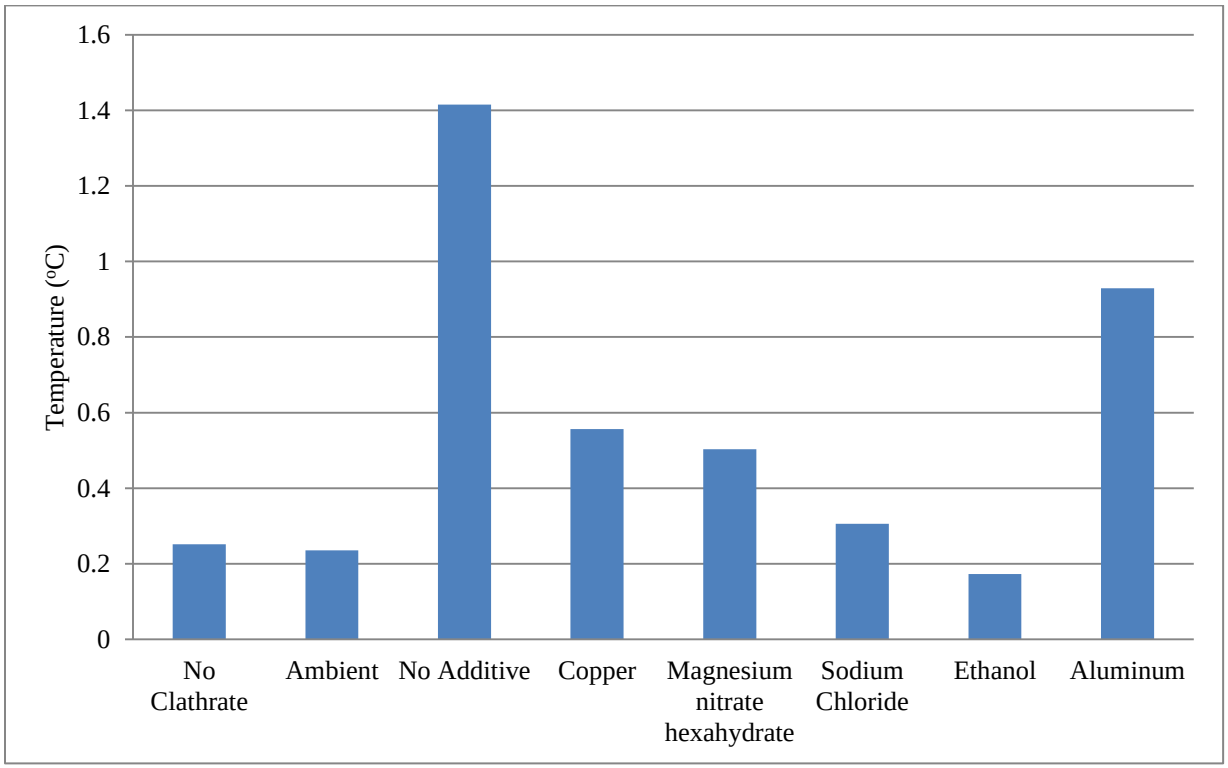

Figure 7.69 Standard deviations of battery cutoff temperatures of PCMs

Figure 7.70 shows the standard deviation associated with the liquid phase specific heat of the PCMs. It is the period before the onset of freezing. PCM with aluminum additive shows the least standard deviation while PCM without any additive shows the most. Standard deviation for base PCM without additive, PCM with ethanol and PCM with magnesium nitrate hexahydrate is high. Copper, aluminum and sodium chloride results show low uncertainty for liquid specific heat. The percent variation for all the tested materials is below 5%. Figure 7.71 shows the standard deviation associated with the liquid phase thermal conductivity of the PCMs. PCM with ethanol additive appear to have the highest standard deviation while PCM without any additive shows to have the least. For all the materials, except for ethanol additive, the percent variation is below 9%. For ethanol additive, the deviation is at 23%. Figure 7.72 shows the standard deviation associated with the mushy phase thermal conductivities of the PCMs. Mushy phase is the period after the onset of freezing until the PCM completely frozen. PCM without additive has the highest standard deviation of 3.5×10^{-2} J/kg K while the lowest is for sodium chloride PCM at 8×10^{-3} J/kg K. PCM without any additive appears to have the highest standard deviation while PCM with sodium chloride has the lowest deviation. For all the materials, except for PCM without additive, the percent variation is below 5%. For PCM without additive, the deviation is at 10%. Figure 7.73 shows the standard deviation associated with the specific latent heat of the PCMs. Specific latent heat is the heat required to change the phase per unit mass. So it is for the period after the onset of freezing until the PCM is completely frozen. PCM without any additive and PCM with sodium chloride additive appear to have the high standard deviations. Ethanol and copper

additive show low deviation in the results at below 1%. For all the other materials, the percent variation is around and above 10%.

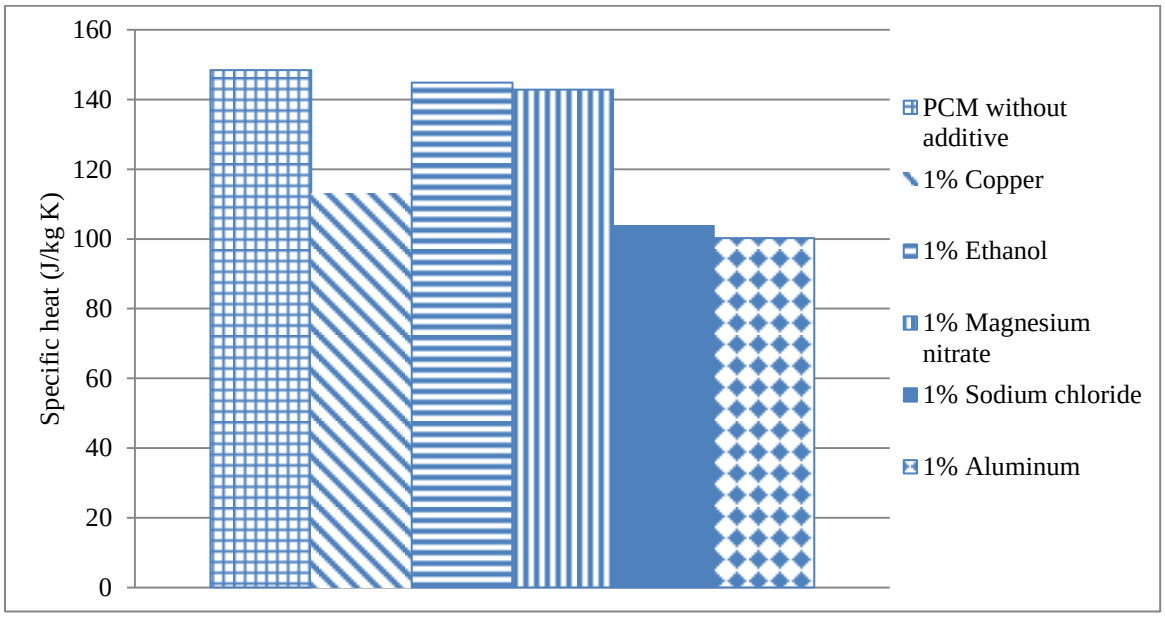

Figure 7.70 Standard deviations in liquid phase specific heat capacity values for PCM with different additives

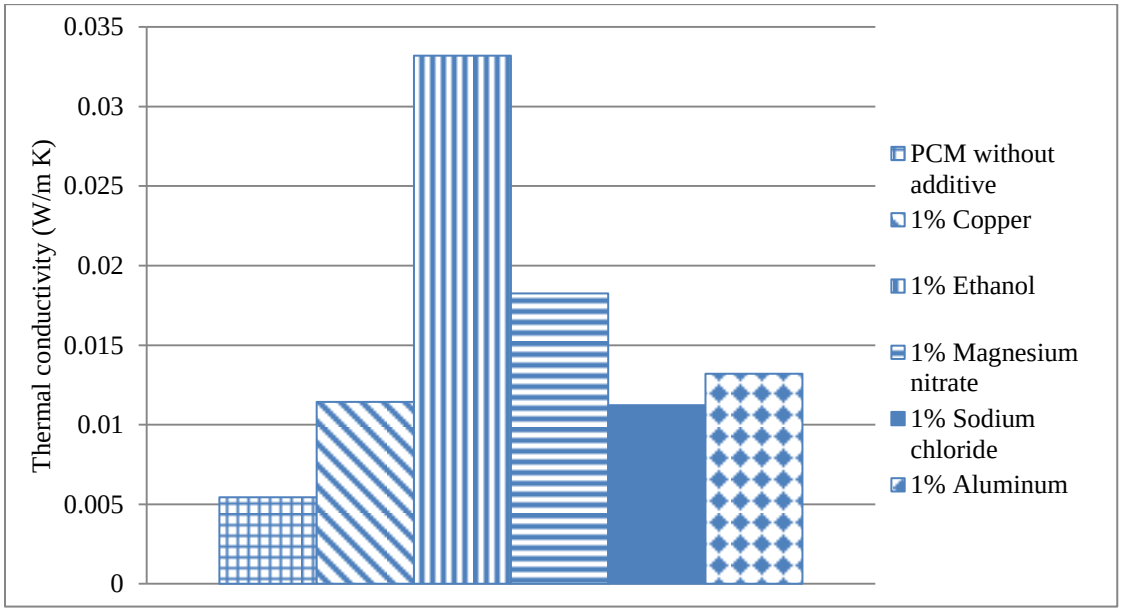

Figure 7.71 Standard deviations in liquid phase thermal conductivity values for PCM with different additives

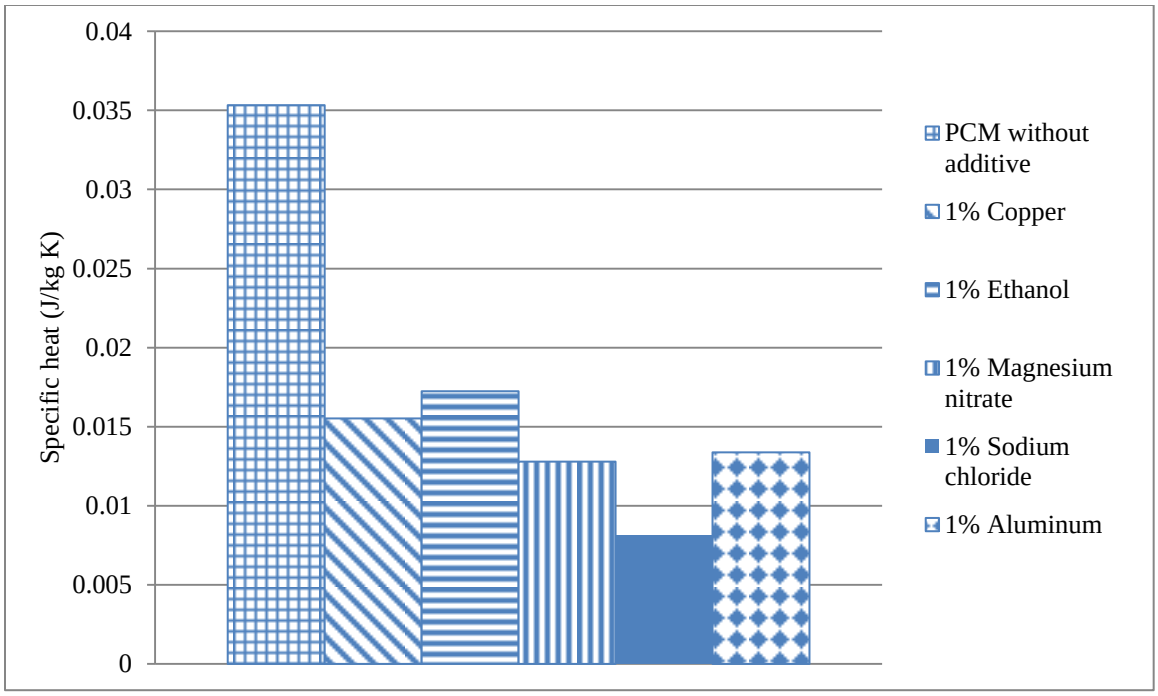

Figure 7.72 Standard deviations in mushy phase thermal conductivity values for PCM with different additives

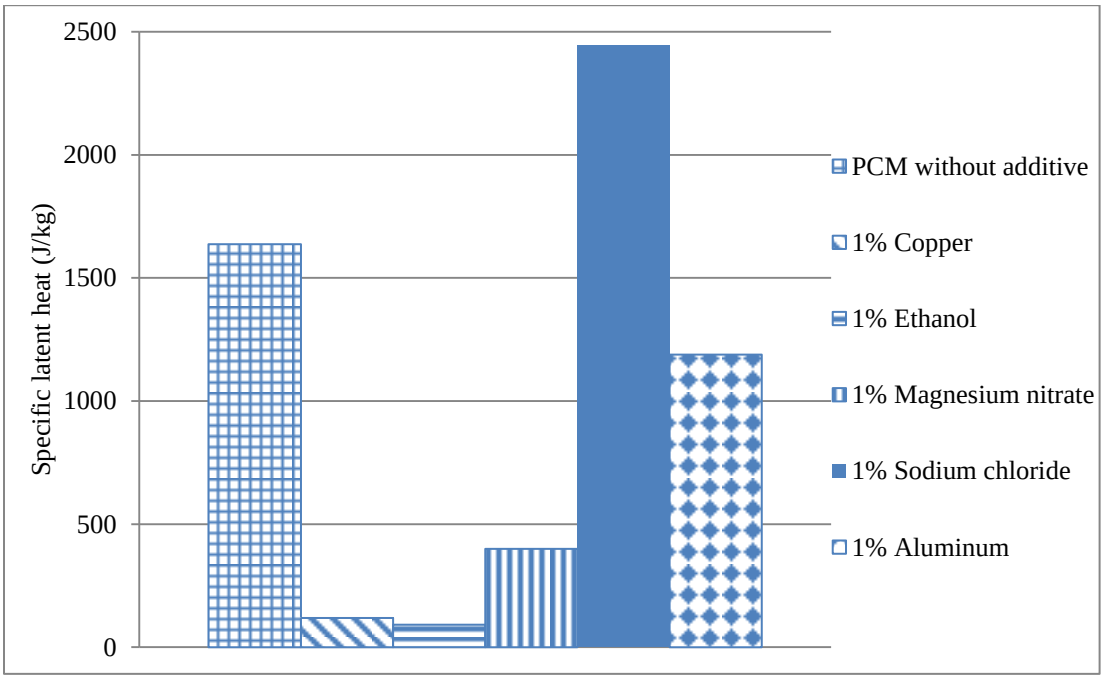

Figure 7.73 Standard deviations in specific latent heat values for PCMs with different additives

Figure 7.74 shows the percent variation in standard deviation for the thermal properties calculated for six different types of PCMs. Most of the results happen to have deviation below 5% while none of the deviations are above 25%. This acceptable standard deviation fraction shows the experimental values are not far away from one another hence can be considered satisfactory.

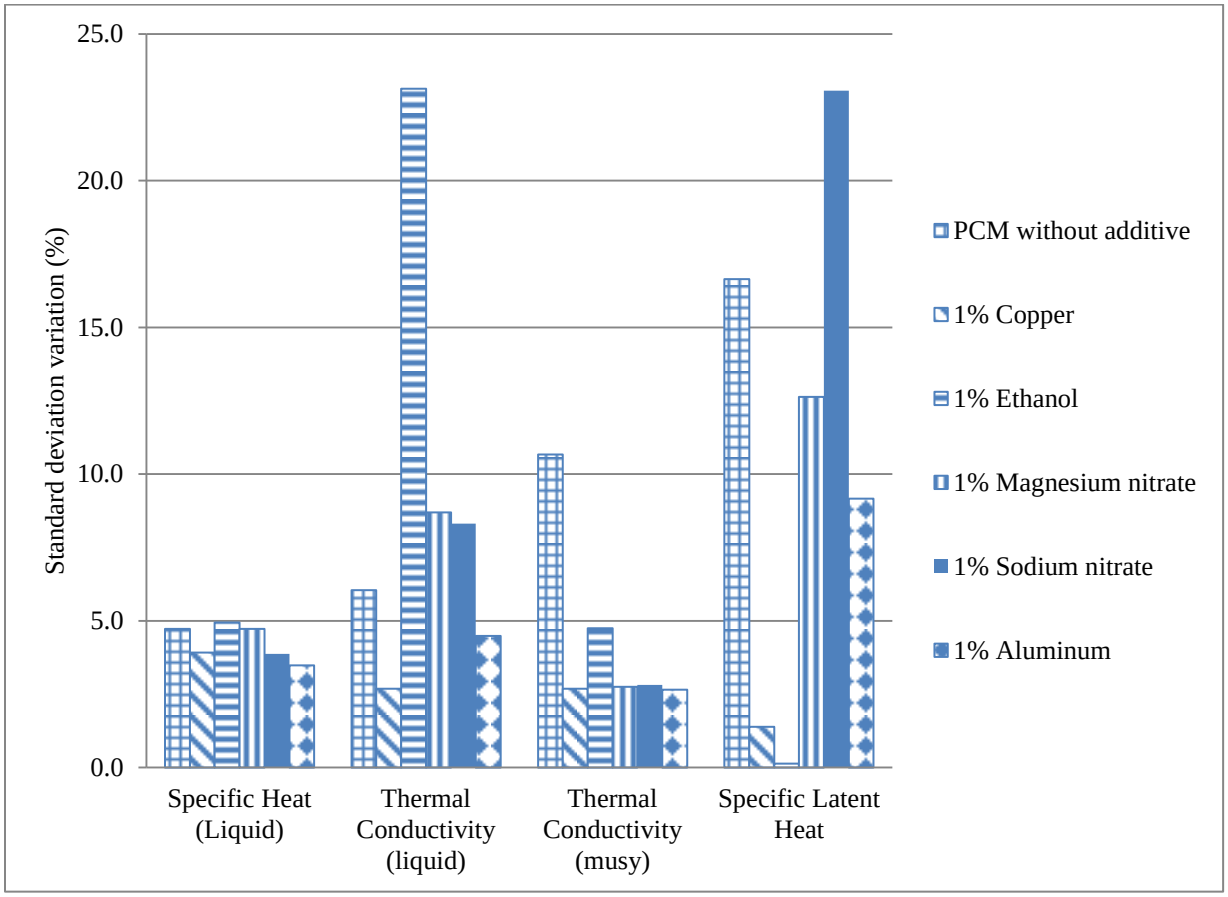

Figure 7.74 Percent variation in standard deviations of PCMs

7.10 Analytical Study Results of Thermal Properties of PCMs

In order to analytically study the influence of additives on refrigerant clathrates, three refrigerant candidates are isolated to see the improvements in specific heats and thermal conductivities. The selected refrigerant candidates are R1234yf, R134a and R32 for this analytical study. R134a is chosen for study due to its widespread use in cooling and heating cycles [41]. R1234yf and R32 are selected to be studied as they have low global warming potential and are considered potential candidates for replacement of existing refrigerants [112].

Several different additives are incorporated with the refrigerant clathrates to improve their thermal properties. Sodium chloride (NaCl) and magnesium nitrate hexahydrate ($(Mg(NO_3)_2.6H_2O$) are added in the refrigerant clathrates to evaluate the change in thermal conductivities and specific heats of the newly formed PCMs. In order to develop PCMs with improved thermal conductivities, nanoparticles of highly conductive materials are added. Aluminum, copper and grapheme nanoparticles are selected as additives to study the improvement in the thermal conductivity of the corresponding clathrate based on the selected refrigerants. The thermal properties are determined for variable fractions of refrigerants since their solubility changes with the change in temperature [89-93].

7.10.1 Specific Heat Results

Specific heat capacity is the ability of the material to absorb heat per unit change of its own temperature. The specific heat of the PCM is calculated using equation (6.5). It is desired to predict the specific heat as it helps in determining the heat capacity of the PCM

during the sensible heat storage temperature. The properties used to calculate the specific heats are listed in Table 7.18.

Table 7.18 Materials and their corresponding specific heat capacities [94-100,113-115]

Materials	Specific heats (J/kg K)
R134a	850
R1234yf	1256
R32	1370
Water	4200
Sodium chloride	880
Magnesium nitrate hexahydrate	4700
Aluminum	910
Copper	390
Graphene	600

Effects of Salts on Specific Heat Values

The effects of salts on the specific heat capacity values of the refrigerant clathrates are studied first. It highlights the effects salts have, as additives, on the refrigerant clathrates' specific heat capacities. This section shows the overall specific heat capacities for each refrigerant based clathrate with the two different salts studied. Figure 7.75 shows the specific heat values of R134a, R1234yf and R32 clathrates with sodium chloride and magnesium nitrate hexahydrate. The results are shown for 0.3 refrigerant mass fraction clathrate. For the sake of simplicity, it will be referred to as percentage refrigerant clathrate. The graph shows the variation in specific heat with respect to the water and salt mass fraction. It shows the linear decrease in specific heat of sodium chloride based PCM as the salt mass fraction increases. This decrease is due to the lower specific heat of sodium chloride as compared to the clathrate. Clathrate based on magnesium nitrate hexahydrate show linear increase in specific heat as the salt mass fraction increases due to its higher specific heat. The figure also shows that R32 based clathrates have the

highest specific heat, closely followed by R1234yf and then R134a. This is simply due to the difference in their individual specific heats. It can be seen from the graph that using magnesium nitrate hexahydrate with the refrigerant clathrate yields significantly high specific heat at high salt mass fraction.

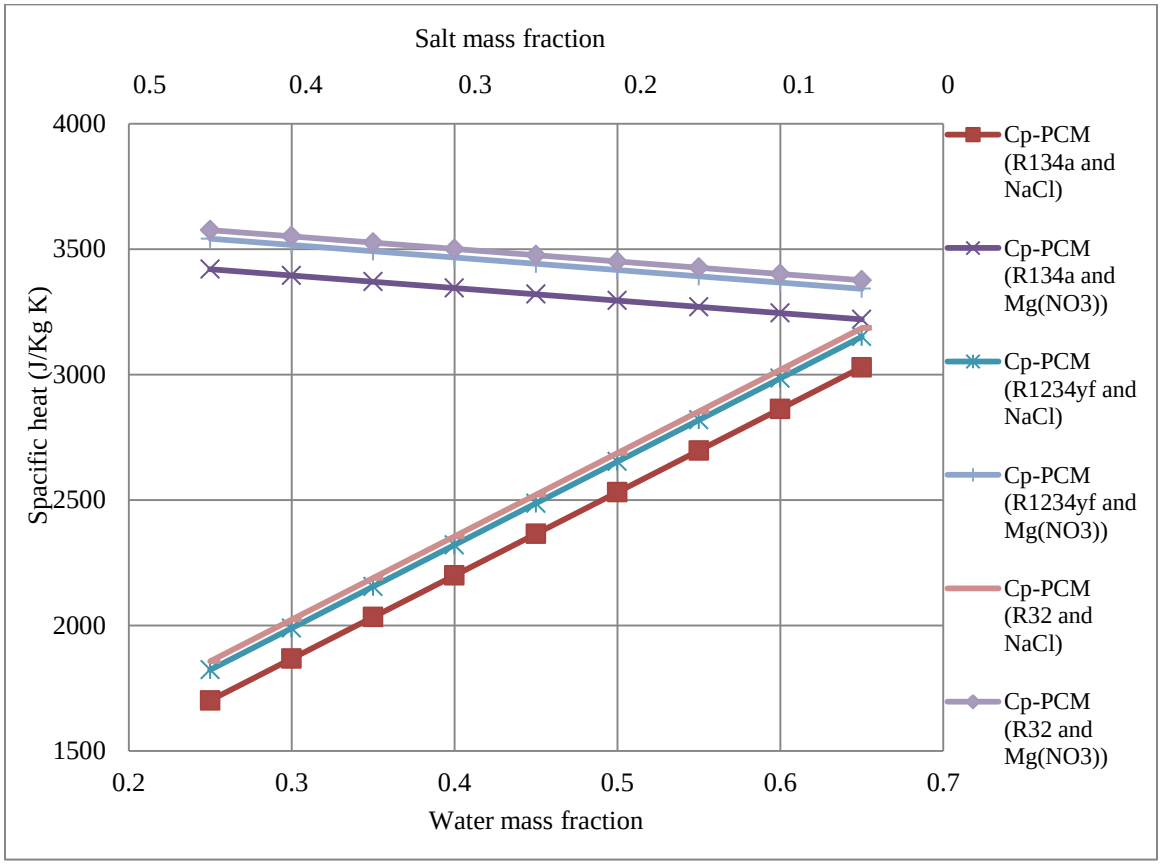

Figure 7.75 Specific heats for different refrigerant clathrates with salts

Figure 7.76 shows the change in specific heat of the PCM based on R32 refrigerant and salts. The variation is shown with respect to the change in salt and refrigerant mass fraction. The specific heat of the PCM increases with the increase in magnesium nitrate hexahydrate mass fraction and decreases with the increase in sodium chloride mass fraction. The increase in specific heat is due to the higher specific heat of

magnesium nitrate hexahydrate whereas the decrease is due to the lower specific heat of sodium chloride, compared to the R32 based clathrate. The specific heat decreases with the increase in refrigerant mass fraction since the refrigerant has lower specific heat compared to water. Using sodium chloride as additive lowers the specific heat of the clathrate. Hence, as a thermal energy storage material during sensible temperature period, it would be a bad choice. Using magnesium nitrate hexahydrate would turn out to be a feasible choice as a sensible thermal energy storage material. The impact of adding salts in clathrate can improve the latent heat. The effect on the phase change temperature of the clathrates is to be observed by conducting the experiments.

Figure 7.77 shows the change in specific heat of the PCM based on R134a refrigerant and salts. The variation is shown with respect to the change in salt and refrigerant mass fraction. Similar to the other refrigerant based PCMs, the specific heat increases with the increase in magnesium nitrate hexahydrate mass fraction and decreases with the increase in sodium chloride mass fraction. The specific heat decreases with the increase in refrigerant mass fraction since the refrigerant R134a has lower specific heat compared to water. Even for R134a based PCMs, using magnesium nitrate hexahydrate would produce the PCM with better specific heat property as compared to sodium chloride.

Figure 7.78 shows the change in specific heat of the PCM based on R1234yf refrigerant and salts. The variation is shown with respect to the change in salt and refrigerant mass fraction. The specific heat trend is found to be the same as with the PCMs based on R134a and R32. The specific heat increases with the increase in magnesium nitrate hexahydrate mass fraction and decreases with the increase in sodium

chloride mass fraction. Once again, using magnesium nitrate hexahydrate would produce the PCM with better specific heat property as compared to sodium chloride.

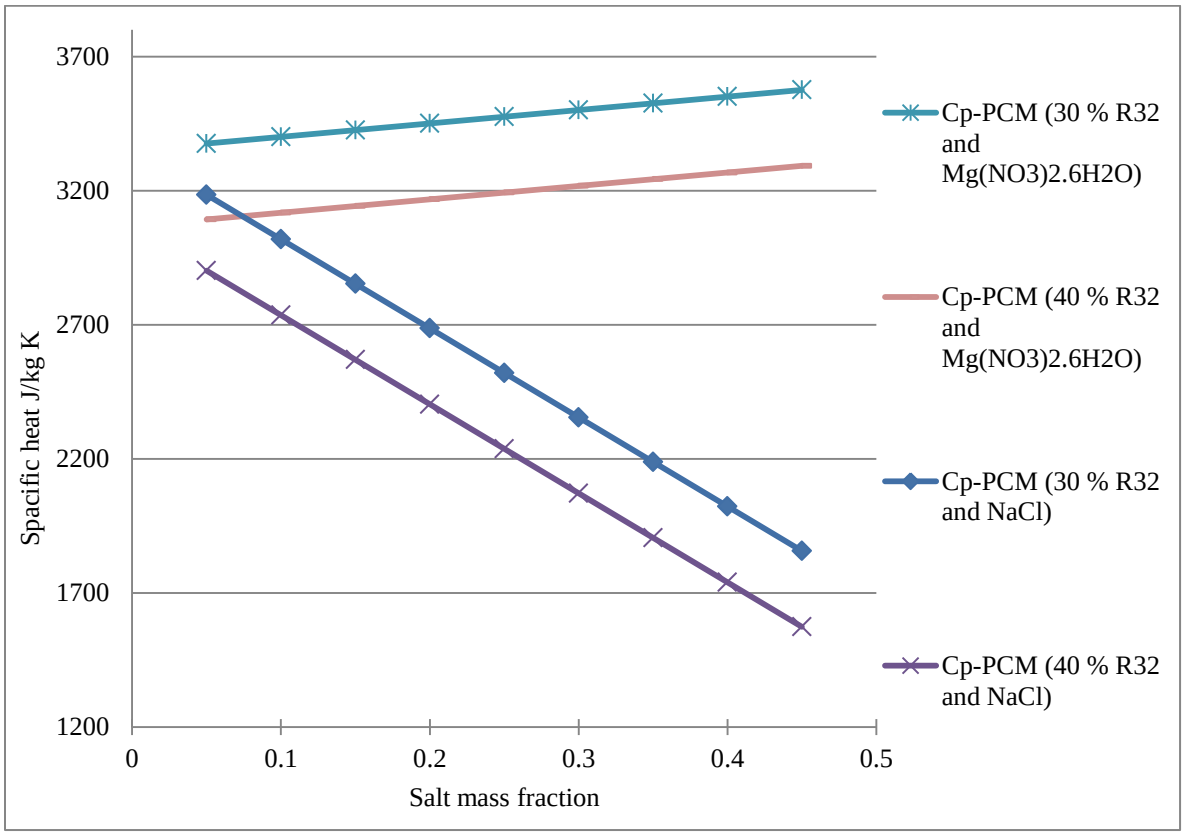

Figure 7.76 R32 clathrates with salts at different refrigerant fractions

Effects of Nanoparticles on Specific Heat Values

The effects of nanoparticles on the specific heat capacity values of the refrigerant clathrates are also studied. This section presents the impact of each nanoparticle material on the refrigerant clathrate‘s specific heat. It also shows how much of an improvement can be achieved by using nanoparticles over salts.

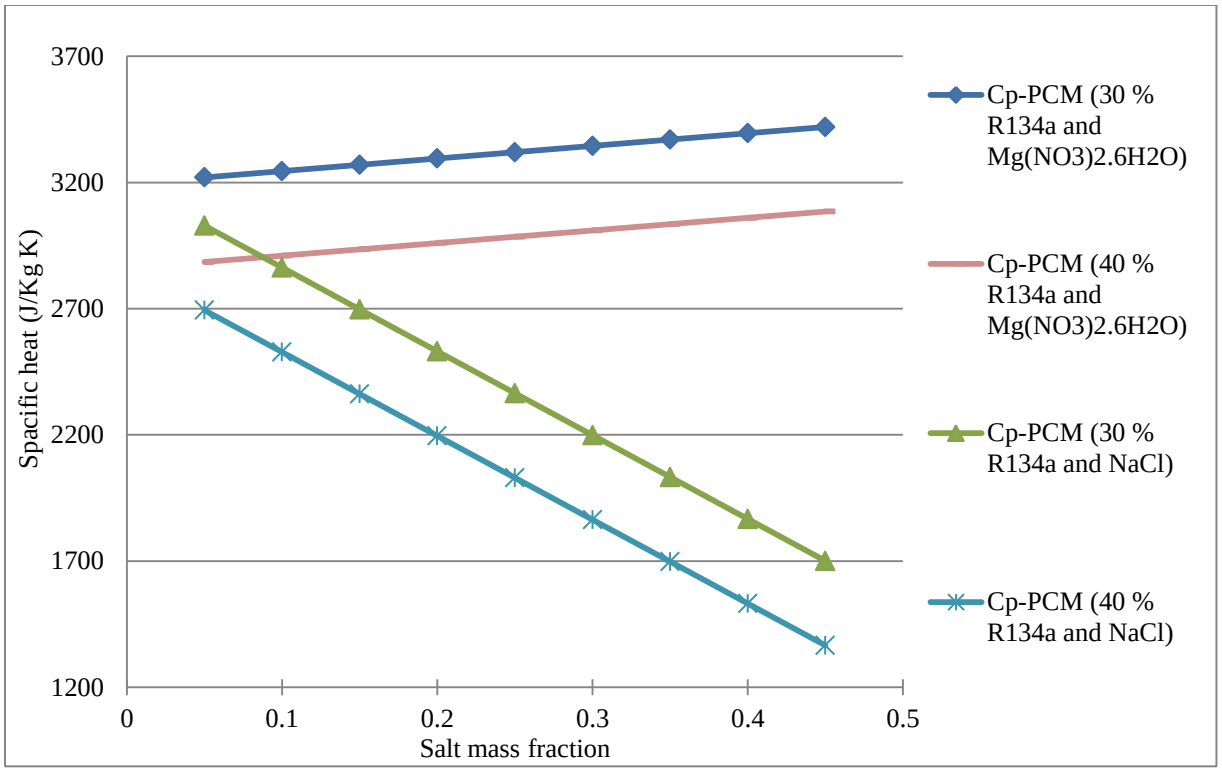

Figure 7.77 R134a clathrates with salts at different refrigerant fractions

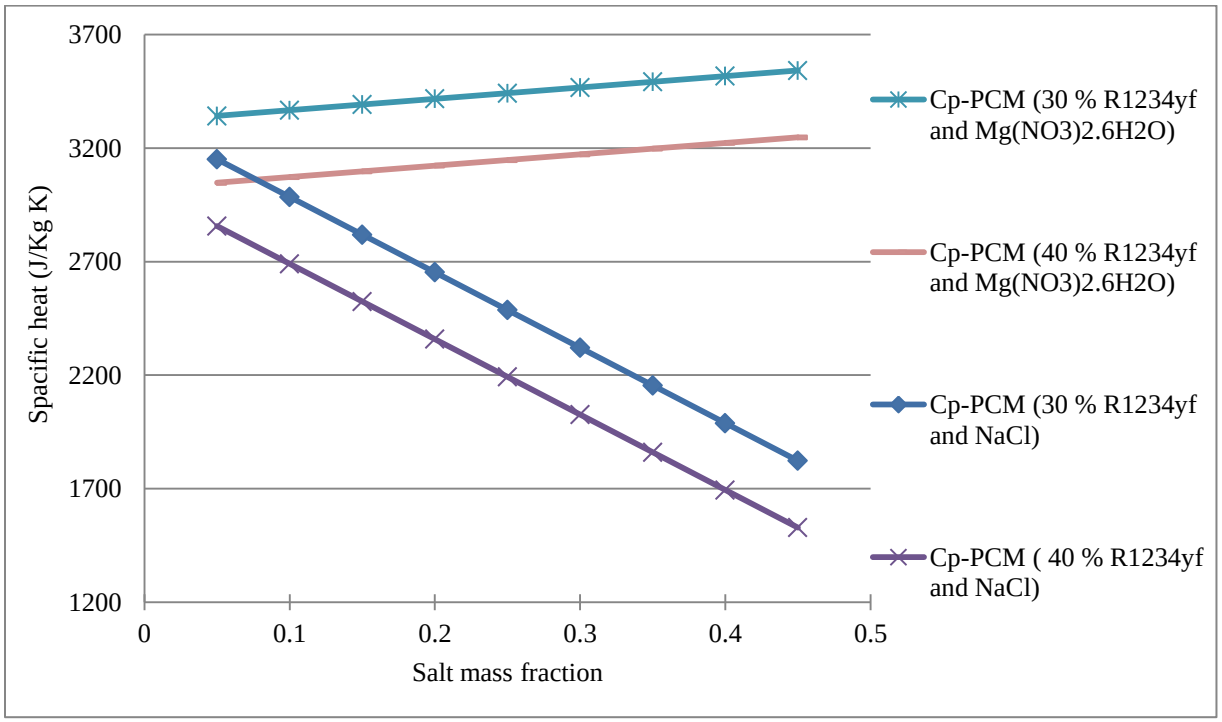

Figure 7.78 R1234yf clathrates with salts at different refrigerant fractions

Figure 7.79 shows the change in specific heat of the PCM based on studied refrigerants and nanoparticles. The variation is shown with respect to the change in water and nanoparticle mass fraction with 0.3 refrigerant mass fraction clathrate. For the sake of simplicity, it will be referred as percentage refrigerant clathrate. For PCM with graphene and copper nanoparticles, the specific heat decreases with the increase in nanoparticles. This trend is due to low specific heat of graphene and copper, compared to any of the studied refrigerant based clathrates. For copper based PCM, the decrease is not as steep as for graphene. PCM with aluminum nanoparticles, however, show an increase in specific heat with the increase in mass fraction of aluminum. Amongst the refrigerants, R32 has the highest specific heat, closely followed by R1234yf and then R134a. The graph shows that PCM based on R32 or R1234yf with aluminum nanoparticles would serve effectively as heat storage medium during sensible temperature region.

Figure 7.80 shows the change in specific heat of the PCM based on R32 and nanoparticles. The variation is shown with respect to the change in refrigerant percent mass fraction and nanoparticle mass fraction. As the nanoparticle mass fraction increases, the specific heat decreases for graphene and copper. For aluminum, the specific heat linearly increases. The specific heat is found to be higher when the refrigerant mass fraction is low. This is due to higher specific heat of water compared to R32. It can be seen from the graph that at low mass fraction of nanoparticles, refrigerant mass fraction has greater effect on the specific heat as compared to the nanoparticles' mass fraction. Figure 7.80 shows that aluminum with low R32 mass fraction appears to have the highest specific heat and it increases with the increase in nanoparticle mass fraction.

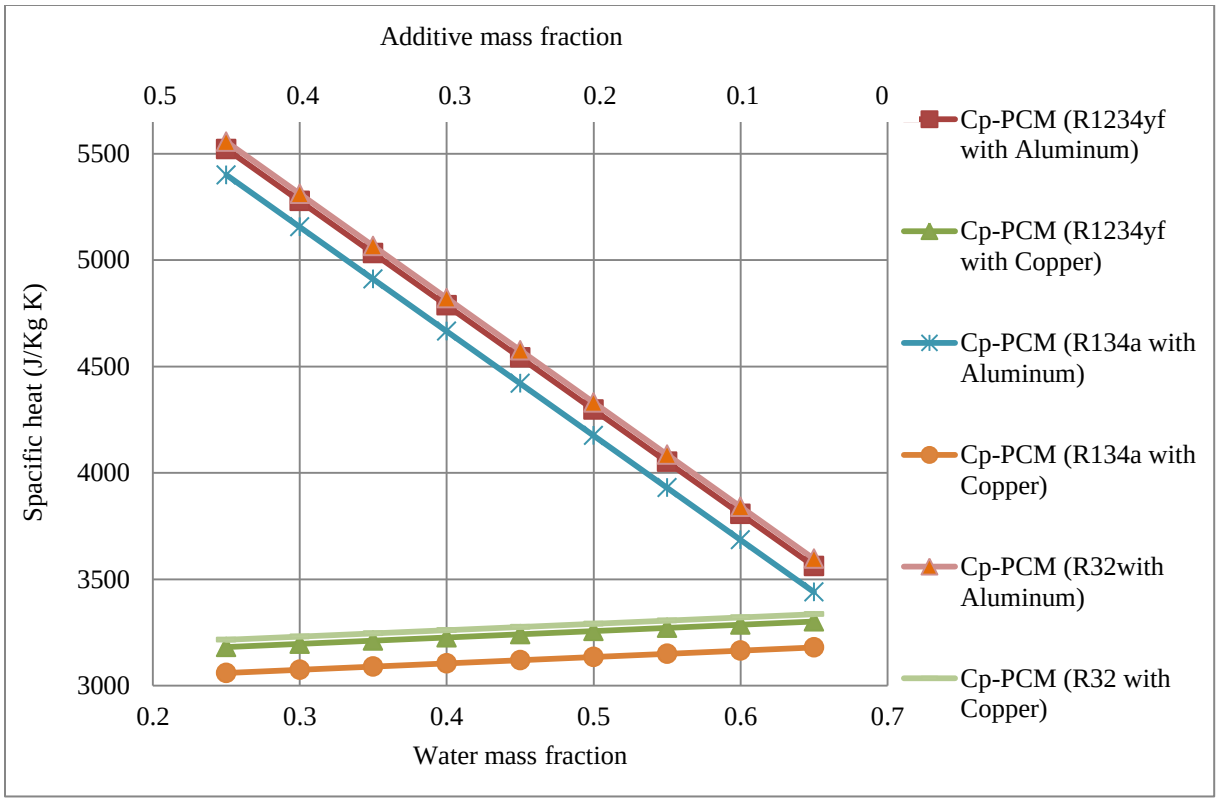

Figure 7.79 Specific heats for the different refrigerant clathrates with nanoparticles

Figure 7.81 shows the change in specific heat of the PCM based on R134a and nanoparticles. The variation is shown with respect to the change in refrigerant percent mass fraction and nanoparticle mass fraction. As the nanoparticle mass fraction increases, the specific heat decreases for graphene and copper. For aluminum, the specific heat linearly increases with the increase in its mass fraction. The specific heat is again found to be higher when the refrigerant mass fraction is low due to higher specific heat of water compared to R134a. For low mass fraction of nanoparticles, the refrigerant mass fraction has greater effect on the specific heat as compared to the nanoparticle's mass fraction. Figure 7.81 shows that aluminum with low R134a mass fraction appears to have the highest specific heat and it increases with the increase in nanoparticle mass fraction.

Figure 7.82 shows the change in specific heat of the PCM based on R1234yf and nanoparticles. The variation is shown with respect to the change in refrigerant percent mass fraction and nanoparticle mass fraction. The trend is found to be similar as with the R32 and R134a based PCMs. As the nanoparticle mass fraction increases, the specific heat decreases for graphene and copper while for aluminum, the specific heat linearly increases. The specific heat is again found to be higher when the refrigerant mass fraction is low due to higher specific heat of water compared to R1234yf. Aluminum with low R1234yf mass fraction appears to have the highest specific heat and it increases with the increase in nanoparticle mass fraction.

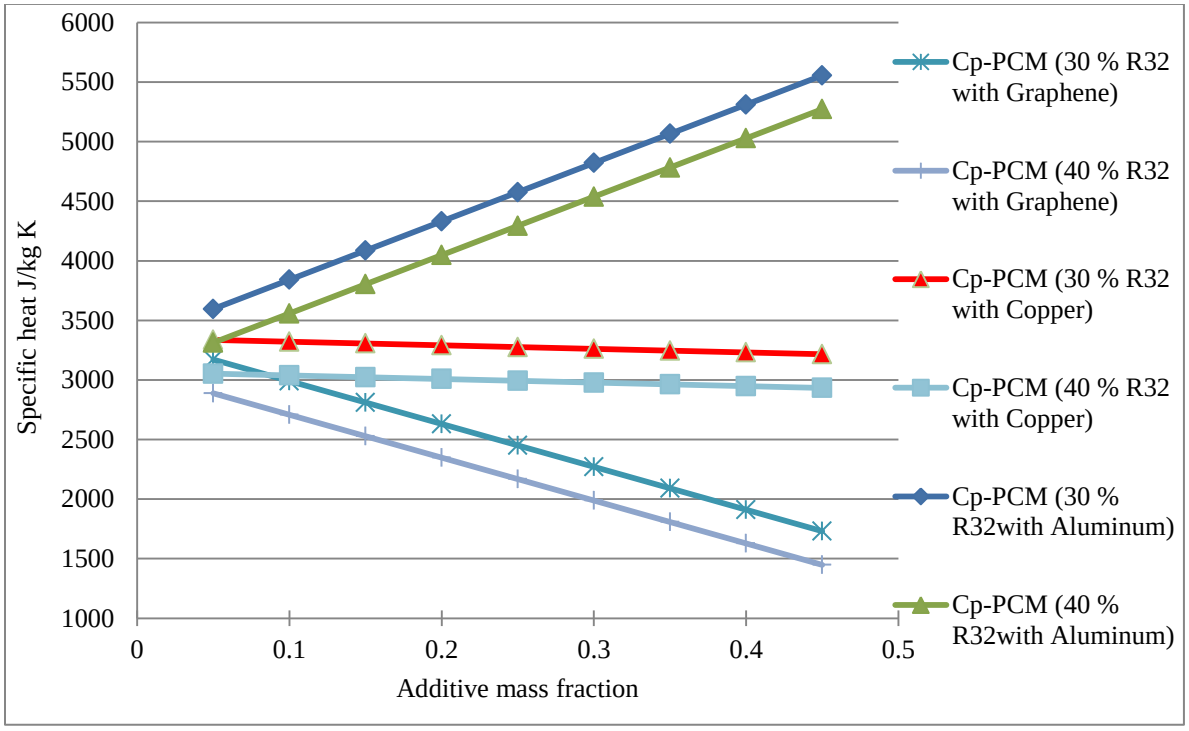

Figure 7.80 R32 clathrates with nanoparticles at different refrigerant fractions

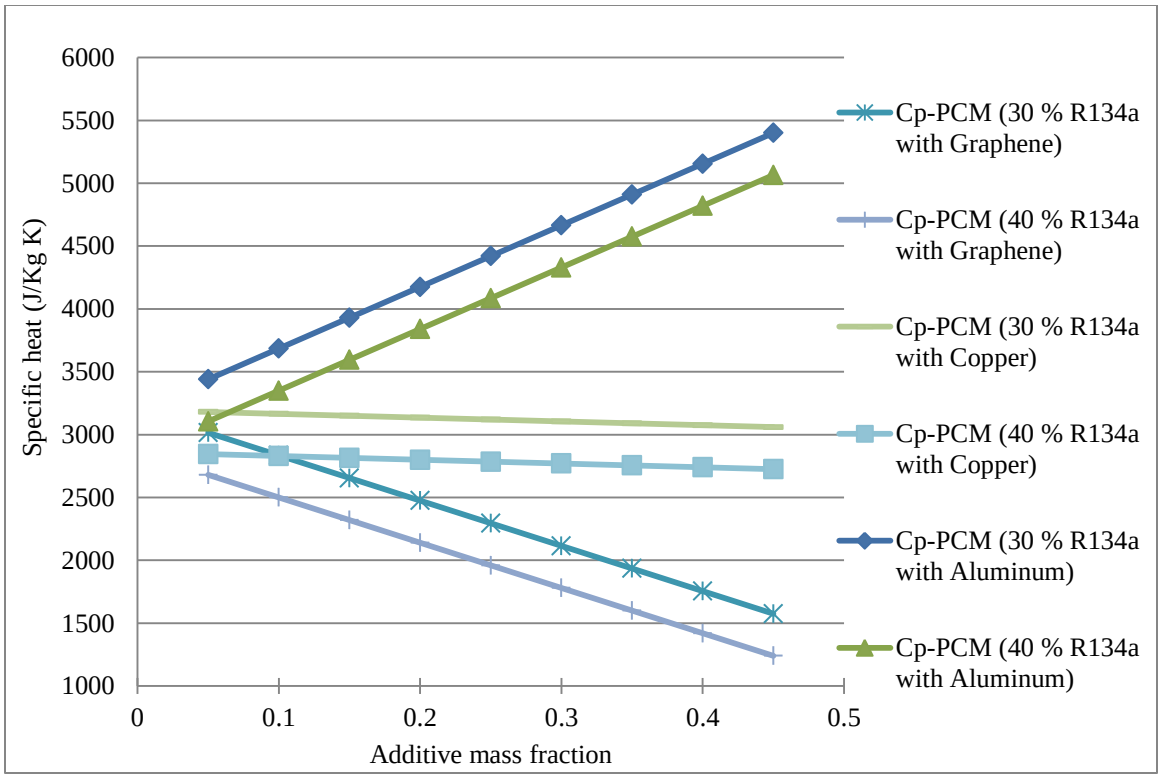

Figure 7.81 R134a clathrates with nanoparticles at different refrigerant fractions

7.10.2 Thermal Conductivity Results

Using equation (6.13), the thermal conductivities of the refrigerant clathrates are calculated. The solubility of the refrigerant in water changes with the operating temperature hence the thermal conductivity is determined for a variety of mass fractions over a range of operating temperatures. The properties used to calculate the thermal conductivities of the clathrates are listed in Table 7.19 as taken from the literature sources [116-120].

Figure 7.83 shows the change in thermal conductivities as the refrigerant mass fraction changes for R134a, R32 and R1234yf refrigerants. The thermal conductivity trend shown in Figure 7.83 is for pure clathrate without any additive or nanoparticles. At low refrigerant mass fraction, the thermal conductivities do not vary a lot for the studied

refrigerants. However, for high refrigerant mass fractions, distinct thermal conductivity starts to appear. Thermal conductivity for R32 based clathrate is the lowest, followed by R134a. R1234yf based clathrate is found to have the highest thermal conductivity. This trend matches with the dipole moment and molar mass of the discussed refrigerants. It appears that the thermal conductivity of the clathrates depend more on the dipole moment than the individual components' thermal conductivities.

Table 7.19 Parameters and their corresponding values for calculation of thermal conductivities of refrigerant clathrates

	Water	**R134a**	**R1234yf**	**R32**
Critical Temperature, T_c	647 K	374 K	368 K	351 K
Thermal Conductivity, k	0.58 W/m K	0.092 W/m K	0.05 W/m K	0.155 W/m K
Dipole Moment, D	6.2×10^{-30} C m	4.8×10^{-30} C m	8.3×10^{-30} C m	2.8×10^{-30} C m
Molar Mass, M	18 mol/g	102 mol/g	114 mol/g	52 mol/g

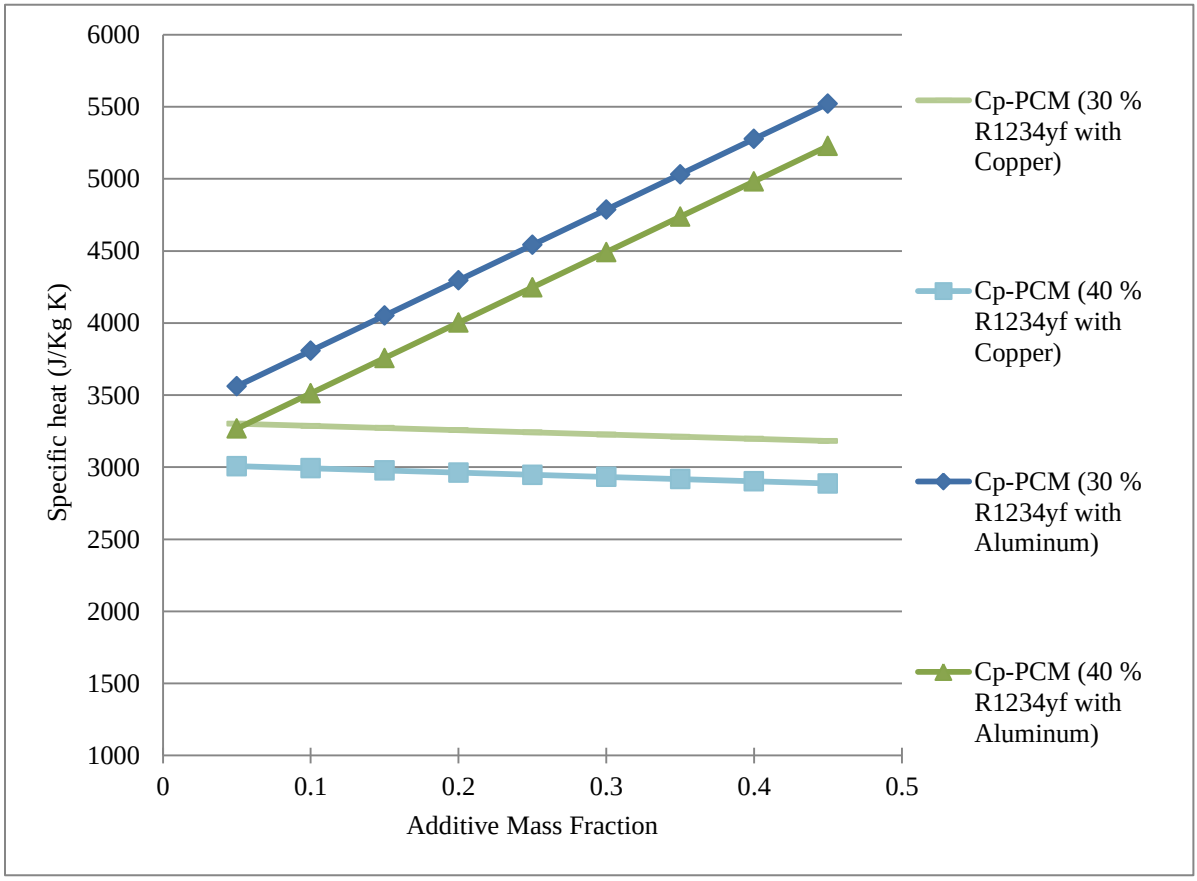

Figure 7.82 R1234yf clathrates with nanoparticles at different refrigerant fractions

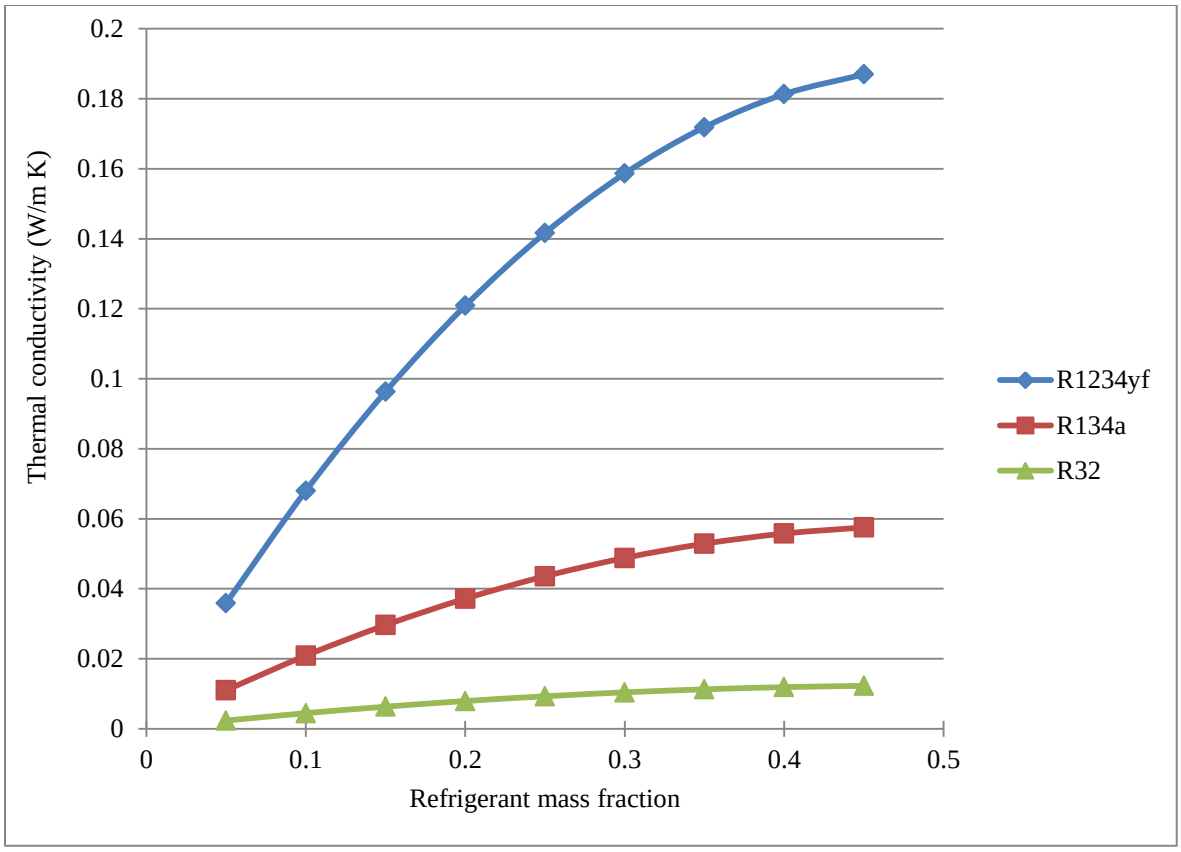

Figure 7.83 Clathrate thermal conductivities with different refrigerants against refrigerant mass fractions

Effects of Nanoparticles on Thermal Conductivity Values

The effects of nanoparticles, as additives, on thermal conductivities of the refrigerant clathrate are evaluated. The thermal conductivity improvement is important to establish as it helps select the most appropriate additive. Using equation (6.20), the thermal conductivity of the PCM containing refrigerant clathrate with nanoparticles, is calculated. The parameters used to determine the thermal conductivities of the PCMs are listed in Table 7.20.

Table 7.20 Parameters and their corresponding values for calculation of thermal conductivities [89, 108 – 111, 121]

Parameter	Value
Thermal interface resistance - R_b	98 x 10^{-10} K m^2/W
Nanoparticle diameter - d_p	10 nm
Reynolds' number – Re	0.029
Nusselt number	1
Thermal conductivity - Aluminum	210 W/m K
Thermal conductivity - Copper	410 W/m K
Thermal conductivity - Graphene	3000 W/m K
Thermal conductivity – Sodium chloride	6.5 W/m K
Thermal conductivity – Magnesium nitrate hexahydrate	0.7 W/m K
A	40,000
m	2.5%

Figure 7.84 shows the variation in thermal conductivities of PCMs with different refrigerants and aluminum nanoparticles. The thermal conductivities are studied over a range of nanoparticle volume fractions. The figure shows the increasing trend in thermal conductivity of the PCM as the aluminum nanoparticles volume fraction increases. The graph also shows that R1234yf based PCM produces the highest thermal conductivity due to the high thermal conductivity of its clathrate. R32 based PCM yields the lowest thermal conductivity. High refrigerant fraction is found to yield greater thermal conductivities since the thermal conductivity increases with the increase in refrigerant fraction.

Figure 7.85 shows the variation in thermal conductivities of the PCMs with copper nanoparticles and different refrigerants. The thermal conductivity is studied over a range of nanoparticle volume fraction. Figure 7.84 also shows the exponentially increasing trend in thermal conductivity of the PCM containing copper nanoparticles. The graph also shows that R1234yf based PCM produces the highest thermal conductivity due

to the high thermal conductivity of the clathrate while R32 based PCM yields the lowest thermal conductivity.

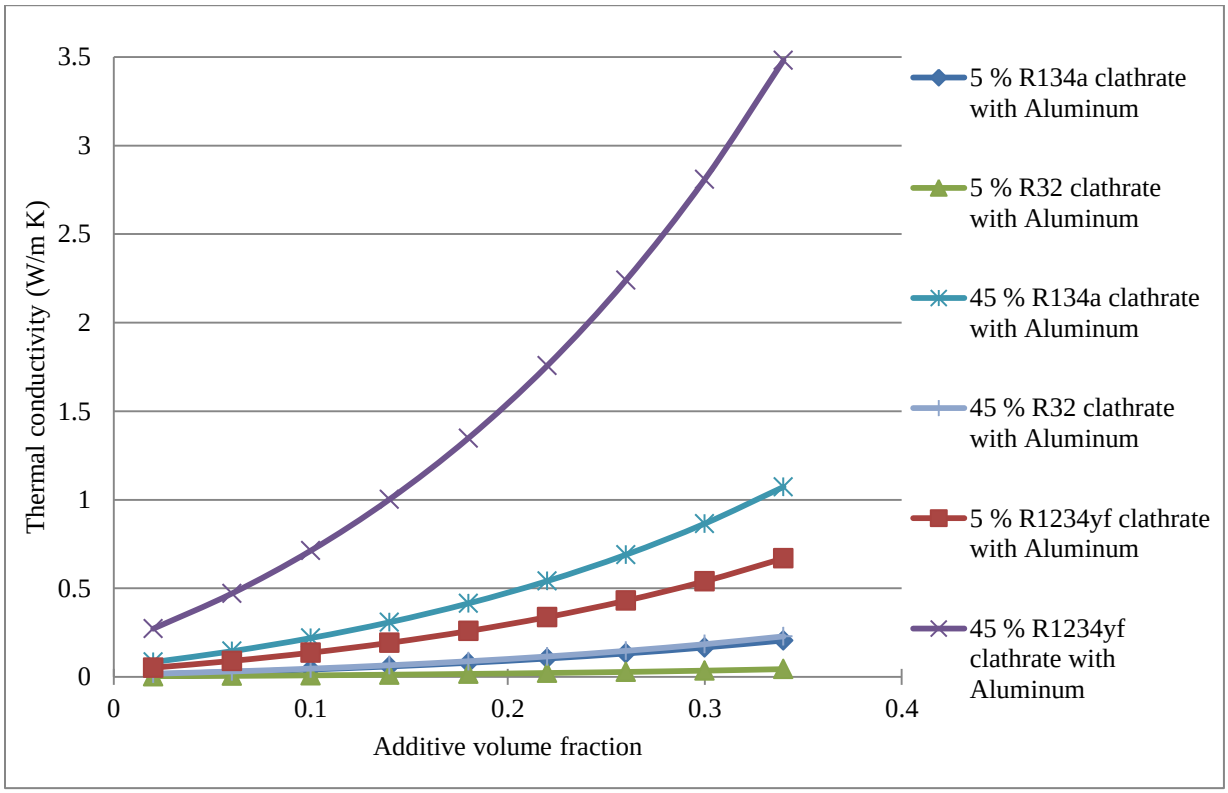

Figure 7.84 Thermal conductivities of refrigerant clathrates with aluminum particles

Figure 7.86 shows the variation in thermal conductivities of the PCMs with graphene nanoparticles and different refrigerants. The graph shows the exponentially increasing trend in thermal conductivity of the PCM containing graphene nanoparticles in spite the fact that graphene has 7 times higher thermal conductivity than copper. The graph also shows that R1234yf based PCM produces the highest thermal conductivity due to the high thermal conductivity of the refrigerant. R32 based PCM yields the lowest thermal conductivity.

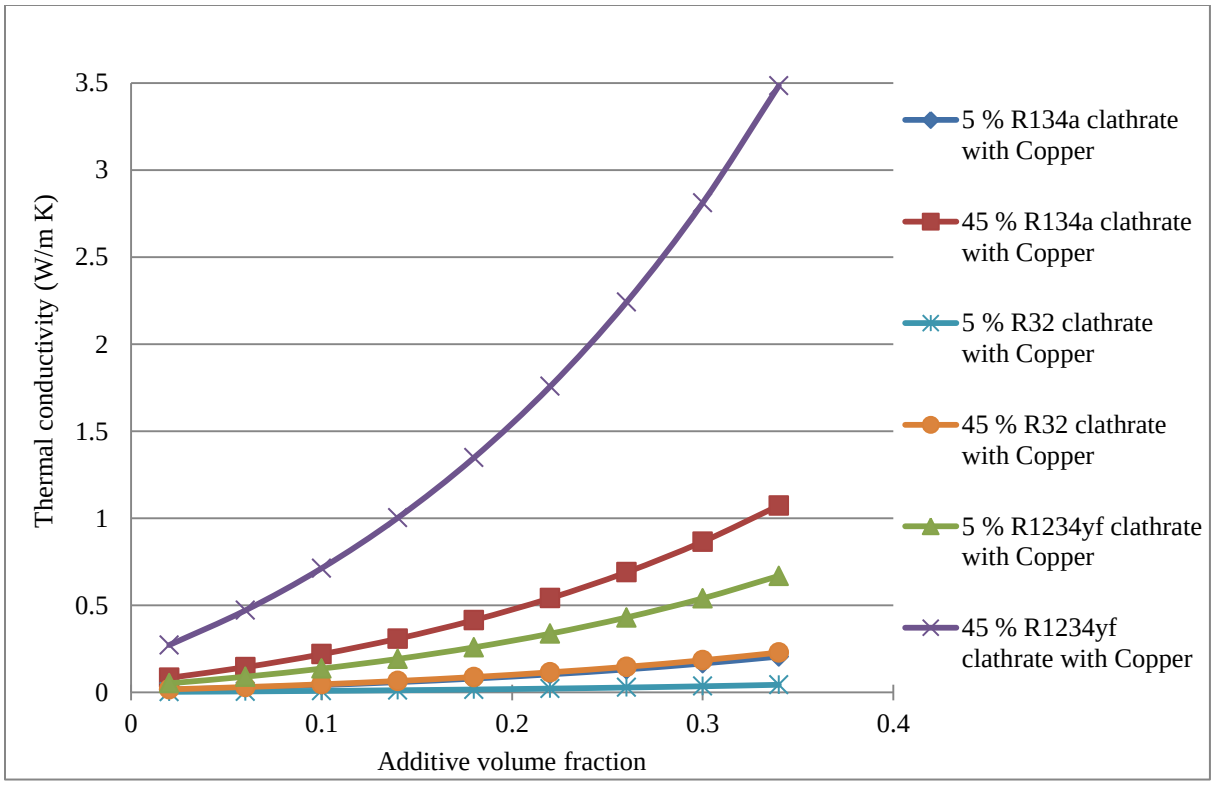

Figure 7.85 Thermal conductivities of refrigerant clathrates with copper particles

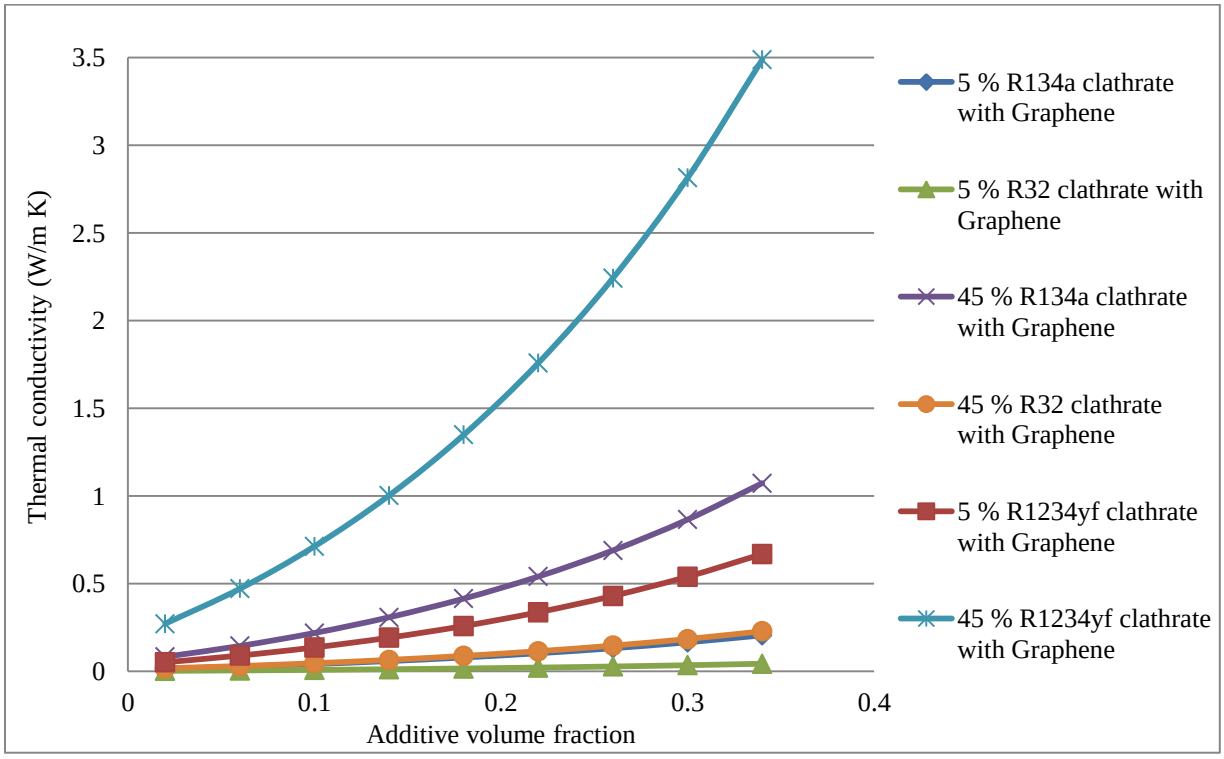

Figure 7.86 Thermal conductivities of refrigerant clathrates with graphene particles

Figure 7.87 shows the improvement in thermal conductivity after using the selected nanoparticles for different refrigerant mass fraction. The graph also shows the baseline thermal conductivity of R1234yf based clathrate. For 0.05 refrigerant mass fraction clathrate, thermal conductivity improves 2.5 times better than base refrigerant clathrate. For 0.45 refrigerant mass fraction clathrate, the improvement is 2.55 times batter. The graph shows that the inclusion of nanoparticles improves the thermal conductivity of the PCM. Graphene improves the thermal conductivity the most, followed by copper and then aluminum. Although the thermal conductivity difference in pure species of nanoparticle is significant, their use as additives in refrigerant clathrate does not yield a significant increase in the thermal conductivity. This is due to the greater influence of thermal transport due to Brownian motion of nanoparticles. For R1234yf clathrates, the difference in thermal conductivities is significant for different refrigerant mass fractions while low refrigerant mass fraction yields low thermal conductivity. The reason for high thermal conductivity with large refrigerant fraction is the increase in thermal conductivity of R1234yf refrigerant clathrate with respect to refrigerant mass fraction.

Figure 7.88 shows the variation in thermal conductivity for PCM with aluminum, copper and graphene nanoparticles for different refrigerant mass fraction. The graph also shows the baseline thermal conductivity of R32 based clathrate. For low refrigerant mass clathrate, the thermal conductivity increases from 2.3×10^{-3} W/m K to 5.9×10^{-3} W/m K for almost all the nanoparticle materials. This represents an increase of 2.6 times, due to the addition of nanoparticles. For 0.45 refrigerant mass fraction clathrate, 1.2×10^{-2} W/m K to 22.9 W/m K which shows that nanoparticles makes, thermal conductivity of the R32 based clathrates, 19 times batter. With a minor difference, graphene improves the thermal

conductivity the most, followed by copper and then aluminum. For R32 clathrates, high refrigerant mass fraction yields slightly higher thermal conductivity for the PCM due to high thermal conductivity of R32 refrigerant clathrate.

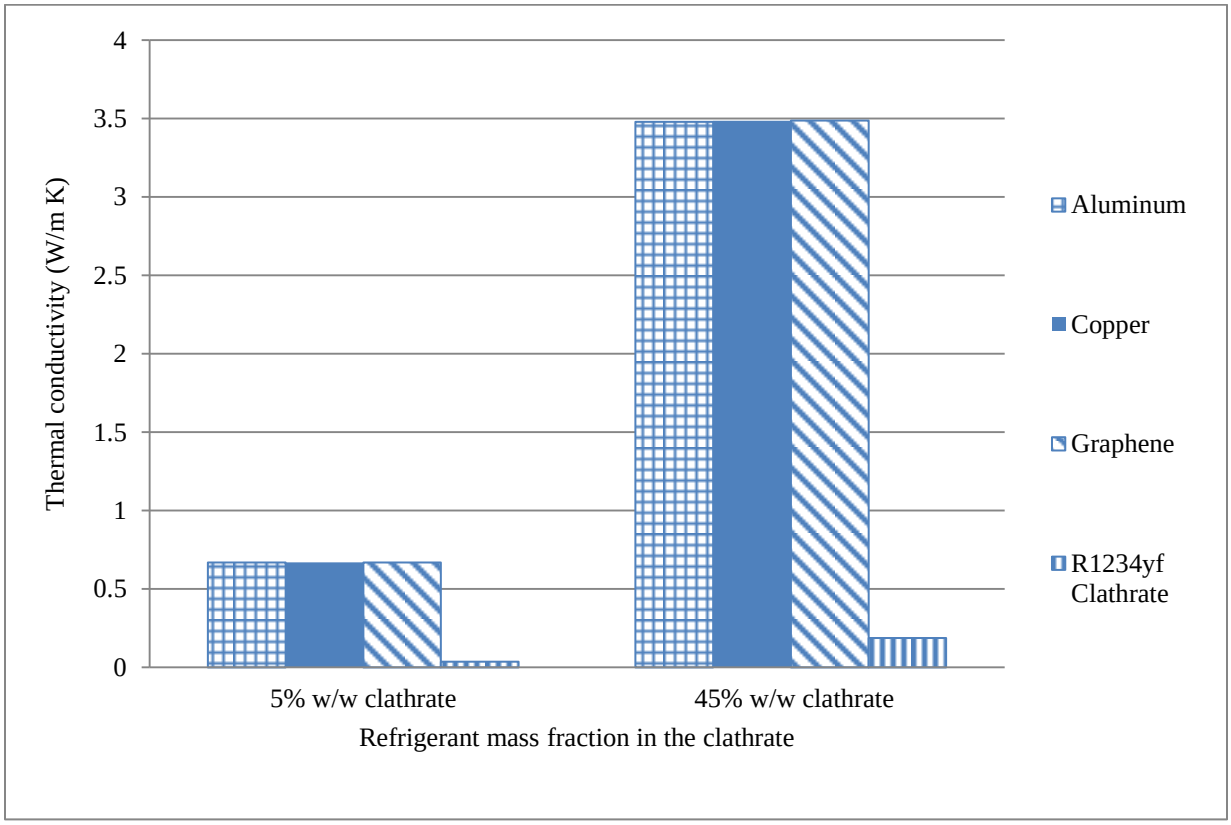

Figure 7.87 Thermal conductivity comparisons for different nanoparticles in R1234yf based clathrates

Figure 7.89 shows the improvement in thermal conductivities after using the selected nanoparticles for different refrigerant mass fraction. At 0.05 refrigerant mass fraction, thermal conductivity improves from 1.1 x 10^{-2} W/m K to 0.2 W/m K due to the presence of nanoparticles. The improvement is 19 times over the baseline thermal conductivity. For 0.45 refrigerant mass fraction clathrate, thermal conductivity improves from 0.06 W/m K to 1.07 W/m K which is an improvement of 18.8 times. Once again, for R134a based PCM, high refrigerant mass fraction yields higher thermal conductivity.

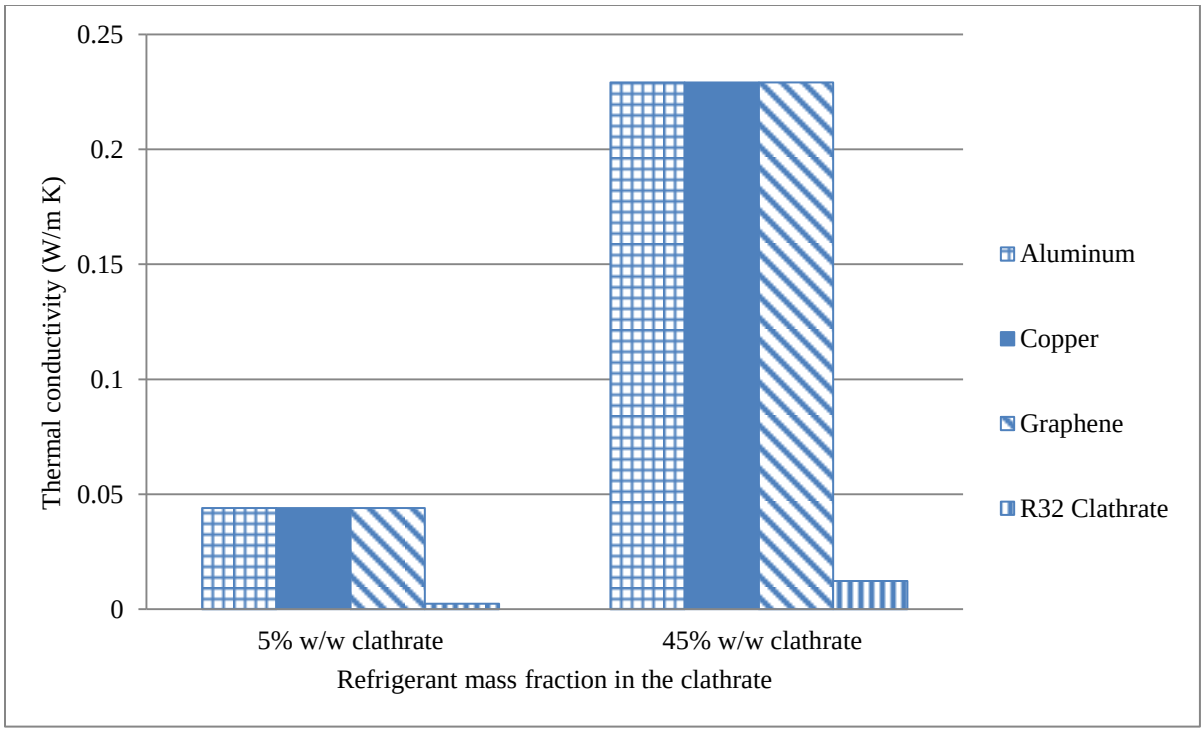

Figure 7.88 Thermal conductivity comparisons for different nanoparticles in R32 based clathrates

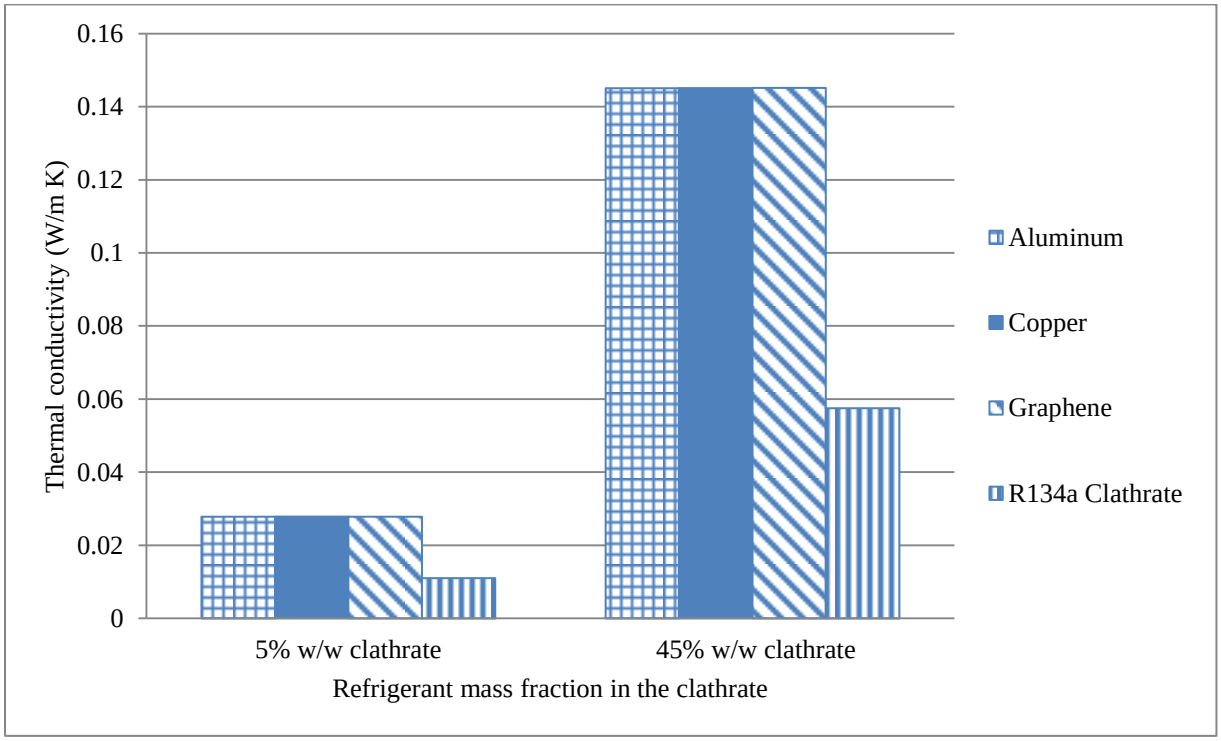

Figure 7.89 Thermal conductivity comparisons for different nanoparticles in R134a based clathrates

Effects of Salts on Thermal Conductivity Values

The effects of salts, as additives, on the thermal conductivities of PCMs are determined. Using equation (6.22), the thermal conductivity of the PCM containing refrigerant clathrate with salts is calculated.

Figure 7.90 shows the thermal conductivities of R134a clathrates with salt additives. The thermal conductivity is plotted against a wide range of salt volume fractions. The studied salts are sodium chloride and magnesium nitrate hexahydrate. Thermal conductivity of both the studied salts is higher hence they both improved the thermal conductivity of the formed PCM. However, sodium chloride improved the thermal conductivity significantly more than magnesium nitrate hexahydrate. Sodium chloride improved the thermal conductivity 19% for high quantity refrigerant clathrate, compared to magnesium nitrate hexahydrate, while the improvement is 3.8% for low quantity refrigerant clathrate. All these improvements are for 0.34 volume fraction of salt. The thermal conductivity increases with the increase in volume fraction of salts. It can also be observed that higher refrigerant mass clathrate yields higher thermal conductivity.

Figure 7.91 shows the thermal conductivities of R1234yf clathrates with salt additives. Thermal conductivities of both the studied salts are higher hence they both improved the thermal conductivity of the formed PCM. However, for high quantity refrigerant clathrate, sodium chloride improved the thermal conductivity 50% more than magnesium nitrate hexahydrate. For low quantity refrigerant clathrate, the thermal conductivity improvement using sodium chloride is 12% over the other studied salt. All these improvements are for 0.34 volume fraction of salt. The thermal conductivity rises with an increase in volume fraction of salts.

Figure 7.92 shows the thermal conductivities of R32 clathrates with salt additives against a wide range of salt volume fractions. Thermal conductivity of both the studied salts improved the thermal conductivity of the formed PCM. For high quantity refrigerant clathrate, sodium chloride improved the thermal conductivity by 4% compared to magnesium nitrate hexahydrate. For low quantity refrigerant clathrate, the improvement is less than 1%. All these improvements are for 0.34 volume fraction of salt. As is the case with other refrigerant PCMs, the thermal conductivity increases with the increase in volume fraction of salts.

Figure 7.93 shows the change in thermal conductivities with respect to the change in salt volume fraction. The graph shows the 0.45 refrigerant mass fraction clathrates. The graph shows that R1234yf refrigerant yields the highest thermal conductivity irrespective of the salt. For sodium chloride as additive, R1234yf based PCM yields 15 times better thermal conductivity than R32 based PCM. For magnesium nitrate hexahydrate, the improvement is 10 times better. When compared to R134a based PCMs, the thermal conductivity of R1234yf based PCM is 3 times better. For magnesium nitrate hexahydrate, the improvement is 2.5 times better. Thermal conductivity with sodium chloride linearly increases with the increase in salt volume fraction. For magnesium nitrate hexahydrate, the thermal conductivity increases but at a shallower rate compared to sodium chloride.

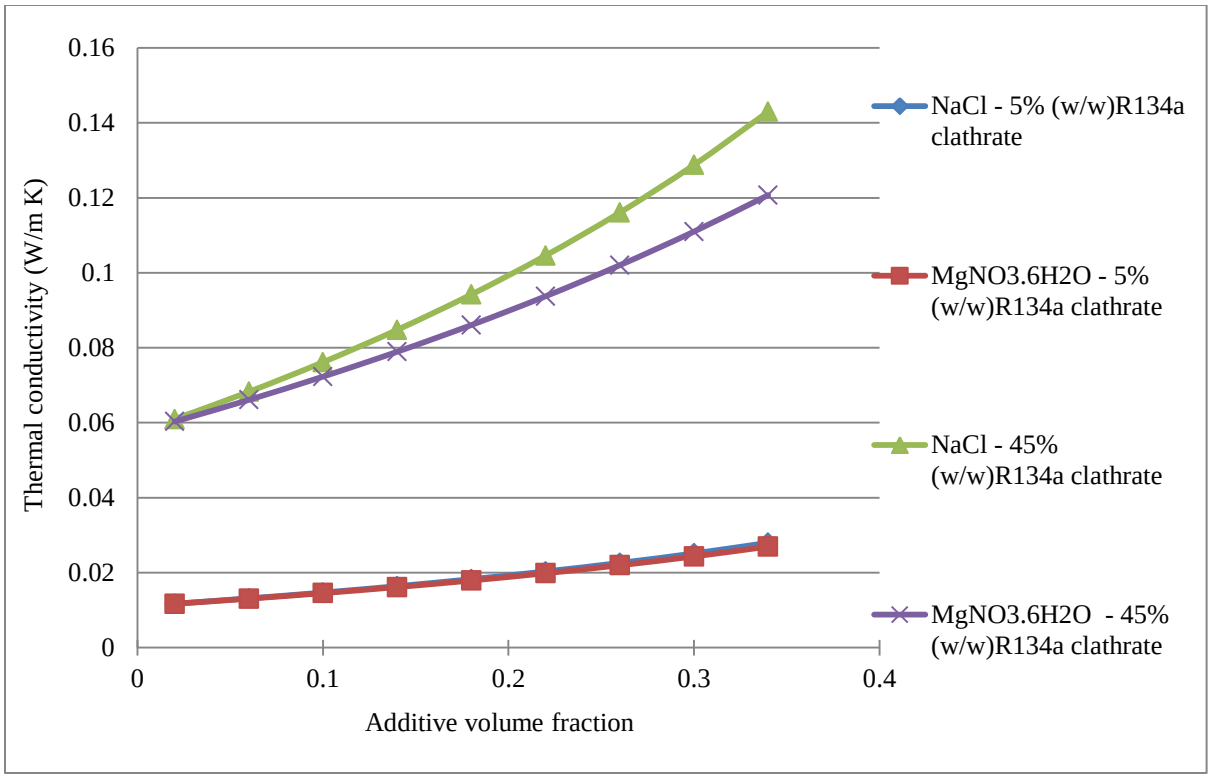

Figure 7.90 Thermal conductivities of R134a clathrates with salts

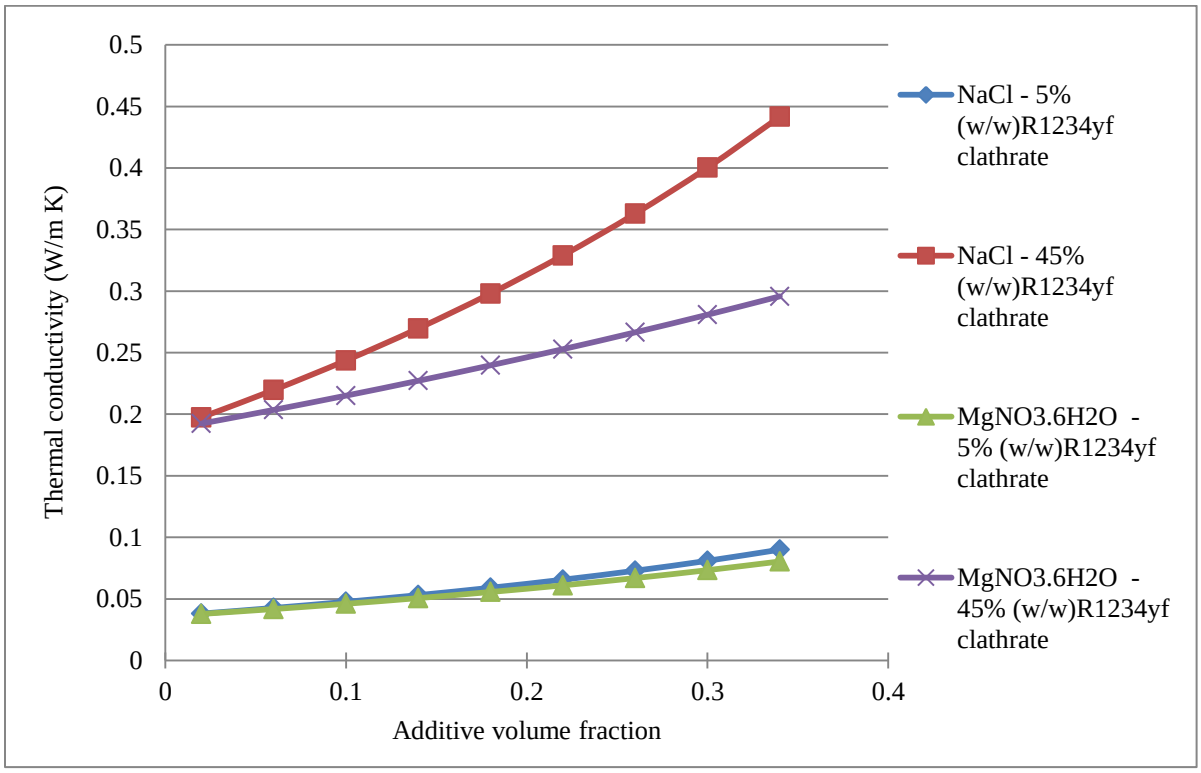

Figure 7.91 Thermal conductivities of R1234yf clathrates with salts

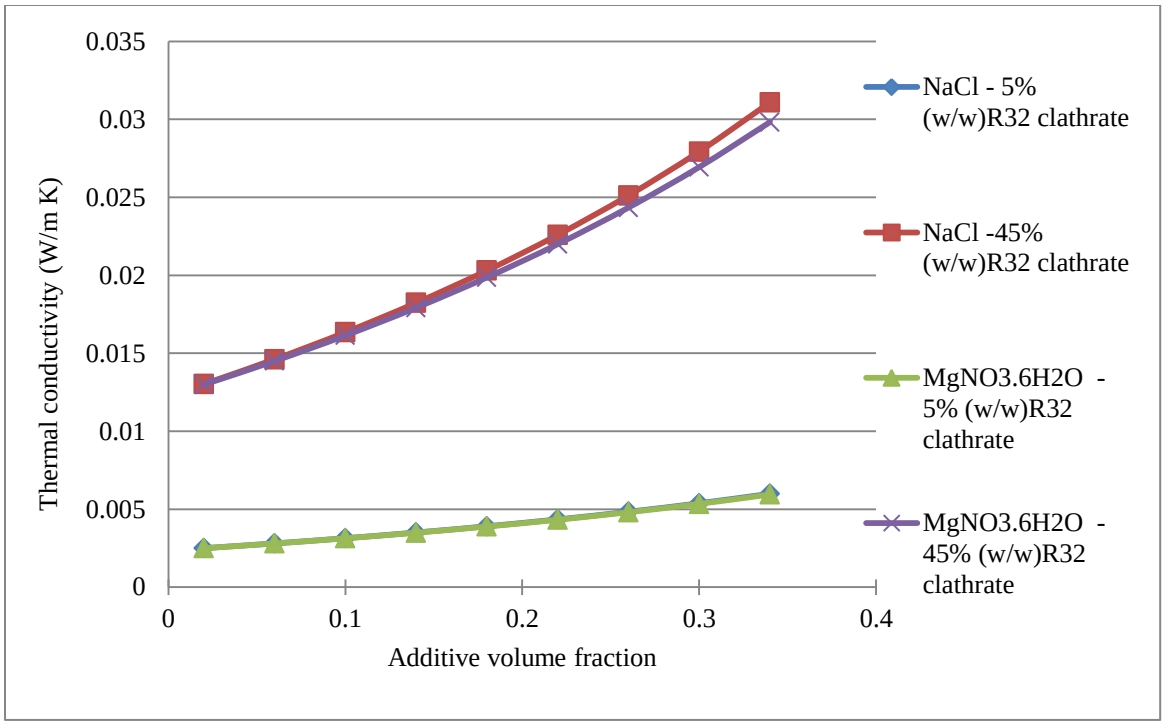

Figure 7.92 Thermal conductivities of R32 clathrates with salts

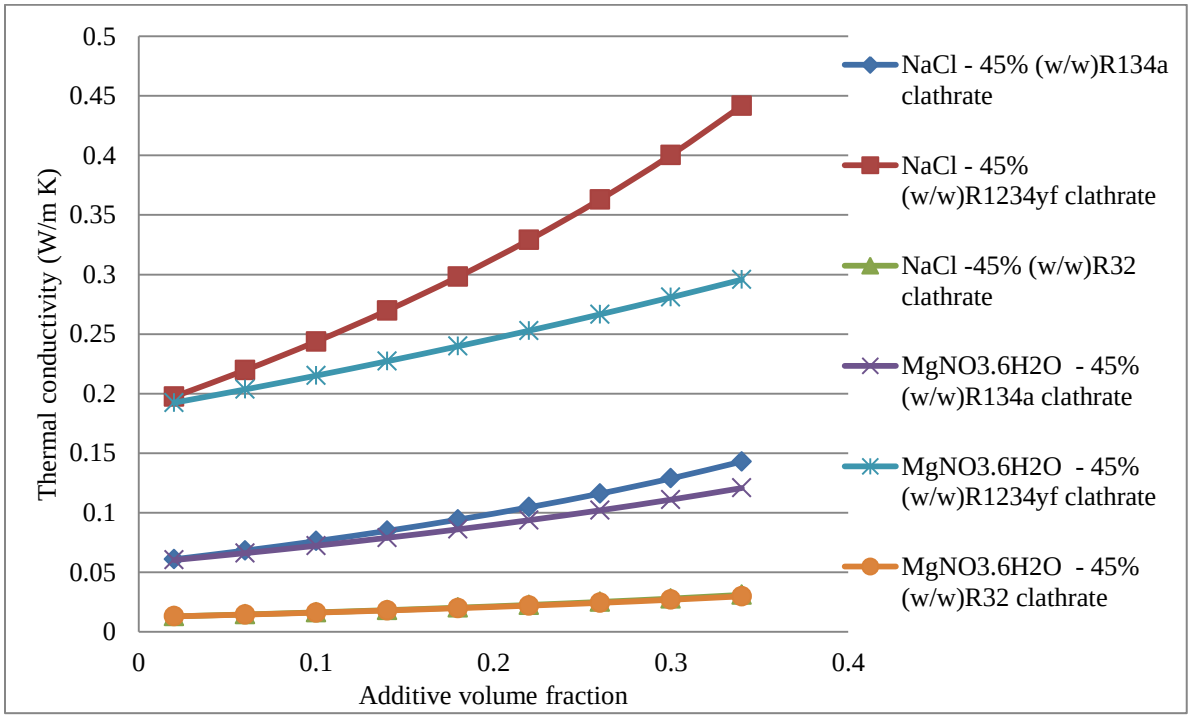

Figure 7.93 Thermal conductivities for different refrigerants with salts

7.10.3 Thermal Property Results with Liquid Additives

Ethylene glycol and propylene glycol are studied as liquid additives. Liquid additives are also studied as they pose integration simplicity when the use of PCM is desired for active cooling. Clathrate with liquid additive can pass through compressors and pumps without causing any significant physical or efficiency loss. Table 7.21 shows the thermal properties of the used liquid additives [122, 123]

Table 7.21 Thermal properties of ethylene glycol and propylene glycol

	Thermal conductivity (W/m K)	**Specific heat (J/kg K)**
Ethylene glycol	0.26	2428
Propylene glycol	0.2	2500

A comparison is made to see the change in thermal properties of R134a clathrate when ethylene glycol and propylene glycol are used as additives. The comparison is made against salt additives. Since this part purely aims to study the difference in thermal properties caused by using glycols, R134a clathrate is chosen to see the difference.

Figure 7.94 shows the variation of specific heats of PCMs over a wide range of volume fraction of additives. The additives are added into 0.4 refrigerant mass fraction clathrate of R134a refrigerant. When compared with salt additives, glycol additives show that they do not improve the specific heat capacity of the clathrate. However, compared to magnesium nitrate hexahydrate additive, glycols result in better specific heat of the PCM. Both glycols have similar specific heat with propylene glycol having slightly better specific heat.

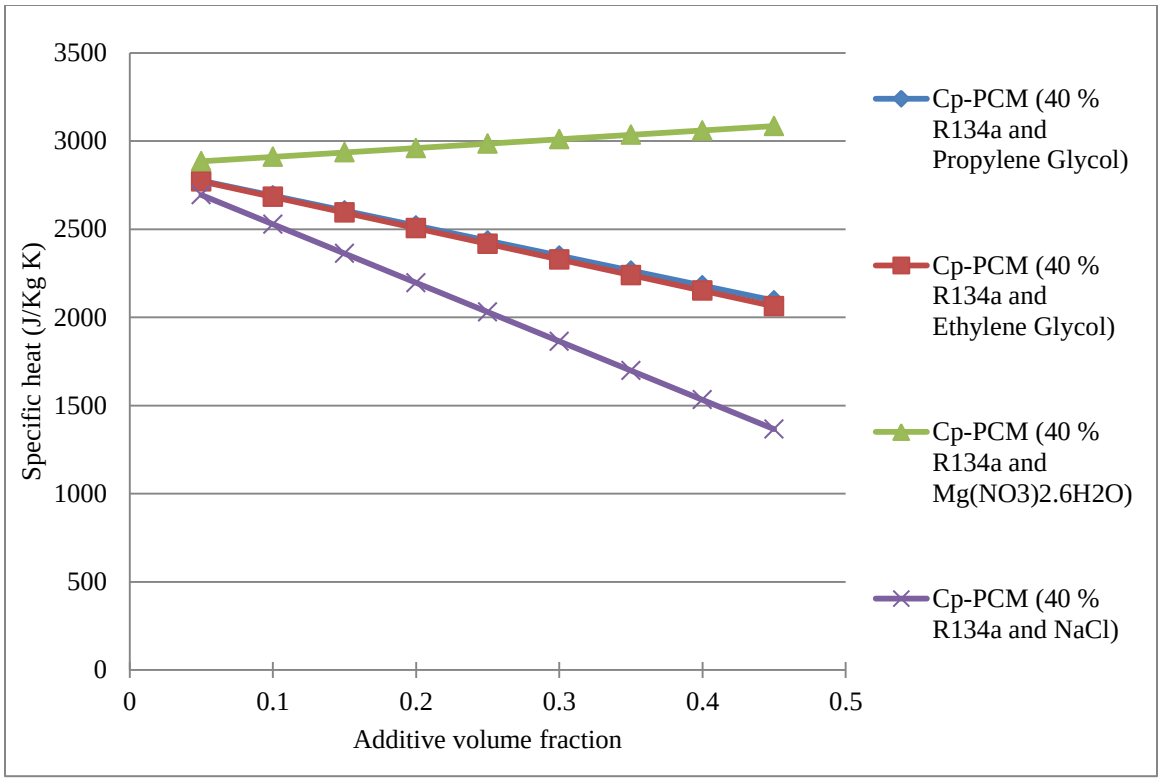

Figure 7.94 Specific heats of R134a clathrates with salts and glycols

Figure 7.95 shows the variation of thermal conductivities of PCMs over the range of volume fraction of additives. The additives are added into the 0.4 refrigerant mass fraction clathrate of R134a refrigerant. When compared with clathrate, propylene and ethylene glycol additives show that they slightly improve the thermal conductivities of the PCMs. However, in comparison with salts, propylene and ethylene glycol additives result in significantly lower thermal conductivity improvement. This reduced improvement is mainly due to the absence of heat transport due to Brownian motion.

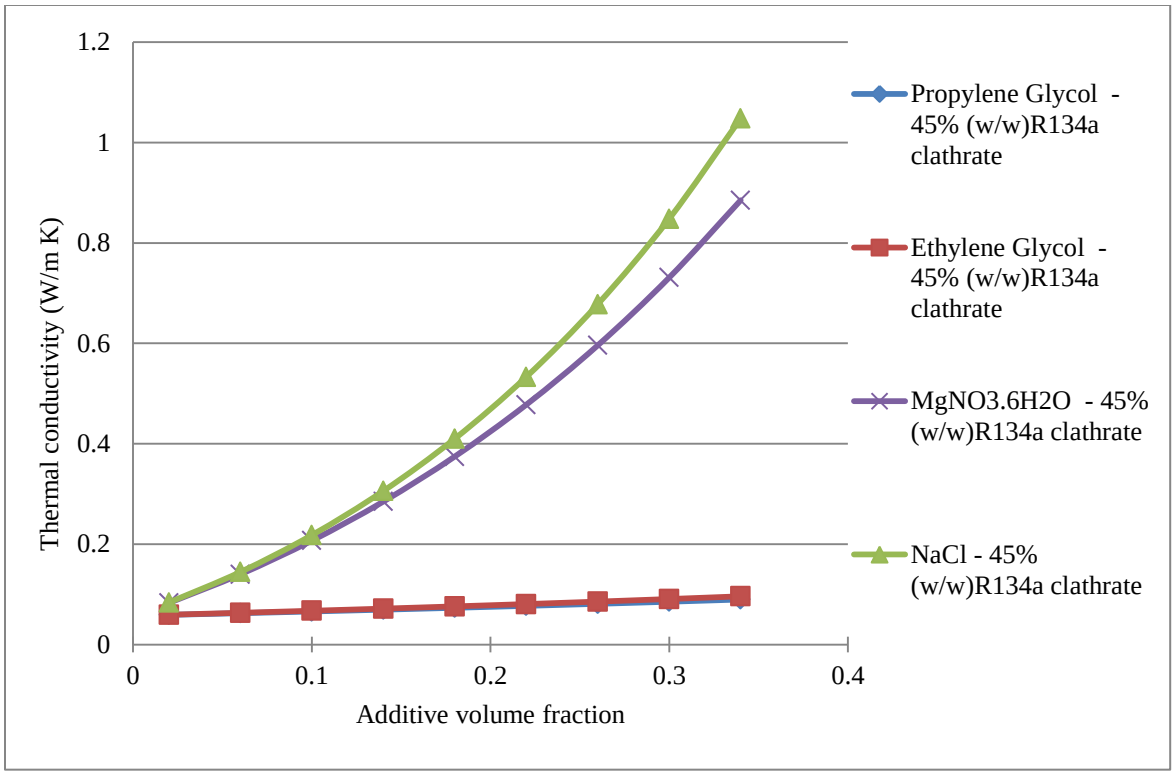

Figure 7.95 Thermal conductivities of R134a clathrates with salts and glycols

7.12 Optimization Results

Using the equations presented in chapter 6 under optimization sections, optimization results are presented here. Glass tube optimization, referred as simple cooling, and battery cooling optimizations are conducted for each additive. In each case, it is desirable to have the optimization factor to be the lowest for the most optimal PCM. Figure 7.96 shows the optimization factor for simple cooling is presented for each PCM. The results show copper to have the highest value for the optimization factor while ethanol has the lowest. Base clathrate has a relatively low optimization factor partly because of low cost, since it has no additive, and partly due to its high energy ratio. Although copper PCM has decent charge to discharge energy ratio, it has a very high cost. The high cost is because

of copper particles that cost more than any other type of additive used. Ethanol has the lowest optimization factor primarily due to its very high energy discharge and partly due to its low cost. Overall, for simple cooling tests, the optimization suggests that ethanol PCM is the best choice as it yields high energy during discharge and has low cost.

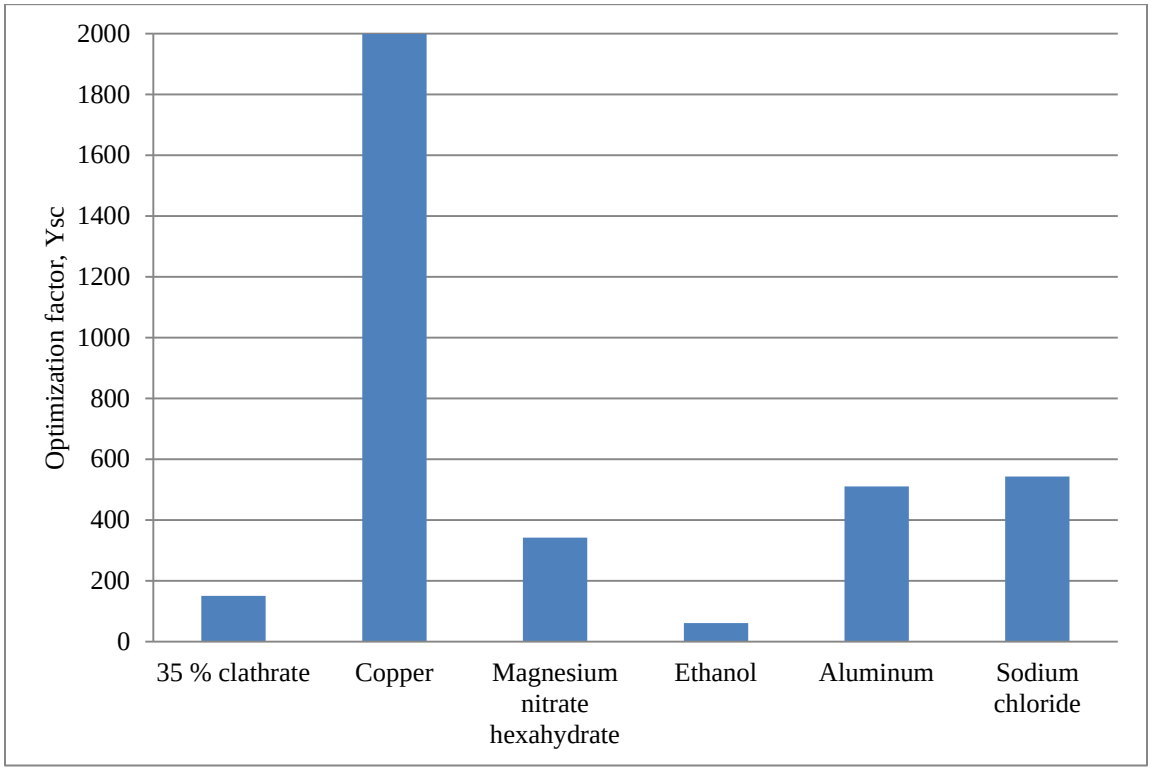

Figure 7.96 Optimization factors for simple cooling for each PCM

Figure 7.97 shows the optimization factor for battery cooling with respect to each PCM. Once again, the results show copper to have the highest value for the optimization factor. But this time the difference between copper and other PCMs are not as great as with simple cooling. Ethanol PCM shows the lowest optimization factor Y_{bc} of 554. Base PCM comes out to be the second best along with aluminum PCM at Y_{bc} value of 1050. Base PCM has a relatively low optimization factor partly because of low cost, since it has

no additive, and partly due to its high energy ratio. Aluminum PCM shows great potential since it shortens the battery cooling time while its cost is not as high as copper additive. Copper PCM has decent charge to discharge energy ratio, however, it has a very high cost. Ethanol has the lowest optimization factor primarily due to its very high energy discharge and partly due to its low cost. Overall, for battery cooling tests, the optimization suggests that ethanol PCM is the best choice as it yields high energy during discharge and has low cost.

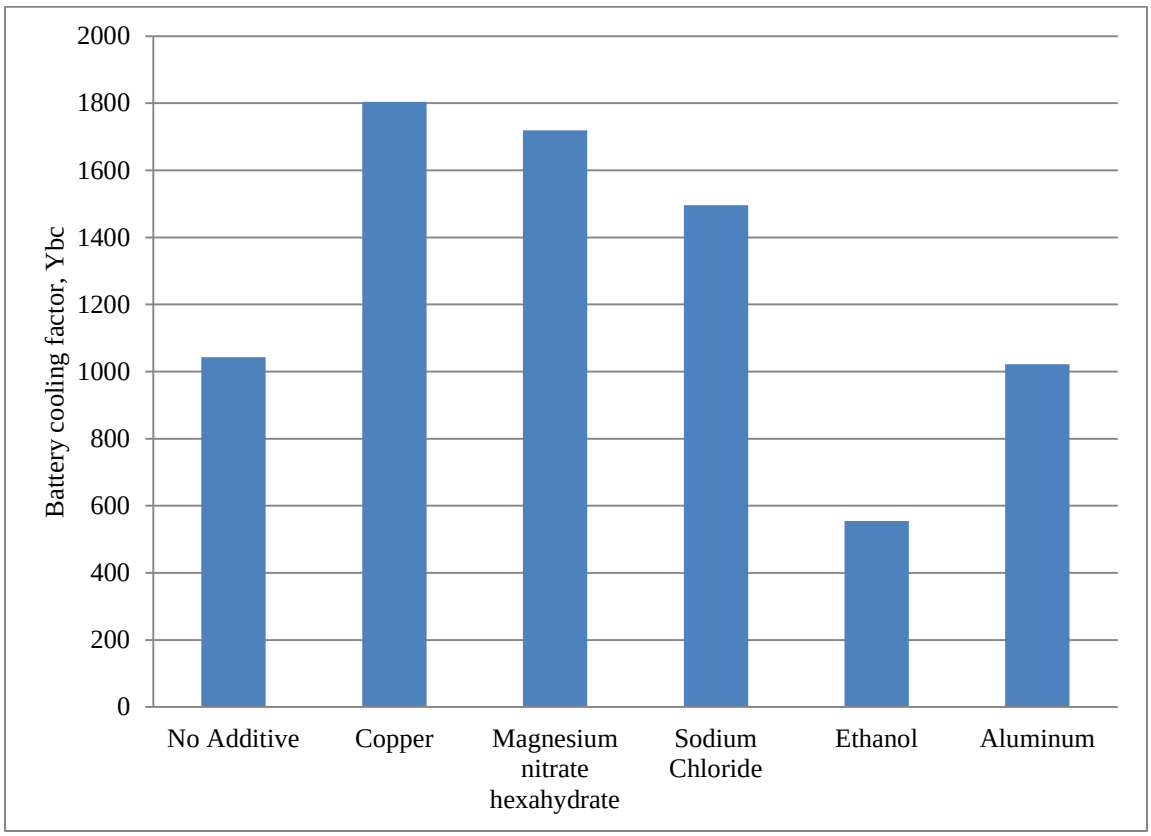

Figure 7.97 Optimization factors for battery cooling with respect to each PCM

7.13 Validation of Results

The thermal properties of the R134a clathrates with the selected additives, namely aluminum, copper, sodium chloride and magnesium nitrate hexahydrate have not been studied before. Additionally, the precise charging time of the PCMs and battery cooling using the PCMs has no previous record either. Therefore, there are no previous studies on the same subject available to compare the results with. There are handful of studies available that have studied R134a and R141b clathrate with some additives. But those studies did not attempt to find the thermal properties nor did they attempt to pinpoint the charging time. Some other studies have attempted to find the thermal properties of fluids with nanoscale particles. Those studies, however, do not use refrigerant clathrate as base fluid. To facilitate the validation requirement, a comparison is made to compare the thermal properties of closest fluid mixture available in the literature. A comparison is also presented for charging time of the clathrate. Thermal conductivity improvement matches positively for metal additives. The charging time improvement also compares favorably with the published results. It is to be noted that charging time gets effected by the material PCMs are encapsulated in. The comparison of previous studies with the thesis results validates the thesis results. This validation makes the results appropriate enough to be used to future research or even for product development for practical use. With ongoing research and development, the results in this thesis can assist the future researches to improve the studies further. It can also help industries to select the right additive for cool thermal energy storage development, depending on its application. As shown in Table 7.22, the available published results are compared with some of the findings on this thesis [38, 47, 124-129].

Table 7.22 Comparison of available published results with the results of the thesis

Base Fluid	**Type**	**Size**	**% volume**	**Source Remarks**	**Comparison with Thesis**
R123, R134a	Carbon nanotubes	20nm × 1 μm	1%	[124] Heat transfer coefficient improved to 36.6%	75% with Cu additive, 52% with Aluminum at 0.01 additive mass fraction
R113	Cupric oxide (CuO)	40nm	0.15–1.5%	[125] Maximum improvement of heat transfer coefficient, 29.7%	75% with Copper additive with 0.01 additive mass fraction
R134a	Cupric oxide (CuO)	-	–	[126] Heat transfer coefficient increased more than 100%	75% with Copper additive with 0.01 additive mass fraction
R134a	Cupric oxide (CuO)	30nm	0.50%	[127] Enhancement of heat transfer coefficient of between 50% and 275%	75% with Copper additive with 0.01 additive mass fraction
Mono-ethlyine Glycol	Cupric oxide (CuO)	Nano	1%	[128] Thermal conductivity improved 50%	75% with Copper additive
R134a	Copper (Cu)	Nano	1%	[47] Charging time improved 63%	25% improvement in charging time when 0.01 copper additive is used
Water	Aluminum Oxide (Al2O	Nano	1% to 4%	[129] Thermal conductivity improved 20%	52% with Aluminum
R141b	Benzene-sulfonic acid sodium salt	-	0.08%	[38] Latent heat of 206.07 MJ/m^3	67 MJ/m^3 for R134a clathrate with Ethanol additive

This thesis shows the experimental results of R134a clathrate based PCM with additives. The results concluded that liquid additive tends to work better than solid additives. Further improvement in the refrigerant clathrate can be made by using liquid additives with better thermal properties than ethanol. Since metal particles tend to settle at the bottom of the tube, metal mesh can alternatively be used to see the improvement in thermal properties of the refrigerant clathrate. New refrigerants with low global warming potential can be used and the results can be compared. R1234yf is a promising replacement for R134a as it has similar working properties. Improvement in techniques to measure the thermal properties can also be part of the future work in this field. Advanced mechanisms can be developed that can seal the thermocouple wires without any leak yet allow some current to flow. All these developments can improve the readings taken for thermal properties.

Chapter 8 Conclusions and Recommendations

This thesis provides the experimental results of several different R134a based PCM materials. A range of refrigerant clathrate is tested and results evaluated. With the selected refrigerant clathrate, five different additives are used to improve the performance of the PCM.

8.1 Conclusions

Experimental studies are conducted on refrigerant clathrates for use in cooling applications. Refrigerant R134a and R141b are used to form the clathrate. Sodium chloride, magnesium nitrate hexahydrate, aluminum particles, copper particles and ethanol is used as an additive to determine their impact on the refrigerant clathrate. Charging time, discharging time, thermal properties, energy, exergy and battery cooling characteristics are evaluated for the PCM. The major findings in this thesis are as follows:

- R141b does not form clathrate at tested temperatures of 276 K.
- Refrigerant R134a mass fraction of 0.35 requires the lowest time to form the complete clathrate with bath temperature of 276 K and 278 K.
- Additives copper, aluminum, magnesium nitrate hexahydrate and ethanol decrease the onset time of the PCM. Whereas, sodium chloride increases the onset time.

- The magnesium nitrate hexahydrate forms the clathrate fastest, followed by copper, ethanol, aluminum and then sodium chloride. The copper and aluminum additives show an improvement of 71%, magnesium nitrate hexahydrate 57% and ethanol by 28%.
- The magnesium nitrate hexahydrate and copper accelerate the clathrate formation while aluminum and ethanol does not affect the charging time much.
- The sodium chloride delays the clathrate formation time while at 0.04 and 0.05 sodium chloride mass fraction, it does not allow clathrate formation.
- Increasing the additive fraction does not help speed up the process while in some cases it slows the charging.
- Energy and exergy values follow the same trend as the charging time.
- Greater charging time does not necessarily mean that the PCM is ineffective for cooling applications.
- The liquid phase specific heat capacity of the base PCM is found to be 3140 J/kg K. Additives reduce the liquid phase specific heat capacity of the base PCM with sodium chloride having the most adverse effect.
- The liquid phase thermal conductivity of the base PCM is found to be 0.09 W/m K. All the additives increased the liquid phase thermal conductivity of the base PCM. Copper additive improved the thermal conductivity by 350%, followed by aluminum at 230%, magnesium nitrate hexahydrate at 134%, ethanol at 60% and sodium chloride at 50%.

- The solid phase thermal conductivity of the base PCM is found to be 0.33 W/m K. Except for sodium chloride; all other additives increase the solid phase thermal conductivity of the base PCM. Copper additive improved the thermal conductivity by 74%, followed by aluminum at 52%, magnesium nitrate hexahydrate at 40% and ethanol at 9%. Sodium chloride reduced the solid phase thermal conductivity by 12%.
- Magnesium nitrate hexahydrate additive lowers the specific latent heat of the PCM by 68%. The specific latent heat of the PCM with ethanol is 600% more than the base PCM.
- Compared to analytical results, all the experimental values for the liquid phase specific heat are found within 14% difference. For liquid phase thermal conductivity, the experimental values are found within 26% difference.
- Ethanol additive lasts the longest during discharge for 435 seconds while magnesium nitrate hexahydrate lasts the shortest at 180 seconds.
- PCM with ethanol additive cools down the battery fastest with copper, aluminum and no additive PCM have similar cooling time. Salt additives have higher cooling time compared to other additives.
- PCM with ethanol and aluminum additive helps battery maintain the lowest temperature. PCMs with salt additives keep the battery temperature higher than the other PCMs. Overall; the PCMs reduce the battery temperature by approximately 5 K.

8.2 Recommendations

Further improvements can be investigated in future studies which can include experimental results to validate the predictions of analytical studies. Experiments can be conducted to compare the results and possibly suggest further improvements in the equations predicting the thermal conductivities. Due to the highly empirical nature of thermal conductivity equations, the thermal conductivity prediction highly depends on the substances being studied, its phase and its surrounding environment. The analyses, results and discussions presented in this thesis can be used to compare the effectives of the refrigerant based PCMs to other PCMs under research. Some results and developments can be directly used for practical passive cooling applications. However, there are several recommendations for the future work.

- Refrigerant clathrate of other refrigerants can be made and studied for their performance on passive cooling applications. R134a refrigerant used in this study has a high global warming potential and it will soon be phased out. New refrigerants such as R1234yf or R32 can be used for a similar study as they have low global warming potential and will soon replace existing refrigerants.
- The studied PCMs are primarily studied for passive cooling applications for electronics. However, they can be used in a cold thermal energy storage system to provide cool energy to cooling fluids. These cooling fluids can then be used for space cooling applications. Colt thermal energy storage system's performance can be evaluated with each additive. The additives may help speed up the charging process, which for a large system, could yield significant improvement.

- Obtaining the thermal properties is a huge challenge. The existing methods to measuring the thermal properties are difficult to apply for this setup as it had pressurized refrigerant. An improved method of obtaining the thermal properties, possibly based on wheat stone bridge circuit can be developed. Such a mechanism would greatly reduce the number of tests results required to obtain thermal properties' values.
- Repeatability and cycling stability tests can also be conducted by future researchers to see if the performance of the PCMs changes. The PCMs can be frozen and melted for several cycles to see if the amount of heat release or absorbed bas changed. The impact of cyclic phase change can also be studied on the freezing temperature and latent heat.
- Visually inspecting the onset and end set phase is something that can be improved. Instead of observing the onset and end set phase, a more improved method is to charge all the PCMs for a specific amount of time, irrespective of its additive.
- Studying the crystal growth can be look at as each additive produces a unique crystal shape which can be studied for its shape and size.
- Discharge the PCM at different temperatures and recording the discharge time is another aspect that can be studied by future researchers. This study would determine the capacity of the PCM for each environmental condition.

References

[1] Chaichana C, Charters WW, Aye L. An ice thermal storage computer model. Applied Thermal Energy 2001;. 21: 1769–1778

[2] Habeebullah B. Economic feasibility of thermal energy storage systems. Energy and Buildings 2007; 39: 355–363

[3] Zafar S, Dincer I, Gadalla M. Experimental testing and analysis of R134a clathrates based PCMs for cooling applications. International Journal of Heat and Mass Transfer 2015; 91: 756-765

[4] Abdullah MO, Yii LP, Junaidi E, Tambi G, Mustapha MA. Electricity cost saving comparison due to tariff change and ice thermal storage (ITS) usage based on a hybrid centrifugal-ITS system for buildings: A university district cooling perspective. Energy and Buildings 2013; 67: 70–78

[5] Sharma CS, Zimmermann S, Tiwari MK, Michel B, Poulikakos D. Optimal thermal operation of liquid-cooled electronic chips Int. J. Heat Mass Transfer 2012;, 55: 1957–1969

[6] Sharma A, Tyagi VV, Chen CR, Buddhi D. Review on thermal energy storage with phase change materials and applications. Renewable and Sustainable Energy Reviews 2009; 13: 318–345.

[7] Khartchenko NV. Advanced energy systems. Berlin: Institute of Energy Engineering & Technology University; 1997

[8] Dincer I, Rosen MA. Thermal energy storage - Systems and Applications. John Wiley & Sons, Chichester (England); 2002

[9] Zalba B, Marín JA, Cabeza LF, Mehling H. Review on thermal energy storage with phase change: materials, heat transfer analysis and applications. Applied Thermal Engineering 2003; 23:251–283

[10] Dutil Y, Rousse DR, Salah NB, Lassue S, Zalewski L. A review on phase-change materials: Mathematical modeling and simulations. Renewable and Sustainable Energy Reviews 2011; 15: 112-130

[11] Abhat A. Low temperature latent heat thermal energy storage: heat storage materials, Solar Energy 1983; 30: 313–332

[12] Pillai KK, Brinkwarth BJ. The storage of low grade thermal energy using phase change materials. Applied Energy 1976; 2: 205–16.

[13] Alkana C, Günthera E, Hieblera S, Ensarib OF, Kahramanb D. Polyurethanes as solid–solid phase change materials for thermal energy storage. Solar Energy 2012; 86: 1761–1769

[14] Gordon J, Passlow L. Introduction to Organic Chemistry: Theory Manual. Chemical, Forensic, Food & Environmental Technology 2009; 1: 2-3

[15] Buddhi D, Sawhney RL.In: Proceedings on thermal energy storage and energy conversion; 1994

[16] Abhat A, Heine D, Heinisch M, Malatidis NA, Neuer G. Development of a modular heat exchanger with an integrated latent heat storage. Report no. BMFT FBT 81-050. Germany Ministry of Science and Technology, Bonn (Germany); 1981

[17] Lane GA. Macro-encapsulation of PCM. Report no. ORO/5117-8. Midland, Michigan: Dow Chemical Company 1978: 152.

[18] Lane GA, Rossow HE. Encapsulation of heat of fusion storage materials. Proceedings of the second south eastern conference on application of solar energy 1976: 442–55

[19] Telkes M. Thermal storage for solar heating and cooling. Proceedings of the workshop on solar energy storage sub-systems for heating and cooling of buildings. University of Virginia, Charlottesville; 1975.

[20] Biswas R. Thermal storage using sodium sulfate decahydrate and water. Solar Energy 1977; 99: 99–100

[21] Encyclopedia Britannica, Paraffin hydrocarbon, http://www.britannica.com/ EBchecked/ topic/ 442584/ paraffin-h ydrocarbon, 2014

[22] Dutch S, Incongruent Melting,http://www.uwgb.edu/dutchs/Petrology/ incongm.HTM, University of Wisconsin - Green Bay, 2014

[23] George A. Hand book of thermal design. Guyer C, editor. Phase change thermal storage materials. McGraw Hill Book Co.; 1989 chapter 1

[24] Sloan ED. Clathrate hydrates of natural gases. Marcel (Bekker, New York) 1990: 641.

[25] Nikbakhta F, Izadpanaha AA, Varaminianb F, Mohammadic AH. Thermodynamic modeling of hydrate dissociation conditions for refrigerants R-134a, R-141b and R-152a. International Journal of Refrigeration 2012; 35: 1914–1920

[26] Tanasawa I, Takao S. Low-temperature storage using clathrate hydrate slurries of tetra-n-butylammonium bromide: thermophysical properties and morphology of clathrate hydrate crystals, Fourth International Conference on Gas Hydrates 2002; 96: Yokohama, Japan: 3–967.

[27] Mori YH, Mori T. Characterization of gas hydrate formation in direct-contact cool storage process. International Journal of Refrigeration 1989; 12: 259–265.

[28] Mori YH, Mori T. Formation of gas hydrate with CFC alternative R-134a. AIChE Journal 1989; 35: 1227–1228.

[29] Mori YH, Isobe F. A model for gas hydrate formation accompanying direct-contact evaporation of refrigerant drops in water. International Communications in Heat Mass Transfer 1991; 18: 599–608.

[30] Carbajo JJ. A direct-contact-charged–direct-contact-discharged cool storage system using gas hydrate. ASHRAE Transaction 1985; 91: 258–266

[31] Bi YH, Guo TW, Zhu TY, Fan SS, Liang DQ, Zhang L. Influence of volumetric-flow rate in the crystallizer on the gas-hydrate cool-storage process in a new gas-hydrate cool-storage system. Applied Energy 2004; 78: 111–121.

[32] Inab H. New challenge in advanced thermal energy transportation using functionally thermal fluids. International Journal of Thermal Science 2000; 39: 991–1003

[33] Eslamimanesh A, Mohammadi AH, Richon D. Thermodynamic model for predicting phase equilibria of simple clathrate hydrates of refrigerants. Chemical Engineering Science 2011; 66: 5439–5445

[34] Guo KH, Shu BF, Meng ZX, Zeng L Direct-contact gas hydrate cool storage vessel and cool storage air-conditioning system. 1995; Chinese Patent No. ZL95107268.4.

[35] Guo KH, Shu BF, Yang WJ. Advances and applications of gas hydrate thermal energy storage technology. 1st Trabzon International Energy and Environment Symposium 1996, Trabzon, Turkey; 1: 381–386.

[36] Guo KH, Shu BF, Zhang Y. Transient behavior of energy charge– discharge and solid–liquid phase change in mixed gas-hydrate formation. In: Wang, B.X. (Ed.), Heat Transfer Science and Technology. Higher Education Press, Beijing, China, 1996: 728–733

[37] Li G, Hwang Y, Radermacher R. Review of cold storage materials for air conditioning application. International Journal of Refrigeration 2012; 35: 2053–2077

[38] Bi Y, Guo T, Zhu T, Zhang L, Chen L. Influences of additives on the gas hydrate cool storage process in a new gas hydrate cool storage system. Energy Conversion and Management 2006; 47: 2974–2982

[39] EngineeringToolBox. Refrigerants - Ozone Depletion (ODP) and Global Warming Potential (GWP); 2013 < http://www.engineeringtoolbox.com/Refrigerants-Environment-Properties-d_1220.html>

[40] Ro ST, Kim JY, Kim DS. Thermal conductivity of R32 and its mixture with R134a. International Journal of Thermophysics 1995; 16: 1193-1201

[41] Wu J, Wang S. Research on cool storage and release characteristics of R134a gas hydrate with additive. Energy and Buildings 2012; 45: 99–105

[42] Bi Y, Guo T, Zhang L, Zhang H, Chen L. Experimental study on cool release process of gas-hydrate with additives. Energy and Buildings 2009; 41: 120–124

[43] Murshed SMS, Leong KC, Yang C. A combined model for the effective thermal conductivity of nanofluids. Applied Thermal Engineering 2009; 29: 2477-2483.

[44] Duangthongsuk W, Wongwises S. Measurement of temperature dependent thermal conductivity and viscosity of TiO2-water nanofluids. Experimental Thermal and Fluid Science 2009; 33: 706-714.

[45] Moghadassi AR, Hosseini SM, Henneke DE. Effect of CuO nanoparticles in enhancing the thermal conductivities of monoethylene glycol and paraffin fluids. Industrial Engineering and Chemistry Research 2010; 49: 1900-1904

[46] Eastman JA, Choi SUS, Li S, Yu W, Thompson LJ. Anomalously increased effective thermal conductivities of ethylene glycol-based nanofluids containing copper nanoparticles. Appied. Physics. Letter 2001; 78: 718–20

[47] Li J, Liang D, Guo K, Wang R, Fan S. Formation and dissociation of HFC134a gas hydrate in nano-copper suspension. Energy Conversion and Management 2006; 47: 201–210

[48] Das SK, Putra N, Thiesen P, Roetzel W. Temperature Dependence of Thermal Conductivity Enhancement for Nanofluids. ASME Journal of Heat Transfer 2003; 125: 567–574.

[49] Vadasz, P. Heat Conduction in Nanofluid Suspensions. ASME Journal of Heat Transfer 2005; 128: 465–477.

[50] Jang SP, Choi SUS. Effects of Various Parameters on Nanofluid Thermal Conductivity. ASME Journal of Heat Transfer 2006; 129: 617–623.

[51] Kim SH, Choi SR, Kim D. Thermal Conductivity of Metal-Oxide Nanofluids: Particle Size Dependence and Effect of Laser Irradiation. ASME Journal of Heat Transfer 2006; 129: 298-307

[52] Mmohammadiun M, Dashtestani F, Alizadeh M. Exergy Prediction Model of a Double Pipe Heat Exchanger Using Metal Oxide Nanofluids and Twisted Tape Based on the Artificial Neural Network Approach and Experimental Results. ASME Journal of Heat Transfer 2015; 138: 011801

[53] Fan J, Wang L. Review of Heat Conduction in Nanofluids. ASME Journal of Heat Transfer 2009; 133: 040801

[54] Bi Y, Guo T, Zhu T, Zhang L, Chen L. Influences of additives on the gas hydrate cool storage process in a new gas hydrate cool storage system. Energy Conversion and Management 2006; 47: 2974–2982

[55] Oró E, deGracia A, Castell A, Farid MM, Cabeza LF. Review on phase change materials (PCMs) for cold thermal energy storage applications. Applied Energy 2012; 99: 513–533

[56] Fang, X., Ding, Q., Fan, L. Thermal Conductivity Enhancement of Ethylene Glycol-Based Suspensions in the Presence of Silver Nanoparticles of Various Shapes. ASME Journal of Heat Transfer 2014; 136: 034501

[57] Calmac, 2014, <http://www.calmac.com/icebank-energy-storage-model-c>

[58] K. Nagano, K. Ogawa, T. Mochida, K. Hayashi, H. Ogoshi, Thermal characteristics of magnesium nitrate hexahydrate and magnesium chloride hexahydrate mixture as a phase change material for effective utilization of urban waste heat. Applied Thermal Engineering 2004; 24 pp. 221 232

[59] U.S. Energy Information Administration. International Energy Outlook 2011. U.S. Energy Information Administration. (Washington) 2011

[60] Brown LR. PLAN B 4.0- Mobilizing to save civilisation. W.W. Norton & Company, (London) 2007

[61] Confederation of International Contractors' Associations, Ed., Industry as a partner for sustainable development-refrigeration. UNEP; 2002

[62] U.S. Energy Information Administration. International Energy Outlook 2013. Report Number: DOE/EIA-0484(2013) < http://www.eia.gov/forecasts/ieo/world.cfm>

[63] Chen K, Li X. Accurate determination of battery discharge characteristics – A comparison between two battery temperature control methods. Journal of Power Sources 2014; 247: 961–966

[64] Kandasamy R, Wang XQ, Mujumdar AS. Transient cooling of electronics using phase change material (PCM)-based heat sinks. Applied Thermal Engineering 2008; 28: 1047–1057

[65] Hunt C. Gas Hydrate Thermal Energy Storage System. US Patent. 1992.

[66] Javanmardi, Moshfeghian M. Energy consumption and economic evaluation of water desalination by hydrate phenomenon. Applied Thermal Engineering 2003; 23: 845–857

[67] The Clifton Range. Chillo Baths NE7 Series 8 <http://nickel-electro.co.uk/water-baths-stirred/ne7-refrigerated-water-baths/>

[68] ACE Glass Incorporated. Pressure Tube 185 mL. Item Number 8648-33 < http://www.aceglass.com/page.php?page=8648>

[69] Omega, CL3512A Digital Thermometer & Calibrator, http://www.omega.com/manuals/manualpdf/M3806.pdf, 2015.

[70] Eagle Tree Systems, Instruction Manual for the eLogger V3, (2012) 1-2

[71] P.A.Hilton, Air Conditioning Laboratory Unit, http://www.p-a-hilton.co.uk/products/A660-Air-Conditioning-Laboratory-Unit, 2015

[72] Dutil Y, Rousse DR, Salah NB, Lassue S, Zalewski L. A review on phase-change materials: Mathematical modeling and simulations. Renewable and Sustainable Energy Reviews 2011; 15: 112–130

[73] Phelan PE, Bhattacharya P, Prasher RS. Nanofluids for Heat Transfer Applications. Annual Review Heat Transfer 2005; 14: 255–275

[74] Kleinstreuer C, Feng Y. Experimental and Theoretical studies of nanofluid thermal conductivity enhancement: a review. Nanoscale Research Letters 2011; 6: 229

[75] Shi L, Liu XJ, Wang X, Zhu MS. Prediction method for liquid thermal conductivity of refrigerant mixtures. Fluid Phase Equilibria 2000; 172: 293–306

[76] Eastman JA, Choi SUS, Li S, Yu W, Thompson LJ. Anomalously increased effective thermal conductivities of ethylene glycol-based nanofluids containing copper nanoparticles. Applied Physics Letters 2001; 78: 718–720

[77] Lansuer R. The electrical resistance of binary metallic mixtures. Journal of Applied Physics 1952; 23: 779

[78] Davis TH, Valencourt LR, Johnson CE. Transport processes in composite media. Journal of American Ceramic Society 1975; 58: 447

[79] Kirkatrick S. Percolation and conduction. Reviews of Modern Physics 1973; 45: 574

[80] Mattea M, Urbicain MJ, Rotstein E .Prediction of Thermal Conductivity of Vegetable Foods by the Effective Medium Theory. Journal of Food Science 1986; 51:113-116

[81] Kopelman IJ. Transient Heat Transfer and Thermal Properties in Food Systems. Doctoral Dissertation 1966. East Lansing: Michigan State University

[82] Maroulis ZB, Drouzas AE, Saravacos GD. Modeling of thermal conductivity of granular starches. Journal of Food Engineering 1990; 11: 255–271

[83] Maroulis ZB, Shah KK, Saravacos GD. Thermal conductivity of gelatinized starches. Journal of Food Science 1991; 56: 773–776

[84] Morley MJ. Thermal conductivities of muscles, fats and bones. Journal of Food Technology 1966; 1: 303–311

[85] Morley MJ, Miles CA. Modelling the thermal conductivity of starch-water gels. Journal of Food Engineering 1997; 33: 1–14

[86] Maxwell JC. A Treatise on Electricity and Magnetism. Oxford: Clarendon Press 1891: 435-441

[87] Heldman DR, Singh RP. Food Process Engineering. Westport: AVI Publishing Co.,Inc 1981: 87–157

[88] Rizvi IH, JainA, Ghosh SK, Mukherjee PS. Mathematical modelling of thermal conductivity for nanofluid considering interfacial nano-layer. Heat and Mass Transfer 2013; 49: 595-600

[89] Prasher R, Bhattacharya P, Phelan PE. Brownian-motion-based convective-conductive model for the effective thermal conductivity of nanofluids. ASME Journal of Heat Transfer 2006; 128: 588-595

[90] Abusoglu A, Kanoglu M. Exergetic and thermoeconomic analyses of diesel engine powered cogeneration: Part 1 – Formulations. Applied Thermal Energy 2009; 29: 234–241

[91] Dincer I, Rosen M. EXERGY Energy, Environment and Sustainable Development. London: Elsevier, 2007

[92] Hernandez O. SIDS Initial Assessment Report for 12th SIAM. UNEP Publications. Paris, France: 2001

[93] DuPont™ Suva® refrigerants. Mutual Solubility of Select HCFCs and HFCs and Water. DuPont USA: 2004

[94] The Linde Group. Refrigerants: Product data summary.2015 http://www.linde-gas.com/internet.global.lindegas.global/en/images/Refrigerants-Product-Data-Summary17_108590.pdf

[95] BOC Gases. Safety Data Sheet: R141b 2001 https://www.boconline.co.uk /internet.lg.lg.gbr/en/images/r141b410_55986.pdf

[96] NFAA. Material Safety Data Sheet: Ethanol 2001. http://www.nafaa.org/ethanol.pdf

[97] ScienceLab. Material Safety Data Sheet: Magnesium nitrate hexahydrate MSDS 2005. http://www.sciencelab.com/msds.php?msdsId=9927355

[98] ScienceLab. Material Safety Data Sheet: Aluminum MSDS 2005 http://www.sciencelab.com/msds.php?msdsId=9922844

[99] ScienceLab. Material Safety Data Sheet: Copper MSDS 2005 http://www.sciencelab.com/msds.php?msdsId=9923549

[100] ScienceLab. Material Safety Data Sheet: Sodium Chloride MSDS 2005 http://www.sciencelab.com/msds.php?msdsId=9927593

[101] NIST Standard Reference Database 69: NIST Chemistry WebBook. Liquid Phase Specific Heat Capacity of Water. 1998 http://webbook.nist.gov/cgi/cbook.cgi?ID=C7732185&Type=JANAFL&Table=on#JANAFL

[102] NIST Standard Reference Database 69: NIST Chemistry WebBook. Isothermal Properties of Water. 1998 http://webbook.nist.gov/cgi/fluid.cgi?T=298&PLow=&PHigh=&PInc=&Applet=on&Digits=5&ID=C7732185&Action=Load&Type=IsoTherm&TUnit=K&PUnit=MPa&DUnit=kg%2Fm3&HUnit=kJ%2Fmol&WUnit=m%2Fs&VisUnit=uPa*s&STUnit=N%2Fm&RefState=DEF

[103] EngineeringToolbox. Water: Thermal Properties. 2015 http://www.engineeringtoolbox.com/water-thermal-properties-d_162.html

[104] NIST Standard Reference Database 69: NIST Chemistry WebBook. Solid Phase Specific Heat Capacity of Sodium Chloride. 2011 <http://webbook.nist.gov/cgi/cbook.cgi?ID=*C7647145&Type=JANAFS&Table=on*>

[105] Shomate CH, Kelley KK. The Specific Heats at Low Temperatures of Nitrates of Magnesium, Calcium, Barium and Aluminum. Journal of American Chemical Society 1944; 66: 1490–1492

[106] NIST Standard Reference Database 69: NIST Chemistry WebBook. Solid Phase Specific Heat Capacity of Aluminum. 2011 http://webbook.nist.gov/cgi/cbook.cgi?ID=*C7647145&Type=JANAFS&Table=on*

[107] White GK, Collocott SJ. Heat Capacity of Reference Materials: Cu and W. Journal of Physical and Chemical Reference Data 1984; 13: 4

[108] NIST Standard Reference Database 69: NIST Chemistry WebBook. Constant Pressure Heat Capacity of Liquid Ethanol. 1998 http://webbook.nist.gov/cgi/cbook.cgi?Name=ethanol&Units=SI&cTC=on

[109] MIT. Sodium Chloride 2009. http://dao.mit.edu/8.231/NaCl.htm

[110] Petravica J. Thermal conductivity of ethanol. The Journal of Chemical Physics 2005; 123:174503

[111] Nagano K, Ogawa K, Mochida T, Hayashi K, Ogoshi H. Performance of heat charge/discharge of magnesium nitrate hexahydrate and magnesium chloride hexahydrate

mixture to a single vertical tube for a latent heat storage system. Applied Thermal Engineering 2004; 24: 209–220

[112] Linde. Refrigerants: R134a 2015. http://www.linde-gas.com/en/products_and_supply/refrigerants/HFC_refrigerants/R134a/index.html

[113] Lemmon EW, Huber ML, McLinden MO. NIST Standard Reference Data 23 REFPROP Ver. 8.0. NIST, USA: 2007

[114] Domanski PA, Yashar D. Comparable Performance Evaluation of HC and HFC Refrigerants in an Optimized System. 7th IIR Gustav Lorentzen Conference on Natural Working Fluids 2006, Trondheim, Norway, May 28-31

[115] NIST Standard Reference Database 69: NIST Chemistry WebBook. Constant Pressure Heat Capacity of Solid Graphite. 2011 http://webbook.nist.gov/cgi/cbook.cgi?ID=C7782425&Mask=2

[116] DuPont™ Suva® refrigerants. Mutual Solubility of Select HCFCs and HFCs and Water. DuPont, USA: 2004

[117] Papadaki M., Schmitt M, Seitz A, Stephan K, Taxis B, Wakeham WA. Thermal conductivity of R134a and R141b within the temperature range 240–307 K at the saturation vapor pressure. International Journal of Thermophysics 1993; 14: 173-181

[118] Benedito JCC, Guedes RC, Pai-Panandikerb RS, Castrob CAN. Hydrogen bonding and the dipole moment of hydrofluorocarbons by density functional theory. Physical Chemistry Chemical Physics 2001; 3: 4200-4207

[119] Mathur GD. Heat Transfer Coefficients and Pressure Gradients during Flow Boiling and Condensation for Refrigerant HFO-1234yf. ARSS Meeting, Phoenix, USA: 2011

[120] Ro ST, Kim JY, Kim DS. Thermal conductivity of R32 and its mixture with R134a. International Journal of Thermophysics 1995; 16: 1193-1201

[121] Pop E , Varshney V , Roy AK. Thermal properties of graphene: Fundamentals and applications. MRS Bulletin 2012; 37: 1273-1281

[122] The Dow Chemical Company. Ethylene Glycol, Physical Properties. 2014 http://www.dow.com/ethyleneglycol/about/properties.htm

[123] Martin AE, Murphy FH. Glycols – Propylene Glycols. Dow Chemical Company 2014; (12): 117-01785-0306 < http://msdssearch.dow.com/PublishedLiteratureDOWCOM/dh_006e/0901b8038006e13c.pdf?filepath=propyleneglycol/pdfs/noreg/117-01785.pdf&fromPage=GetDoc>

[124] Park KJ, Jung DS. Boiling heat transfer enhancement with carbon nanotubes for refrigerants used in building air conditioning. Energy and Buildings 2007; 39: 1061–1064

[125] Hao P, Guoliang D, Weiting J, Haitao H, Yifeng G. Heat transfer characteristics of refrigerant-based nanofluid flow boiling inside a horizontal smooth tube. International Journal of Refrigeration 2009; 32: 1259–1270

[126] Fu L, Wang R, Cong W, Li Q, Wu Y. Experiment study on performance of refrigerator using nano-particle additive. Journal of Xi'an Jiaotong University 2008; 42: 852–854

[127] Kedzierski MA, Gong M. Effect of CuO nanolubricant on R134a pool boiling heat transfer with extensive measurement and analysis details. NISTIR 7336. National Institute of Standards and Technology, USA: 2007

[128] Moghadassi AR, Hosseini SM, Henneke DE. Effect of CuO nanoparticles in enhancing the thermal conductivities of monoethylene glycol and paraffin fluids. Industrial Engineering and Chemistry Research 2010, 49:1900-1904

[129] Murshed SMS, Leong KC, Yang C. A combined model for the effective thermal conductivity of nanofluids. Applied Thermal Engineering 2009, 29:2477-2483